Department of Chemical Engineering

Towards the Development of an Aptamer-based Polymeric Biosensor for Biomolecular Screening

Caleb Acquah

This thesis is presented for the Degree of
Doctor of Philosophy
of
Curtin University

October 2017

GENERAL DECLARATION

The thesis generated twelve original papers which were published in and submitted to international peer reviewed journals, one accepted book chapter and three postgraduate student colloquiums. The thrust of this thesis was geared "towards the development of an aptamer-based polymeric biosensors for biomolecular screening".

The conceptualisation of ideas and write-up were the sole responsibility of the research candidate, working within the confines of the Department of Chemical Engineering and Curtin Malaysia Research Institute (CMRI) under the primary supervision of Professor Michael K. Danquah and co-supervised by Dr. Charles K.S. Moy, Dr. Lau Sie Yon and Dr. Clarence Ongkudon. Sections of the experiment were also actively conducted in collaboration with other Universities in Malaysia and China. The presence of co-authors in the manuscripts are an indication of the active internal and external collaborations within the core thematic framework of this research.

To the best of my knowledge and belief this thesis contains no material previously published by any other person except where due acknowledgment has been made and contains no material which has been accepted for the award of any other degree or diploma in any university. The proposed research study had low animal ethical clearance with an approval number CSEA 051214.

Signed by: _____   Date: 24/10/2017   .

Caleb Acquah
(Phd Candidate)

The table below lists scientific peer-reviewed articles of the research candidate in formulating this thesis.

Article	Thesis Chapter	Title of Publication	Status of Publication	Contribution of Candidate
1	2	Development and characteristics of polymer monoliths for advanced LC bioscreening applications: A review	Journal of Chromatography B 1015, 121-134. (2016)	Conceptualisation, write-up [85%]
2	2	SELEX Modifications and Bioanalytical Techniques for Aptamer–Target Binding Characterization	Critical reviews in analytical chemistry 46, 521-537. (2016)	Conceptualisation, write-up [40%]
3	2	A review on immobilised aptamers for high throughput biomolecular detection and screening	Analytica chimica acta 888, 10-18. (2015)	Conceptualisation, write-up [75%]
4	3	In-process thermochemical analysis of in situ poly (ethylene glycol methacrylate-co-glycidyl methacrylate) monolithic adsorbent synthesis	Journal of Applied Polymer Science 133, 1-9. (2016)	Conceptualisation, experimental design, data interpretation and write-up [85%]
5	3	Parametric investigation of polymethacrylate monolith synthesis and stability via thermogravimetric characterisation	Asia-Pacific Journal of Chemical Engineering 12, 352-364. (2017)	Conceptualisation, experimental design, data interpretation and write-up [80%]
6	3	Thermogravimetric characterization of ex situ polymethacrylate (EDMA-co-GMA) monoliths	The Canadian Journal of Chemical Engineering 9999,1-7. (2017)	Conceptualisation, experimental design, data interpretation and write-up [80%]
7	4	Characterisation of charge distribution and stability of aptamer-	Process Biochemistry	Conceptualisation, data interpretation,

		thrombin binding interaction		and write-up [40%]
8	4	Aptamer-anchored macroporous poly(EDMA-*co*-GMA) monolith for high throughput affinity binding	Under Review	Conceptualisation, experimental design, data interpretation and write-up [75%]
9	5	Chromatographic characterisation of poly(EDMA-co-GMA) disk aptasensor monolithic format for protein binding and separation	Under Review	Conceptualisation, experimental design, data interpretation and write-up [75%]

The following articles and manuscripts have been developed out of this research but not included in the current dissertation.

Article/	Thesis Chapter	Title of Publication	Status of Publication	Contribution of Candidate
1	Appendix A8	Deploying aptameric sensing technology for rapid pandemic monitoring	Critical reviews in biotechnology 36, 1010-1022. (2016)	Conceptualisation, write-up [75%]
2	Appendix A9	Nano-Doped Monolithic Materials for Molecular Separation	Separations 4, 1-22. (2017).	Conceptualisation, write-up [75%]
3		Prospects in the use of aptamers for characterizing the structure and stability of bioactive proteins and peptides in food	Manuscript Accepted – Analytical and bioanalytical Chemistry	Conceptualisation, write-up [40%]
4		Aptameric sensing in food safety	Book chapter accepted in "Handbook of Food Bioengineering", Volume 16, 2017 (Elsevier)	Conceptualisation, write-up [70%]

The following conference and colloquiums presentations resulted from this research.

Abstract	Thesis Chapter	Title of Publication	Colloquium and Conference	Contribution of Candidate
1	Appendix B1	Immobilised aptamers for real-time bio-sensing and screening	Curtin-UNIMAS Postgraduate Colloquium 2015.	Conceptualisation, write-up [80%]
2	Appendix B2	Thermometric characterisation of methacrylate polymer synthesis	North Borneo Postgraduate Research Colloquium 2016.	Conceptualisation, write-up [85%]
3	Appendix B3	Thermal Stability and Kinetic Modelling of Ex-Situ Polymethacrylate Monoliths	5th Postgraduate Borneo Research Colloquium 2017	Conceptualisation, write-up [75%]

Signed by: _____   Date: 24/10/2017   .

Professor Michael K. Danquah
(Primary Supervisor)

Signed by: _____   Date: 24/10/2017   .

Dr. John Lau Sie Yon
(Co-supervisor)

ACKNOWLEDGEMENTS

ABSTRACT

The development of polymeric aptasensors for high throughput bioscreening including pathogen detection and bio-separation applications has become a major research endeavour in the wake of rampant infectious disease outbreaks, and preparative manufacturing of novel biomolecules. Thrombin biomolecules and thrombin binding aptamers are widely used in the development of model aptasensors. Presently, there are a limited number of reported studies on the development and characterisation of monolithic aptasensors compared to reports on immunoassays for high throughput bioscreening applications.

Current research efforts in monolithic aptasensors have been mainly geared towards post-polymerisation characterisation and separation applications with limited focus on understanding the thermo-molecular relationship between in-process synthesis conditions and post-polymerisation characteristics, and the effects on separation performance. Diverse monolithic architectural formats such as annular, cylindrical, conical and disk have been synthesised for various chromatographic binding and separation applications. Nevertheless, studies on aptamer coupling on monolithic supports have so far been limited to cylindrical rods/column and microfluidic formats. Disk monoliths possess almost homogeneous pore structure, can enable fast mobile phase transfer, can exhibit low back pressure, are scalable, require less quantities of reagents, and are uniquely place for the development of high throughput bioscreening technologies. As such, this work reports on the development of a disk-aptasensor using a thrombin-binding aptameric ligand immobilised on polymethacrylate monolith for convective binding and isolation of thrombin molecules.

Characterisation of the polymethacrylate monolith was performed under *in process* and *ex situ* polymerisation conditions to investigate characteristic relationships between the polymer synthesis conditions and the physical and functional properties of the monolith. The impact of exotherm build-up on the thermal stability of the monolith was investigated. Established theoretical models such as Avrami and thermal isoconversional models were employed to further investigate the kinetics of *in situ* polymerisation and thermal stability of the monolith, respectively. Data from Avrami's isothermal analysis was consistent with experimental data in terms of the polymerisation rate post-initiation. Porogen to

monomer ratio and polymerisation temperature were found to be significant factors affecting the thermal stability of the monolith. Increasing the porogen (P) to monomer (M) ratio increased the thermal stability of the monolith, whereas decreasing the polymerisation temperature increased the thermal stability of the monolith. Kinetic studies from the thermal isoconversional models showed that an increase in monomer concentration above 20% significantly enhanced the thermal stability of the monolith under elevated non-isothermal conditions.

The hydrodynamic size and surface charge distribution of the thrombin binding aptamer and target thrombin molecules were characterised under varying physicochemical conditions using dynamic light scattering and zeta analysis to probe their impacts on binding stability. The thrombin binding aptamer molecules showed electronegativity at pH > 5, with a high degree of dispersion and stability at pH > 9. The aptamer molecules were coupled on the disk monolith using Schiff-base covalent immobilisation chemistry to form the monolithic aptasensor with a ligand density of 480 pmol/uL. The disk-aptasensor showed good permeability in the range $1.67 \pm 0.05 \times 10^{-14} \, m^2$ (RSD = 3.2%) with a marginal drop in permeability by 1.12 fold relative to the activated disk monolith. Chromatographic analysis of the aptasensor was performed to investigate the hydrodynamic characteristics and binding performance of the matrix under continuous flow conditions. Column efficiency analysis revealed an optimum linear velocity of 126 cm/min ($\approx$ 0.25 mL/min) at room temperature $25 \pm 2 \, ^{\circ}C$, with corresponding theoretical number of plates of 128.2 and HETP of 0.022 mm. Binding studies demonstrated that flow rate variation had minimal impact on dynamic binding capacity of the disk-aptasensor, whiles feed concentration showed a significant effect. Efficient thrombin isolation recovery was obtained at 6% gradient elution from a crude protein mixture. The findings from this work are important in advancing current scientific knowledge in the development of polymeric aptasensors for high throughput bioscreening applications.

PUBLICATION DETAILS

I would like to acknowledge that the submitted thesis was formulated from the literature review and experimental results from this research published and submitted to internationally recognised peer reviewed journals, postgraduate colloquiums and two international exhibition conferences. The entire list of publication reference is listed below in ascending order of year of publication and submission.

Review Articles

Caleb Acquah, Michael K. Danquah, John LS Yon, Amandeep Sidhu, and Clarence M. Ongkudon. "A review on immobilised aptamers for high throughput biomolecular detection and screening." *Analytica chimica acta* 888 (2015): 10-18.

Caleb Acquah, Charles KS Moy, Michael K. Danquah, and Clarence M. Ongkudon. "Development and characteristics of polymer monoliths for advanced LC bioscreening applications: A review." *Journal of Chromatography B* 1015 (2016): 121-134.

Caleb Acquah, Michael K. Danquah, Dominic Agyei, Charles KS Moy, Amandeep Sidhu, and Clarence M. Ongkudon. "Deploying aptameric sensing technology for rapid pandemic monitoring." *Critical reviews in biotechnology* 36, no. 6 (2016): 1010-1022.

Sze Y. Tan, **Caleb Acquah**, Sidhu Amandeep, Ongkudon M. Clarence, Yon S. Lau, and Danquah K. Michael. "SELEX Modifications and Bioanalytical Techniques for Aptamer–Target Binding Characterization." *Critical reviews in analytical chemistry* 46, no. 6 (2016): 521-537.

Caleb Acquah, Eugene Marfo Obeng, Dominic Agyei, Clarence M. Ongkudon, Charles KS Moy, and Michael K. Danquah. "Nano-Doped Monolithic Materials for Molecular Separation." *Separations* 4, no. 1 (2017): 2.

Dominic Agyei, **Caleb Acquah,** Kei Xian Tan, Hii Hieng Kok, Rajendran Subin, Udenigwe Chibuike, Michael K. Danquah. Aptameric characterization of the structure and stability of bioactive proteins and peptides in food. Analytical and Bioanalytical Chemistry – Accepted.

Experimental Articles

Caleb Acquah, Michael K. Danquah, Charles KS Moy, and Clarence M. Ongkudon. "In-process thermochemical analysis of in situ poly (ethylene glycol methacrylate-co-glycidyl methacrylate) monolithic adsorbent synthesis." *Journal of Applied Polymer Science* 133 (2016): 1-9.

Caleb Acquah, Michael K. Danquah, Charles KS Moy, Mahmood Anwar, and Clarence M. Ongkudon. "Parametric investigation of polymethacrylate monolith synthesis and stability via thermogravimetric characterisation." *Asia‐Pacific Journal of Chemical Engineering* (2017).

Caleb Acquah, Michael K. Danquah, Charles KS Moy, Mahmood Anwar, and Clarence M. Ongkudon. "Thermogravimetric characterization of ex situ polymethacrylate (EDMA-co-GMA) monoliths." *The Canadian Journal of Chemical Engineering* (2017).

Sze Y. Tan, **Caleb Acquah**, Sing Y. Tan, Clarence M. Ongkudon, and Michael K. Danquah. Characterisation of charge distribution and stability of aptamer-thrombin binding

interaction. Process Biochemistry. Available from. DOI https://doi.org/10.1016/j.procbio.2017.06.003. (2017)

Caleb Acquah, Michael K. Danquah, Yi Wei Chan, Charles K.S. Moy, Lau Sie Yon, Clarence M. Ongkudon. 'Aptamer-anchored poly(EDMA-co-GMA) monolith for high throughput affinity binding' (under review).

Caleb Acquah, Michael K. Danquah, Yi Wei Chan, Charles K. S. Moy, Clarence M. Ongkudon, Lau Sie Yon. 'Chromatographic characterisation of aptamer-modified poly(EDMA-co-GMA) monolithic disk format for protein binding and separation.' (Under Review).

Book Chapter

Caleb Acquah, Dominic Agyei, Monney Isaac, Sharadwata Pan, Michael K. Danquah. Aptameric sensing in food safety (2018). In Food Control and Biosecurity, Volume 16, Elsevier (Accepted).

SPECIAL DEDICATIONS

TO

VICTORIA ACQUAH

&

YAA SERWAA-AKOTO AMOAH

TABLE OF CONTENTS

CHAPTER ONE

INTRODUCTION

1.1 BACKGROUND

Pathogenic activities are the cause of many infectious diseases (Longo *et al.*, 2014; Yu *et al.*, 2017). It is estimated that 40% of global mortality result from pathogenic infections (Leonard *et al.*, 2003). According to World Health Organisation (WHO) report as of 2015, 10% of the global population contract infectious diseases through food annually (WHO, 2017). The effect of not detecting pathogens early enough causes minor infections to escalate into severe outbreaks and even pandemics. Consequently, there is a need for the development of robust biosensing devices for rapid detection and isolation of pathogens and pathogenic molecules with high specificity and sensitivity. Bioaffinity sensing offers the opportunity to identify specific cellular and biomolecular species with high selectivity and specificity. The binding mechanism is fundamentally based on affinity recognition of target species using biological ligands or probes. Monoclonal antibodies are common affinity probes and are predominantly used in immunoassay development for pathogen detection with reduced assay times (Marzouk *et al.*, 2011; Sakurai *et al.*, 2014). Notwithstanding, the development and application of antibodies for biosensing are challenged with ethical issues, production cost, batch-to-batch inconsistency, false results, shelf life, and lack of stability especially under harsh matrix conditions (Jayasena, 1999; Velusamy *et al.*, 2010; Wark *et al.*, 2010).

Significant research advances in bioaffinity interactions over the past three decades have resulted in the development and application of short single stranded synthetic nucleic acid molecules known as aptamers (Ellington and Szostak, 1990; Robertson and Joyce, 1990; Tuerk and Gold, 1990). They are generated *in vitro* through a robust repetitive and amplification process called Systematic Evolution of Ligands by Exponential Enrichment (SELEX). Aptamers possess high target binding specificity and selectivity, high binding strength (low dissociation constant, K_D), chemical and biophysical stability, fast binding kinetics, and can be generated for a wide range of target molecules (Kuehne *et al.*, 2017; Sharma *et al.*, 2017). Aptamers are smaller in size compared to antibodies, and this enables effective immobilisation on solid platforms such as nanoparticles, monoliths, microfluidic substrates, paper, and glass slides to form high density layers which are reusable (Xu *et al.*, 2010; Acquah *et al.*, 2015) and are generally referred to as 'aptasensors'. Furthermore,

the characteristics of the solid platform and the immobilisation chemistry are essential to attain high ligand density and retention, convective mass transport, and optimal binding efficiency.

Conventional stationary supports for bio-separation using liquid chromatography supports typically depend on diverse particulate polymeric materials as the support matrix and antibodies as the ligand in a process generally referred to as 'immunochromatography'. Although protocols for these types of assays are well standardised, they are tagged with significant setbacks such as matrix effect, slow diffusive fluid transport, clogging of large target molecules, and intensive sample pre-treatment steps. The development of aptamers and continuous stationary adsorbent create an opportunity to enhance bio-separation efficiency and target specificity for high throughput application.

Romig *et al.* (1999) pioneered work on aptamer immobilisation on stationary support using biotin-avidin chemistry for bio-separation application. Their work focused on the purification of recombinant L-selectin–Ig fusion protein produced from Chinese hamster ovary (CHO) and obtained a recovery rate 83% in a unitary step using 0.1 M sodium citrate (pH 3.0) for elution. Remarkably, the success of their work sprung a multitude of ground-breaking biomolecular binding and separation applications in life sciences using diverse particulate adsorbents as stationary phases (Deng *et al.*, 2001; Michaud *et al.*, 2004; Ruta *et al.*, 2007). Ruta *et al.* (2008) further demonstrated an anti-D-adenosine aptameric chiral separation system using carboxylic acid based silica particles. Their immobilisation strategy resulted in the formation of covalent amide bonds linking the aptamer molecules and the silica particles. This resulted in improved resistance to harsh separation conditions, high aptamer retention and enhanced enantioselectivity.

The use of magnetic nanoparticles has been demonstrated by Faraji *et al.* (2010) and Wu *et al.* (2011) to generate improved chromatographic performances than silica based particles in terms of ligand density, diffusivity, and binding capacity. Madru *et al.* (2011) also performed a parametric analysis into the effect of various chemistries and adsorbent particles on cocaine recovery using a cocaine aptamer. They obtained a recovery range of 86%-89% for cyanogen-bromide activated sepharose; 74%-89% for streptavidin-activated agarose; and ~20% for glutaraldehyde-activated silica; and ~20% for thiol-activated

sepharose. The low recoveries of the latter two were**:** (i) the existence of an hydrophilic polyethylenimine coating around the silica beads along with potential binding of cations to the polyanionic aptamer at the medium pH; and (ii) hydrolysis of the NHS-ester moiety, dis-oriented aptamer immobilisation and low deoxygenation of binding solutions (Madru *et al.*, 2011). Other innovative static phase systems that have been explored for aptamer immobilisation include glass nanopores (Ding *et al.*, 2009), and charged membranes (Katayama *et al.*, 2002).

Even though the introduction of aptamers has improved affinity chromatography assays in terms of target binding specificity and selectivity, there still exist challenges particularly relating to high throughput continuous applications. The small pore size and the diffusive mass transport phenomenon associated with the commonly used particle-based stationary support system make them unreliable for high throughput applications. According to Arrua *et al.* (2009), the intra-particle void fraction (ε) of most conventional particulate stationary support systems is estimated to be between 30-50% of the entire domain volume for rapid diffusion devoid of channelling. Diffusivity is the rate determining step governing the solid phase mass transfer process for large target molecules including DNA, proteins, enzymes and cells. Such targets are also liable to clogging pore spaces of particulate static phase adsorbents. These challenges have compelled the search for new and improved affinity chromatographic supports for high throughput applications.

The utilisation of continuous stationary supports (monoliths) as stationary adsorbents for aptamer coupling is gaining prominence due to the unique convective mass transfer characteristics of monoliths. Monolithic support systems have been used for rapid chromatographic binding and separation of a wide range of biomolecules (Uzun *et al.*, 2005; Danquah and Forde, 2008; Ongkudon *et al.*, 2013; Wang *et al.*, 2017). Monoliths are solo continuous porous structured chromatographic supports synthesised in an unstirred mould (Danquah and Forde, 2007; Desire *et al.*, 2017). They possess good permeability, convective mass transfer characteristics, ease of pore size fine-tuning, and ease of functionalisation (Svec, 2004; Pfaunmiller *et al.*, 2013). Polymethacrylate monoliths represent one of the predominant monolithic adsorbents investigated for biomolecular separation to date. They are simple to synthesise with tuneable pore and

surface characteristics. They are synthesised via free radical polymerization initiated thermally or by radiation (Schlemmer *et al.*, 2009; Svec, 2010; Vonk *et al.*, 2015).

1.2   RESEARCH GAPS AND PROJECT NOVELTY

Owing to the small size of aptamers, their immobilisation onto polymethacrylate monoliths results in a porous aptasensor with a high ligand density which are also responsible for the binding performance of the aptasensor. Recent reports from different researchers have yielded different ligand densities for polymethacrylate aptasensors. Zhao *et al.* (2008) reported of a ligand density of 170 pmol/µL, whereas Han *et al.* (2012) and Du *et al.* (2015) reported of higher ligand densities of 290 pmol/µL and 25.356 nmol/µL, respectively. Improvements in aptamer density and efficiency of immobilisation can be achieved by creating multilayers using grafting tentacles such as D-glucosamine or spacer arms on the monolith (Deng *et al.*, 2012; Du *et al.*, 2015); optimising the time duration for monolith activation (Deng *et al.*, 2012; Brothier and Pichon, 2014); eliminating non-specific binding (Gao *et al.*, 2013); optimising the immobilisation temperature (Brothier and Pichon, 2014); implementing the right immobilisation chemistry based on polymer moieties (Zhao *et al.*, 2008; Deng *et al.*, 2012; Marechal *et al.*, 2015; Wang *et al.*, 2015). Effective aptamer immobilisation on the monolithic support system is critical to enhance target binding performance and durability of the aptasensor system. Also, major challenges associated with the development and application of polymethacrylate monolithic supports need to be addressed to enable the creation of robust polymethacrylate-based aptasensor platforms. Some of these challenges include lack of pore homogeneity, thermal inhibition, matrix cracking and shrinking, wall channelling, and limited variety of suitable chaotropic organic reagents for target elution (Podgornik *et al.*, 2000; Danquah *et al.*, 2008).

Current research efforts in aptamer modified-monoliths have been mainly geared towards post-polymerisation characterisation and separation applications with limited focus on understanding the thermo-molecular relationship between in-process synthesis conditions and post-polymerisation characteristics, and the effects on separation performance. Various architectural formats of monoliths including annular, cylindrical, conical and disk have been synthesised for various chromatographic binding and separation applications

(Roberts *et al.*, 2009; Ongkudon *et al.*, 2014). Studies on aptamer coupling on monolithic supports have so far been limited to cylindrical rods and microfluidic formats. However, morphological and hydrodynamic studies on column monoliths have revealed vast heterogeneity in pore structure and the existence of elevated back pressure which impedes continuous mobile phase flow (Podgornik *et al.*, 2013). Short format disk monoliths with thickness ≤1.5 cm possess almost homogeneous pore structure, can enable fast mobile phase transfer, can exhibit low back pressure, are scalable, require less quantities of reagents, and are uniquely place for the development of preparation kits (Prasanna and Vijayalakshmi, 2010; Podgornik *et al.*, 2013; Isakari *et al.*, 2016). As a result, the development of aptasensors using disk monoliths is hypothesised to facilitate continuous and high throughput bimolecular separation under highly selective and specific binding conditions. This is illustrated in Figure 1. This dissertation focuses on the synthesis and thermo-molecular characterisation of polymethacrylate monoliths, development of a disk-aptasensor monolith, and chromatographic characterisation and application of the disk-aptasensor for target binding and isolation.
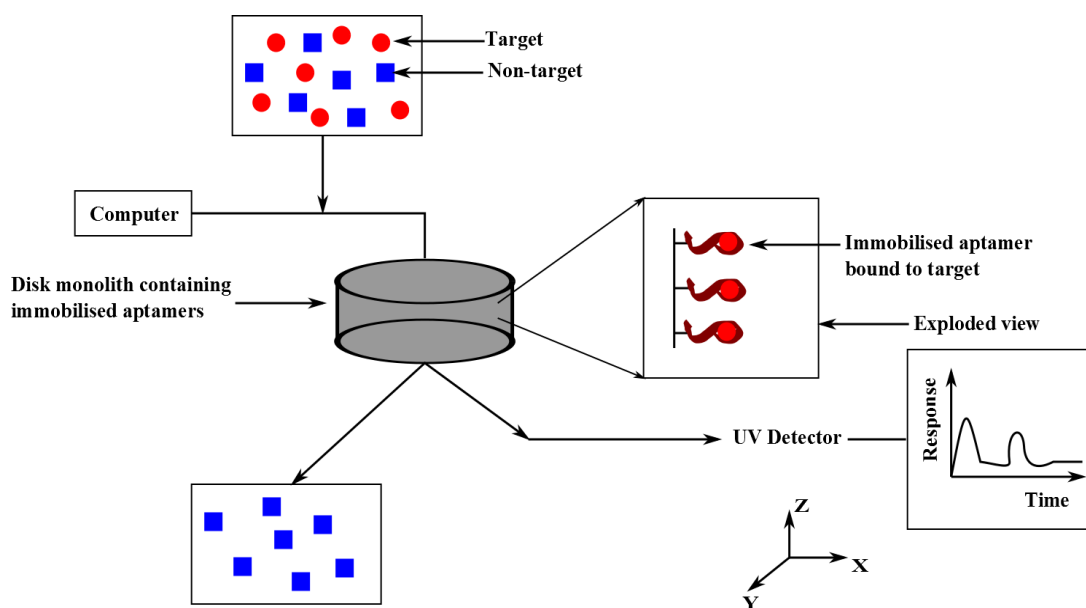

Figure 1. Schematic illustration of disk aptasensor system for selective target binding and isolation.

1.3   RESEARCH QUESTIONS

The development of robust monolithic aptasensors is gaining research prominence. Nevertheless, progress in enhancing their applications for high throughput bioscreening

applications has been identified to be fraught with some challenges such as the build-up of exotherm, chemical and thermal stability, lack of non-destructive models, limited ligand and adsorbent biophysical characterisation studies, and limited studies on their chromatographic performance under various physicochemical conditions. As such, the thrust of this research was formulated from the following research questions:

- What is the thermo-molecular relationship between in process synthesis conditions and thermal build-up during the synthesis of polymethacrylate monoliths, and their impact on the physicochemical characteristics?
- What is the thermo-molecular relationship between in process and post-polymerisation conditions on the chemical and thermal stability of polymethacrylate monoliths?
- What is the effect of micro-environment and physicochemical conditions on the biophysical features of aptamers, their complexes and the development of aptasensors?
- What is the chromatographic performance of disk-monolithic aptasensors under different isocratic and physicochemical conditions for effective bioscreening?

1.4   MAIN OBJECTIVE

The main objective of this research is to develop a novel aptasensor device based on disk polymethacrylate monolithic adsorbent for rapid real-time bioscreening applications.

1.4.1   Specific Objectives

a.   To determine *in situ* thermo-molecular mechanisms governing the synthesis of poly(EDMA-co-GMA) monoliths.

b.   To investigate the relationship between poly(EDMA-co-GMA) synthesis parameters and the thermal stability of the monolith.

c.   To determine factors affecting efficient immobilisation of aptameric ligand onto poly(EDMA-co-GMA) monolith for target binding.

d.   To characterise a polymeric aptasensor for high throughput affinity binding and removal of target biomolecules.

1.5   SIGNIFICANCE OF RESEARCH

This project focuses on the development of a new and improved aptasensor technology using a disk monolith with convective mass transfer characteristics. The aptasensor would find applications in high throughput bioscreening relating to bio-separation and pathogen detection. Apart from this, the project will extend scientific knowledge in bioaffinity systems through; (i) the development of robust polymeric systems with biophysical and chemically resilient properties, tuneable porous network, homogenous surface characteristics with low flow backpressure; (ii) aptamer coupling onto monolithic systems using stable covalent activation and immobilisation chemistries to develop robust aptasensor platforms; (iii) the application of chromatographic analysis to determine mass transfer characteristics, flow hydrodynamics in monolithic systems, and biomolecular separation efficiency. As mentioned earlier, the aptasensor would be useful for domestic and clinical pathogen detection due to its rapidity, and specificity and the non-requirement for sample preparation. This would improve patient health care and potentially reduce the cost of clinical diagnosis. The ease of use would also promote the commercialisation of 'at home' usage and point of health care diagnostic kits. The technology can provide the platform for rapid detection and screening of people at immigrations borders for various diseases. Various food items and agricultural materials can also be screened for specific disease pathogens as well as the detection of illegal chemicals such as cocaine in blood samples using the technology. As the epidemiological features of most pandemic strains show that an almost instantaneous specific detection of initial cases would help in tracking and mitigating transmission, the need for a reliable technology to accurately and rapidly identify pandemic pathogens is very critical. The aptasensor would provide the capacity to detect pandemic pathogens from various transmission sources in the early stages in order to contain the pathogens and associated biotoxins. The technology will create new opportunities for bioseparation and purification of biomolecules and cells in life science industries.

1.6   RESEARCH SCOPE

This research project seeks to develop a robust monolithic aptasensor for rapid biomolecular binding and isolation. There are a limited number of reported studies

focusing on the development and characterisation of monolithic aptasensors compared to reports on immunoassay development. The present work utilises an aptameric ligand and monolithic polymer in the development of an aptasensor with convective flow properties. The thrombin binding DNA aptamer (TBA) with the sequence 5'-/5AmMC6/GGT TGG TGT GGT TGG-3' is used as the aptameric ligand in this work. Findings from this work would be essential in predicting the characteristics of other aptamer-target systems. Key design criteria considered for aptasensor development include ease of regeneration to enable multiple use, covalent locking of immobilised aptamer molecules, convective mass transfer characteristics, and physicochemical stability. Polymethacrylate disk monolith is used as the synthetic base for covalent immobilisation of aptamer molecules. Strong covalent immobilisation of aptamer molecules enables aptasensor reusability by minimising potential ligand leaching. Key fundamental research insights that are covered in this project include *in situ* thermo-molecular and thermal stability analysis of polymethacrylate monolith synthesis, kinetic modelling of polymethacrylate monolith degradation, characterisation of aptamer charge distribution and stability, effect of temperature on immobilisation efficiency and ligand density, effect of ions and pH on the binding performance of the disk aptasensor, effect of flow rate on the binding performance and target selectivity. These insights are critical in building the theoretical framework around the development and application of monolithic aptasensors for optimal performance output.

1.7   THESIS LAYOUT

In the proceeding chapters, a critical literature review covering biophysical characterisation techniques for monoliths and aptamers, as well as bioscreening applications of aptasensors is presented in **Chapter 2**. The review of literatures reveals that the synergy between in-process polymerisation conditions and the resultant physicochemical effects on monoliths are essential to optimise chromatographic performance.

Chapter 3 in relation to the first specific objective describes the synthesis and characterisation of polymethacrylate monoliths via *in situ* thermochemical analysis. A

kinetic model of polymethacrylate monolith synthesis was also carried out by means of Avrami's isothermal analysis.

Chapter 4 is in two sections describing the thermal stability of polymethacrylate monoliths by varying *in situ* and *ex situ* synthesis conditions and investigating their synergistic effects. Section 4.1 describes a thermogravimetric parametric analysis of polymethacrylate monoliths and section 4.2 describes an isoconvensional kinetic modelling of polymethacrylate monolith synthesis. This chapter seeks to fulfil the second specific objective of this research.

Chapter 5 is in two sections. Section 5.1 describes the application of dynamic light scattering via zeta analysis as a biophysical tool to characterise the charge distribution and stability of aptamer binding to target molecule under different physicochemical conditions. It also describes a theoretical kinetic model for thrombin binding aptamers under varying pH conditions. Section 5.2 describes the aptamer-monolith immobilisation chemistry and the effects of key process parameters on target binding performance. Findings from Chapter Five are linked to the third specific objective.

Chapter 6 describes the effect of temperature on aptamer immobilisation, column efficiency, and the chromatographic binding performance of the disk monolithic aptasensor for target binding and isolation for a multi-component mixture. Findings from Chapter Six are associated with the fourth specific objective of this research.

Chapter 7 presents the conclusion with a summary of key findings from this research and recommendations for future work.

REFERENCES

Acquah, C., M.K. Danquah, J.L.S. Yon, A. Sidhu and C.M. Ongkudon, 2015. A review on immobilised aptamers for high throughput biomolecular detection and screening. Analytica chimica acta, 888: 10-18. Available from http://www.sciencedirect.com/science/article/pii/S0003267015008016. DOI http://dx.doi.org/10.1016/j.aca.2015.05.050.

Arrua, R.D., M.C. Strumia and C.I. Alvarez Igarzabal, 2009. Macroporous monolithic polymers: Preparation and applications. Materials, 2(4): 2429-2466. DOI 10.3390/ma2042429.

Brothier, F. and V. Pichon, 2014. Miniaturized DNA aptamer-based monolithic sorbent for selective extraction of a target analyte coupled on-line to nanolc. Analytical and bioanalytical chemistry, 406(30): 7875-7886. Available from http://www.ncbi.nlm.nih.gov/pubmed/25335821. DOI 10.1007/s00216-014-8256-z.

Danquah, M.K. and G.M. Forde, 2007. Towards the design of a scalable and commercially viable technique for plasmid purification using a methacrylate monolithic stationary phase. Journal of Chemical Technology & Biotechnology, 82(8): 752-757. DOI 10.1002/jctb.1733.

Danquah, M.K. and G.M. Forde, 2008. Large-volume methacrylate monolith for plasmid purification. Process engineering approach to synthesis and application. Journal of chromatography. A, 1188(2): 227-233. Available from http://www.ncbi.nlm.nih.gov/pubmed/18329651. DOI 10.1016/j.chroma.2008.02.045.

Danquah, M.K., J. Ho and G.M. Forde, 2008. A thermal expulsion approach to homogeneous large-volume methacrylate monolith preparation; enabling large-scale rapid purification of biomolecules. Journal of Applied Polymer Science, 109(4): 2426-2433. DOI 10.1002/app.28346.

Deng, N., Z. Liang, Y. Liang, Z. Sui, L. Zhang, Q. Wu, K. Yang, L. Zhang and Y. Zhang, 2012. Aptamer modified organic-inorganic hybrid silica monolithic capillary columns for highly selective recognition of thrombin. Analytical chemistry, 84(23): 10186-10190. Available from http://www.ncbi.nlm.nih.gov/pubmed/23137349. DOI 10.1021/ac302779u.

Deng, Q., I. German, D. Buchanan and R.T. Kennedy, 2001. Retention and separation of adenosine and analogues by affinity chromatography with an aptamer stationary phase. Analytical chemistry, 73(22): 5415-5421. DOI 10.1021/ac0105437.

Desire, C.T., E.F. Hilder and R.D. Arrua, 2017. Monolithic high-performance liquid chromatography columns. Encyclopedia of Analytical Chemistry.

Ding, S., C. Gao and L.-Q. Gu, 2009. Capturing single molecules of immunoglobulin and ricin with an aptamer-encoded glass nanopore. Analytical chemistry, 18(16): 6649.

Du, K., M. Yang, Q. Zhang and S. Dan, 2015. Highly porous polymer monolith immobilized with aptamer (rna) anchored grafted tentacles and its potential for the purification of lysozyme. Industrial & Engineering Chemistry Research.

Ellington, A.D. and J.W. Szostak, 1990. In vitro selection of rna molecules that bind specific ligands. Nature, 346(6287): 818-822.

Faraji, M., Y. Yamini and M. Rezaee, 2010. Magnetic nanoparticles: Synthesis, stabilization, functionalization, characterization, and applications. Journal of the Iranian Chemical Society, 7(1): 1-37.

Gao, C., X. Sun and A.T. Woolley, 2013. Fluorescent measurement of affinity binding between thrombin and its aptamers using on-chip affinity monoliths. Journal of chromatography. A, 1291: 92-96. Available from http://www.ncbi.nlm.nih.gov/pubmed/23587316. DOI 10.1016/j.chroma.2013.03.063.

Han, B., C. Zhao, J. Yin and H. Wang, 2012. High performance aptamer affinity chromatography for single-step selective extraction and screening of basic protein lysozyme. Journal of chromatography. B, Analytical technologies in the biomedical and life sciences, 903: 112-117. Available from http://www.ncbi.nlm.nih.gov/pubmed/22841745. DOI 10.1016/j.jchromb.2012.07.003.

Isakari, Y., A. Podgornik, N. Yoshimoto and S. Yamamoto, 2016. Monolith disk chromatography separates pegylated protein positional isoforms within minutes at low pressure. Biotechnology journal, 11(1): 100-106.

Jayasena, S.D., 1999. Aptamers: An emerging class of molecules that rival antibodies in diagnostics. Clin. Chem., 45(9): 1628-1650.

Katayama, H., A. Shimasaki and S. Ohgaki, 2002. Development of a virus concentration method and its application to detection of enterovirus and norwalk virus from coastal seawater. Applied and environmental microbiology, 68(3): 1033.

Kuehne, C., S. Wedepohl and J. Dernedde, 2017. Single-step purification of monomeric l-selectin via aptamer affinity chromatography. Sensors, 17(2): 226.

Leonard, P., S. Hearty, J. Brennan, L. Dunne, J. Quinn, T. Chakraborty and R. O'Kennedy, 2003. Advances in biosensors for detection of pathogens in food and water. Enzyme and Microbial Technology, 32(1): 3-13. Available from http://www.sciencedirect.com/science/article/pii/S0141022902002326. DOI http://dx.doi.org/10.1016/S0141-0229(02)00232-6.

Longo, A.V., P.A. Burrowes and K.R. Zamudio, 2014. Genomic studies of disease-outcome in host–pathogen dynamics. Integrative and Comparative Biology, 54(3): 427-438. DOI 10.1093/icb/icu073.

Madru, B., F. Chapuis-Hugon and V. Pichon, 2011. Novel extraction supports based on immobilised aptamers: Evaluation for the selective extraction of cocaine. Talanta, 85(1): 616-624. Available from http://www.ncbi.nlm.nih.gov/pubmed/21645749. DOI 10.1016/j.talanta.2011.04.016.

Marechal, A., F. Jarrosson, J. Randon, V. Dugas and C. Demesmay, 2015. In-line coupling of an aptamer based miniaturized monolithic affinity preconcentration unit with capillary electrophoresis and laser induced fluorescence detection. Journal of Chromatography A, 1406: 109-117.

Marzouk, M., I.B. Kahla, N. Hannachi, A. Ferjeni, W.B. Salma, S. Ghezal and J. Boukadida, 2011. Evaluation of an immunochromatographic assay for rapid identification of mycobacterium tuberculosis complex in clinical isolates. Diagnostic microbiology and infectious disease, 69(4): 396-399. Available from http://www.ncbi.nlm.nih.gov/pubmed/21396535. DOI 10.1016/j.diagmicrobio.2010.11.009.

Michaud, M., E. Jourdan, C. Ravelet, A. Villet, A. Ravel, C. Grosset and E. Peyrin, 2004. Immobilized DNA aptamers as target-specific chiral stationary phases for resolution of nucleoside and amino acid derivative enantiomers. Analytical chemistry, 76(4): 1015-1020.

Ongkudon, C.M., T. Kansil and C. Wong, 2014. Challenges and strategies in the preparation of large-volume polymer-based monolithic chromatography adsorbents. Journal of separation science, 37(5): 455-464.

Ongkudon, C.M., S. Pan and M.K. Danquah, 2013. An innovative monolithic column preparation for the isolation of 25 kilo base pairs DNA. Journal of chromatography. A, 1318: 156-162. Available from http://www.ncbi.nlm.nih.gov/pubmed/24209297. DOI 10.1016/j.chroma.2013.10.011.

Pfaunmiller, E., M. Paulemond, C. Dupper and D. Hage, 2013. Affinity monolith chromatography: A review of principles and recent analytical applications. Analytical and bioanalytical chemistry, 405(7): 2133-2145. DOI 10.1007/s00216-012-6568-4.

Podgornik, A., M. Barut, A. Strancar, D. Josić and T. Koloini, 2000. Construction of large-volume monolithic columns. Analytical chemistry, 72(22): 5693.

Podgornik, A., S. Yamamoto, M. Peterka and N.L. Krajnc, 2013. Fast separation of large biomolecules using short monolithic columns. Journal of chromatography. B, Analytical technologies in the biomedical and life sciences, 927: 80-89. Available from http://www.ncbi.nlm.nih.gov/pubmed/23465515. DOI 10.1016/j.jchromb.2013.02.004.

Prasanna, R.R. and M.A. Vijayalakshmi, 2010. Characterization of metal chelate methacrylate monolithic disk for purification of polyclonal and monoclonal immunoglobulin g. Journal of Chromatography A, 1217(23): 3660-3667.

Roberts, M.W., C.M. Ongkudon, G.M. Forde and M.K. Danquah, 2009. Versatility of polymethacrylate monoliths for chromatographic purification of biomolecules. Journal of separation science, 32(15-16): 2485-2494. Available from http://www.ncbi.nlm.nih.gov/pubmed/19603394. DOI 10.1002/jssc.200900309.

Robertson, D.L. and G.F. Joyce, 1990. Selection in vitro of an rna enzyme that specifically cleaves single-stranded DNA. Nature, 344(6265): 467-468.

Romig, T.S., C. Bell and D.W. Drolet, 1999. Aptamer affinity chromatography:: Combinatorial chemistry applied to protein purification. Journal of Chromatography B: Biomedical Sciences and Applications, 731(2): 275-284.

Ruta, J., C. Grosset, C. Ravelet, J. Fize, A. Villet, A. Ravel and E. Peyrin, 2007. Chiral resolution of histidine using an anti-d-histidine l-rna aptamer microbore column. Journal of Chromatography B, 845(2): 186-190.

Ruta, J., C. Ravelet, J. Désiré, J.-L. Décout and E. Peyrin, 2008. Covalently bonded DNA aptamer chiral stationary phase for the chromatographic resolution of adenosine. Analytical and bioanalytical chemistry, 390(4): 1051-1057.

Sakurai, A., K. Takayama, N. Nomura, N. Yamamoto, Y. Sakoda, Y. Kobayashi, H. Kida and F. Shibasaki, 2014. Multi-colored immunochromatography using nanobeads for rapid and sensitive typing of seasonal influenza viruses. Journal of virological methods, 209: 62-68. Available from http://www.ncbi.nlm.nih.gov/pubmed/25218175. DOI 10.1016/j.jviromet.2014.08.025.

Santosh, B. and P.K. Yadava, 2014. Nucleic acid aptamers: Research tools in disease diagnostics and therapeutics. BioMed research international, 2014: 540451. Available from http://www.ncbi.nlm.nih.gov/pubmed/25050359. DOI 10.1155/2014/540451.

Schlemmer, B., R. Bandari, L. Rosenkranz and M.R. Buchmeiser, 2009. Electron beam triggered, free radical polymerization-derived monolithic capillary columns for high-performance liquid chromatography. Electron beam triggered, free radical polymerization-derived monolithic capillary columns for high-performance liquid chromatography, 1216(13): 2664-2670.

Sharma, T.K., J.G. Bruno and A. Dhiman, 2017. Abcs of DNA aptamer and related assay development. Biotechnology advances, 35(2): 275-301. Available from http://www.sciencedirect.com/science/article/pii/S0734975017300034 [Accessed 2017/4//]. DOI https://doi.org/10.1016/j.biotechadv.2017.01.003.

Svec, F., 2004. Preparation and hplc applications of rigid macroporous organic polymer monoliths. Journal of separation science, 27(10-11): 747-766. DOI 10.1002/jssc.200401721.

Svec, F., 2010. Porous polymer monoliths: Amazingly wide variety of techniques enabling their preparation. Journal of Chromatography A, 1217(6): 902-924.

Tuerk, C. and L. Gold, 1990. Systematic evolution of ligands by exponential enrichment: Rna ligands to bacteriophage t4 DNA polymerase. Science, 249(4968): 505-510.

Uzun, L., R. Say and A. Denizli, 2005. Porous poly (hydroxyethyl methacrylate) based monolith as a new adsorbent for affinity chromatography. Reactive and Functional Polymers, 64(2): 93-102.

Velusamy, V., K. Arshak, O. Korostynska, K. Oliwa and C. Adley, 2010. An overview of foodborne pathogen detection: In the perspective of biosensors. Biotechnology advances, 28(2): 232-254. Available from http://www.ncbi.nlm.nih.gov/pubmed/20006978. DOI 10.1016/j.biotechadv.2009.12.004.

Vonk, R., S. Wouters, A. Barcaru, G. Vivó-Truyols, S. Eeltink, L. Koning and P. Schoenmakers, 2015. Post-polymerization photografting on methacrylate-based monoliths for separation of intact proteins and protein digests with comprehensive two-dimensional liquid chromatography hyphenated with high-resolution mass spectrometry. Analytical and bioanalytical chemistry, 407(13): 3817-3829. DOI 10.1007/s00216-015-8615-4.

Wang, J., S. Shen, X. Lu and F. Ye, 2017. One-pot preparation of an organic polymer monolith by thiol-ene click chemistry for capillary electrochromatography. Journal of separation science.

Wang, Z., J.-C. Zhao, H.-Z. Lian and H.-Y. Chen, 2015. Aptamer-based organic-silica hybrid affinity monolith prepared via "thiol-ene" click reaction for extraction of thrombin. Talanta, 138: 52-58. DOI 10.1016/j.talanta.2015.02.009.

Wark, A.W., J. Lee, S. Kim, S.N. Faisal and H.J. Lee, 2010. Bioaffinity detection of pathogens on surfaces. Journal of Industrial and Engineering Chemistry, 16(2): 169-177. DOI 10.1016/j.jiec.2010.01.061.

WHO, 2017. Food safety. World Health Organistaion, http://www.who.int/mediacentre/factsheets/fs399/en/.

Wu, X., J. Hu, B. Zhu, L. Lu, X. Huang and D. Pang, 2011. Aptamer-targeted magnetic nanospheres as a solid-phase extraction sorbent for determination of ochratoxin a in food samples. Journal of chromatography. A, 1218(41): 7341-7346. Available from http://www.ncbi.nlm.nih.gov/pubmed/21890142. DOI 10.1016/j.chroma.2011.08.045.

Xu, Y., X. Yang and E. Wang, 2010. Review: Aptamers in microfluidic chips. Analytica chimica acta, 683(1): 12-20.

Yu, M., H. Wang, F. Fu, L. Li, J. Li, G. Li, Y. Song, M. Swihart and E. Song, 2017. Dual-recognition förster resonance energy transfer based platform for one-step sensitive detection of pathogenic bacteria using fluorescent vancomycin-gold nanoclusters and aptamer-gold nanoparticles. Analytical chemistry, 89(7): 4085. DOI 10.1021/acs.analchem.6b04958.

Zhao, Q., X.-F. Li and X.C. Le, 2008. Aptamer-modified monolithic capillary chromatography for protein separation and detection. Analytical chemistry, 80(10): 3915-3920. DOI 10.1021/ac702567x.

Zhao, Q., X.-F. Li, Y. Shao and X.C. Le, 2008. Aptamer-based affinity chromatographic assays for thrombin. Analytical chemistry, 80(19): 7586-7593.

CHAPTER TWO

LITERATURE REVIEW

SECTION 2.1

Development and characteristics of polymer monoliths for advanced LC bioscreening applications: A review

Caleb Acquah, Charles K.S. Moy, Michael K. Danquah, Clarence M. Ongkudon

DECLARATION FOR THESIS SECTION 2.1

Development and characteristics of polymer monoliths for advanced LC bioscreening applications: A review

The candidate will like to declare that there is no conflict of interests involved in this work and that my extent of contribution as candidate is as shown below:

Contribution of Candidate	Conceptualisation, initiation and write-up	85%

The following co-authors were involved in the development of this publication and attest to the candidate's contribution to a joint publication as part of his thesis. Permission by co-authors are as follows:

Name	Signature	Date
Michael K. Danquah		13.07.2017
Charles K.S. Moy		13.07.2017
Clarence M. Ongkudon		13.07.2017

ABSTRACT

Biomedical research advances over the past two decades in bioseparation science and engineering have led to the development of new adsorbent systems called monoliths, mostly as stationary supports for liquid chromatography (LC) applications. They are acknowledged to offer better mass transfer hydrodynamics than their particulate counterparts. Also, their architectural and morphological traits can be tailored *in situ* to meet the hydrodynamic size of molecules which include proteins, pDNA, cells and viral targets. This has enabled their development for a plethora of enhanced bioscreening applications including biosensing, biomolecular purification, concentration and separation, achieved through the introduction of specific functional moieties or ligands (such as triethylamine, N,N-dimethyl-N-dodecylamine, antibodies, enzymes and aptamers) into the molecular architecture of monoliths. Notwithstanding, the application of monoliths presents major material and bioprocess challenges. The relationship between in-process polymerisation characteristics and the physicochemical properties of monolith is critical to optimise chromatographic performance. There is also a need to develop theoretical models for non-invasive analyses and predictions. This review article therefore discusses in-process analytical conditions, functionalisation chemistries and ligands relevant to establish the characteristics of monoliths in order to facilitate a wide range of enhanced bioscreening applications. It gives emphasis to the development of functional polymethacrylate monoliths for microfluidic and preparative scale bio-applications.

Keywords: Monoliths; Polymethacrylate; Bio-screening; Chromatography; Polymerisation; Biomolecules

1. INTRODUCTION

Bioscreening enables the selective identification and isolation of biomolecular and cellular species through specific interactions with biomarkers or ligands. Bioscreening encompasses a series of processes relating to target binding, isolation and/or purification. Research advances in bio-recognition and bioscreening has led to the synthesis of a number of specific bio-ligands, immobilisation chemistries and adsorbent supports with the aim of achieving improved screening performance under high throughput conditions; increasing the specificity and selectivity of the binding process; eliminating matrix effects; reducing the analysis time and quantity of reagent; and reducing process cost. Conventional LC assays for biomolecular screening mostly rely on fixed particulate polymeric packings as the stationary phase (Chapuis-Hugon *et al.*, 2011; Madru *et al.*, 2011; Ali and Pichon, 2014). Other types of stationary adsorbents for bioseparation include but not limited to glass nanopores (Ding *et al.*, 2009), and charged membranes (Katayama *et al.*, 2002). Even though these adsorbents have improved target binding capacities, they are mostly not suitable for high throughput continuous applications. This drawback is driven by their diffusive mass transfer which results in slow hydrodynamics and pressure build-up; small particle pore size which results in clogging; and the difficulty in tailoring their pore size distribution to the target hydrodynamic size (Unger *et al.*, 2008; Gutiérrez-Aguirre *et al.*, 2009; Roberts *et al.*, 2009).

Polymeric monoliths such as polymethacrylates represent a fourth generation of chromatographic adsorbent supports synthesised in a preferred mould by means of free radical polymerisation to form a solo continuous phase with high porosity and interconnectivities (Danquah and Forde, 2007; Jungbauer and Hahn, 2008; Wang *et al.*, 2014). Polymeric monoliths have been demonstrated for high throughput chromatographic separation and purification of diverse biomolecules such as proteins, pDNA and cellular targets (Danquah and Forde, 2008; Jungbauer and Hahn, 2008; Nischang, 2013), and are more suitable than particulate adsorbents. The governing feature for high throughput in both adsorbents lies in their respective bed morphologies. Whereas the chromatographic performance of particulate adsorbents hinges on the nature of the particles, their size and mode of packing resulting in slow diffusive transport, monoliths

are devoid of interstitial spaces and, possess tuneable cross-sectional area in their morphology and architectural skeleton which facilitates an axial convective transport of samples. Gagnon (2012) inferred that a 35 L particle column having a capacity of 35 g/L will yield 20 kg of IgG in 85 h whilst an 8 L monolithic column possessing a capacity of 10 g/L will yield 20 kg of IgG in just 27 h. Polymeric monoliths can be synthesised to have good mechanical stability, biocompatibility, high porosity, chemical resistivity, sufficient access sites for ligand-target interaction and low back pressure for high throughput application of micro- and macromolecules (Arrua *et al.*, 2009; Roberts *et al.*, 2009; Pichon *et al.*, 2015). The shape and size of the mould dictates the final monolithic-polymer formed and the pattern of the flow hydrodynamics. Different architectural shapes synthesised for polymer monoliths include annular, cylindrical, conical and disks (Roberts *et al.*, 2009; Pfaunmiller *et al.*, 2013). Various types of polymeric monoliths can be synthesised based on the type of monomers and/or polymerisation process employed for synthesis (Qin *et al.*, 2014), and they can be molecularly engineered to possess varying physicochemical properties. Polymeric monoliths such as polymethacrylates have functional moieties on their interconnected pores that can be activated for ligand immobilisation, allowing a variety of activation chemistries to be applied for the formation of covalent and non-covalent bonding with ligands (Mallik and Hage, 2006; Pichon *et al.*, 2015). In addition, ligands such as antibodies, protein A, histadine, aptamer, diethylamine (DEA) and 2-chloro-N, N-diethyl ethylamine hydrochloride (DEAE-Cl) have been utilised for different applications including affinity chromatography (Deng *et al.*, 2012), hydrophobic interaction (Hemström *et al.*, 2006), ion-exchange interaction (Ongkudon and Danquah, 2011; Aydoğan, 2015) and enzymatic digestion (de Lathouder *et al.*, 2008; Lin *et al.*, 2015). The efficiency of LC bioscreening assay for biomolecular separation is dependent on the type and biophysical characteristics of the adsorbent support, activation chemistry and specificity/selectivity of the ligand immobilised on the support (Zhang *et al.*, 2013).

In-depth understanding of the polymer formation and post-polymerisation modification processes has further widened the bioseparation applications of polymeric monoliths for cellular (Ott *et al.*, 2011; Mai *et al.*, 2014), viral (Zaveckas *et al.*, 2015) and, diverse biomolecular targets (Yuan *et al.*, 2014; Chen *et al.*, 2015) to achieve optimal

chromatographic performances. Various process parameters such as temperature, polymerisation time, presence of oxygen, initiator concentration, monomer-porogen ratio and concentration, have been identified to have effects on the porosity, morphology, physicochemical properties, hydrodynamic and mass transfer characteristics of the monoliths in relation to analytes (Mihelic *et al.*, 2001; Danquah and Forde, 2008; Nischang *et al.*, 2010; Alves *et al.*, 2013). Several good review articles have discussed research advancements made in the synthesis and application of polymeric monoliths for small molecule applications in an isocratic mode (Svec, 2012), fast biomolecule isolation (Podgornik and Krajnc, 2012; Podgornik *et al.*, 2013) and preparative chromatography (Jungbauer and Hahn, 2008; Ongkudon *et al.*, 2014). However, there exist to-date limited discussions essential to formulate the relationship between in-process polymerisation mechanism and conditions, and post-polymerisation physicochemical characteristics of polymeric monoliths. This relationship will facilitate predictive modelling and, effective process engineering and tuning of the characteristics and chromatographic features of polymer monoliths for enhanced bioscreening performance of a wide range of target molecules. This review article discusses analytical process conditions relevant to establish the characteristics of polymethacrylate monoliths in order to facilitate a wide range of bioscreening applications. Also, research advances in the application of polymethacrylate monolithic adsorbents for high efficiency bioseparation is presented.

2.   TYPES OF MONOLITHS

Different kinds of monolithic adsorbent systems have been developed for various applications. These can be broadly classified into 3 groups; organic monoliths, inorganic monoliths and hybrid organic-inorganic monoliths (Hjerten *et al.*, 1989; Tennikova *et al.*, 1991; Svec and Fréchet, 1995; Minakuchi *et al.*, 1997). Figure 1 shows examples of commonly used monolithic adsorbents under each classification.
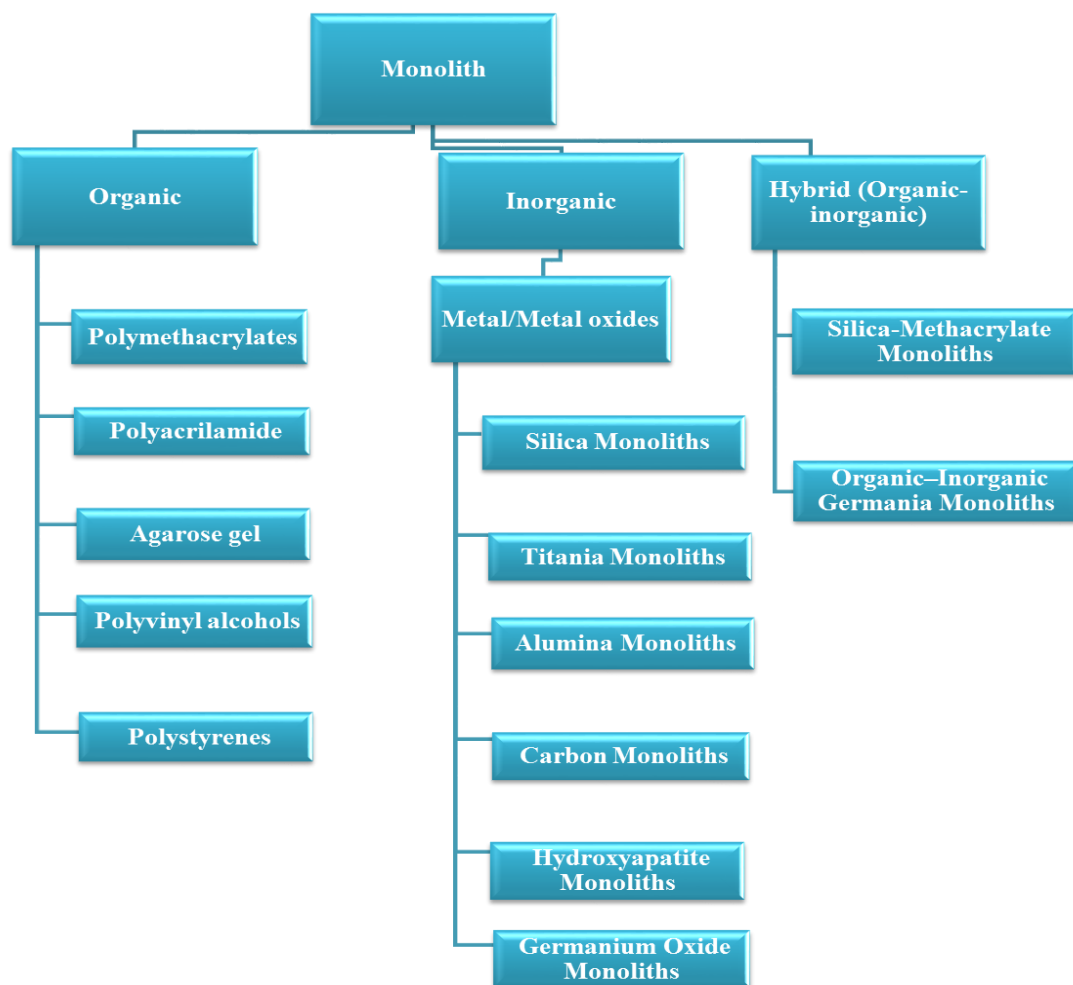
Figure 1. Examples of commonly used monolithic adsorbents classified under organic, inorganic and hybrid systems (Hjerten *et al.*, 1989; Xu and Anderson, 1994; Svec and Fréchet, 1995; Svec and Fréchet, 1995; Minakuchi *et al.*, 1997; Nandakumar *et al.*, 2000; Liang *et al.*, 2003; Kucheyev *et al.*, 2006; Fang *et al.*, 2007; Yu *et al.*, 2008; Hasegawa *et al.*, 2009; Zajickova *et al.*, 2011; Xiaoxia *et al.*, 2013; Yang *et al.*, 2015).

Generally, organic monoliths are resistant to pH, biocompatible, easy to synthesise mostly via polymerisation and possess high interconnectivities (Walsh *et al.*, 2012; Wang *et al.*, 2014). However, they are susceptible to swelling, shrinkage and are unstable under extreme temperature conditions of above 200 ºC (Mayr *et al.*, 2002; Walsh *et al.*, 2012), and prolonged exposure to harsh solvents. For instance, it has been reported that the presence of tetrahydrofuran conferred structural alterations to poly(styrene–co-divinylbenzene), resulting in changes in pore distribution, reduction in permeability, increased back pressure, and reduced life span (Oberacher *et al.*, 2004). Notably, amongst organic monoliths, polymethacrylate and polystyrene monoliths demonstrate unique

physicochemical properties, such as good resistance to pH, resistant to some alkaline solvents, ease of tuning pore and surface characteristics, biocompatibility and macroporosity which enables efficient mass transfer by convection (Roberts *et al.*, 2009; Podgornik *et al.*, 2013). Polymethacrylates are also noted as the most utilised monoliths for bioseparation applications (Podgornik *et al.*, 2013). Inorganic monoliths mostly have limited operational pH ranges. For example, silica monoliths have an operational pH range of 2-8, and their synthesis and pore/surface engineering is quite challenging. However, they have good mechanical stability at temperatures above 750 ^{o}C, and a high surface area of ~ 648 g/m^2 (Walsh *et al.*, 2012; Wang *et al.*, 2014). Hybrid monoliths are designed to possess intermediary properties of organic and inorganic monoliths (Wang *et al.*, 2014).

3.   MODE OF SYNTHESIS OF POLYMERIC MONOLITHS

A wide range of techniques exist for the synthesis of a variety of polymeric monoliths. Some of these techniques have contributed to reduce synthesis time, enhance reaction conversion, and reduce energy consumption and heat dissipation for the development of different geometrical structures of miniaturised and large-scale monoliths. These polymerisation techniques include free radical polymerisation (thermal initiation, radiation, photopolymerisation), sol–gel synthesis, living polymerisation, polycondensations, polyemulsions and xerogels-derived (Danquah and Forde, 2007; Svec, 2010). Free radical copolymerisation is a commonly used technique to enable effective control of the pore size distribution and surface area of the monolith (Mayr *et al.*, 2002; Alves *et al.*, 2013). A summary of the comparison between free radical polymerisation processes by radiation, thermal and photo initiation is presented in Table 1.

Table 1. Comparison of free radical polymerisation processes with different initiation mechanisms for polymer monolith synthesis.

Parameter	Thermal	Photo-polymerisation	Radiation
Polymerisation initiation mechanism	Thermal energy from water bath or oven (Ji *et al.*, 2015)	UV light (Vonk *et al.*, 2015)	Electron beams or γ-radiations (Vizioli *et al.*, 2005)

Mold	Generally requires any thermally conductive mold	Requires molds that are fully or partially UV accessible (Svec, 2004; Szumski and Buszewski, 2009; Yang *et al.*, 2015)	Generally applicable to all molds
Operating Temperature	Not applicable at room temperature due to the high decomposition temperatures of chemical initiators	Can take place at any arbitrary operating temperature (Hirano *et al.*, 2009; Szumski and Buszewski, 2009)	Arbitrary temperature set point
Porogen	Has a relatively limited number of suitable porogens (Not suitable for porogens with lower boiling points) (Svec, 2010)	Has a large number of porogen types that can be utilised	No known documentation of unsuitable porogen
Monomer	No restriction to the types of monomers	Requires UV transparent monomers (Svec, 2010)	No known documentation of unsuitable monomer
Initiator	Any initiator that decomposes at the specified operating temperature can be used.	Requires initiators that can form free radicals at specified wavelength	Not a prerequisite due to the inherent intense energy from the radiations (Svec, 2010)
Polymerisation time	The synthesis process takes hours	Rapid (Chen *et al.*, 2015)	Rapid (Vizioli *et al.*, 2005)
Safety ethics	Approach generally safe with low risk	Generally safe	The use of γ-radiation is hazardous

4. EFFECT OF SYNTHESIS CONDITIONS ON THE MORPHOLOGICAL FEATURES OF POLYMERIC MONOLITHS

The morphological features of polymeric monoliths are mostly dictated by the conditions of their synthesis process, and this offers the opportunity to engineer their pore size, surface characteristics and porosity (Jungbauer and Hahn, 2008). The morphological characteristics and rate of polymerisation of monoliths are dependent on synthesis conditions such as operating temperature, type and composition of porogen, initiator, and monomers as well as the polymerisation time (Svec, 2012). Commonly used thermally-initiated process commences with a clear liquid mixture of the monomers, initiator and porogen(s) placed in a temperature controlled reactor to commence free radical copolymerisation after initiator decomposition to form the polymer resin (Mihelic *et al.*, 2001; Danquah and Forde, 2008). Heat build-up within the mould, which is a summation of the heat contribution from the operating temperature and heat released during the reaction, plays a critical role in formulating the morphological characteristics of the monolith (Mihelic *et al.*, 2001; Danquah and Forde, 2008). During the polymerisation process, initiators decompose to form free radicals and the process results in the release of exothermic heat. The extent of the reaction can be represented by the following equation:

$$\frac{d\xi}{dt} = (1 - \xi)^n A e^{(-\frac{E_a}{RT})} \tag{1}$$

Where; ξ is the extent of the reaction, n is the order of the reaction, A is the pre-exponential factor, E_a is the activation energy, R is the gas constant, and T is temperature in Kelvin (Mihelic *et al.*, 2001).

The polymerisation process proceeds with the formation of nuclei resulting from free radical-driven monomeric interactions, and this acts as the seeding nucleus for the formation of microglobules. Aggregated microglobules precipitate out of the solution to form the polymer. The coagulation of microglobules and aggregated microglobules controls the formation of irregular pores with high interconnectivities, and this defines the pore characteristics of the polymer with the geometric shape being that of the mould (Ongkudon *et al.*, 2013). Microscopic analysis indicates that the formed pores comprise

of asymmetrical voids between the following: globules of a certain cluster, clusters of globules, and intra-globular pores (Danquah and Forde, 2008). The pore sizes of most polymeric monoliths could easily be engineered to range from micropores to macropores. The macropores facilitates high throughput convective mass flow whilst the micropores offer high surface area for ligand immobilisation and target binding (Danquah and Forde, 2008). The surface area of the monolithic adsorbent can be represented by the following equation:

$$S_a = N_T K_v d_v^2 \tag{2}$$

where S_a is the surface area of the monolith; K_v is the constant of proportionality of pore shape; d_v is the pore linear dimension assumed to be repetitive; and N_T is the total number of pores (Podgornik *et al.*, 2013). The end of the polymerisation process results in the formation of a 2-phase system; an inert liquid porogenic system within the pores of white continuous solid structure (monoliths) (Mihelic *et al.*, 2001).

4.1 Porogen effect

The physicochemical properties of the porogenic medium affect the pore formation process of the polymer resin as they control cluster/globular mobility and association to ensure optimal pores homogeneity (uni-modal or bi-modal) and permeability during phase separation of cross-linked nuclei and globules (Santora *et al.*, 2001; Danquah and Forde, 2008; Vonk *et al.*, 2015). There are a variety of porogens with different physicochemical properties and impacts. These include: (i) microporogens (such as cyclohexanol), which act as a good solvent for the separation of cross-linked nuclei (Mayr *et al.*, 2002); (ii) macroporogens (such as dodecanol), which act as a poor solvent for rapid phase separation and large pore formation (Danquah and Forde, 2008; Nischang *et al.*, 2010); (iii) solid porogens such as sodium carbonate, which can induce pore size increase through the release of gaseous species (Danquah and Forde, 2008); and (iv) Polymer solvent porogens such as poly(ethylene glycol) and poly(ethylene oxide) (Viklund *et al.*, 2001; Chen *et al.*, 2015). An increase in porogen concentration results in the enlargement of monolithic pores as well as a decrease in the mechanical strength of the polymer. Our previous work, as shown in Figure 2A, reported the effect of increasing cyclohexanol porogen

concentration from 40% - 80% for the synthesis of polymethacrylate monoliths, and the resulting pore size increase from 116 nm – 876 nm respectively was observed (Danquah and Forde, 2008).
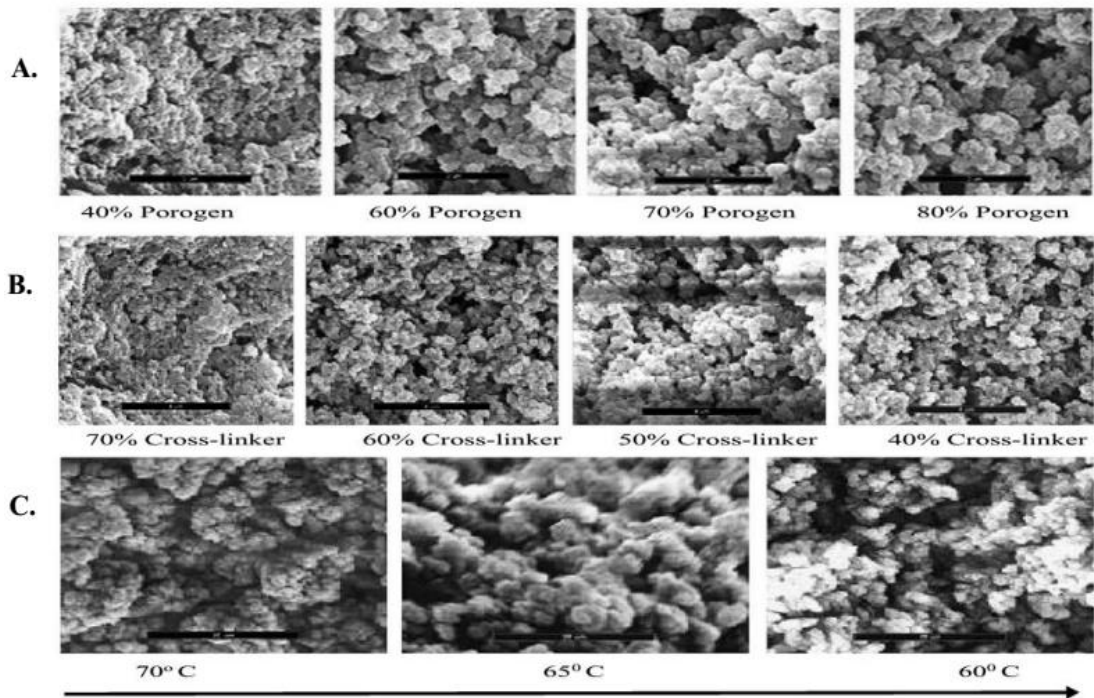

Figure 2. Scanning Electron Micrographs displaying the effects of engineering different polymerisation conditions on GMA-co-EDMA monolith pore size. Figure is adapted from (Danquah and Forde, 2008).

4.2 Monomer effect

Synthesis of polymeric monoliths by copolymerisation involves two monomers; the functional and cross-linker monomers. The monomers contribute different physicochemical properties to the polymer. A high concentration of the cross-linker monomer results in a tight globular network and this decreases the monolith pore size, pore volume and permeability (Bisjak *et al.*, 2007; Danquah and Forde, 2008) as shown in Figure 2B. Also, there is a resultant increase in covalent interconnectivities between nuclei, globules and cluster of globules, and this leads to an increase in the mechanical strength and surface area of the polymer. The interconnectivities restrain the swelling and amalgamation of nuclei to cause the formation of small internal channels (Danquah and Forde, 2008). Studies have shown that the pore size distribution of polymeric monoliths can be tailored to a variety of target molecules with different hydrodynamic sizes by

27

altering the type and concentration of the cross-linker monomer (Urban *et al.*, 2010; Jandera *et al.*, 2013; Staňková *et al.*, 2013; Alshitari *et al.*, 2015). It is possible to change the macroporous features of methacrylate monoliths by using cross-linker monomers with a high number of repeating non-polar methylene groups to increase microporosity for small target molecules application. Polymethacrylate monoliths synthesised with ethylene glycol dimethacrylate (EDMA) having one repeating methylene non-polar group had >90% of pores with gyration radius above 50 nm. Also, hexamethylene dimethacrylate (HEDMA) having 3 repeating methylene non-polar groups generated ~70% of pores in the same region. Tetraoxyethylene dimethacrylate (TeEDMA) having 6 repeating methylene non-polar groups produced 66%-73% (Jandera *et al.*, 2013). Conversely, an increase in the concentration of the functional monomer relative to the cross-linker increases the epoxy density for activation and ligand immobilisation. Nevertheless, this results in the formation of larger pore monoliths with low mechanical strength. The trade-off between the relative concentrations of functional and cross-linker monomers is essential to tailor the polymer characteristics for different bioscreening application.

4.3   Temperature Effect

The polymerisation temperature is an important parameter that controls the kinetics of polymer formation, and this affects the pore and surface characteristics of the monolith. Temperature affects the rate of collision of reactant molecules and this dictates the probability of product formation. An increase in temperature results in enhanced intermolecular collision and this causes a spontaneous increase in the heat of reaction as shown in equation (1). Under elevated temperature conditions, the initiator decomposes faster to generate more free radicals relative to available monomers per unit time. This results in a simultaneous increase in the number of nuclei and small pore size interconnectivities (Bisjak *et al.*, 2007; Danquah and Forde, 2008; Hirano *et al.*, 2009). The effect of temperature variation on the morphology of the monoliths is shown with scanning electron microscopic images in Figure 2C.

4.4 Initiator Effect

The decomposition of initiators for the synthesis of polymeric monolith results in the emission of large amounts of heat in the mould. The initiator decomposes to form free radicals for the commencement of the polymerisation process (Svec and Fréchet, 1995). The rate of initiator decomposition and specificity of initiation reactions is dependent on the polymerisation temperature and, types of porogen(s) and monomers. Porogens can have a limiting effect on the specificity of free radicals by causing undesirable side reactions such as recombining the free radicals to inactivate the initiators as the solution becomes more viscous. An increase in the amount of initiator corresponds with an increase in the rate of polymerisation and late separation of the solid phase from solution. This causes the formation of monoliths with smaller pore sizes and large surface area (Danquah and Forde, 2008). Similar finding were obtained for the study of initiator effects on vinylPOSS monoliths (Alves *et al.*, 2013). Svec and Fréchet (1995) also demonstrated that the initiator type can influence the pore size distribution.

4.5 Oxygen Effect

The presence of oxygen in the monomer mixture can have negative impacts on the rate and type of products formed during the polymerisation process. Oxygen reacts with a series of free radicals to form unreactive peroxy radicals by means of coupling or disproportionation reactions (Mihelic *et al.*, 2001). Also, the presence of oxygen can introduce structural non-uniformity to polymer formation and this can affect the pore size distribution (Alshitari *et al.*, 2015). Oxygen can also contribute to mass loss by reacting with carbon chains of monomers or initiators to form CO and CO_2 products hence, the need for nitrogen sparging or deoxygenating before polymerisation.

4.6 Polymerisation Time Effect

The polymerisation time can affect the physicochemical characteristics and the adsorptive performance of polymeric monoliths. The polymerisation time dictates the extent of polymerisation reaction and the degree of structural formation. It has been demonstrated that for styrene-based monoliths, longer polymerisation times resulted in higher amounts of monomer conversion (Greiderer *et al.*, 2009; Trojer *et al.*, 2009). For a thermal free

29

radical polymerisation process in the presence of azobisisobutyronitrile (AIBN) as the initiator, a conversion of >99% was obtained at 600 min whereas 58% conversion was achieved at 60min for the same polymerisation conditions and compositions (Greiderer *et al.*, 2009). It was shown that a significant strutural transformation ensued with increasing polymerisation time for the synthesis of poly(1,2-bis(p-vinylphenyl))ethane monoliths. These transformations relate to (i) the pore size distribution: from unimodal distribution to bimodal distribution; (ii) porosity: from 73.8% to 81.4%; and (iii) Surface area: an increment by three fold (Greiderer *et al.*, 2009). A similar trend in the reduction of permeability, porosity, and the formation of more interconnectivities was observed for organic monoliths, prepared from pentaerythriol tetra(3-mercaptopropionate)-co-1,2,4-trivinylcyclohexane, synthesised by photopolymerisation with UV (Chen *et al.*, 2015).

5. HYDRODYNAMICS OF POLYMER MONOLITHS

The fundamental hydrodynamics of fluid flow through monolithic adsorbents hinge on the laws of conservation of mass and momentum. In addition, the flow of fluids through monoliths is generally regarded to be Newtonian thus, can be described by Navier-stokes equations. Different polymer monoliths can be synthesised to possess similar physicochemical properties such as stability, low swelling propensity and porosity but with varying pore size distributions (Podgornik *et al.*, 2013). It has been demonstrated that a linear correlation exists between the flow of fluids in monoliths, the pressure drop and the pore size (Leinweber and Tallarek, 2003; Mihelič *et al.*, 2005). Several in-depth hydrodynamic studies of the behaviour of different monolithic systems have been carried out to demonstrate superiority over particulate systems (Leinweber *et al.*, 2002; Leinweber and Tallarek, 2003; Mihelič *et al.*, 2005; Vervoort *et al.*, 2005; Danquah and Forde, 2008; Jungreuthmayer *et al.*, 2015). These studies have led to the development of a modified Carman-Kozeny equation for incompressible fluids in laminar flow, equation (3), to a more accurate prediction, equation (4), for monolithic beds (Podgornik *et al.*, 2013):

$$\Delta P = (k_s)(v)(L)(\mu)\left(\frac{1}{D_s^2}\right)\left(\frac{(1-\varepsilon)^2}{\varepsilon^3}\right) \tag{3}$$

$$\Delta P = 2(v)(L)(\mu)\left(\frac{a_w^2}{\varepsilon^3}\right) \tag{4}$$

Whereas equation (3) is based on particle diameter, which is less suitable for monoliths, equation (4) is based on the assumption of wetted surface area of monoliths. Given that the wetted surface area is:

$$a_w = \frac{surface\ area}{total\ pore\ volume} = (\varepsilon)(k_v)\left(\frac{1}{D_v}\right) \tag{5}$$

Equation (4) can be rearranged based on equation (5) to fit the Carman-Kozeny equation as follows:

$$\Delta P = 2(k_v^2)(v)(L)(\mu)\left(\frac{1}{D_v^2}\right)\left(\frac{1}{\varepsilon}\right) \tag{6}$$

where; k_s is the structural constant for particulate bed; k_v is the structural constant for monolithic bed; v is the linear velocity of the fluid; L is the length of monolith; μ is the average viscosity of the fluid; D_s is the diameter of particles; D_v is the pore linear dimension of monoliths; a_w is the wetted surface area/surface area of pores; ε is monolith porosity (Podgornik *et al.*, 2013). A mathematical analysis of the extent of pore size distribution by considering a two case scenario; monoliths with a bi-modal parallel non-uniformity against monoliths prepared from the same resin composition but with a bi-modal non-uniformity of pore size distribution has also revealed that lower pressure drops for fluid flow can be obtained by simply altering pore size ranges along the length of the monolith during the formation process (Danquah and Forde, 2007; Roberts *et al.*, 2009). Furthermore, Jungbauer's group recently demonstrated through the use of experimental and computational fluid dynamics (CFD) the existence of intermittent distribution and networking of large and small pores which leads to lateral low of samples with fluctuating velocity in the channels (Jungreuthmayer *et al.*, 2015). The fluctuating velocity is explained to be potentially responsible for the lower back pressure and excellent separation properties of polymer monoliths for macromolecules. In addition, their computational analysis further proves the drawbacks in using particulate adsorbent flow models for polymeric monoliths.

6. MASS TRANSFER CHARACTERISTICS OF MONOLITHIC POLYMERS

Monoliths have superior convective mass transfer properties (Mayr *et al.*, 2002; Jungbauer and Hahn, 2008) compared to other adsorbent matrices such as particulate beds (Deng *et al.*, 2001), glass nanopores (Ding *et al.*, 2009; Gao *et al.*, 2009) and open tubular capillaries (Dick Jr *et al.*, 2004; Connor and McGown, 2006). The mass transfer characteristics of monolithic adsorbents have been extensively investigated using pulse response experiments and frontal analysis using dynamic binding capacity (Jungbauer and Hahn, 2008). Owing to their convective mass transfer properties, monolithic chromatography can be optimised based on their binding and elution gradients to have a reduced analysis time coupled with high resolution (Podgornik and Krajnc, 2012; Podgornik *et al.*, 2013). Podgornik *et al.* (2013) reported that the use of short monoliths such as disk monoliths can be effective in getting rapid analysis time and small peak broadening initiated by sharpening effect for even larger molecules such as protein, plasmid DNA, RNA and viruses. Also, an increase in the convective mass transfer coefficient significantly increases the allowable throughput for large molecules binding though this has no significant effect on the dynamic binding capacity of monoliths especially for protein adsorption.

7. FUNCTIONALIZATION OF POLYMERIC MONOLITHS

The degree of ligand immobilisation is dependent on physicochemical characteristics such as pH, temperature, available reactive moieties, extent of ligand concentration and reaction time (Ongkudon and Danquah, 2010; Sinitsyna *et al.*, 2012). For example, pH increase has been investigated to enhance the reactivity of epoxy moieties on polymethacrylate monoliths (Ongkudon and Danquah, 2010). Nevertheless, a balance is required in order not to affect the stability of pH sensitive ligands such as protein and peptide ligands (Jiang *et al.*, 2005; Ongkudon and Danquah, 2010). An increase in temperature also yields positive results for ligand immobilisation and ligand density though high temperatures can degrade thermally sensitive ligands. Although immobilising ligands on solid adsorbents can reduce activity, it enhances ligand reusability and stability (Zhang *et al.*, 2013). Engineering the pore and surface area of monolithic adsorbents can

result in the optimisation of ligand density and ligand binding sites for better interactions with the target. Also, surface areas of monoliths could be enhanced through the introduction of diverse nanoparticles into monoliths either during the preparation of polyresin or in the post-polymerisation stage for enhanced bioscreening conditions (Tang *et al.*, 2014).

Functional chemistries employed in the activation of monoliths for ligand immobilisation include but not limited to direct coupling on monolithic moiety such as the epoxy group (Gao *et al.*, 2013); glutaraldehyde activation (Deng *et al.*, 2012); disuccinimidyl carbonate activation (Jiang *et al.*, 2005); hydrazide activation (Jiang *et al.*, 2005); streptavidin activation (Zhao *et al.*, 2008); and carbonyldiimidazole activation (Jiang *et al.*, 2005). The choice of chemistry is dependent on the adsorbent moieties, the type of ligand and the purpose of application. Generally, the most preferred approach to immobilise ligands is through chemistries that lead to covalent bonding with minimal non-specific adsorption. Although covalent chemistries are quite challenging to achieve, they are robust, economical in the long term and can be used multiple times (Bănică, 2012; Acquah *et al.*, 2015). For example, immobilisation of ligands on monoliths by means of streptavidin-biotinylation interaction is relatively easy to achieve and requires less time (Zhao *et al.*, 2008; Brothier and Pichon, 2014). However, due to non-covalent interactions existing between the activated supports and the immobilised ligands, the bond is easily hydrolysed in the presence of organic solvents, causing ligand leaching and reduced life span (Brothier and Pichon, 2014; Pichon *et al.*, 2015). Insights into the characteristics of various covalent chemistries for ligand retention are discussed.

7.1 Epoxy Method

Epoxy activation is a simple method of covalent immobilisation (Mallik and Hage, 2006). Free radical copolymerisation of methacrylate monoliths with glycidyl methacrylate (GMA) as the functional monomer introduces reactive epoxy moiety into the structural make-up of the monolith and this enables nucleophilic interaction with amine, sulfhydryl and/or hydroxyl groups on ligands (Hee Seung and David, 2005; Mallik and Hage, 2006; Gao *et al.*, 2013). However, epoxy activation has a slow reaction rate, low level of ligand

immobilisation and the binding is liable to hydrolytic reactions (Mallik and Hage, 2006; Pfaunmiller *et al.*, 2013).

7.2   Schiff Base activation

Schiff base activation occurs when an aldehyde-functionalized group reacts with an amine-containing ligand to form a covalent bond (Pfaunmiller *et al.*, 2013). There are two basic mechanism by which this results: (i) the conversion of the monolithic surface into an amine form using ethylenediamine or hexanediamine and subsequently reacting them with dialdehydes such as glutaraldehyde; and (ii) activation of the monolithic surface using sodium periodate or periodic acid to oxidise the diol-functionalised surface into aldehyde residuals (Hee Seung and David, 2005; Mallik and Hage, 2006). Although the former aids in minimising steric hindrance through the formation of longer spacer arms, it requires more steps (Mallik and Hage, 2006; Han *et al.*, 2012; Brothier and Pichon, 2014). The latter has a faster rate of reaction with a higher ligand activity but it requires the use of a reducing agent (sodium cyanoborohydride and sodium borohydride) to stabilise the amine-aldehyde reaction, and this can negatively affect the ligand activity and also pose some hazards to the user (Hee Seung and David, 2005; Mallik and Hage, 2006).

7.3   Carbonyldiimidazole (CDI) activation

This approach requires the functionalization of monolithic surface into diols and reacting it with 1,19-carbonyldiimidazole (CDI) to yield imidazolyl carbamate groups (Jiang *et al.*, 2005; Mallik and Hage, 2006). This results in the formation of a covalent bond between the amine ligands and the CDI activated monolithic surfaces (Kim and Hage, 2006; Mallik and Hage, 2006). In comparison to epoxy activation and Schiff base methods, CDI immobilisation is noted to be faster and requires fewer process steps (Mallik and Hage, 2006).

7.4   Disuccinimidylcarbonates (DSC) activation

This approach requires the functionalization of monolithic surfaces with diol groups and reacting them with disuccinimidyl carbonate groups to form covalent bonds with amine ligands (Ott *et al.*, 2011; Pfaunmiller *et al.*, 2013). Although this approach is also noted to

be fast, it has a low stability and the bonding is liable to hydrolysis (Mallik *et al.*, 2004; Mallik and Hage, 2006; Pfaunmiller *et al.*, 2013).

7.5   Hydrazide activation

The methodology for hydrazide activation is the same as the Schiff base approach, and this results in the formation of aldehydes on the surface of the monoliths using reagents such as adipicdihydrazide in a phosphate buffer (Mallik and Hage, 2006). The aldehyde groups are then reduced to alcohols by reacting with sodium borohydride. This method of monolith activation is suitable for ligands possessing carbohydrate groups or a member of the glycoprotein family. Such ligands are oxidised to form aldehyde functional ends to enable reaction with the hydrazide groups (Mallik *et al.*, 2004; Mallik and Hage, 2006; Pfaunmiller *et al.*, 2013).

7.6   Azlactone activation

Monoliths can also be synthesised to possess azlactone (lactone-based) pendant moieties that experiences ring-opening reactions whiles their vinyl end binds to the surface of the monolith (Alwael *et al.*, 2011). This method of activation is appropriate for nucleophilic modified molecules such as primary amines-, alcohols- or thiol-based ligands (Delplace *et al.*, 2015). Incorporation of lactone-based moieties into monoliths can occur *in-situ* by using vinyl azlactone as a functional monomer or *ex-situ* grafting by means of pumping vinyl azlactone through the monolith (Connolly *et al.*, 2010; Alwael *et al.*, 2011). Advantages of this method of monolith activation includes its relative stability to hydrolysis and ease of rapid interactions in the absence of catalysts at room temperature (Delplace *et al.*, 2015).

8.   BIOSCREENING APPLICATIONS AND THEIR CORRESPONDING FIELDS

The biocompatible features of polymeric monoliths and the ability to tune their pore and surface characteristics to suit a variety of biomolecules and cells enable a substantial number of analytical and preparative-scale bioseparation and bioscreening applications in

diverse fields. Some of these applications include ion-exchange, hydrophobic and affinity binding and separations.

8.1 Ion-exchange separation

Ion-exchange separation of biomolecules is based on the charge and molecular size of the analyte and this leads to either a cation- or anion-exchange separation. Anion-exchange separation is the most commonly used ion-exchange chromatographic separation due to the fact that biomolecules are predominantly negatively charged (Roberts *et al.*, 2009). The pore surfaces of the stationary adsorbents are functionalized with positively charged ligands, as shown in Figure 3, for target binding. Examples of anion-exchange ligands include 2-chloro-N,N-diethylethylamine hydrochloride (DEAE-Cl), hexylamine (HxA), tripropylamine (TPA), diethylamine(DEA), N,N- dimethylbutylamine (DMBA) and triethylamine (TEA) (Danquah and Forde, 2007; Ongkudon and Danquah, 2010; Sharma *et al.*, 2012).
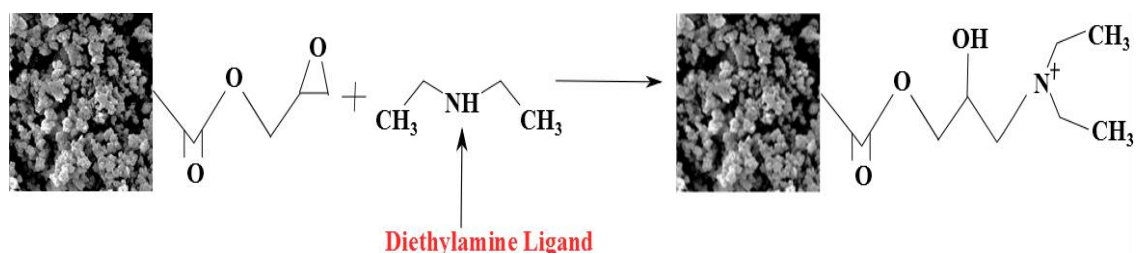

Figure 3. Immobilisation of DEA ligands on polymethacrylate monoliths for anion-exchange separation applications.

An electrostatic interaction is thus set in place between positively charged ligands and negatively charged analyte molecules. Elution of targets is by means of increasing order of surface-charge density and molecular conformation. The strength of ligand-target bonding can be decreased by increasing the ionic concentration, protonating (or deprotonating) the matrix to reduce the net charge, and altering the molecular conformation of the target (Ongkudon and Danquah, 2010; Ruščić *et al.*, 2015). Ongkudon and Danquah (2011) demonstrated that optimal conditions for anion-exchange purification of plasmid DNA (pcDNA3F) hinge on the plasmid size, buffer conditions, porosity of the adsorbent and conductivity. It was also shown that TEA-activated

monoliths enhanced binding performance as compared to DEA-activated monoliths. Guo and Carta (2015) studied the application of sulfonate cation exchange monolithic system for the analysis of bovine serum albumin tryptic digest with a loading capacity of ~15 pmol using 10^{-5} M angiotensin II. Binding analysis was performed by creating a dynamic pH junction via the preparation of samples in an acidic buffer before ejecting them into the cation-monolith and eluting them with a basic buffer.

8.2   Hydrophobic separations

The separation of biomolecules based on hydrophobic interactions is another versatile LC separation method especially for protein targets. Hydrophobic ligands are immobilised on the pore surface of the monolith for hydrophobic interaction with the target. Protein molecules have an inherent degree of hydrophobicity, and the separation efficiency of proteins is dependent on the surface hydrophobicity, density and the nature of the hydrophobic ligands (Zou *et al.*, 2002; Roberts *et al.*, 2009). A decrease in the concentration gradient of salt in the mobile phase results in the separation of molecules in order of increasing hydrophobicity (Urban and Jandera, 2008). Alternatively, salt concentration can be maintained whiles modulating temperature to eventually dictate the hydrophobic-hydrophilic interaction transition of the functionalised ligands (Zou *et al.*, 2002). Remarkably, polystyrene and polybutyl methacrylate based organic monoliths are recognised as strong hydrophobic adsorbents and can be used directly for reversed-phase and precipitation–redissolution chromatography as well as hydrophobic interaction chromatography (Zou *et al.*, 2002; Urban and Jandera, 2008). Hydrophobic separations are also popularly used to complement other types of bioseparation technologies in a mixed mode format (Zou *et al.*, 2002). Ligands such as N,N-dimethyl-N-dodecylamine can be functionalized on monolithic columns, as shown in Figure 4, to obtain a mixed mode anion/hydrophobic separation system for organic and inorganic compounds such as phenols, alkylbenzenes, nitrate, bromide, nitrite, thiocyanate and iodide (Aydoğan, 2015).
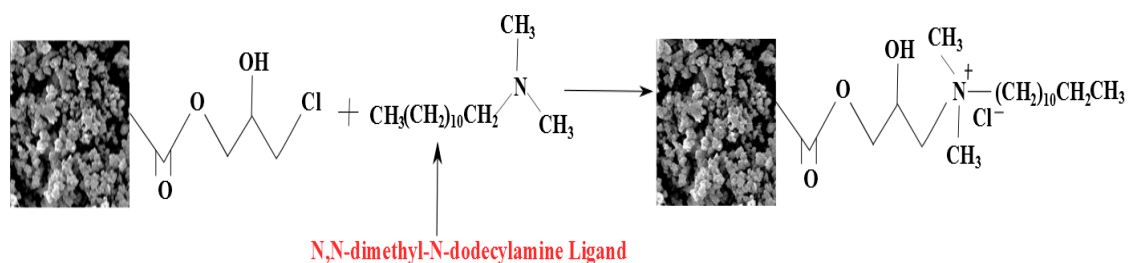
Figure 4. Immobilisation of N,N-dimethyl-N-dodecylamine ligands on polymethacrylate monoliths for mixed mode anion/hydrophobic screening application adapted from (Aydoğan, 2015).

8.3 Affinity Separations

Research and technological advancements have led to the discovery and application of a plethora of ligands that are specific in interacting with their respective cognate targets with high binding affinities. Some of these affinity ligands include DNA molecules, protein receptors, peptide receptors, enzyme receptors, antibodies and aptamers. An example of an affinity ligand (such as aptamer) is shown in Figure 5 for affinity separations.
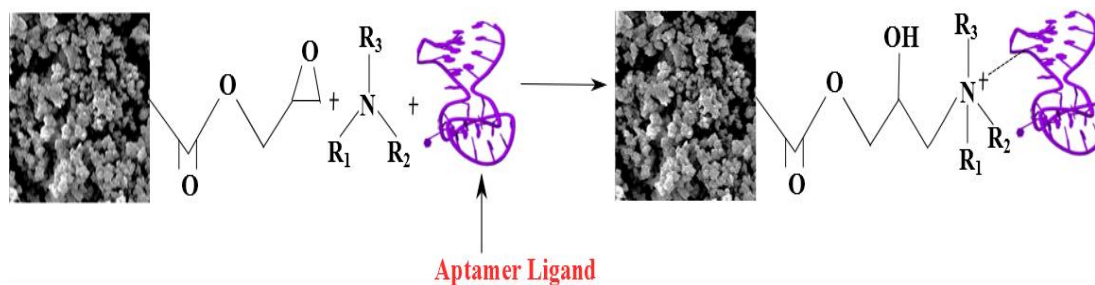

Figure 5. Illustration of affinity separations through the use of an affinity ligand.

8.3.1 Protein receptors

Protein A ligands are classical examples of protein bioaffinity ligands used for biomolecular separation, and are derived from the cell wall of *Staphylococcus aureus*. They have a molecular mass of 42 kDa with a unique affinity for the F_c region of antibodies (Pan *et al.*, 2002; Zou *et al.*, 2002; Gagnon, 2012). Bioanalysis of human IgG with protein A was performed within 3 min using immobilised monolithic adsorbents at a flow rate of 1.0 ml/min (Zou *et al.*, 2002). However, the use of protein A as ligands is expensive, unstable, and plagued with ethical issues (Zou *et al.*, 2002; Gagnon, 2012). Other types of protein ligands include histadine, gelatin and Protein G.

8.3.3 Enzyme receptors

Monolithic adsorbents for immobilised enzymes have become the ideal support for non-destructive, rapid and high throughput application that enables the enzymes to access substrate active sites with low back pressure (Josić and Buchacher, 2001). Trypsin is one of the most utilised enzymes for bioaffinity applications. Ma et al., studied the immobilisation of trypsin on hybridised organic-inorganic monoliths for myoglobin digestion and observed that the immobilisation of trypsin on monoliths yielded 92% digestion in 30 seconds whereas free trypsin achieved the same yield in 12 h (Ma *et al.*, 2008). Similar trends in high performance of enzymatic monolithic reactors were discussed by Josić and Buchacher (2001) in comparison to chromatographic bead operations. Zhang *et al.* (2013) also immobilised 30l g/mg of α-glucosidase on a polymethacrylate monolith for the digestion of pNPG. The enzymatic reactor exhibited 80% bioactivity after 25 runs and only 7.6% of bioactivity was lost after 6 assays within 31 days compared to free enzymes in solution which lost 37.7% of its activity in 7 days (Zhang *et al.*, 2013).

8.3.4 Antibody receptors

Application of receptors based on molecular recognition is another approach by which bioaffinity interactions with analytes occur. One of such molecular recognition ligands is the antibody. Immobilisation of antibodies on adsorbents generates 'immunosorbents' for bioseparation applications. Antibody-target recognition is analogous to antibody-antigen interaction. The availability of antibodies through the development of hybridoma technologies and their high binding selectivity make them ligands of interest for affinity chromatography, especially, for large molecules (Hennion and Pichon, 2003; Acquah *et al.*, 2015). Brgles *et al*. (2014) demonstrated the use of antibodies for the identification of Atx protein molecules in horned viper (*Vipera ammodytes ammodytes*). However, the use of antibodies are faced with a number of challenges such as ethical issues, large molecular mass, high cost, non-resistant to toxic targets such as Ochratoxin A in food and austere environments (Brothier and Pichon, 2014).

8.3.5   Synthetic receptors

Synthetic receptors are emerging ligands engineered to enhance the performance of bioaffinity separation over a wide range of target application. These include synthetic peptide and DNA/RNA aptameric receptors for target recognition and binding. The mode of interaction of synthetic receptors with cognate targets is also based on affinity interactions but has been demonstrated to be superior over antibodies (Zhao *et al.*, 2012; Brothier and Pichon, 2014). Synthetic receptors are robust, not faced with any ethical issues, economical to generate, have a small molecular size, can be used in austere environments, simple and rapid to synthesise. As a result, their immobilisation results in high ligand densities for high throughput screening (Neff and Jungbauer, 2011; Acquah *et al.*, 2015; Pichon *et al.*, 2015). Streptavidin chemistry has been employed to immobilise aptamers (ligand density of 250 pmol/µL) on a methacrylate monolith for a sandwich chromatographic separation of thrombin via its fibrinogen and heparin binding-site (Zhao *et al.*, 2008). Wang *et al.* (2015) also immobilised aptamers on silica-monoliths by means of thiol-ene click reaction to achieve an enhanced immobilisation density of 420 pmol/µL for the extraction of thrombin in human serum. However, extensive research is required to standardise the generation and performance of synthetic receptors for bioaffinity chromatographic applications.

9.   VIRAL AND CELLULAR SCREENING APPLICATION

Chromatographic screening of pathogens, virus-like particles and cells, as simplified in Figure 6, require the engineering of stationary supports to suit the hydrodynamic and functional characteristics of the targets for high throughput application. For example, the size of parvovirus is 30 nm, orthomyxovirus is 250 nm, paramyxovirus can be 14 µm, and bacteria cells being ≥400 nm. These targets require macroporous adsorbents with tuneable binding features for high performance screening. Suitable macroporous adsorbents for this purpose have been solely based on cryogel-based monoliths, CIM methacrylate monoliths and CIM styrene monoliths. Although cryogels (macroporous monoliths synthesised in sub-zero temperature) inherently have huge pores relative to CIM methacrylate monoliths, the latter is often preferred by biotechnologist due to the ease of fine-tuning pore size distribution, and immobilising ligands suitable for the cellular target.
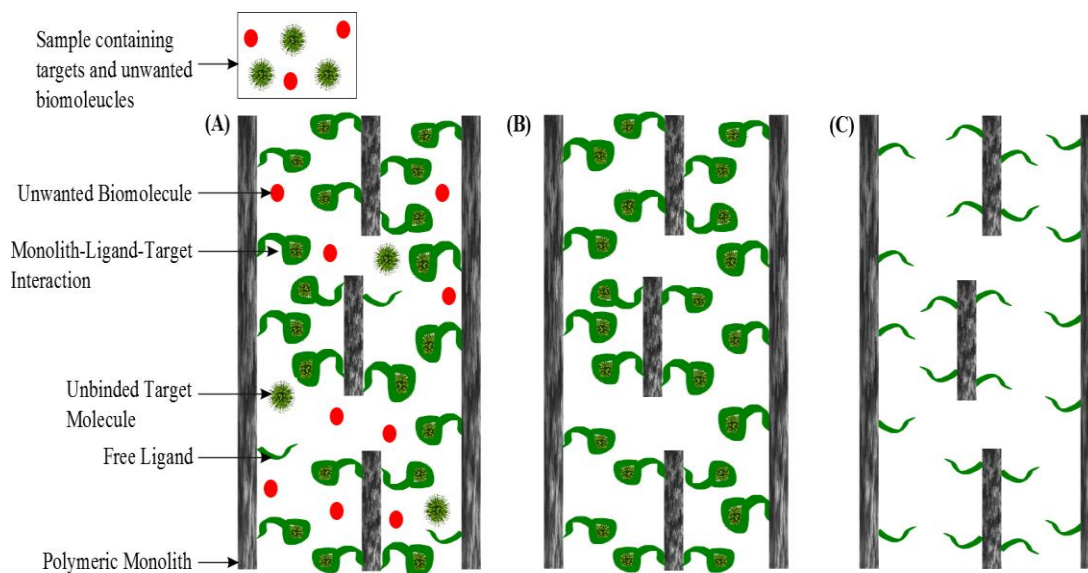
Figure 6. Bioscreening and bioseparation of target molecules using functionalised monoliths. (A) Interaction between immobilised ligands and their cognate targets. (B) After washing of monolithic column to remove unwanted or loosely molecules. (C) Regeneration of the functionalised monolith by means of elution to enable reuse.

Viruses can be engineered as vaccine delivery vectors, phage display, specific phage typing, and for gene delivery therapy (Jungbauer and Hahn, 2008; Podgornik and Krajnc, 2012). The most notable chromatographic processes extensively utilised for viral purification are ion-exchange and size-exclusion. Monolithic adsorbents have found applications in ion-exchange and size exclusion as a stationary phase for the purification and maintenance of infectivity for live attenuated vaccines (Jungbauer and Hahn, 2008). Table 2 summarises the biophysical characteristics of proteins and cells for chromatographic separation.

Table 2.   Comparative biophysical characteristics of proteins and cells.

Characteristics	Protein	Cells
Hydrodynamic size	Small-moderate	High
Response to Mechanical Impact	Moderate	High
Mobility by Diffusion	Significant	Insignificant
Mobility by Convection	Significant	Significant
Number of binding sites	Low	High

Elution of molecules	Simple	Tedious effort
Recovery yield	High	Low

9.1   Pathogen screening

Monoliths have been utilised for selective concentration of various types of pathogens (Gutiérrez-Aguirre *et al.*, 2009; Kovač *et al.*, 2009). Gutiérrez-Aguirre *et al.* (2009) demonstrated the use of CIM monoliths for the concentration of rotavirus. These viral pathogens are the causative agents for diarrhoea in children. In comparison to the use of charged membranes for the concentration of enteric viruses from tap water as per the US environmental protection agency, CIM monoliths were demonstrated to have superior advantages in terms of rapidity, single-step concentration, and high recovery (Gutiérrez-Aguirre *et al.*, 2009). Kovač *et al.* (2009) also demonstrated the use of CIM monoliths for the concentration of hepatitis A virus (HAV) and feline calicivirus (FCV) with improved recoveries compared to conventional methods. The use of butyl–based and styrene-divinyl benzene monoliths have also been applied for the screening of HA1 subunits of different strains of Influenza virus such as A/Solomon Islands/3/2006 (H1N1), A/Wisconsin/67/2005 (H3N2) and B/Malaysia/2506/2004 (Urbas *et al.*, 2011). Their analysis were conducted in reverse phase and it showed that the working linear range, limit of detection and limit of quantification were $1.60x10^{10}$-$1.64x10^{11}$, $2.56x10^9$ and $5.12x10^9$ viral particles/ml, respectively. In addition, SDS-page analysis confirmed that the eluted portion was purely HA1 (Urbas *et al.*, 2011). Zaveckas *et al.* (2015) also developed a 2 step protocol involving a Q Sepharose XL and cation-exchange CIM-monoliths for the purification of virus-like particles, Porcine circovirus 2 (PCV2), responsible for causing post weaning multisystemic wasting syndrome. The percentage purities obtained were 4–7% and 40% as well as a recovery of 5-7% and 15-18% for the two respective columns (Zaveckas *et al.*, 2015). Jungbauer's group also developed a protocol for the purification of infectious baculoviruses within a time frame of 20 h for a volume of 1150 mL cell culture supernatant in a 1mL radial flow monolith requiring a single purification cycle (Gerster *et al.*, 2013). This was achieved through the use of CIM monoliths as an optional pre-column to clarify lipids out of the mixture. Anion exchange monoliths were then employed to screen the baculovirus out of a cell cultured medium

obtained from Spodoptera frugiperda cells. Notably, the rate of recovery ranged from 20% - 99% and above. The wide variation in recovery was attributed to the impact of the age and composition of the supernatant (Gerster *et al.*, 2013).

9.2   Cell isolation and purification

The development of an effective system for cell separation poses more challenges than protein molecules as indicated in Table 2. Due to the number of available binding sites and the hydrodynamic size of cells, suitable adsorbents functionalised with ligands for cell separation should be binding-specific with convective mass transfer characteristics resulting from macroporosity to prevent clogging as well as reduce shear stress damage (Kumar *et al.*, 2003; Dainiak *et al.*, 2006). In light of this, a cryogel monolith with an immobilised protein A ligand was developed and demonstrated successful separation of B-lymphocytes from A-lymphocytes. The recovery rate for B-lymphocytes in the elution fraction was about 60-70% (Kumar *et al.*, 2003). The purification of bacteriophages are highly essential in the production of vaccines and are currently being considered as a complement and/or supplement to antibiotics (Kramberger *et al.*, 2015). *Staphylococcus aureus* bacteriophages VDX-10 from bacteria cell lysate was purified in a single elution step with the host cell DNA >99%, proteins > 90% and about 60% of viable phages recovered. A dynamic binding capacity of 1.1 x 10^{10} pfu/mL of CIM quaternary amine methacrylate monolith was achieved (Kramberger *et al.*, 2010). Liu *et al*., purified mycobacteriophage D29 using CIM methacrylate monoliths functionalised with diethyl amine in a double stage purification process to yield > 99% purity and a recovery of 10-30% for viable phages (Liu *et al.*, 2012). Oksanen *et al*. (2012) demonstrated the use of diethyl aminoethyl and quaternary amine functionalized CIM monoliths for the purification of filamentous phage phi05_2302 and icosahedral bacteriophage PRD1 species and achieved a purification yield of 80% and a recovery of 5 mg/mL.

9.3   Cell binding and targeting

Arvidsson *et al*. (2002) demonstrated the use of an anion-exchange and Cu^{2+} metal affinity cryogel for cellular binding and elution of Escherichia coli with a selective recovery of ~70–80% and ~80% respectively. The pore size of the monolith was in the region of 10-

100 μm. A mixture of *Escherichia coli* and *Saccharomyces cerevisiae* cells was also successfully separated through the use of a cryogel-based monolith with immobilised Concanavalin A (Dainiak *et al.*, 2006). Results from the analysis in a 96-mini column plate format indicated that the flow out, *Escherichia coli*, was~100% pure. *Saccharomyces cerevisiae* was separated from the cryogel monolith by means of compression and a purity of ~95% was obtained (Dainiak *et al.*, 2006). Peskoller *et al*. (2009) also developed a polyglycerol-3-glycidyl monolith synthesised by means of self-polymerization at room temperature for an hour. The monolith was immobilised with polymyxin B as the ligand and had a pore size of about 22 μm and 79% porosity. The immobilised monolith was used for selective binding of *Escherichia coli* with a recovery of ~100% was obtained in 5 min. In addition, an epoxide monolith with pore size of about 20 μm was synthesised by Ott *et al*. (2011) for the selective binding of *Staphylococcus aureus* by means of immunofiltration prior to its bioanalysis with a flow cytometer. Immunofiltration of 1 L sample took 145 min and the sensitivity of the post-analysis flow cytometry was increased by 130 folds from $5.5x10^3$ S. aureus/mL to 42.3 S. aureus/mL in terms of detection limit. Although the immunofiltration process was specific, it was less efficient when compared to ionic interaction of cells in monolithic columns (Ott *et al.*, 2011).

10.   APPLICATION OF MONOLITHS IN MICROFLUIDIC SYSTEMS

The development of effective microfluidic systems for bioscreening have been fraught with a number of challenges relating to surface area to volume ratio and sample preparation for the solid phase component (Tripp *et al.*, 2004; Gao *et al.*, 2013). The use of well-characterised monolithic phases present a unique way of tackling these challenges (Tripp *et al.*, 2004). Monoliths can be easily incorporated into microfluidic devices together with other bioanalytical systems to develop a portable, rapid, and economical system for a wide range of bioscreening applications (Tripp *et al.*, 2004; Gao *et al.*, 2013; Chan *et al.*, 2014). An example of a microfluidic system is shown in Figure 7. Microfluidic systems are economical due to the requirement for minute amounts of samples, reagents and analysis time.
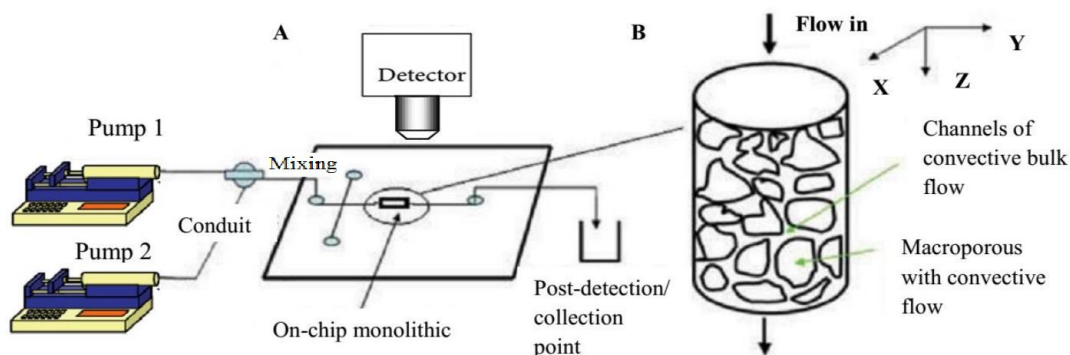
Figure 7. (A) Illustration of a microfluidic system with an embedded methacrylate monolith for rapid LC bioscreening applications. **(B)** An exploded view of the monolithic phase on the microfluidic platform (Chan *et al.*, 2014).

The use of a microfluidic system with an embedded monolithic stationary phase immobilised with trypsin for enzymatic digestion demonstrated 57 seconds analysis time at a flow rate of 0.5 μl/min compared to conventional microfluidic devices which require 3-15 min reaction time (Peterson *et al.*, 2002). Rapid results were obtained in the former as a result of convective mass transport of fluids and a high binding frequency to and from the binding sites. Parameters essential to improve the efficiency of anion-exchange methacrylate monoliths (Chan *et al.*, 2014) and reverse phase silica monolith (Chan *et al.*, 2014) in microfluidic systems for rapid application has been investigated. It was reported that the dynamic binding capacity of the anion-exchange monolithic microfluidic system for protein binding is not affected by flow rate. However, an increase in pH above the isoelectric point (pI = 4.6) of the protein (BSA) resulted in an improved binding capacity, whereas strong ionic concentration (>0.6 M NaCl) resulted in a low dynamic binding capacity (Chan *et al.*, 2014). In a recent work by Yang et al., varieties of monomers (Methyl methacrylate, MMA; butyl methacrylate, BMA; octyl methacrylate, OMA; and lauryl methacrylate, LMA) were applied for the development of a microfluidic system (Yang *et al.*, 2015). Notably, the retention of BSA increased with higher carbon chain lengths as a result of increasing hydrophobicity (Yang *et al.*, 2015). The use of a hybrid monolithic, poly(MAA-co-EGDMA)-γ-Al2O3, microfluidic system has been utilised for the identification and extraction of 2-amino-4-chlorophenol (ACP) in chlorzoxazone tablet, and various parameters such as pH and sample / eluent flow rates were optimised for the extraction process (Zhang *et al.*, 2013). Gao *et al.*, (2013) also demonstrated the use of an aptamer-based microfluidic system for real-time fluorescent monitoring of

biointeractions between a thrombin binding aptamer and thrombin within 3 min. Different chaotropic reagents were tested for the bound thrombin and their respective elution conditions and efficiencies were (i) 200 mM acetic acid + 2 M NaCl (75%), (ii) 1 M NH_4OH (40%), (iii) 4 M urea (40%), (iv) 200 mM glycine (30%), (v) 2 M KSCN + 2 M $MgCl_2$ (25%), and (vi) 2 M $NaClO_4$ (0%).

11. BIOPROCESS CHALLENGES TO THE APPLICATION OF POLYMERIC MONOLITHS FOR HIGH THROUGHPUT APPLICATIONS

To date, the highest volumetric capacity of polymeric monolithic columns is 8 L (Urthaler *et al.*, 2005). Despite the numerous advantages of monoliths for high performance bioseparation, there has been limited progress in producing large volume monoliths for large-scale applications. Factors leading to these challenges can be broadly categorised under (i) thermal inhibition, (ii) maintenance of mechanical and chemical stability, (iii) wall channelling, and (iv) insufficient non-invasive characterisation techniques for process standardization.

The control of temperature associated with the exothermic reaction of the synthesis process of polymeric monoliths is important to produce large uniform monoliths (Mihelic *et al.*, 2001). The generation of large amounts of heat in the mould is explained to have a detrimental effect relating to the formation of heterogeneous pores and non-uniformity along the length of monoliths (Danquah *et al.*, 2008; Ongkudon *et al.*, 2014). To avoid this effect, large scale monoliths have previously been prepared through the embedment of varied annulus monoliths in one another (Podgornik *et al.*, 2000). Though this technique has somewhat been successful, the embedment of annulus monoliths are complex to achieve and could lead to the presence of large nesting dead volumes in the finished monolith (Danquah and Forde, 2008; Danquah *et al.*, 2008). An alternative approach, which happens to be much more effective and simpler, is by heat expulsion (Danquah *et al.*, 2008). However, the use of heat expulsion is suspected to have a negative consequential effect on pore formation in relation to structural interconnectivities and subsequently the mechanical properties of the monolith as the size is further scaled-up (Ongkudon *et al.*, 2014).

Mechanical and chemical stability is also another hurdle requiring in-depth investigations for large monoliths (Bisjak *et al.*, 2007; Vidič *et al.*, 2007). Contrary to particulate supports experiencing minimal or no effect from shrinkage and swelling of their pore size and column stability, monoliths tend to have a pronounced effect when they come in contact with harsh mobile phases (Vidič *et al.*, 2007). Monoliths, by virtue of their continuous block nature, have tangible effect which could lead to cracks upon mechanical stress and this is prevalent in large monoliths (Vidič *et al.*, 2007). Nevertheless, Jungbauer and Hahn (2008) expounded on the fact that polymethacrylate monoliths are resistant to deformation by means of pressure. They can also undergo series of regeneration processes with suitable chaotropic reagents and can be stored for over a year under suitable conditions (Jungbauer and Hahn, 2008; Ongkudon *et al.*, 2014). The maximum volumetric capacity available for silica monoliths is in the region of 50 mL, a volume far below that achieved for polymeric monoliths. This is due to the fact that current methods in synthesising silica monoliths results in shrinkages and cracks during calcinations for scaling up processes (Ongkudon *et al.*, 2014).

Wall channelling is another limitation to the formation and application of large monoliths (Jungbauer and Hahn, 2008; Ongkudon *et al.*, 2014). The formation of monoliths often reveals the existence of a gap between the column wall and monoliths. Channelling can also result from relatively large heterogeneous pores within the monolith matrix, creating a unidirectional preferential pathway for fluid flow. This is more pronounced in large volume polymeric monoliths. Channelling can be minimised by silanisation of the column walls before synthesis of monolith (Greiderer *et al.*, 2009), the use of an innovative-conical moulds (Ongkudon and Danquah, 2011), temperature control, and by swelling of monoliths with tetrahydrofuran to fill the gaps (Urban *et al.*, 2010).

Unlike particulate supports where a small quantity of the particulate material can be sampled for biochemical analysis, monoliths will undergo destruction for a similar biochemical analysis to be carried out (Lendero *et al.*, 2005; Jungbauer and Hahn, 2008). Nevertheless, there have been developments of some non-invasive techniques for biochemical analysis of monoliths. Lendero *et al.* (2005) demonstrated the use of acid-based titration curves to understand the ionic composition of monoliths. The technique

has been shown to be contamination-free and suitable for biopharmaceutical application (Lendero *et al.*, 2005; Jungbauer and Hahn, 2008). Other reports on non-invasive methods for monolith characterisation have been developed for the determination of pore size, flow uniformity, binding capacity, active group types and ionic capacity (Podgornik *et al.*, 2005; Podgornik *et al.*, 2013).

12.   CONCLUSION

Polymeric monoliths are adsorbent matrices suitable for rapid and high throughput bioscreening of biomolecular, viral and cellular targets. Owing to advances in the mechanism of synthesis of polymeric monoliths in relation to polymerisation time, cost of synthesis, engineering of pores and surface areas, monoliths are now easily developed for a wide range of applications. Monolithic stationary adsorbents also provide downstream process advantages for short analysis time and optimal gradient slope for elution under reduced back pressure. In addition, monoliths have led to the reduction in turn around and residence time in industrial preparative-scale applications. The ability to activate and functionalize polymeric monoliths with diverse kind of ligands makes them an ideal support for biomolecular and cellular purification and concentration, as well as the design of enzymatic reactors for biointeractions. Nevertheless, there remain significant research gaps to be accomplished. There are limited or no standard protocols for non-invasive characterisation of monoliths for bioseparation. Theoretical models describing the molecular phenomenon of the pore formation process, essential to accurately predict pore characteristics based on the synergistic effects of multiple polymerisation parameters, are not available. Knowledge on the mechanisms to engineer the physicochemical properties of monoliths is limited as compared to the worth of research interest generated around the application of monoliths as well as in comparison to other polymeric materials. Issues relating to polymeric swelling and cracks as monoliths are further scaled-up remain a huge challenge for large volume monoliths development and application.

13.   ACKNOWLEDGEMENT

the Fundamental Research Grant Scheme (FRGS) and Curtin Flagship schemes respectively.

14. REFERENCES

Acquah, C., M.K. Danquah, D. Agyei, C.K. Moy, A. Sidhu and C.M. Ongkudon, 2015. Deploying aptameric sensing technology for rapid pandemic monitoring. Critical Reviews in Biotechnology(ahead-of-print): 1-13.

Acquah, C., M.K. Danquah, J.L.S. Yon, A. Sidhu and C.M. Ongkudon, 2015. A review on immobilised aptamers for high throughput biomolecular detection and screening. Analytica chimica acta, 888: 10-18. Available from http://www.sciencedirect.com/science/article/pii/S0003267015008016. DOI http://dx.doi.org/10.1016/j.aca.2015.05.050.

Ali, W.H. and V. Pichon, 2014. Characterization of oligosorbents and application to the purification of ochratoxin a from wheat extracts. Analytical and bioanalytical chemistry, 406(4): 1233-1240. Available from http://www.ncbi.nlm.nih.gov/pubmed/24309623. DOI 10.1007/s00216-013-7509-6.

Alshitari, W., C.L. Quigley and N. Smith, 2015. Fabrication and evaluation of an organic monolithic column based upon the polymerisation of hexyl methacrylate with 1,6-hexanediol ethoxylate diacrylate for the separation of small molecules by capillary liquid chromatography. Talanta, 141: 103-110. DOI 10.1016/j.talanta.2015.03.064.

Alves, F., P. Scholder and I. Nischang, 2013. Conceptual design of large surface area porous polymeric hybrid media based on polyhedral oligomeric silsesquioxane precursors: Preparation, tailoring of porous properties, and internal surface functionalization. ACS applied materials & interfaces, 5(7): 2517-2526. Available from http://www.ncbi.nlm.nih.gov/pmc/articles/PMC3624795/. DOI 10.1021/am303048y.

Alwael, H., D. Connolly, P. Clarke, R. Thompson, B. Twamley, B. O'Connor and B. Paull, 2011. Pipette-tip selective extraction of glycoproteins with lectin modified gold nano-particles on a polymer monolithic phase. The Analyst, 136(12): 2619. DOI 10.1039/c1an15137a.

Arrua, R.D., M.C. Strumia and C.I. Alvarez Igarzabal, 2009. Macroporous monolithic polymers: Preparation and applications. Materials, 2(4): 2429-2466. DOI 10.3390/ma2042429.

Arvidsson, P., F.M. Plieva, I.N. Savina, V.I. Lozinsky, S. Fexby, L. Bülow, I. Yu. Galaev and B. Mattiasson, 2002. Chromatography of microbial cells using continuous supermacroporous affinity and ion-exchange columns. Journal of Chromatography A, 977(1): 27-38. DOI 10.1016/S0021-9673(02)01114-7.

Aydoğan, C., 2015. A new anion-exchange/hydrophobic monolith as stationary phase for nano liquid chromatography of small organic molecules and inorganic anions. Journal of Chromatography A, 1392: 63-68. Available from http://www.sciencedirect.com/science/article/pii/S0021967315003970. DOI http://dx.doi.org/10.1016/j.chroma.2015.03.014.

Bănică, F.G., 2012. Nucleic acids in chemical sensors. In: Chemical sensors and biosensors: Fundamentals and applications. John Wiley & Sons Inc, West Sussex, U.K: pp: 118-134.

Bisjak, C.P., L. Trojer, S.H. Lubbad, W. Wieder and G.K. Bonn, 2007. Influence of different polymerisation parameters on the separation efficiency of monolithic poly(phenyl acrylate- co-1,4-phenylene diacrylate) capillary columns. Journal of Chromatography A, 1154(1): 269-276. DOI 10.1016/j.chroma.2007.03.100.

Brgles, M., T. Kurtovic, L. Kovacic, I. Krizaj, M. Barut, M. Balija, G. Allmaier, M. Marchetti-Deschmann and B. Halassy, 2014. Identification of proteins interacting with ammodytoxins in vipera ammodytes ammodytes venom by immuno-affinity chromatography. Anal. Bioanal. Chem., 406(1): 293-304. DOI 10.1007/s00216-013-7453-5.

Brothier, F. and V. Pichon, 2014. Miniaturized DNA aptamer-based monolithic sorbent for selective extraction of a target analyte coupled on-line to nanolc. Analytical and bioanalytical chemistry, 406(30): 7875-7886. Available from http://www.ncbi.nlm.nih.gov/pubmed/25335821. DOI 10.1007/s00216-014-8256-z.

Chan, A.S., M.K. Danquah, D. Agyei, P.G. Hartley and Y. Zhu, 2014. A parametric study of a monolithic microfluidic system for on-chip biomolecular separation. Separation Science and Technology, 49(6): 854-860. DOI 10.1080/01496395.2013.872144.

Chan, A.S., M.K. Danquah, D. Agyei, P.G. Hartley and Y. Zhu, 2014. A simple microfluidic chip design for fundamental bioseparation. 2014. DOI 10.1155/2014/175457.

Chapuis-Hugon, F., A. du Boisbaudry, B. Madru and V. Pichon, 2011. New extraction sorbent based on aptamers for the determination of ochratoxin a in red wine. Analytical and bioanalytical chemistry, 400(5): 1199-1207. Available from http://www.ncbi.nlm.nih.gov/pubmed/21221554. DOI 10.1007/s00216-010-4574-y.

Chen, L., J. Ou, Z. Liu, H. Lin, H. Wang, J. Dong and H. Zou, 2015. Fast preparation of a highly efficient organic monolith via photo-initiated thiol-ene click polymerization for capillary liquid chromatography. Journal of Chromatography A, 1394: 103-110. DOI 10.1016/j.chroma.2015.03.054.

Connolly, D., B. Twamley and B. Paull, 2010. High-capacity gold nanoparticle functionalised polymer monoliths. Chemical communications, 46(12): 2109-2111. DOI 10.1039/b924152c.

Connor, A.C. and L.B. McGown, 2006. Aptamer stationary phase for protein capture in affinity capillary chromatography. Journal of Chromatography A, 1111(2): 115-119. DOI 10.1016/j.chroma.2005.05.012.

Dainiak, M.B., I.Y. Galaev and B. Mattiasson, 2006. Affinity cryogel monoliths for screening for optimal separation conditions and chromatographic separation of cells. Journal of chromatography. A, 1123(2): 145.

Danquah, M.K. and G.M. Forde, 2007. The suitability of deae-cl active groups on customized poly(gma-co-edma) continuous stationary phase for fast enzyme-free isolation of plasmid DNA. Journal of chromatography. B, Analytical technologies in the biomedical and life sciences, 853(1-2): 38-46. Available from

http://www.ncbi.nlm.nih.gov/pubmed/17400523.   DOI 10.1016/j.jchromb.2007.02.050.

Danquah, M.K. and G.M. Forde, 2008. Preparation of macroporous methacrylate monolithic material with convective flow properties for bioseparation: Investigating the kinetics of pore formation and hydrodynamic performance. Chemical   Engineering   Journal,   140(1-3):   593-599.   DOI 10.1016/j.cej.2008.02.012.

Danquah, M.K., J. Ho and G.M. Forde, 2008. A thermal expulsion approach to homogeneous large-volume methacrylate monolith preparation; enabling large-scale rapid purification of biomolecules. Journal of Applied Polymer Science, 109(4): 2426-2433. DOI 10.1002/app.28346.

de Lathouder, K., M. Smeltink, A. Straathof, M.A. Paasman, E. van de Sandt, F. Kapteijn and J. Moulijn, 2008. Hydrogel coated monoliths for enzymatic hydrolysis of penicillin g. J. Ind. Microbiol. Biotechnol., 35(8): 815-824. DOI 10.1007/s10295-008-0353-6.

Delplace, V., J. Nicolas, S. Harrisson, H.T. Ho, S. Pascual, L. Fontaine, A. Tardy and Y. Guillaneuf, 2015. One-step synthesis of azlactone-functionalized sg1-based alkoxyamine for nitroxide-mediated polymerization and bioconjugation. Macromolecules, 48(7): 2087-2097. DOI 10.1021/acs.macromol.5b00178.

Deng, N., Z. Liang, Y. Liang, Z. Sui, L. Zhang, Q. Wu, K. Yang, L. Zhang and Y. Zhang, 2012. Aptamer modified organic-inorganic hybrid silica monolithic capillary columns for highly selective recognition of thrombin. Analytical chemistry, 84(23):   10186-10190.   Available   from http://www.ncbi.nlm.nih.gov/pubmed/23137349. DOI 10.1021/ac302779u.

Deng, Q., I. German, D. Buchanan and R.T. Kennedy, 2001. Retention and separation of adenosine and analogues by affinity chromatography with an aptamer stationary phase. Analytical chemistry, 73(22): 5415-5421. DOI 10.1021/ac0105437.

Dick Jr, L.W., B.J. Swinteck and L.B. McGown, 2004. Albumins as a model system for investigating separations of closely related proteins on DNA stationary phases in capillary electrochromatography. Analytica chimica acta, 519(2): 197-205. Available   from http://www.sciencedirect.com/science/article/pii/S0003267004005409.   DOI http://dx.doi.org/10.1016/j.aca.2004.04.051.

Ding, S., C. Gao and L.-Q. Gu, 2009. Capturing single molecules of immunoglobulin and ricin with an aptamer-encoded glass nanopore. Analytical chemistry, 18(16): 6649.

Fang, L., S. Kulkarni, K. Alhooshani and A. Malik, 2007. Germania-based, sol-gel hybrid organic-inorganic coatings for capillary microextraction and gas chromatography. Analytical chemistry, 79(24): 9441-9451. DOI 10.1021/ac071056f.

Gagnon, P., 2012. Technology trends in antibody purification. Journal of chromatography. A, 1221: 57. DOI 10.1016/j.chroma.2011.10.034.

Gao, C., S. Ding, Q. Tan and L. Gu, 2009. Method of creating a nanopore-terminated probe for single-molecule enantiomer discrimination. Anal. Chem., 81(1): 80-86. DOI 10.1021/ac802348r.

Gao, C., X. Sun and A.T. Woolley, 2013. Fluorescent measurement of affinity binding between thrombin and its aptamers using on-chip affinity monoliths. Journal of chromatography.   A,   1291:   92-96.   Available   from

http://www.ncbi.nlm.nih.gov/pubmed/23587316.   DOI
10.1016/j.chroma.2013.03.063.

Gerster, P., E.-M. Kopecky, N. Hammerschmidt, M. Klausberger, F. Krammer, R.
Grabherr, C. Mersich, L. Urbas, P. Kramberger, T. Paril, M. Schreiner, K.
Nöbauer, E. Razzazi-Fazeli and A. Jungbauer, 2013. Purification of infective
baculoviruses by monoliths. Journal of Chromatography A, 1290: 36-45.
Available   from
http://www.sciencedirect.com/science/article/pii/S0021967313005128.   DOI
http://dx.doi.org/10.1016/j.chroma.2013.03.047.

Greiderer, A., L. Trojer, C.W. Huck and G. Bonn, 2009. Influence of the polymerisation
time on the porous and chromatographic properties of monolithic poly(1,2-bis(p-
vinylphenyl))ethane capillary columns. J. Chromatogr. A, 1216(45): 7747-7754.
DOI 10.1016/j.chroma.2009.08.084.

Guo, J. and G. Carta, 2015. Unfolding and aggregation of monoclonal antibodies on cation
exchange columns: Effects of resin type, load buffer, and protein stability. Journal
of Chromatography A. DOI 10.1016/j.chroma.2015.02.047.

Gutiérrez-Aguirre, I., M. Banjac, A. Steyer, M. Poljšak-Prijatelj, M. Peterka, A. Štrancar
and M. Ravnikar, 2009. Concentrating rotaviruses from water samples using
monolithic chromatographic supports. Journal of Chromatography A, 1216(13):
2700-2704. DOI 10.1016/j.chroma.2008.10.106.

Han, B., C. Zhao, J. Yin and H. Wang, 2012. High performance aptamer affinity
chromatography for single-step selective extraction and screening of basic protein
lysozyme. Journal of chromatography. B, Analytical technologies in the
biomedical   and   life   sciences,   903:   112-117.   Available   from
http://www.ncbi.nlm.nih.gov/pubmed/22841745.   DOI
10.1016/j.jchromb.2012.07.003.

Hasegawa, J., K. Kanamori, K. Nakanishi, T. Hanada and S. Yamago, 2009. Rigid
crosslinked polyacrylamide monoliths with well-defined macropores synthesized
by living polymerization. Macromolecular Rapid Communications, 30(12): 986-
990.   Available   from   http://dx.doi.org/10.1002/marc.200900066.   DOI
10.1002/marc.200900066.

Hee Seung, K. and S.H. David, 2005. Immobilization methods for affinity
chromatography. In: Handbook of affinity chromatography, second edition. CRC
Press: pp: 36-78.

Hemström, P., A. Nordborg, K. Irgum, F. Svec and J.M. Fréchet, 2006. Polymer-based
monolithic microcolumns for hydrophobic interaction chromatography of
proteins. Journal of separation science, 29(1): 25.

Hennion, M.-C. and V. Pichon, 2003. Immuno-based sample preparation for trace
analysis. Journal of Chromatography A, 1000(1): 29-52. DOI 10.1016/S0021-
9673(03)00529-6.

Hirano, T., S. Kitagawa and H. Ohtani, 2009. Methacrylate-ester-based reversed phase
monolithic columns for high speed separation prepared by low temperature uv
photo-polymerization. Analytical Sciences, 25(9): 1107-1113.

Hjerten, S., J. Liao and R. Zhang, 1989. High-performance liquid-chromatography on
continuous polymer beds. Journal Of Chromatography, 473(1): 273-275.

Jandera, P., M. Staňková, V. Škeříková and J. Urban, 2013. Cross-linker effects on the
separation efficiency on (poly)methacrylate capillary monolithic columns. Part i.

Reversed-phase liquid chromatography. Journal of Chromatography A, 1274(0): 97-106. Available from http://www.sciencedirect.com/science/article/pii/S0021967312018420. DOI http://dx.doi.org/10.1016/j.chroma.2012.12.003.

Ji, X., D. Li and H. Li, 2015. Preparation and application of a novel molecularly imprinted solid-phase microextraction monolith for selective enrichment of cholecystokinin neuropeptides in human cerebrospinal fluid. Biomedical Chromatography. DOI 10.1002/bmc.3418.

Jiang, T., R. Mallik and D.S. Hage, 2005. Affinity monoliths for ultrafast immunoextraction. Analytical chemistry, 77(8): 2362-2372.

Josić, D. and A. Buchacher, 2001. Application of monoliths as supports for affinity chromatography and fast enzymatic conversion. Journal of Biochemical and Biophysical Methods, 49(1): 153-174. DOI 10.1016/S0165-022X(01)00195-6.

Jungbauer, A. and R. Hahn, 2008. Polymethacrylate monoliths for preparative and industrial separation of biomolecular assemblies. Journal of chromatography. A, 1184(1-2): 62-79. Available from http://www.ncbi.nlm.nih.gov/pubmed/18241874. DOI 10.1016/j.chroma.2007.12.087.

Jungreuthmayer, C., P. Steppert, G. Sekot, A. Zankel, H. Reingruber, J. Zanghellini and A. Jungbauer, 2015. The 3d pore structure and fluid dynamics simulation of macroporous monoliths: High permeability due to alternating channel width. Journal of Chromatography A, 1425: 141-149.

Katayama, H., A. Shimasaki and S. Ohgaki, 2002. Development of a virus concentration method and its application to detection of enterovirus and norwalk virus from coastal seawater. Applied and environmental microbiology, 68(3): 1033.

Kim, H.S. and D.S. Hage, 2006. Immobilization methods for affinity chromatography. Handbook of Affinity Chromatography: 35-78.

Kovač, K., I. Gutiérrez-Aguirre, M. Banjac, M. Peterka, M. Poljšak-Prijatelj, M. Ravnikar, J.Z. Mijovski, A.C. Schultz and P. Raspor, 2009. A novel method for concentrating hepatitis a virus and caliciviruses from bottled water. Journal of virological methods, 162(1): 272-275. DOI 10.1016/j.jviromet.2009.07.013.

Kramberger, P., R.C. Honour, R.E. Herman, F. Smrekar and M. Peterka, 2010. Purification of the staphylococcus aureus bacteriophages vdx-10 on methacrylate monoliths. Journal of virological methods, 166(1): 60-64. DOI 10.1016/j.jviromet.2010.02.020.

Kramberger, P., L. Urbas and A. Štrancar, 2015. Downstream processing and chromatography based analytical methods for production of vaccines, gene therapy vectors, and bacteriophages. Human Vaccines & Immunotherapeutics, 11(4): 1010-1021. DOI 10.1080/21645515.2015.1009817.

Kucheyev, S.O., T.F. Baumann, Y.M. Wang, T.v. Buuren, J.F. Poco, J.H. Satcher, Jr and A.V. Hamza, 2006. Monolithic, high surface area, three-dimensional geo nanostructures. Applied Physics Letters, 88: 103117. DOI 10.1063/1.2182064.

Kumar, A., F.M. Plieva, I.Y. Galaev and B. Mattiasson, 2003. Affinity fractionation of lymphocytes using a monolithic cryogel. Journal of Immunological Methods, 283(1): 185-194. DOI 10.1016/j.jim.2003.09.017.

Leinweber, F.C., D. Lubda, K. Cabrera and U. Tallarek, 2002. Characterization of silica-based monoliths with bimodal pore size distribution. Analytical chemistry, 74(11): 2470-2477.

Leinweber, F.C. and U. Tallarek, 2003. Chromatographic performance of monolithic and particulate stationary phases: Hydrodynamics and adsorption capacity. Journal of Chromatography A, 1006(1): 207-228. DOI 10.1016/S0021-9673(03)00391-1.

Lendero, N., J. Vidič, P. Brne, A. Podgornik and A. Štrancar, 2005. Simple method for determining the amount of ion-exchange groups on chromatographic supports. Journal of Chromatography A, 1065(1): 29-38. DOI 10.1016/j.chroma.2004.10.072.

Liang, C., S. Dai and G. Guiochon, 2003. A graphitized-carbon monolithic column. Analytical chemistry, 75(18): 4904.

Lin, L., S. Liu, Z. Nie, Y. Chen, C. Lei, Z. Wang, C. Yin, H. Hu, Y. Huang and S. Yao, 2015. Automatic and integrated micro-enzyme assay (aiμea) platform for highly sensitive thrombin analysis via an engineered fluorescence protein-functionalized monolithic capillary column. Analytical chemistry, 87: 4552-4559. DOI 10.1021/acs.analchem.5b00723.

Liu, K., Z. Wen, N. Li, W. Yang, L. Hu, J. Wang, Z. Yin, X. Dong and J. Li, 2012. Purification and concentration of mycobacteriophage d29 using monolithic chromatographic columns. Journal of virological methods, 186(1-2): 7-13. DOI 10.1016/j.jviromet.2012.07.016.

Ma, J., Z. Liang, X. Qiao, Q. Deng, D. Tao, L. Zhang and Y. Zhang, 2008. Organic−inorganic hybrid silica monolith based immobilized trypsin reactor with high enzymatic activity. Analytical chemistry, 80(8): 2949-2956. Available from http://dx.doi.org/10.1021/ac702343a. DOI 10.1021/ac702343a.

Madru, B., F. Chapuis-Hugon and V. Pichon, 2011. Novel extraction supports based on immobilised aptamers: Evaluation for the selective extraction of cocaine. Talanta, 85(1): 616-624. Available from http://www.ncbi.nlm.nih.gov/pubmed/21645749. DOI 10.1016/j.talanta.2011.04.016.

Mai, J., V. Abhyankar, M.E. Piccini, J.P. Olano, R. Willson and A. Hatch, 2014. Rapid detection of trace bacteria in biofluids using porous monoliths in microchannels. Biosens. Bioelectron., 54: 435-441. DOI 10.1016/j.bios.2013.11.012.

Mallik, R. and D.S. Hage, 2006. Affinity monolith chromatography. Journal of separation science, 29(12): 1686-1704.

Mallik, R., T. Jiang and D.S. Hage, 2004. High-performance affinity monolith chromatography: Development and evaluation of human serum albumin columns. Analytical chemistry, 76(23): 7013.

Mayr, B., G. Hölzl, K. Eder, M.R. Buchmeiser and C.G. Huber, 2002. Hydrophobic, pellicular, monolithic capillary columns based on cross-linked polynorbornene for biopolymer separations. Analytical chemistry, 74(23): 6080-6087.

Mihelic, I., M. Krajnc, T. Koloini and A. Podgornik, 2001. Kinetic model of a methacrylate-based monolith polymerization. Ind. Eng. Chem. Res., 40(16): 3495-3501.

Mihelič, I., D. Nemec, A. Podgornik and T. Koloini, 2005. Pressure drop in cim disk monolithic columns. Journal of Chromatography A, 1065(1): 59-67.

Minakuchi, H., K. Nakanishi, N. Soga, N. Ishizuka and N. Tanaka, 1997. Effect of skeleton size on the performance of octadecylsilylated continuous porous silica

columns in reversed-phase liquid chromatography. Journal of Chromatography A, 762(1): 135-146. DOI 10.1016/S0021-9673(96)00944-2.

Nandakumar, M.P., E. Pålsson, P.-E. Gustavsson, P.-O. Larsson and B. Mattiasson, 2000. Superporous agarose monoliths as mini-reactors in flow injection systems. Bioseparation, 9(4): 193-202.

Neff, S. and A. Jungbauer, 2011. Monolith peptide affinity chromatography for quantification of immunoglobulin m. Journal of Chromatography A, 1218(17): 2374-2380. DOI 10.1016/j.chroma.2010.10.053.

Nischang, I., 2013. Porous polymer monoliths: Morphology, porous properties, polymer nanoscale gel structure and their impact on chromatographic performance. Journal of Chromatography A, 1287: 39-58.

Nischang, I., I. Teasdale and O. Brüggemann, 2010. Towards porous polymer monoliths for the efficient, retention-independent performance in the isocratic separation of small molecules by means of nano-liquid chromatography. Journal of Chromatography A, 1217(48): 7514-7522. Available from http://www.sciencedirect.com/science/article/pii/S0021967310013427. DOI http://dx.doi.org/10.1016/j.chroma.2010.09.077.

Oberacher, H., A. Premstaller and C.G. Huber, 2004. Characterization of some physical and chromatographic properties of monolithic poly(styrene–co-divinylbenzene) columns. Journal of Chromatography A, 1030(1): 201-208. DOI 10.1016/j.chroma.2004.01.009.

Oksanen, H.M., A. Domanska and D. Bamford, 2012. Monolithic ion exchange chromatographic methods for virus purification. Virology, 434(2): 271-277. DOI 10.1016/j.virol.2012.09.019.

Ongkudon, C.M. and M.K. Danquah, 2010. Process optimisation for anion exchange monolithic chromatography of 4.2 kbp plasmid vaccine (pcdna3f). Journal of Chromatography B, 878(28): 2719-2725. DOI 10.1016/j.jchromb.2010.08.011.

Ongkudon, C.M. and M.K. Danquah, 2011. Anion exchange chromatography of 4.2kbp plasmid based vaccine (pcdna3f) from alkaline lysed e. Coli lysate using amino functionalised polymethacrylate conical monolith. Separation and Purification Technology, 78(3): 303-310. DOI 10.1016/j.seppur.2011.01.039.

Ongkudon, C.M., T. Kansil and C. Wong, 2014. Challenges and strategies in the preparation of large-volume polymer-based monolithic chromatography adsorbents. Journal of separation science, 37(5): 455-464.

Ongkudon, C.M., S. Pan and M.K. Danquah, 2013. An innovative monolithic column preparation for the isolation of 25 kilo base pairs DNA. Journal of chromatography. A, 1318: 156-162. Available from http://www.ncbi.nlm.nih.gov/pubmed/24209297. DOI 10.1016/j.chroma.2013.10.011.

Ott, S., R. Niessner and M. Seidel, 2011. Preparation of epoxy-based macroporous monolithic columns for the fast and efficient immunofiltration of staphylococcus aureus. Journal of separation science, 34(16-17): 2181-2192. DOI 10.1002/jssc.201100208.

Pan, Z., H. Zou, W. Mo, X. Huang and R. Wu, 2002. Protein a immobilized monolithic capillary column for affinity chromatography. Analytica chimica acta, 466(1): 141-150. DOI 10.1016/S0003-2670(02)00511-1.

Peskoller, C., R. Niessner and M. Seidel, 2009. Development of an epoxy-based monolith used for the affinity capturing of eschericha coli bacteria. Journal of Chromatography A, 1216(18): 3794-3801.

Peterson, D.S., T. Rohr, F. Svec and J.M. Frechet, 2002. High-throughput peptide mass mapping using a microdevice containing trypsin immobilized on a porous polymer monolith coupled to maldi tof and esi tof mass spectrometers. Journal of proteome research, 1(6): 563-568.

Pfaunmiller, E., M. Paulemond, C. Dupper and D. Hage, 2013. Affinity monolith chromatography: A review of principles and recent analytical applications. Analytical and bioanalytical chemistry, 405(7): 2133-2145. DOI 10.1007/s00216-012-6568-4.

Pichon, V., F. Brothier and A. Combes, 2015. Aptamer-based-sorbents for sample treatment-a review. Anal. Bioanal. Chem., 407: 681-698. DOI 10.1007/s00216-014-8129-5.

Podgornik, A., M. Barut, A. Štrancar, D. Josic and T. Koloini, 2000. Construction of large-volume monolithic columns. Analytical chemistry, 72(22): 5693-5699.

Podgornik, A. and N.L. Krajnc, 2012. Application of monoliths for bioparticle isolation. Journal of separation science, 35(22): 3059-3072.

Podgornik, A., V. Smrekar, P. Krajnc and A. Strancar, 2013. Estimation of methacrylate monolith binding capacity from pressure drop data. Journal of chromatography. A, 1272: 50-55. Available from http://www.ncbi.nlm.nih.gov/pubmed/23261298. DOI 10.1016/j.chroma.2012.11.057.

Podgornik, A., J. Vidic, J. Jancar, N. Lendero, V. Frankovic and A. Strancar, 2005. Noninvasive methods for characterization of large-volume monolithic chromatographic columns. Chem. Eng. Technol., 28(11): 1435-1441. DOI 10.1002/ceat.200500170.

Podgornik, A., S. Yamamoto, M. Peterka and N.L. Krajnc, 2013. Fast separation of large biomolecules using short monolithic columns. Journal of chromatography. B, Analytical technologies in the biomedical and life sciences, 927: 80-89. Available from http://www.ncbi.nlm.nih.gov/pubmed/23465515. DOI 10.1016/j.jchromb.2013.02.004.

Qin, W., H. Lü and Z. Xie, 2014. Preparation and evaluation of o -phenanthroline immobilized on a hybrid silica monolith modified with ionic liquids for reversed-phase pressurized capillary electrochromatography. Journal of separation science, 37(24): 3722-3728. DOI 10.1002/jssc.201400773.

Roberts, M.W., C.M. Ongkudon, G.M. Forde and M.K. Danquah, 2009. Versatility of polymethacrylate monoliths for chromatographic purification of biomolecules. Journal of separation science, 32(15-16): 2485-2494. Available from http://www.ncbi.nlm.nih.gov/pubmed/19603394. DOI 10.1002/jssc.200900309.

Ruščić, J., I. Gutiérrez-Aguirre, M. Tušek Žnidarič, S. Kolundžija, A. Slana, M. Barut, M. Ravnikar and M. Krajačić, 2015. A new application of monolithic supports: The separation of viruses from one another. Journal of Chromatography A. DOI 10.1016/j.chroma.2015.01.097.

Santora, B.P., M.R. Gagné, K.G. Moloy and N.S. Radu, 2001. Porogen and cross-linking effects on the surface area, pore volume distribution, and morphology of macroporous polymers obtained by bulk polymerization §. Macromolecules, 34(3): 658-661. DOI 10.1021/ma0004817.

Sharma, V.K., J. Glick and P. Vouros, 2012. Reversed-phase ion-pair liquid chromatography electrospray ionization tandem mass spectrometry for separation, sequencing and mapping of sites of base modification of isomeric oligonucleotide adducts using monolithic column. Journal of Chromatography A, 1245(0): 65-74. Available from http://www.sciencedirect.com/science/article/pii/S0021967312007054. DOI http://dx.doi.org/10.1016/j.chroma.2012.05.003.

Sinitsyna, E.S., J.G. Walter, E.G. Vlakh, F. Stahl, C. Kasper and T.B. Tennikova, 2012. Macroporous methacrylate-based monoliths as platforms for DNA microarrays. Talanta, 93: 139-146. DOI 10.1016/j.talanta.2012.01.064.

Staňková, M., P. Jandera, V. Škeříková and J. Urban, 2013. Cross-linker effects on the separation efficiency on (poly)methacrylate capillary monolithic columns. Part ii. Aqueous normal-phase liquid chromatography. Journal of Chromatography A, 1289(0): 47-57. Available from http://www.sciencedirect.com/science/article/pii/S0021967313004639. DOI http://dx.doi.org/10.1016/j.chroma.2013.03.025.

Svec, F., 2004. Preparation and hplc applications of rigid macroporous organic polymer monoliths. Journal of separation science, 27(10-11): 747-766. DOI 10.1002/jssc.200401721.

Svec, F., 2010. Porous polymer monoliths: Amazingly wide variety of techniques enabling their preparation. Journal of Chromatography A, 1217(6): 902-924.

Svec, F., 2012. Quest for organic polymer-based monolithic columns affording enhanced efficiency in high performance liquid chromatography separations of small molecules in isocratic mode. Journal of Chromatography A, 1228: 250-262.

Svec, F. and J.M.J. Fréchet, 1995. Modified poly(glycidyl metharylate-co-ethylene dimethacrylate) continuous rod columns for preparative-scale ion-exchange chromatography of proteins. Journal of Chromatography A, 702(1–2): 89-95. Available from http://www.sciencedirect.com/science/article/pii/0021967394010216. DOI http://dx.doi.org/10.1016/0021-9673(94)01021-6.

Svec, F. and J.M.J. Fréchet, 1995. Temperature, a simple and efficient tool for the control of pore size distribution in macroporous polymers. Macromolecules, 28(22): 7580-7582.

Szumski, M. and B. Buszewski, 2009. Effect of temperature during photopolymerization of capillary monolithic columns. J. Sep. Sci., 32(15-16): 2574-2581. DOI 10.1002/jssc.200900220.

Tang, S., Y. Guo, C. Xiong, S. Liu, X. Liu and S. Jiang, 2014. Nanoparticle-based monoliths for chromatographic separations. The Analyst, 139(17): 4103-4117.

Tennikova, T.B., M. Bleha, F. Švec, T.V. Almazova and B.G. Belenkii, 1991. High-performance membrane chromatography of proteins, a novel method of protein separation. Journal of Chromatography A, 555(1–2): 97-107. Available from http://www.sciencedirect.com/science/article/pii/S0021967301871703. DOI http://dx.doi.org/10.1016/S0021-9673(01)87170-3.

Tripp, J.A., F. Svec, J.M. Fréchet, S. Zeng, J.C. Mikkelsen and J.G. Santiago, 2004. High-pressure electroosmotic pumps based on porous polymer monoliths. Sensors and Actuators B: Chemical, 99(1): 66-73.

Trojer, L., C.P. Bisjak, W. Wieder and G.K. Bonn, 2009. High capacity organic monoliths for the simultaneous application to biopolymer chromatography and the separation of small molecules. Journal of Chromatography A, 1216(35): 6303-6309. Available from http://www.sciencedirect.com/science/article/pii/S0021967309010449. DOI http://dx.doi.org/10.1016/j.chroma.2009.07.010.

Unger, K.K., R. Skudas and M.M. Schulte, 2008. Particle packed columns and monolithic columns in high-performance liquid chromatography-comparison and critical appraisal. Journal of Chromatography A, 1184(1): 393-415.

Urban, J. and P. Jandera, 2008. Polymethacrylate monolithic columns for capillary liquid chromatography. Journal of separation science, 31(14): 2521-2540.

Urban, J., F. Svec and J.M.J. Fréchet, 2010. Hypercrosslinking: New approach to porous polymer monolithic capillary columns with large surface area for the highly efficient separation of small molecules. Journal of Chromatography A, 1217(52): 8212-8221. DOI 10.1016/j.chroma.2010.10.100.

Urbas, L., B. Košir, M. Peterka, B. Pihlar, A. Štrancar and M. Barut, 2011. Reversed phase monolithic analytical columns for the determination of ha1 subunit of influenza virus haemagglutinin. Journal of Chromatography A, 1218(17): 2432-2437. DOI 10.1016/j.chroma.2010.12.082.

Urthaler, J., R. Schlegl, A. Podgornik, A. Strancar, A. Jungbauer and R. Necina, 2005. Application of monoliths for plasmid DNA purification: Development and transfer to production. Journal of Chromatography A, 1065(1): 93-106.

Vervoort, N., H. Saito, K. Nakanishi and G. Desmet, 2005. Experimental validation of the tetrahedral skeleton model pressure drop correlation for silica monoliths and the influence of column heterogeneity. Analytical chemistry, 77(13): 3986-3992.

Vidič, J., A. Podgornik, J. Jančar, V. Frankovič, B. Košir, N. Lendero, K. Čuček, M. Krajnc and A. Štrancar, 2007. Chemical and chromatographic stability of methacrylate-based monolithic columns. Journal of Chromatography A, 1144(1): 63-71. Available from http://www.sciencedirect.com/science/article/pii/S0021967306021327. DOI http://dx.doi.org/10.1016/j.chroma.2006.11.030.

Viklund, C., A. Nordstrom, K. Irgum, F. Svec and J. Frechet, 2001. Preparation of porous poly(styrene-co-divinylbenzene) monoliths with controlled pore size distributions initiated by stable free radicals and their pore surface functionalization by grafting. Macromolecules, 34(13): 4361-4369.

Vizioli, N., M. Rusell, M. Carbajal, C. Carducci and M. Grasselli, 2005. On-line affinity selection of histidine-containing peptides using a polymeric monolithic support for capillary electrophoresis. Electrophoresis, 26(15): 2942-2948. DOI 10.1002/elps.200410416.

Vonk, R., S. Wouters, A. Barcaru, G. Vivó-Truyols, S. Eeltink, L. Koning and P. Schoenmakers, 2015. Post-polymerization photografting on methacrylate-based monoliths for separation of intact proteins and protein digests with comprehensive two-dimensional liquid chromatography hyphenated with high-resolution mass spectrometry. Analytical and bioanalytical chemistry, 407(13): 3817-3829. DOI 10.1007/s00216-015-8615-4.

Walsh, Z., B. Paull and M. Macka, 2012. Inorganic monoliths in separation science: A review. Analytica chimica acta, 750: 28-47. Available from

http://www.sciencedirect.com/science/article/pii/S0003267012006241. DOI http://dx.doi.org/10.1016/j.aca.2012.04.029.

Wang, H., J. Ou, H. Lin, Z. Liu, G. Huang, J. Dong and H. Zou, 2014. Chromatographic assessment of two hybrid monoliths prepared via epoxy-amine ring-opening polymerization and methacrylate-based free radical polymerization using methacrylate epoxy cyclosiloxane as functional monomer. Journal of Chromatography A, 1367: 131-140. DOI 10.1016/j.chroma.2014.09.072.

Wang, Z., J.-c. Zhao, H.-z. Lian and H.-y. Chen, 2015. Aptamer-based organic-silica hybrid affinity monolith prepared via "thiol-ene" click reaction for extraction of thrombin. Talanta, 138: 52-58. Available from http://www.sciencedirect.com/science/article/pii/S003991401500082X. DOI http://dx.doi.org/10.1016/j.talanta.2015.02.009.

Xiaoxia, S., F. Takashi and U. Hiroshi, 2013. Fabrication of a poly(vinyl alcohol) monolith via thermally impacted non-solvent-induced phase separation. Polymer Journal, 45(10): 1101. DOI 10.1038/pj.2013.18.

Xu, Q. and M.A. Anderson, 1994. Sol–gel route to synthesis of microporous ceramic membranes: Preparation and characterization of microporous tio2 and zro2 xerogels. Journal of the American Ceramic Society, 77(7): 1939-1945.

Yang, R., J.V. Pagaduan, M. Yu and A.T. Woolley, 2015. On chip preconcentration and fluorescence labeling of model proteins by use of monolithic columns: Device fabrication, optimization, and automation. Analytical and bioanalytical chemistry, 407(3): 737-747. Available from http://www.ncbi.nlm.nih.gov/pubmed/25012353. DOI 10.1007/s00216-014-7988-0.

Yang, X., L. Tan, L. Xia, C.D. Wood and B. Tan, 2015. Hierarchical porous polystyrene monoliths from polyhipe. Macromolecular rapid communications, 36(17): 1553-1558.

Yu, S., J. Geng, P. Zhou, J. Wang, X. Chen and J. Hu, 2008. New hydroxyapatite monolithic column for DNA extraction and its application in the purification of bacillus subtilis crude lysate. Journal of Chromatography A, 1183(1): 29-37.

Yuan, H., L. Zhang and Y. Zhang, 2014. Preparation of high efficiency and low carry-over immobilized enzymatic reactor with methacrylic acid–silica hybrid monolith as matrix for on-line protein digestion. Journal of Chromatography A, 1371: 48-57.

Zajickova, Z., E. Rubi and F. Svec, 2011. In situ sol–gel preparation of porous alumina monoliths for chromatographic separations of adenosine phosphates. Journal of Chromatography A, 1218(22): 3555-3558. Available from http://www.sciencedirect.com/science/article/pii/S0021967311004171. DOI http://dx.doi.org/10.1016/j.chroma.2011.03.054.

Zaveckas, M., S. Snipaitis, H. Pesliakas, J. Nainys and A. Gedvilaite, 2015. Purification of recombinant virus-like particles of porcine circovirus type 2 capsid protein using ion-exchange monolith chromatography. Journal of Chromatography B, 991: 21-28. DOI 10.1016/j.jchromb.2015.04.004.

Zhang, A., F. Ye, J. Lu and S. Zhao, 2013. Screening alpha-glucosidase inhibitor from natural products by capillary electrophoresis with immobilised enzyme onto polymer monolith modified by gold nanoparticles. Food chemistry, 141(3): 1854-

1859. Available from http://www.ncbi.nlm.nih.gov/pubmed/23870901. DOI 10.1016/j.foodchem.2013.04.100.

Zhang, J., G. Chen, M.M. Tian, R.G. Li, X. Quan and Q. Jia, 2013. A novel organic-inorganic hybrid monolithic column prepared in-situ in a microchip and its application for the determination of 2-amino-4-chlorophenol in chlorzoxazone tablets. Talanta, 115: 801-805. DOI 10.1016/j.talanta.2013.06.058.

Zhao, Q., X. Li, Y. Shao and X.C. Le, 2008. Aptamer-based affinity chromatographic assays for thrombin. Anal. Chem., 80(19): 7586-7593. DOI 10.1021/ac801206s.

Zhao, Q., M. Wu, X. Chris Le and X.-F. Li, 2012. Applications of aptamer affinity chromatography. TrAC Trends in Analytical Chemistry, 41: 46-57. DOI 10.1016/j.trac.2012.08.005.

Zou, H., X. Huang, M. Ye and Q. Luo, 2002. Monolithic stationary phases for liquid chromatography and capillary electrochromatography. Journal of Chromatography A, 954(1): 5-32. DOI 10.1016/S0021-9673(02)00072-9.

SECTION 2.2

SELEX Modifications and Bioanalytical Techniques for Aptamer–Target Binding Characterization

Sing Y. Tan, **Caleb Acquah**, Amandeep Sidhu, Clarence M. Ongkudon, Lau Sie Yon, Michael K. Danquah,

DECLARATION FOR THESIS SECTION 2.2

SELEX Modifications and Bioanalytical Techniques for Aptamer–Target Binding Characterization

The candidate will like to declare that there is no conflict of interests involved in this work and that my extent of contribution as candidate is as shown below:

Contribution of Candidate	Conceptualisation, initiation and write-up	40%

The following co-authors were involved in the development of this publication and attest to the candidate's contribution to a joint publication as part of his thesis. Permission by co-authors are as follows:

Name	Signature	Date
Michael K. Danquah		13.07.2017
Lau Sie Yon		13.07.2017
Amandeep Sidhu		18.07.2017
Clarence M. Ongkudon		13.07.2017
Sze Y. Tan		13.07.2017

ABSTRACT

The quest to improve the detection of biomolecules and cells in health and life sciences has led to the discovery and characterisation of various affinity bioprobes. Libraries of synthetic oligonucleotides (ssDNA/ssRNA) with randomized sequences are employed during Systematic Evolution of Ligands by Exponential enrichment (SELEX) to select highly specific affinity probes called aptamers. With much focus on the generation of aptamers for a variety of target molecules, conventional SELEX protocols have been modified to develop new and improved SELEX protocols yielding highly specific and stable aptamers. Various techniques have been used to analyse the binding interactions between aptamers and their cognate molecules with associated merits and limitations. This article comprehensively reviews research advancements in the generation of aptamers, analyses physicochemical conditions affecting their binding characteristics to cellular and biomolecular targets, and discusses various field applications of aptameric binding. Biophysical techniques employed in the characterisation of the molecular and binding features of aptamers to their cognate targets are also discussed.

Keywords: Aptamer; SELEX; Biophysical Techniques; Biomolecules; Cellular Targets.

1. INTRODUCTION

The drive to improve preventive healthcare delivery through pathogen detection has resulted in tremendous research into the development of ligands such as monoclonal antibodies and subsequently aptamers. Monoclonal antibodies are protein-based ligands produced via *in vivo* processes with significant biochemical limitations. Unlike antibodies, nucleic acid aptamers are single stranded oligonucleotides selected *in vitro* by means of a stringent iterative procedure known as Systematic Evolution of Ligands by Exponential enrichment (SELEX) (Ellington and Szostak, 1990; Robertson and Joyce, 1990; Tuerk and Gold, 1990). DNA/RNA aptamers have a high binding specificity, can be generated for an infinite pool of biological targets irrespective of their biochemical characteristics, are modifiable with functional moieties, easily immobilised on solid support systems, have an inexpensive production process, are chemically stable, can be molecularly engineered to possess a longer life span, and can be subjected to frequent denaturation and renaturation processes without affecting their affinity binding potential (Jayasena, 1999; Andrea *et al.*, 2011; Acquah *et al.*, 2015). Owing to these competitive advantages, aptamers are heralding innovations in biomarker development for applications in diverse fields such as cell targeting in therapeutic delivery, clinical diagnosis and prognosis, detection of environmental-related targets, mitigation of biotoxins and illicit drugs such as cocaine. Despite their superior traits, the application of aptamers is fraught with a number of setbacks ranging from SELEX, standardisation protocols and in their applications documented in the literature (Baird, 2010; McKeague and Derosa, 2012; Acquah *et al.*, 2015)

Various advances have been made in the application of SELEX for the development of aptamers. These advancements include modifying the library domain, elimination of non-specific binding, targeting of complex/living cells, modification of the selection and partitioning steps, and sequencing (McKeague and Derosa, 2012; Sun and Zu, 2015). Aquino-Jarquin and Toscano-Garibay (2011) previously did a comprehensive discussion solely on the history of SELEX and their modifications. McKeague and Derosa (2012) also reviewed the generation and application of aptamers for small target molecules. Also, a description of the advances made in SELEX was also presented though the analysis was

mainly geared towards small target molecules. Sun and Zu (2015) recently discussed various chemical and structural modification techniques applied to enhance the bioavailability of aptamers as well as achieving a rapid SELEX technology. In addition, Darmostuk *et al.* (2015) presented a comprehensive discussion on SELEX covering conventional assays, advancements, post-SELEX modifications and aptamer databases. Whilst all these previously reported articles focus on SELEX advancements, none discusses aptamer generation in relation to binding features, analytical characterisation and the effects of physicochemical conditions on affinity performance. This relationship is necessary to engineer the binding characteristics of aptamers for enhanced binding performance. Aptamers have distinct secondary structures together with their primary sequence that enable high specific interaction with their cognate target to form complexes. A unique stable structure is formed as a tertiary complex with the complementary target (Abe *et al.*, 2011; Santosh and Yadava, 2014). Remarkably, aptamer-target affinity interaction is affected by the pH, ionic strength, and the temperature of the binding medium (Hianik *et al.*, 2007; Li *et al.*, 2008; Lin *et al.*, 2011; Kang *et al.*, 2012; Krishnan *et al.*, 2013; Chang *et al.*, 2014)**,** and these can be characterized using techniques such as: Isothermal Titration Calorimetry (ITC), Capillary Electrophoresis (CE), Circular Dichroism (CD), Microscale Thermophoresis (MST), Quartz Crystal Microbalance (QCM), Photonic Crystal Surface Wave (PC SW) and Surface Plasmon Resonance (SPR). Whereas CE and CD are used to determine conformational changes of bound aptamers upon binding (Girardot *et al.*, 2010; Lin *et al.*, 2011), QCM, PC SW, MST and SPR provide real-time monitoring of the affinity interactions and associated kinetics devoid of labelling (Konopsky and Alieva, 2009; Chang *et al.*, 2014; Tatarinova *et al.*, 2014). In addition, they are not affected by background signals arising from aptamer labelling which can potentially distort the molecular conformation of the aptamer. However, the challenge lies in effectively coupling the aptamer to a solid detection surface without compromising on the binding affinity (Hianik *et al.*, 2007; Lin *et al.*, 2011). MST and ITC are used to study the thermodynamic characteristics of the aptamer binding process (Lin *et al.*, 2011; Chang *et al.*, 2014). MST technology offers precise and real-time results devoid of molecular labelling by employing inherent fluorescence properties of one of the binding species (Entzian and Schubert, 2015; Stoltenburg *et al*., 2015). This article presents an

extensive discussion covering the generation of aptamers via SELEX and its modifications, biophysical techniques necessary to characterise aptamer-target binding, and physicochemical conditions that can affect binding potency and specificity. It aims at highlighting the synergies between the relevant areas of aptamer science, thus formulating a fundamental understanding essential to optimise the performance of aptameric binding post-SELEX.

2. SYSTEMATIC EVOLUTION OF LIGANDS BY EXPONENTIAL ENRICHMENT (SELEX)

Contrary to the natural biological approach of synthesizing oligonucleotide sequences, i*n vitro* chemical synthesis, pioneered by Todd and Michelson, proceeded in the 3' to 5' direction. Chemically synthesized RNA/DNA oligonucleotides are used as precursors in setting up a randomised library for SELEX to expedite the simulation and evolution of synthetic ligands with high affinity. Thus, making SELEX technology advantageous in terms of chemical modifications of oligonucleotides prior to SELEX, avoidance of animal ethic issues and cost of production. Notably, the use of RNA oligonucleotides takes a longer time for the selection of aptamer sequences in SELEX as compared to DNA libraries. This is attributed to the reverse transcription of RNA molecules into cDNA molecules to enable sequencing and amplification before being transcribed from cDNA into an RNA molecule (Tuerk and Gold, 1990).

2.1 Conventional SELEX

SELEX is a stringent *in vitro* process for rapid selective development of single stranded oligonucleotides termed as aptamers from nucleic acid libraries. The generated aptamers are characterised by a low dissociation, K_d, thus possess the capacity to bind strongly to their cognate targets compared to antibodies. In general, SELEX protocol has 4 main steps namely; variation, selection, partition and amplification (Tuerk and Gold, 1990; Yang *et al.*, 2007). The variation step involves the generation of random combinatorial libraries of nucleic acid sequences up to 10^{16}. The synthesized combinatorial libraries have random sequences flanked at either ends with fixed 3' and 5' primers. The length of the sequence is often within 20-40bp (Guo *et al.*, 2008). The libraries are incubated with the target

molecules under specified conditions of buffer composition and temperature. Non-selected sequences are partitioned from the selected ones by washing with a suitable reagent, leaving the bound sequences on the immobilised targets, which are also subsequently eluted. Separation techniques such as membrane filtration and affinity chromatography are employed during the partitioning step to identify the bound sequences (Yang *et al.*, 2007; Pinto *et al.*, 2014). The bound sequences are eluted and amplified by PCR or RT-PCR (specifically for RNA aptamers). The stringency of elution (temperature, pH and buffer compositions) is increased through successive cycles of SELEX. The iterative process of selection and amplification proceeds (often ≤15 cycles) (Han, 2013; Radom *et al.*, 2013) to obtain an enriched pool, otherwise known as candidate aptamers (Pinto *et al.*, 2014). The candidate aptamers are then cloned, sequenced and analysed to obtain a selected aptamer with the best binding affinity and specificity towards the target (Andrew and Jack, 1990; Stoltenburg *et al.*, 2007). The selected aptamer is then chemically synthesized for further characterisations and applications. The type of target and the stringency of the conditions employed during the iterative process determine the total number of aptamers generated during cloning and sequence analysis (Stoltenburg *et al.*, 2007). The schematic iterative process is presented in Figure 1.
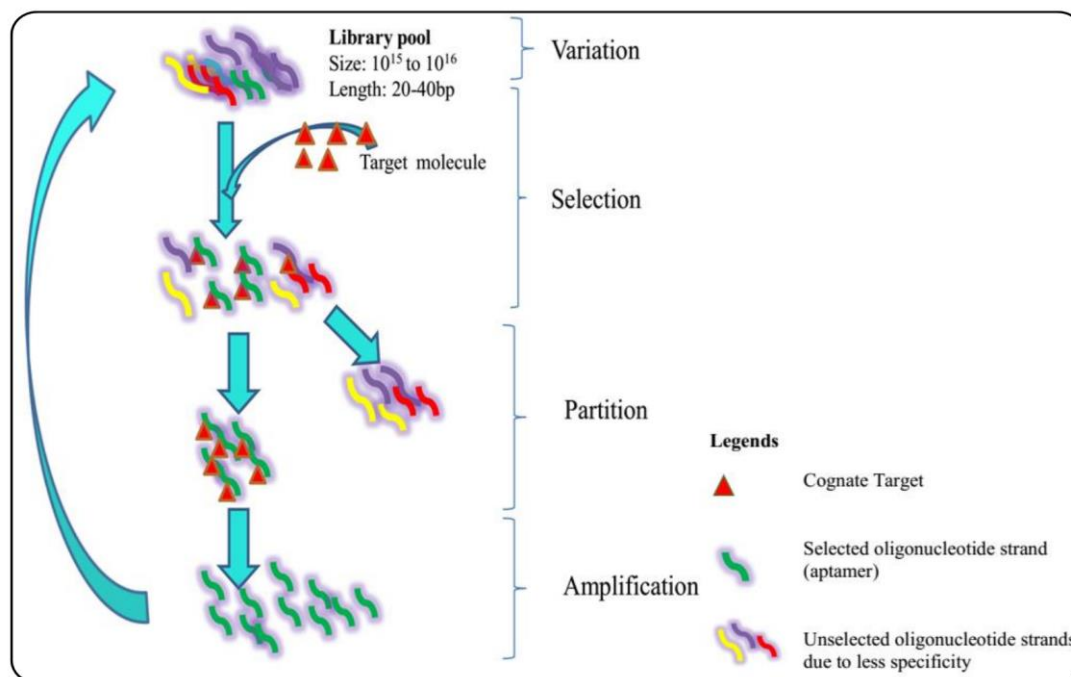
Figure 1. Schematic description of SELEX showing four repetitive steps; variation, selection, partition and amplification.

2.2 Advancement in SELEX Technology

Conventional SELEX technology is notably fraught with a significant number of challenges. Some of these challenges include (i) the duration of selection; (ii) occurrence of non-specific binding of oligonucleotides; (iii) formation of concatamers from PCR artifacts; (iv) low molar ratio of DNA/RNA library to the target; and (v) unavailability of chemistries and technologies capable of achieving a high throughput SELEX (McKeague and Derosa, 2012; Radom *et al.*, 2013; Blind and Blank, 2015; Ouellet *et al.*, 2015). Essential benchmarks applied to the selection of aptamer ligands with high affinity include reduction in non-specific binding, high partition efficiency (PE) and a reduced number of selection rounds needed to attain a low K_d value (Berezovski *et al.*, 2005; Lou *et al.*, 2009). The purity of the separation process is a direct function of the PE value (Lou *et al.*, 2009). For instance, Berezovski *et al.* (2005) demonstrated the application of a technique called 'Non-equilibrium Capillary Electrophoresis of Equilibrium Mixtures (NCEEM)' to attain a PE of $1x10^5$ as compared to conventional techniques yielding 10-1000 PEs. Similarly, Lou *et al.* (2009) obtained a PE of $\sim 1.4 \pm 0.6 \ x10^6$ for a micromagnetic microfluidic SELEX approach by coating carboxylic acid on magnetic beads to reduce non-specific adsorption. In addition, Ouellet *et al.* (2015) recently developed a SELEX technology termed as Hi-Fidelity (Hi-Fi) SELEX. The chemistry of the target-display surface as well as equilibrium conditions and solvents were optimized to reduce non-specific adsorption. Relative to the conventional approach, the following performance characteristics were obtained through the first round: a reduction in sequence diversity by 10^5-10^6 orders of magnitude, a partition efficiency of $8.0 \ x \ 10^5$ and a retention of 10^8-10^9 unique library sequences (Ouellet *et al.*, 2015). These and many other varied improvements in SELEX have led to the development of about 32 different types of SELEX assays (Sun and Zu, 2015). Some of these are described in Table 1 highlighting the main areas of improvement/modification.

Table 1. Summary of some advances in SELEX technology for aptamer generation.

Method	Section of SELEX Modification	Description	Reference(s)
Negative -SELEX	*Conventional technique	Removal of non-specific binding that arises from the matrix binding aptamer.	(Andrew and Jack, 1990)
Counter SELEX	Selection and partitioning step	Elimination of non-specific binding resulting from enantiometric targets.	(Jenison *et al.*, 1994)
Crosslinking SELEX or Photo SELEX	Library domain	Introduction of photo / crosslink group to the library pool to enable higher affinity and specificity binding of aptamer by crosslink to the target molecule following UV radiation.	(Jensen *et al.*, 1995)
cDNA SELEX or Genomic SELEX	Library domain	Modification done in the nucleic acid library domain with the target's own genome. The sequences that are present after co-immunoprecipitation are then amplified.	(Dobbelstein and Shenk, 1995)
In Vivo SELEX	Complex/living cells	SELEX procedure performed on vertebrate cells (living cells)	(Coulter *et al.*, 1997)
Chimeric SELEX	Library domain	Generation of dual function aptamers using a library with fused aptamers that bind independently to different targets.	(Burke and Willis, 1998)
Multistage SELEX	Library domain Selection step	To generate allosteric aptamers. Aptamers that bind to different target molecules are generated separately through conventional SELEX. These aptamers then fused to form longer oligonucleotides. Fused	(Wu and Curran, 1999)

		aptamer then go through counter selection to identify aptamers that have binding affinity of desired target.	
Cell SELEX	Complex targets	Using whole cells as targets. Aptamers with high affinity to a specific surface protein have been identified.	(Homann and Goeringer, 1999)
Indirect SELEX	Library domain	Divalent cations are added to the library pool to generate ion-dependent aptamer. Ion-dependent aptamers have a better binding affinity due to inductive conformation change effect in the presence of specific divalent cation	(Kawakami *et al.*, 2000)
Toggle SELEX	Selection step	Generation of aptamers that have cross reactivity with proteins of different species or subgroups by toggling two homologous proteins during selection.	(Rebekah *et al.*, 2001)
SELEX SAGE	Library domain	Combination of SELEX with serial analysis of gene expression (SAGE) protocols for quantitative modelling and generation of aptamers with large sequence libraries.	(Roulet *et al.*, 2002)
Tailored-SELEX	Amplification step	Swift generation of aptamers with short sequences ~ 10 nt. Primers are added by means of ligation to the 10 fixed nucleotide sequence prior to amplification in the SELEX process.	(Vater *et al.*, 2003)
Primer-free Genomic SELEX	Genomic library domain	Elimination of primer-annealing sequence from random sequence library to avoid interference from primer-binding sequence	(Wen and Gray, 2004)

		in aptamer complex binding.	
FluMag-SELEX	Library domain Selection and partitioning step	Introduction of fluorescent tagging of aptamers as well as target functionalization on magnetic beads in lieu of the conventional radioactive compounds. This increases the rapidity, ease of use, and efficiency of aptamer selection.	(Stoltenburg *et al.*, 2005)
Non-Selex (NECEEM-based)	Selection and partitioning step No amplification	A unique form of SELEX devoid of amplification steps and solely based on the principles of non-equilibrium capillary electrophoresis. High affinity aptamers are produced in an hour as compared to the conventional, which requires several days.	(Berezovski *et al.*, 2006)
NanoSelection	Library domain Selection and partitioning step	Combination of Atomic Force Microscopy (AFM) with Fluorescence Microscopy employed on a nano scale for specific selection of aptamers bound to a target from a smaller domain of nucleic acid sequences.	(Peng *et al.*, 2007)
Monolex	Selection and partitioning step Amplification	High affinity aptamers generated through a single round of elution and amplification and specifically designed for orthopovirus targets.	(Nitsche *et al.*, 2007)
Bind-n-Seq Massive parallel SELEX	Library domain Selection step	This involves the extraction of motifs from bound sequences after incubation of proteins with random nucleic acids. The developed protocol gives room for the generation of > 10 base pair binding	(Zykovich *et al.*, 2009)

		sites, parallel multiplexing with bar coded nucleic acids.	
Microfluidic SELEX	Selection and partitioning step Amplification	An automated rapid miniaturised microfluidic system consisting of a magnetic bead for target coupling with an on-chip amplification module for amplifying selected oligonucleotide sequences.	(Huang *et al.*, 2010)
SOMAmer (Slow Off- rate Modified Aptamer)	Library domain	This is based on the pre-modification of sequences of nucleic acids prior to the SELEX process to generate aptamers with enhanced properties for protein targets previously unbounded. It also capitalises on the unique sequences of each nucleic acids as well as their structural properties.	(Gold *et al.*, 2010)
MAI-SELEX (Multivalent aptamer isolation)	Library domain Selection step	The uniqueness of this assay is embodied in its 2 modules, which are used in aptamer pair selection for distinct site-specific binding interactions on the same target with less cross reactivity.	(Gong *et al.*, 2012)
Single Walled Carbon Nanotubes (SWCNTs)-assisted cell-SELEX	Cellular target	Reduction in the selection cycles and inefficiencies in the separation of specific and non-specific aptamers in each cycle to yield high affinity uncompromised aptamers specifically for cellular detection (cell-SELEX). Principle of separation hinges on the chemistries of nano-materials.	(Tan *et al.*, 2014)

Hi-Fidelity (Hi-Fi) SELEX	Library domain	Hi-Fi SELEX is distinctive by means of: (i) enhancing the diversity in functional aptamer sequences in the start-up library, (ii) elimination of pre-screening library sequences by immobilising targets on photo-coupled polyethylene glycol layers which passivates the surface against non-specific adsorption of oligonucleotides, (iii) application of digital qPCR to obtain high fidelity and, (iv) stoichiometric conversion of amplicons by λ-exonuclease into their related ssDNA aptamer libraries.	(Ouellet *et al.*, 2015)
	Selection and partitioning step		
	Amplification technique		

3.   APTAMER-TARGET BINDING MECHANISMS

Aptamers have secondary structures that enable binding with a wide variety of target molecules. These structures are stable and distinct with different nucleotide sequences for any target molecule, and can have one of the following conformations; stems, loops, bulges, hairpins, pseudoknots, triplexes or quadruplexes (Strehlitz *et al.*, 2012). For instance, the stability of the guanine quadruplex of a DNA aptamer is often reliant on the 3-D structure of the guanine quartet. The shape of the guanine quadruplex can be engineered to form either a linear or folded shape. The former is as a result of four oligonucleotide strands, whereas the latter results from one or two strands of oligonucleotide (Smirnov and Shafer, 2000). Howbeit, the fact that aptamers can be synthesized for a wide range of target molecules results in a number of challenges during the SELEX process for anionic and hydrophobic targets from an unmodified sequence of libraries (Amaya-González *et al.*, 2014). In contrast, protein-binding ligands are versatile in binding to complementary targets due to the presence of amino acid moieties, whereas aptamers have one function; to form a binding complex with their cognate targets. As a

73

result, aptamers tend to be highly specific in terms of binding affinity in comparison to antibodies and other protein binding ligands (Hermann and Patel, 2000).

Aptamer-target complex formation is broadly based on any of the following interactions or multiple combinations; aromatic stacking of flat moieties, hydrogen bond formation, van der Waals interaction, hydrophobic interaction and molecular shape complimentary interaction (Amaya-González *et al.*, 2014; Santosh and Yadava, 2014; Acquah *et al.*, 2015). For instance; aromatic targets bind to aptamers by means of stacking and hydrogen bonding (Hermann and Patel, 2000; Long *et al.*, 2008). Amino acids bind to aptamers by means of hydrogen bonding, driven by the orientation of polar moieties (Hermann and Patel, 2000). Oligosaccharides such as antibiotics complex with aptamers through non-Watson base pairing, electrostatic force of attraction, and intermolecular hydrogen bonds (Jiang *et al.*, 1999; Hermann and Patel, 2000). Thrombin interacts with an RNA aptamer having a stem–loop secondary structure through multiple combinations of ion pair interactions between the thrombin protein and the phosphate backbone of the RNA aptamer (Long *et al.*, 2008).

Interactions between RNA aptamers and proteins are based on base pairings within the aptamer and this influences the 3-D structures of RNA aptamers. 3-D structures of aptamers possess special recognition sites for specific protein target binding and for distinguishing between enantiomeric targets. Both DNA and RNA aptamers can bind to a specified target but with different mechanisms of interaction (Song *et al.*, 2012; Acquah *et al.*, 2015). For instance, whereas the 15-mer DNA thrombin binding aptamer binds to the exosite-1 of thrombin with van der Waals forces and hydrogen bonding stabilised by a G-quadruplex structure, Toggle 25t (an RNA aptamer) binds to the opposite end (exosite-2) with van der Waals forces, ionic interactions, hydrogen bonds and π-π stackings (Long *et al.*, 2008). Other studies reported on the interactions of RNA and DNA aptamers with interferon-γ revealed different dissociation constants of 8.7±1.2 and 63.8±7.4 nM respectively, with corresponding detection limits of 100 fM and 1pM (Min *et al.*, 2008). Allers *et al.* (2001) discussed that whilst RNA recognition sites for protein targets relate to the utilisation of polypeptide backbone, amide and carbonyl groups to result in base specific hydrogen bonding, DNA molecules rely on their bases and residues

of amino acids for the formation of the tertiary complexes (Allers and Shamoo, 2001). Generally, the phosphate backbone of nucleic acids binds more readily to positively charged amino acid residues (arginine, lysine and serine) than amino acids such as cytosine (Luscombe *et al.*, 2001).

3.1 Factors affecting aptameric binding performance

3.1.1 Aptamer stability

The stability and functionality of unmodified aptamers are affected by nuclease degradation in biological matrices (Bouchard *et al.*, 2010; Santosh and Yadava, 2014). The Stability of aptamers during intracellular activities is of major concern in medical applications. Aptamer stability can be enhanced, from minutes to hours, through chemical modifications or the selection of a polyvalent aptamer for the target (Musumeci and Montesarchio, 2012). Chemical modifications to aptamers can be performed pre- or post-SELEX by either terminal modification (addition of modified nucleotides to the aptamer backbone) or nucleotide modifications with locked nucleic acids such as 2'-amino, 2'-fluoro, 2'-O-methyl-nucleotides, phosphorothioate and polyethylene glycol (Bouchard *et al.*, 2010; Musumeci and Montesarchio, 2012; Santosh and Yadava, 2014). The challenge with this approach is associated to cost and concerns of chemical toxicity in medical applications (Musumeci and Montesarchio, 2012). Tatarinova *et al.* (2014) compared some selected chemical modification approaches (thiophosphoryl, triazole, and alpha-thymidine modifications) and the addition of a duplex module to a thrombin aptamer to investigate effects on stability. Although the chemically modified aptamers generally had an increase in stability, they were faced with a number of challenges such as poor predictions with the modification effects, identification of suitable positions for chemical modification, possible negative effects on thermostability and selectivity. Modifications by duplex module addition mimicked the effect of an *in vivo* G-quadruplex, and this modification can be implemented on any kind of DNA aptamer (Tatarinova *et al.*, 2014). Alternatively, the engineering of a polyvalent aptamer to establish multivalent interactions with target molecules can be performed to enhance stability. This can be achieved with the use of suitable linkers to covalently connect the aptamers, or by coupling aptamers to nanoparticles (Musumeci and Montesarchio, 2012). With any of these two approaches for

engineering polyvalent aptamers, multiple copies of a selected aptamer interact with target molecules in the same scaffold resulting in a multi-aptamer with an increased stability. Furthermore, polyvalent aptamers have a low dissociation constant, thus, higher binding affinity (Musumeci and Montesarchio, 2012). Seferos *et al.*, (2008) demonstrated that gold nanoparticle-conjugates of polyvalent oligonucleotide have enhanced nuclease stability. The application of the concept of spiegelmers are also known to be workable in the enhancement of aptamer stability and performance (Bouchard *et al.*, 2010). Esposito *et al.* (2014) also demonstrated that aptamer affinity, thermostability and half-life are enhanced through the inversion of polarity at the ends of the sequence for a G-quadruplex thrombin binding aptamer.

3.1.2   Metal Ion

The interaction of metal ions with nucleic acid ligands predominantly occur at the phosphate backbone, base keto oxygens, sugar backbone, N3 of adenine and N7 of guanine (Sundaresan and Suresh, 2007; Girardot *et al.*, 2010). The presence of a metal ion in a medium can cause alterations in the conformation of an aptamer, thus affecting its thermal stability (Smestad and Maher, 2012). The effect of monovalent and divalent cations to stabilise and induce a G-quadruplex structure has been demonstrated to follow the pattern (i) $K^+ > NH_4^+ > Rb^+ > Na^+ > Cs^+ > Li^+$ (Wong   and   Wu,   2003)   and   (ii) $Sr^{2+} > Ba^{2+} > Ca^{2+} > Mg^{2+}$ (Venczel   and   Sen,   1993),   respectively.   Statistical analyses conducted by McKeague *et al.* (2015) also suggested that there exists a positive correlation between a lower metal ion concentration and higher binding affinity. Nevertheless, a negative correlation was observed between Na^+ and viral targets. A number of specific proof-of-concepts have been probed. Lin *et al.*, (2011) demonstrated that the formation of G-quadruplex 15mer thrombin binding aptamer (TBA) was induced by K^+ monovalent ion, whereas A-form duplex formation of a 29mer TBA was induced by Mg^{2+}. André *et al.*, (2005) observed that the presence of Na^+ or Ni^{2+} decreased the affinity constant of adenosine aptamer contrary to the presence of Mg^{2+}. The presence of Mg^{2+} enhanced stabilisation of aptamer secondary structure. Thus, conformational change and binding affinity of aptamers are affected by the presence of metal ions. DNA-metal ion interaction is also dependent on the nature of the metal, size and charges (André *et al.*, 2005).

However, the effect of metal ions such as Na^+ and K^+ on the binding affinity is dependent on the type of binding interactions between the aptamer and the target. For instance, increasing the ionic strength for an electrostatic interaction with Na^+ and K^+ can lead to a reduction in the binding affinity as a result of shielding effect on the phosphate backbone of the aptamer. Thus, the effect of metal ion interactions on aptamer binding affinity is essential in predicting effective binding affinity. Lin *et al.*, (2011) demonstrated the effects of Na^+ on binding affinities of 15-mer, 29-mer and 32-mer TBA. It was observed that an increase in Na^+ concentration results in a significant reduction of the binding affinity with the exception of 29-mer. In addition, the ionic concentration led to a reduction in the binding affinity for electrostatic force of attraction. The decrease in binding affinity was due to the shielding effect of the metal ion (counter ion) (Hianik *et al.*, 2007; Lin *et al.*, 2011). However, this was not observed in the 29-mer TBA due to the involvement of hydrophobic moieties (Lin *et al.*, 2011) which further supports works done by Buff and co-workers (Buff *et al.*, 2009).

Monovalent and divalent ions interact with the aromatic bases and phosphate backbone of aptamers. The presence of Mg^{2+} was observed to increase the affinity of RNA to theophylline by 10^4 fold by stabilising the secondary structure (André *et al.*, 2005; Latham *et al.*, 2009). Cruz-Aguado and Penner (2008) observed that Mg^{2+} and Ca^{2+} enhanced affinity binding by forming a coordination complex with the target Ochratoxin A. Also, the presence of these two divalent ions facilitates aptamer conformational changes to favour target binding (Cruz-Aguado and Penner, 2008). Girardot *et al.* (2010) demonstrated that the addition of divalent Mg^{2+} improved the binding affinity of lysozyme-aptamer interactions due to favourable conformational changes of the aptamer. Moreover, dication interactions results in stronger stabilization of complex conformation (Girardot *et al.*, 2010).

Ionic strength also affects the binding affinity of aptamers and targets by affecting the secondary structure of the aptamer. Effect of divalent Mg^{2+} on binding affinity is very dependent on the structural composition of the target. Mg^{2+} exhibit shielding effect on N1 and N7 of adenine which are the main interaction site with aptamer and thus affect the binding. For AMP, ADP, ATP with structural composition is similar with a phosphate

side chain, increase in Mg^{2+} increase the binding affinity by interaction with the phosphate side chain and reduce the Coulombic repulsion between aptamer and these target molecules (Deng *et al.*, 2001).

3.1.3 Structure of aptamer sequences

The aptamer sequence, length of aptamer and loop conformation have an impact on the binding affinity of aptamers (Smirnov and Shafer, 2000; Musafia *et al.*, 2014). Changes in the nucleotide sequence results in mutation, and this causes variations in the secondary structure of the aptamer (Musafia *et al.*, 2014). It has been demonstrated that longer aptamers could have good binding affinities (Musafia *et al.*, 2014). However, the cost of aptamer production is a significant factor in accounting for the optimal length for effective binding (Smirnov and Shafer, 2000; Musafia *et al.*, 2014). Hence, they could be cleaved and shortened to the binding region to offer a high affinity as the original. In addition, a statistical proof of minimal correlation between the length of aptamers and targets in general has been reported. Relative to the length of aptamers, their specific sequence, structure and type of target are essential in enhancing their affinity (McKeague *et al.*, 2015). Studies by Smirnov and Shafer (2000) on the thermodynamic stability of loop sequence alteration using a thrombin binding DNA aptamer indicate that changes in the loop sequence, conformation and loop length can have significant impacts on the stability of aptamers. 15-mer thrombin binding aptamer (TBA) folds into a unique two guanine quartets by intermolecular interaction such as stacking and hydrogen bonding to gain the structural stability. Changing the loop sequence affects the formation of this unique complex thus affecting the stability of the aptamer. For instance; Musafia *et al.* (2014) demonstrated that the size of aptamers, nature of secondary structure, size of the loop, and loop perturbation affect the binding affinity of an anti-influenza. Changing the loop size or altering the loop composition affects the secondary structure of the aptamer (such as from quadruplex to hairpin), causing the emergence of different recognition regions (Smirnov and Shafer, 2000; Musafia *et al.*, 2014).

3.1.4 pH

Binding-linked protonation processes have been demonstrated to be critical in stabilising the tertiary complex formed between an aptamer and a target (Kaul *et al.*, 2003; Lin *et al.*, 2011), enhancing their binding specificity through the formation of hydrogen bonds (Nguyen *et al.*, 2006; Lin *et al.*, 2011; Nguyen and Vu, 2012). At pH above the target pKa value, a complex can be formed as a result of protonation. When a target is fully protonated at a pH below its pKa value, bioaffinity interactions with the aptamer do not involve binding linked protonation. Pilch *et al.* (2003) showed that pH affects thethermodynamic stability of an RNA-aminoglycoside complex. At a lower pH, aptamer protonation reduced the coulombic repulsion between the target and aptamer to yield a better retention time (Pilch *et al.*, 2003).

3.1.5 Temperature

Binding of aptamers with their cognate targets is a thermodynamic process involving enthalpy (ΔH) and entropy (ΔS) changes that can be defined by Gibbs energy shown in equation 1 (Velazquez-Campoy *et al.*, 2000; Lin *et al.*, 2011; Wang *et al.*, 2013). Thus, temperature is inevitably an important factor affecting the binding affinity.

$$\Delta G = \Delta H - T\Delta S \tag{1}$$

The most studied temperature for aptamer selection is reported to be at 25 °C (McKeague *et al.*, 2015). However, the optimum temperature for high affinity and binding kinetics is obtained around that of physiological conditions, 37 °C according to (Wang *et al.*, 2013; McKeague *et al.*, 2015). At such conditions, aptamers form unique 3-dimensional conformations that facilitates effective interactions (Wang *et al.*, 2013). That notwithstanding, aptamer-target interactions exhibiting endothermic reactions are also thought of to be favoured with high affinity by high temperatures and vice versa for exothermic reactions (Wickiser *et al.*, 2005).

4. CHARACTERISATION OF APTAMER-TARGET BINDING

A distinguishing feature between the generation of aptamers for biomolecular and cellular targets is the non-reliance on molecular signature for cellular targets. In addition, aptamer

selection is relative to their native conformation and physiological environment in cell-SELEX as compared to SELEX for biomolecules (Meyer *et al.*, 2011; Ninomiya *et al.*, 2013). Due to the complexity of cell membrane surface, cell-SELEX bear the risk of selecting molecules different from the desired target protein (Meyer *et al.*, 2011), though this can be overcome by performing counter selection (Van Simaeys *et al.*, 2010).

Binding interactions between aptamers and cellular targets entails secondary structural changes as discussed for biomolecular targets, and these secondary structures are essential for cellular recognition and specificity (Graham and Zarbl, 2012). Aptamer interactions with cellular targets consist of a host of binding forces including hydrogen bonding, van der Waals interactions, electrostatic bonding, aromatic ring stacking, non-Watson-Crick interaction or a combination of these (Graham and Zarbl, 2012). For instance, electrostatic interactions with the phosphate backbone results when the cognate molecule on the cell membrane surface is a protein with positively charged amino acid residues. As living cells are targets for cellular binding and cell surface moieties varying at different growth phases and conditions, cell cultivation and growth pattern is essential to achieve desired binding characteristics (Cao *et al.*, 2009; Suh *et al.*, 2014). At different growth stages, bacteria cells express different molecules that undergo antigenic variations, and this could result in the generation of false-negative results during cellular binding. Also, there is the tendency for aptamers to not recognise bacteria cells with positive charges on their surface and do not express the specific target molecule of interest during cell growth.

Cross-over SELEX is an alternative technique to address the challenges of cell-SELEX in generating aptamers for complex or cellular targets. In this process, a number of SELEX rounds is performed against the cellular target based on the interaction between the nucleic acids and the surface biomarkers expressed on the cell membrane, whiles the remaining rounds of conventional SELEX are performed against a selected purified biomarker and vice versa (Cibiel *et al.*, 2011; Hicke *et al.*, 2001).

Multiple aptamers for target cells based on different cell surface moieties can also be generated (Cao *et al.*, 2009). Multiple aptamers can increase the sensitivity by synergetic effect when the complex target is detected (Cao *et al.*, 2009; Suh *et al.*, 2014). Cao *et al.*

(2009) combined five aptamers for *Staphylococcus aureus* and this resulted in better binding characteristics compared to a single aptamer.

4.1 Instrumentations for probing aptamer-based binding

The extent of affinity between an aptamer-target interaction is estimated by means of the dissociation constant, K_d,(Jing and Bowser, 2011) which is mathematically expressed as:

$$K_d = \frac{(A)(T)}{(C)} \tag{2}$$

Where A is aptamer concentration, T is target concentration and C is the concentration of aptamer-target complex. The advancement in aptamer technology over the past two decades has led to the establishment of analytical methods and tools to characterise the binding affinity of aptamers through the measurement of affinity constant; reaction kinetics; conformational changes during the formation of aptamer-ligand complexes; and real-time monitoring of affinity interactions. Various biophysical techniques or instruments often deployed in characterising aptameric binding features are generally discussed in this section.

4.1.1 Affinity chromatography

High Performance Liquid Chromatographic (HPLC) techniques can be used to analyse aptamer-target binding qualitatively and quantitatively. The mechanism of operation is based on the flow of liquid solvent under pressurised conditions through an aptamer-immobilised adsorbent column as shown in Figure 2. Results are shown in a chromatogram with concentration of analytes against retention time. HPLC technique provides information regarding the equilibrium distribution of aptamer, target and aptamer-target complex which can be used to estimate the K_d value (Deng *et al.*, 2001).

In addition, this technique is useful in investigating the binding affinity of aptamers towards complex samples. With such samples, the binding between aptamers and targets are shown with different peaks in the chromatogram to aid in their comparison (Deng *et al.*, 2001). More so, Deng *et al.*, (2001) characterised the binding of a DNA aptamer to adenosine by affinity chromatography with varying parameters such as pH, ionic strength and concentration of divalent Mg^{2+}.
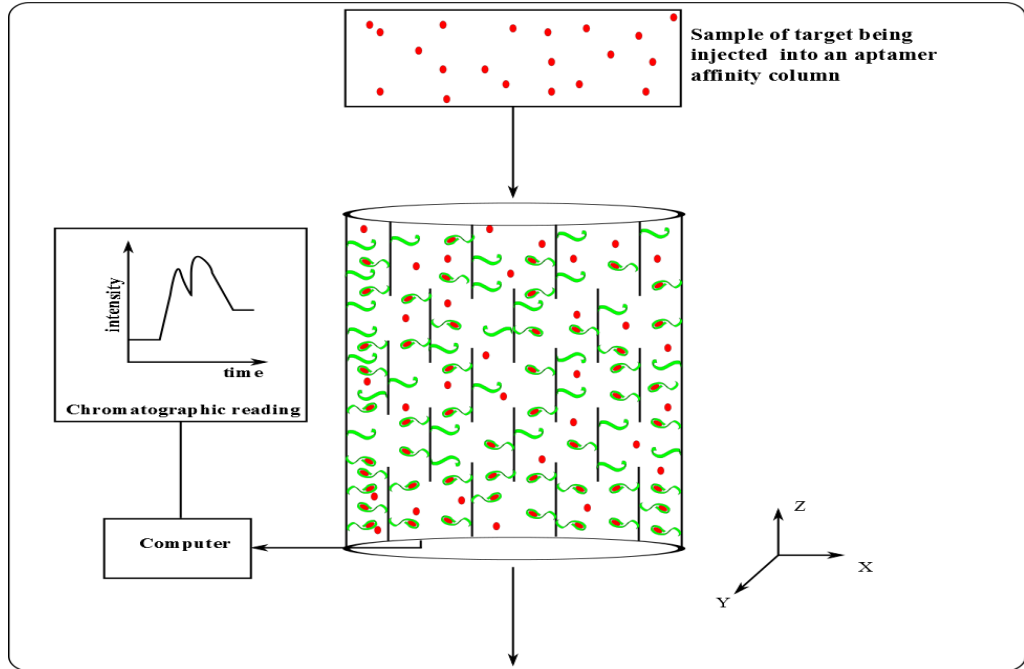
Figure 2. Schematic representation of a biophysical technique (affinity chromatography) used to characterise aptamer-target binding. Movement of fluid through an affinity chromatographic column is via concave flow.

4.1.2 Electrophoresis

The application of electrophoresis to study aptamer-target interactions could be in diverse forms such as gel electrophoresis, affinity capillary electrophoresis and microchip electrophoresis. Gel Electrophoresis (GE) is a commonly used technique for studying the binding characteristics between an aptamer and a target. Aptamers are negatively charged hence possess a negative electrophoretic mobility whereas protein targets have a low polar mobility. As a result, the aptamer-target tertiary complex formed has an intermediate electrophoretic mobility (Jing and Bowser, 2011). Aptamer concentrations can be determined by means of blotting, staining of the protein or aptamer, p-labelling of nucleic acids, and UV–absorbance (Jing and Bowser, 2011). Although, this process is economical and has a high sensitivity, it is time consuming. Due to the prolonged period needed for separation, the association and dissociation rates of the aptamer-target complex are considered to obtain a distinct band for validation.

An improved alternative to gel electrophoresis is affinity capillary electrophoresis (ACE). This is based on the size and charge of the aptamer and target in a free solution under an electric field (Jing and Bowser, 2011; McKeague and Derosa, 2012). Figure 3 shows the electrophoretic mobility. ACE can be grouped into two forms: non-competitive and competitive. The non-competitive assay is associated with running the mixture through capillary electrophoresis with laser-induced fluorescence detection (LIF) mechanism. Quantification is achieved through peak analysis for the aptamer and the tertiary complex (Le *et al.*, 2005; Stratis-Cullum *et al.*, 2009).The competitive electrophoresis assay utilises two aptamers having a competitive effect on a target, with one of the aptamers tagged with a fluorescent label (say, APL). When the non-labelled aptamer (AP) is introduced, it competes for target binding and, as a result, the fluorescent intensity of the complex (APL-T) decreases due to the competitive effect of AP with an increasing intensity of APL. This two-peak information can be used in the quantification of binding affinity (Le *et al.*, 2005). There is no need for aptamer immobilisation during ACE as the process occurs in solution (Stratis-Cullum *et al.*, 2009). Flow through the capillary is via plug flow. However, the aptamer has to be stable within its half-life in order to avoid distorted peaks.
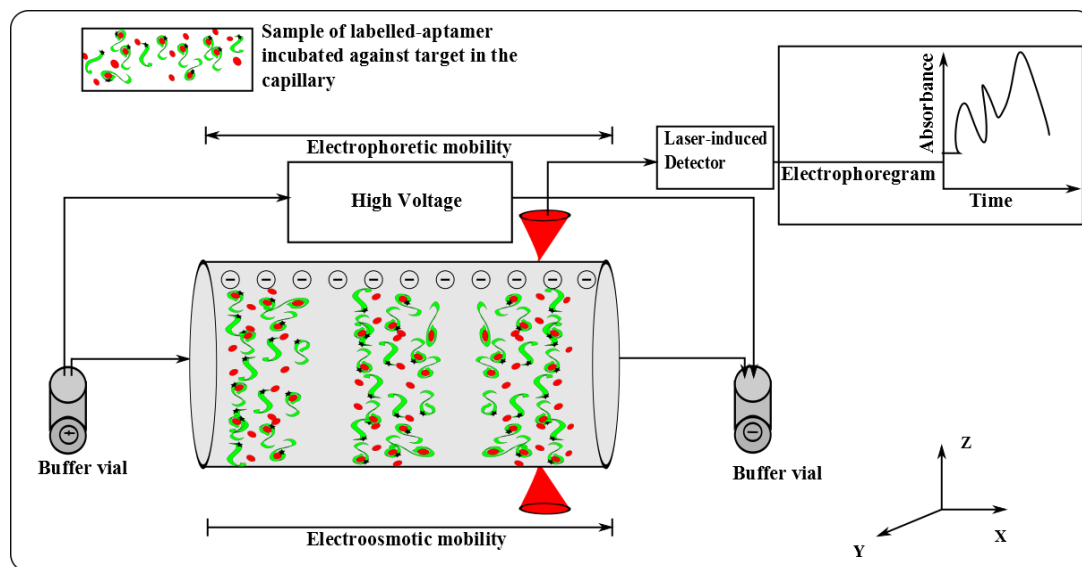
Figure 3. Illustration of an aptamer-target characterisation process using capillary electrophoresis.

Microchip electrophoresis (ME) or automated microchip electrophoresis (AME) is also used for electrophoresis binding studies. Molecular detection is achieved with an intercalating fluorescent dye. Compared to GE and ACE, the following benefits are

associated with the use of microchip electrophoresis: shorter sensing time (<3min); avoidance of gel casting; reduction in volume of sample and reagents needed; capacity to characterise the binding of small-molecules such as adenosine triphosphate ATP; a digital output for the results (Nishikawa *et al.*, 2006; Hu and Easley, 2011). Nevertheless, their application is limited in basic laboratories due to the complexity in developing a special platform to undergo electrophoresis (Darmostuk *et al.*, 2015).

4.1.3   Surface conjugation analysis

Surface plasmon resonance (SPR) technology is a high-throughput, label-free and real-time technique used to characterize the binding affinity of aptamer and its target (Kwon *et al.*, 2001; Win *et al.*, 2006; Lin *et al.*, 2011). The technique allows for immobilisation of either the target or aptamer onto the surface of a chip with varying concentrations of non-tethered ligands flowing through as shown in Figure 4. The binding affinity is determined by measuring the changes in refractive index resulting from the formation of the tertiary complex (McKeague and Derosa, 2012)**.** SPR technique involves either a direct or an in direct functionalization of the target on the chip surface. Indirect functionalization involves the use of a linker such as biotin and streptavidin, whereas the direct approach requires no linker. Though linkers can enhance the immobilisation stability for better accessibility to target molecules, they can interact with the aptamer to result in non-specific binding (Win *et al.*, 2006).
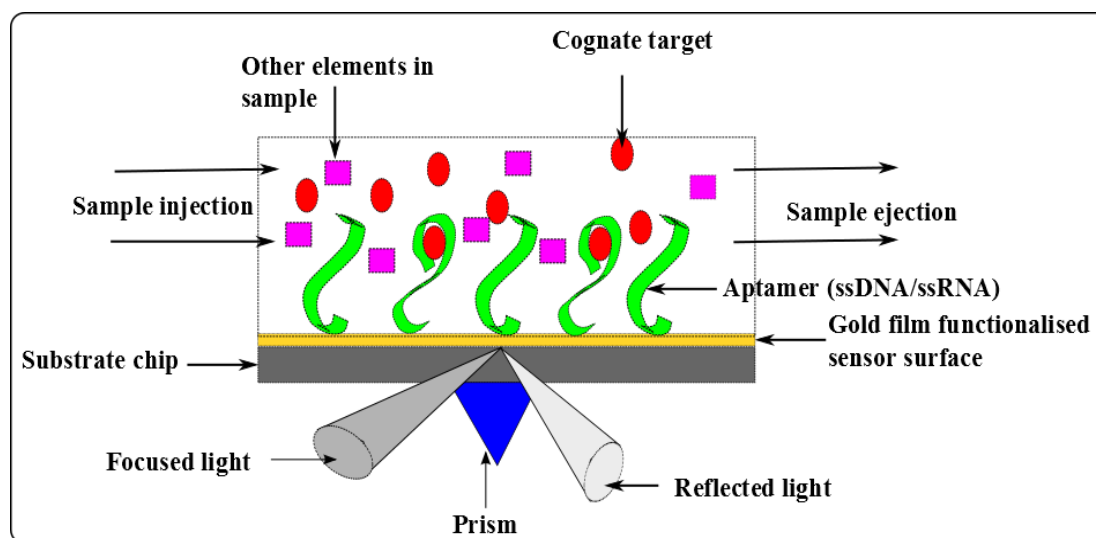
Figure 4. Characterisation of aptamer-target interactions with Surface Plasmon Resonance (SPR).

During an SPR analysis, samples are injected over the aptamer-immobilized surface to examine the binding response (RU) until an equilibrium response is obtained depicting the associate constant (K_{on}). Dissociate constant, $K_{off,}$ is obtained with an injected sample free-solution until the point of equilibrium. Then the binding equilibrium (K_d) can be derived from the graph of RU against sample concentration whereby K_d will be the concentration of sample when half of the maximal response is achieved (Win *et al.*, 2006). Notably, the biophysical study of aptamer-target interactions between RNA molecules are seldom performed in the lab owing to their likely chance of degradation due to the presence of magnesium ions or contaminating nucleases during handlings. Nevertheless, protocols to alleviate such fears has been recently demonstrated to be effective to aid in RNA-molecule studies involving nucleic acids (Di Primo *et al.*, 2011).

4.1.4 Quartz crystal microbalance measurements

Quartz crystal microbalance (QCM) analysis is a label free, real time, sensitive and stable method for studying the interactions between an aptamer and a target molecule. The sensitivity and specificity of this method are based on the immobilization of aptamers on a surface (mostly quartz) recognition layer (Heydari, 2014)**.** The frequency of the quartz decreases when immobilised aptamers on the surface of the QCM bind to target molecules at a measurable mass per unit binding area (Win *et al.*, 2006; McKeague and Derosa, 2012). QCM techniques are cost effective, require less time, and have no interferences that result from labelling. The efficiency of immobilisation of aptamers to the surface is a function of the surface area and surface material type. For instance, the use of a thiolated-modified ssDNA on a gold surface is observed to have a better specificity with an improved surface density than non-thiolate ssDNA. The occurrence of a shift in Frequency (ΔF) when a target is introduced to interact with an immobilized aptamer indicates the occurrence of binding between the pair. Figure 5 gives a schematic view of an aptamer-target interaction monitored with QCM. The higher the frequency shift, the better the binding of the target by the aptamer (Win *et al.*, 2006; Chen *et al.*, 2009; Sultan *et al.*, 2009). The mass changes upon binding provide information on the concentration of target bound and further enable to calculate the binding affinity (K_d) of the aptamer (Cooper and Singleton, 2007).
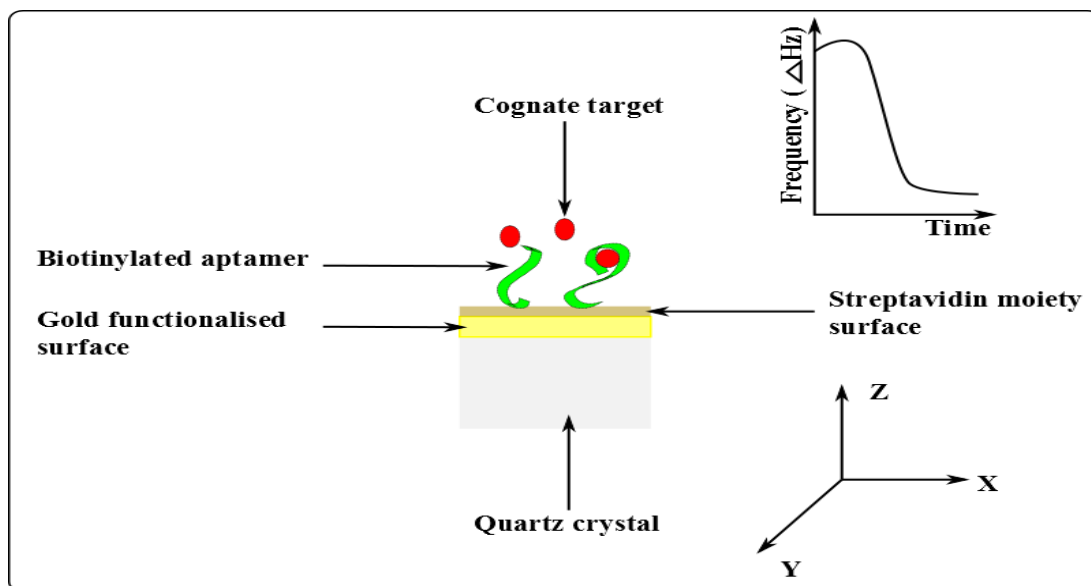
Figure 5. An illustration of aptamer-target analysis with the use of a Quartz Crystal Microbalance Instrument.

4.1.5 Spectra based methods

UV-Vis absorption is a widely used method of characterising the binding characteristics of aptamers and their cognate targets due to its affordability and the absence of labelling. The K_d value is estimated through changes in the absorbance with varying target concentrations but a fixed aptamer concentration. DNA aptamers are noted to have maximum absorption at 260 nm whilst protein targets have maximum absorption in the range of 250 nm to 300 nm (Jing and Bowser, 2011).

On a different note, Circular dichroism (CD) is also a spectrum based technique used in studying conformational changes in the secondary structure of an aptamer towards the formation of tertiary complexes (Jing and Bowser, 2011; Lin *et al.*, 2011; McKeague and Derosa, 2012). By referring to the CD spectra, the secondary structure of the aptamer can be identified (Nagatoishi *et al.*, 2007; Lin *et al.*, 2011). Different well-defined secondary structures possess different CD spectra patterns (Nagatoishi *et al.*, 2007; Jing and Bowser, 2011). G-quadruplex gives a CD spectra with negative band at 255 nm and positive bands at 245nm and 290nm. A CD spectra with negative band at 240 nm and positive band at 265nm could be an aptamer in A form duplex structure (Lin *et al.*, 2011). This method is useful in investigating the structural swift of aptamers upon binding by reading their CD

spectrum as shown in Figure 6.
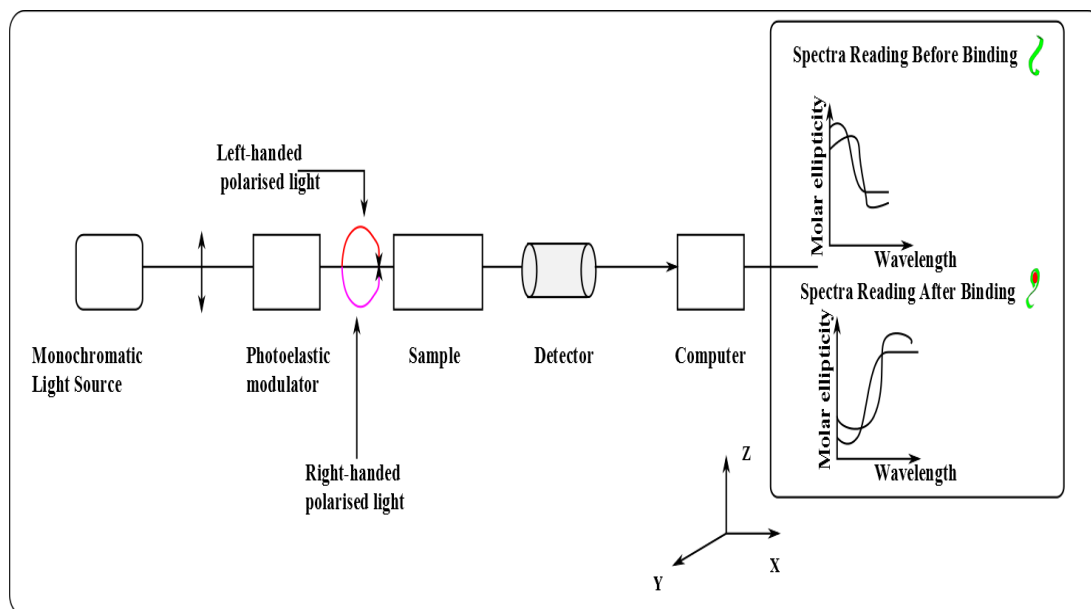
Figure 6. Analysis of aptamer-target interactions using circular dichroism (CD).

Nuclear magnetic resonance (NMR) spectroscopy is used in characterising the aptamer binding affinity and conformational changes by formulating an atomic resolution structure of the aptamer, its target and the tertiary complex formed (Macaya *et al.*, 1993; Sakamoto *et al.*, 2005; McKeague and Derosa, 2012). An external magnetic field is applied to the nuclei to generate the spectrum of interest. However, NMR technique is restricted to only small molecules with size less than 40 kDa (Ruigrok *et al.*, 2012).

4.1.6 Thermodynamic characterisation

Isothermal titration calorimetry (ITC) and Microscale Thermophoresis (MST) are both examples of thermodynamic related techniques applicable for characterising the affinity between aptamers and their targets (McKeague and Derosa, 2012; Stoltenburg *et al.*, 2015). With the ITC technique, a specified concentration of either the aptamer or the target as the titrant is added against varying concentrations of the complementary molecule as the analyte. As the formation of tertiary complex is the only desired exothermic process, the cell temperature is kept at the same temperature as the control cell, whiles circumventing all other possible exothermic sources. Also, removal of the injection volume out of the sample cell before each injection is eminent to ensure a constant sample volume (Jing and Bowser, 2011). Figure 7 shows the use of ITC for aptamer-target binding

87

characterisation based on the energy change generated relative to the reference cell. The energy change is proportional to the quantum of binding.
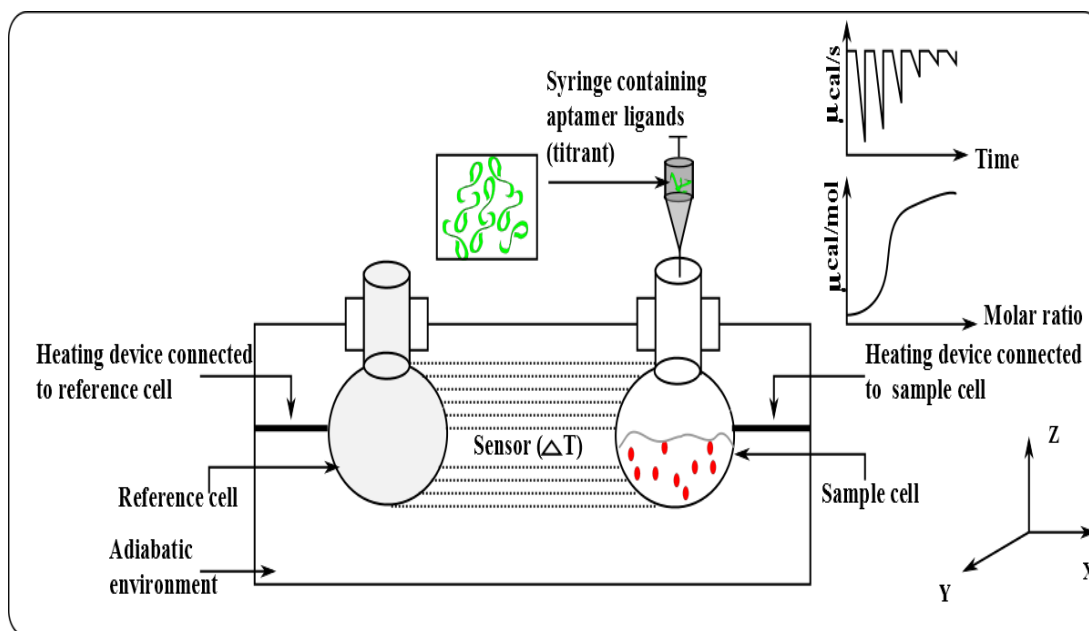
Figure 7. Isothermal titration calorimetry for aptamer-target binding characterisation.

Microscale Thermophoresis (MST) is a relatively new biophysical thermal gradient technique for rapid and precise quantification of biomolecular interactions irrespective of their molecular size in solution (Entzian and Schubert, 2015; Stoltenburg *et al.*, 2015; Amero *et al.*, 2016), and this is applicable for aptamer-target binding characterisations. The thermal gradient is generated by means of infra-red laser. Inherent features such as molecular size, charge, solvation shell and/or conformation dictate the thermophoretic mobility of biomolecules (Jerabek-Willemsen *et al.*, 2014; Stoltenburg *et al.*, 2015). The baseline of the aforementioned features is altered upon the formation of aptamer-target complexes, resulting in a change in mobility that can be used to quantify their binding affinity. Due to the rapidity, specificity and versatility of MST, it is anticipated to soon rival other existing biophysical technologies (Jerabek-Willemsen *et al.*, 2014).

4.1.7 Laser-based (Flow Cytometry)

Flow cytometry is a laser-based method with the capacity to characterise the physical and chemical properties of thousands of particles in a second. The technique has been adapted to characterise the binding of aptamers and whole cells due to its reproducibility, high

degree of statistical accuracy on a large number of analysed cells, and the capacity to quantify results with much rapidity (Jayasena, 1999; Shangguan *et al.*, 2008; Cibiel *et al.*, 2011). The aptamer is first labelled with a fluorescence dye for example FITC dye (fluorescein isothiocyanate) and incubated with the target cell. The binding interaction is determined from the fluorescence intensity of the labelled cells. The intensity of the fluorescence gives the indication of the binding affinity of the aptamer towards the targeted cell. Thus, the higher the intensity the higher the binding capacity of the aptamer towards the cell (Shangguan *et al.*, 2006). Histogram and dot plot are the two main output of the flow cytometer wherein dot plot allows the comparison of the binding of different aptamers and types of cells to be carried out simultaneously (Shangguan *et al.*, 2006; Shangguan *et al.*, 2008). A schematic representation of the principle underpinning flow cytometry for aptamer-target interaction is shown in Figure 8.
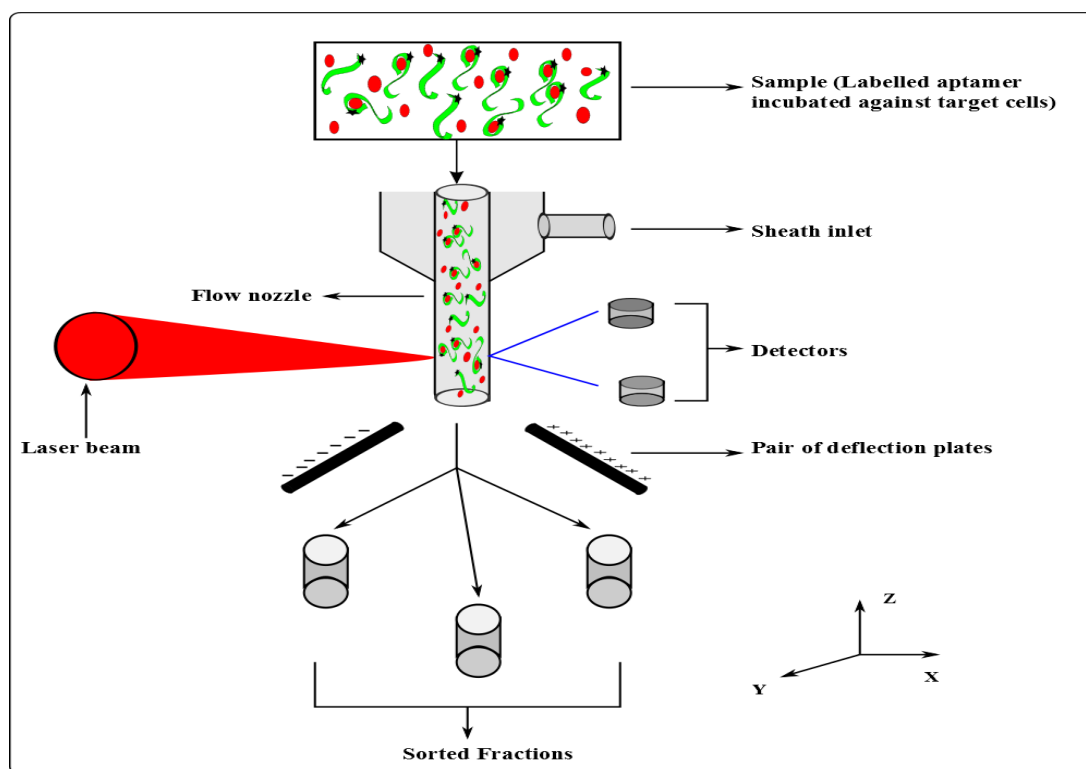
Figure 8. Characterisation of aptamer-target binding affinity by flow cytometry.

4.1.8   Atomic force microscopy

Atomic Force Microscope (AFM) is a scanning probe based microscopy technique which allows high quality nanoscale structure imaging (Kailas *et al.*, 2009; Lonergan *et al.*,

2014). Using a probe call cantilever, AFM can be used to scan the imperceptible sample surface and detect the affinity force between the sample surface and the cantilever as shown in Figure 9. Due to this advantage, it is suitable to study the binding affinity of aptamer to biomolecule (Miyachi *et al.*, 2009). Fixation and dehydration of sample is not required for AFM, thus a cell is able to be observed under aqueous conditions and its latent format (Kailas *et al.*, 2009; Lonergan *et al.*, 2014). This uniqueness makes AFM most suitable for studying the surface protein and topology of live cell. The analysis of AFM can be presented in a force histogram and topology image. The peak of histogram in the measurement of adhesion (pN) at certain data point is used to evaluate the affinity force of binding between aptamer and target. The higher the pN value, the higher the affinity force, which means the better the binding affinity (Miyachi *et al.*, 2009). Topology imaging gives information on the surface conformation of target to give a picture of how the binding of aptamer changes the surface conformation of target (Lonergan *et al.*, 2014).
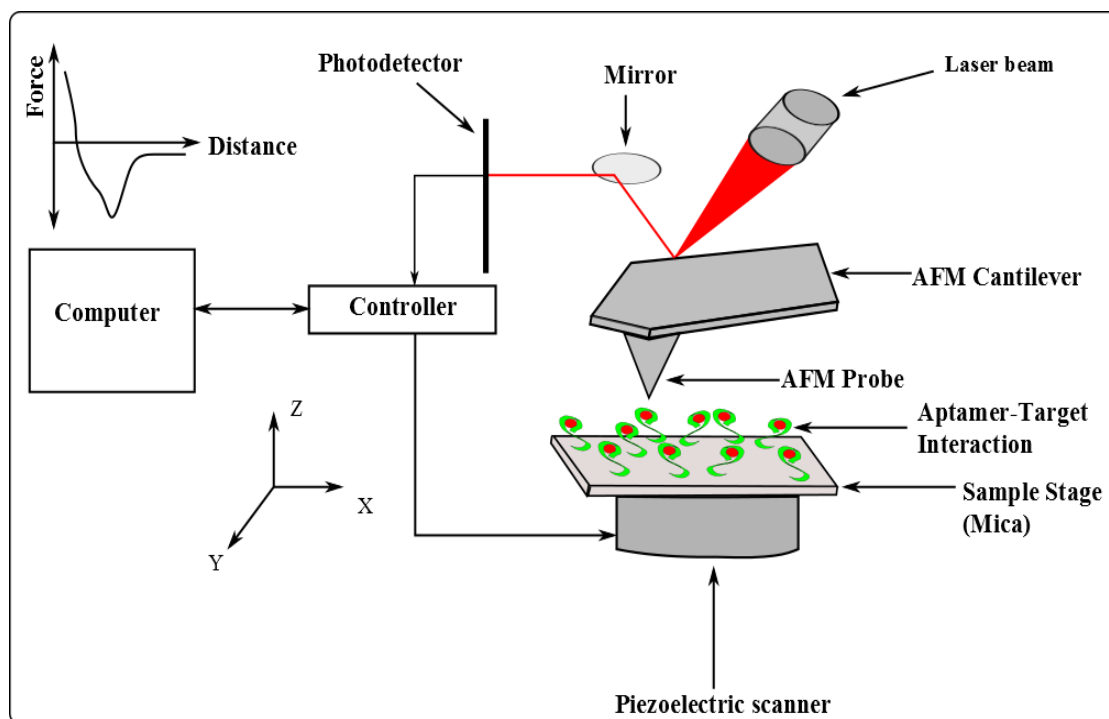
Figure 9. Characterisation of aptamer-target affinity binding strength by atomic force microscopy (AFM).

5.   APPLICATIONS OF APTAMER-BASED BINDING

As discussed earlier, aptamers can be generated for a wide range of target molecules. They have reproducible synthesis and binding characteristics, possess efficient bio-stability, and

have a high affinity and specificity (Yang *et al.*, 2007; Santosh and Yadava, 2014). This has enabled application over wide of range of fields including medical diagnostics, therapeutic manufacturing and delivery, environmental and molecular analysis. Table 2 gives a summary of recently identified aptamers, their associated affinity constant and specific applications.

Table 2. Synthesised aptamers with their associated affinity constant and application.

Aptamer	K_d (nM)	Application and Remark	Reference(s)
Anti-Staphylococcal enterotoxin B SEB aptamer (ssDNA)	64	Therapeutic application: For the inhibition of staphylococcal enterotoxin B (SEB) to mediate staphylococcal toxic shock syndrome (TSS). Affinity constant K_d determined by means of non-linear regression analysis.	(Wang *et al.*, 2015)
CD4 cell expressing aptamer (ssDNA)	1.59	Therapeutic application: Possess high *in vivo* stability and affinity necessary to disrupt the transmission of HIV-1 by ensuring 70% binding-inhibition of viral gp120 to CD4-expressing cells. Affinity constant K_d determined by means of non-linear regression analysis. Flow cytometry employed to determine the ability of the aptamer to bind to the cell.	(Zhao *et al.*, 2014)
Hsp70-ATP Inhibitory aptamer (ssRNA)	61.3±6.6	Therapeutic application: Has a high specificity in binding to a particular conformation of Hsp70-ATP thereby inhibiting its biological activities without stimulating the activity of Hsp40-ATP. This has a high propensity of success in cancer therapy to prevent proliferation of cancerous cells.	(Thirunavukarasu and Shi, 2015)

Epithelial cell adhesion molecule apt (ssRNA)	N/A	Therapeutic and diagnostic application: Chemically modified aptamer functionalised on curcumin-encapsulated nanoparticle to facilitate effective therapy in colon cancer treatment.	(Li *et al.*, 2014)
DNA aptamer HA09	103.61±35.05 for aptamer–HepG2; 35.8±31.0 for aptamer-QGY-7703; 190.2±50.9 for aptamer-Huh7.	Therapeutic and diagnostic applications: Support live imaging and chemotherapy treatment of human liver cancer cells and detect paraffin-embedded human hepatocellular carcinoma tissues.	(Lu *et al.*, 2014)
M. tuberculosis aptamer (ssRNA)	8.04 ± 1.90 for G43 aptamer; 78.85 ± 9.40 for G78 aptamers.	Diagnosis of Mycobacterium Tuberculosis: Development of an aptamer specifically for detecting EsxG Protein of M. Tuberculosis by means of surface plasmon resonance-based SELEX.	(Ngubane *et al.*, 2014)
NOX-G15 (DNA/RNA-Spiegelmer)	3	Diabetes therapy: NOX-G15 has been demonstrated to extremely lessen hyperglycemia in type 1 and type 2 diabetes by binding to glucagon and inhibiting its bioactivities.	(Vater *et al.*, 2013)

Bacillus S8 aptamer (ssRNA)	110 ± 30	Environmental pathogens: Studied the secondary structural changes between RNA aptamers in the free and bound state towards Bacillus S8 proteins.	(Davlieva et al., 2014)
OmpC protein of Salmonella Typhimurium (ssRNA)	20	Environmental pathogens: Identified and characterised nuclease resistant aptamers modified with 2'-fluoro-2'-deoxyribonucleotide specific for the detection of OmpC proteins of Salmonella.	(Han, 2013)
SEC 1 aptamer (ssDNA)	65.14 ± 11.64	Environmental pathogens: Aptamers having molecular recognition for Staphylococcus aureus enterotoxin C1 (SEC 1) proteins.	(Huang et al., 2015)
DNA Apt22	47 ± 3	Environmental pathogen diagnosis: Aptamers with high affinity and specificity developed by whole-cell-SELEX for the detection of Salmonella Paratyphi A and its incorporation into a single walled carbon nanotube for diagnosis in food, environmental and clinical samples.	(Yang et al., 2013)

5.1   Therapeutics

Aptamers are applicable in the development and formulation of therapeutics owing to their inherent ability to inhibit protein functions and modifiable biostability. The biostability of aptamers can be modified with polyethylene glycol, cholesterol molecule and through the creation of spiegelmers (Anthony et al., 2010). As a result of their non-recalcitrant, biostability and bioavailability, they can be deployed readily for cell imaging and single-protein imaging (Song et al., 2012). One of such is the use of tenascin-binding aptamer for cancer imaging (Guo et al., 2008). Factors advantageous to aptamer for therapeutic

applications include cost of high throughput production, duration of therapeutic effect, and binding affinity (Anthony *et al.*, 2010). Aptamers with a short half-life are advantageous in the treatment of transient conditions such as blood clotting (Guo *et al.*, 2008).

5.2   Medical diagnostics

The mortality and morbidity rate caused by pathogenic infections is high especially in developing nations with increasing cases of pathogen resistance against current therapeutic treatment. Such challenges necessitates the need in developing rapid and high affinity detection and screening methods of pathogens; even in its latent form (Zimbres *et al.*, 2013). The high affinity and specificity of aptamers and the ability of aptasensors in offering instantaneous on-site screening makes aptamers high in-demand for pathogen detection, therapeutic analysis and patient prognosis. They have been demonstrated to be able to detect or identify pathogens and also further used in therapeutics for example as an antimycobacterial agent and pathogenic growth inhibitor (Zimbres *et al.*, 2013).

The ability of aptamers in detecting whole cell (Cell-SELEX) has advanced the application of aptamers as a new biomarker discovery which further facilitates early stage diagnosis of cancer (Chang *et al.*, 2013; Santosh and Yadava, 2014). The high affinity of aptamers towards its target enables discrimination between stereoisomeric targets which helps in the identification of cancerous cells over normal cells with detection limits of as low as 90 cells as well as varied subtypes of cancer cells present (Zhang *et al.*, 2010; Chang *et al.*, 2013). One of the numerous successes of cell-SELEX in new biomarker discovery is the identification of protein tyrosine kinase 7 (PTK7) as biomarkers for T-cell acute lymphoblastic leukaemia by using sgc 8 aptamer (Chang *et al.*, 2013).

5.3   Monitoring of environmental related targets

Aptamers have been used to identify toxic substances in food, and trace pharmaceutical residues such as antibiotics, hormones and pesticides in surface, ground and drinking water (Rodriguez-Mozaz *et al.*, 2006; Strehlitz *et al.*, 2012). Owing to their high binding specificity, aptamers can also be used in sample enrichment to overcome challenges faced with the detection of low concentrations of toxic targets such as ochratoxin A and ricin

(Strehlitz *et al.*, 2012). Aptasensors generally do not require additional processing steps such as sample preparation unlike conventional bioanalytical methods, and have the propensity of detecting complex samples. These features makes aptasensors a great tool for onsite field monitoring of environmental contaminants (Rodriguez-Mozaz *et al.*, 2006). Shi *et al.* (2013) demonstrated the use of aptamers as biosensors in detecting acetamiprid pesticides component in soil. Acetamiprid can be toxic to consumers. The use of aptamers in detecting cocaine has been demonstrated to further enhance rapid and real-time drug detection technology for narcotic control (Kawano *et al.*, 2011). The significance of aptamers in food safety has also been discussed recently (Dong *et al.*, 2014).

6.   CONCLUSION

Biomedical research advances have led to SELEX modifications to enhance aptamer production time, cost reduction, biostability, and specific affinity binding to biomolecular and cellular targets. Aptamers form three-dimensional structures that possess specific binding affinity towards target molecules. The binding of aptamer and targets involve combinations of van der Waals, electrostatic, and hydrogen bonding. However, the binding of aptamers and their targets is affected by physiochemical parameters such as temperature, pH and metal ion. Conspicuously, there exists limited knowledge of the biophysical interactions and mechanisms between aptamers and various specified target molecules and this has retarded advances in their generation and applications. Most research breakthroughs have been centred on thrombin analysis, with cancer cell studies gradually gaining prominence. Although bioanalytical studies of aptasensors has taken centre stage in bioaffinity research for diverse applications, there still remain significant gaps needed to be filled to enable practitioners and researchers adequately understand binding interactions and functionalities in biosensing formats under varying physicochemical conditions.

7.   ACKNOWLEDGMENT

8. REFERENCES

Abe, K., D. Ogasawara, W. Yoshida, K. Sode and K. Ikebukuro, 2011. Aptameric sensors based on structural change for diagnosis. Faraday discussions, 149: 93-106.

Acquah, C., M.K. Danquah, D. Agyei, C.K. Moy, A. Sidhu and C.M. Ongkudon, 2015. Deploying aptameric sensing technology for rapid pandemic monitoring. Critical reviews in biotechnology: 1-13. Available from http://www.ncbi.nlm.nih.gov/pubmed/26381238. DOI 10.3109/07388551.2015.1083940.

Acquah, C., M.K. Danquah, J.L.S. Yon, A. Sidhu and C.M. Ongkudon, 2015. A review on immobilised aptamers for high throughput biomolecular detection and screening. Analytica chimica acta, 888: 10-18. Available from http://www.sciencedirect.com/science/article/pii/S0003267015008016. DOI http://dx.doi.org/10.1016/j.aca.2015.05.050.

Allers, J. and Y. Shamoo, 2001. Structure-based analysis of protein-rna interactions using the program entangle. Journal of molecular biology, 311(1): 75-86.

Amaya-González, S., N. de-los-Santos-Álvarez, A.J. Miranda-Ordieres and M.J.s. Lobo-Castañón, 2014. Aptamer binding to celiac disease-triggering hydrophobic proteins: A sensitive gluten detection approach. Analytical chemistry, 86(5): 2733-2739.

Amero, P., C.L. Esposito, A. Rienzo, F. Moscato, S. Catuogno and V. de Franciscis, 2016. Identification of an interfering ligand aptamer for ephb2/3 receptors. Nucleic acid therapeutics.

André, C., A. Xicluna and Y.C. Guillaume, 2005. Aptamer–oligonucleotide binding studied by capillary electrophoresis: Cation effect and separation efficiency. Electrophoresis, 26(17): 3247-3255.

Andrea, R., H. Ulrich and M. Cindy, 2011. Cell-specific aptamers as emerging therapeutics. Journal of Nucleic Acids, 2011 (2011). DOI 10.4061/2011/904750.

Andrew, D.E. and W.S. Jack, 1990. In vitro selection of rna molecules that bind specific ligands. Nature, 346(6287): 818. DOI 10.1038/346818a0.

Anthony, D.K., P. Supriya and E. Andrew, 2010. Aptamers as therapeutics. Nature Reviews Drug Discovery, 9(8): 660. DOI 10.1038/nrd3249.

Aquino-Jarquin, G. and J.D. Toscano-Garibay, 2011. Rna aptamer evolution: Two decades of selection. International journal of molecular sciences, 12(12): 9155-9171. DOI 10.3390/ijms12129155.

Baird, G.S., 2010. Where are all the aptamers? American journal of clinical pathology, 134(4): 529-531. Available from http://www.ncbi.nlm.nih.gov/pubmed/20855632. DOI 10.1309/AJCPFU4CG2WGJJKS.

Berezovski, M., A. Drabovich, S.M. Krylova, M. Musheev, V. Okhonin, A. Petrov and S.N. Krylov, 2005. Nonequilibrium capillary electrophoresis of equilibrium mixtures: A universal tool for development of aptamers. Journal of the American Chemical Society, 127(9): 3165.

Berezovski, M., M. Musheev, A. Drabovich and S.N. Krylov, 2006. Non-selex selection of aptamers. Journal of the American Chemical Society, 128(5): 1410.

Blind, M. and M. Blank, 2015. Aptamer selection technology and recent advances. Molecular Therapy—Nucleic Acids, 4(1): e223.

Bouchard, P., R. Hutabarat and K. Thompson, 2010. Discovery and development of therapeutic aptamers. Annual review of pharmacology and toxicology, 50: 237-257.

Buff, M.C., F. Schäfer, B. Wulffen, J. Müller, B. Pötzsch, A. Heckel and G. Mayer, 2009. Dependence of aptamer activity on opposed terminal extensions: Improvement of light-regulation efficiency. Nucleic acids research: gkp1148.

Burke, D.H. and J.H. Willis, 1998. Recombination, rna evolution, and bifunctional rna molecules isolated through chimeric selex. Rna, 4(9): 1165-1175.

Cao, X., S. Li, L. Chen, H. Ding, H. Xu, Y. Huang, J. Li, N. Liu, W. Cao and Y. Zhu, 2009. Combining use of a panel of ssdna aptamers in the detection of staphylococcus aureus. Nucleic acids research, 37(14): 4621-4628.

Chang, A., M. McKeague, J. Liang and C. Smolke, 2014. Kinetic and equilibrium binding characterization of aptamers to small molecules using a label-free, sensitive, and scalable platform. Analytical chemistry, 86(7): 3273.

Chang, Y.M., M.J. Donovan and W. Tan, 2013. Using aptamers for cancer biomarker discovery. Journal of nucleic acids, 2013.

Chen, S.-H., Y.-C. Chuang, Y.-C. Lu, H.-C. Lin, Y.-L. Yang and C.-S. Lin, 2009. A method of layer-by-layer gold nanoparticle hybridization in a quartz crystal microbalance DNA sensing system used to detect dengue virus. Nanotechnology, 20(21): 215501.

Cibiel, A., D.M. Dupont and F. Ducongé, 2011. Methods to identify aptamers against cell surface biomarkers. Pharmaceuticals, 4(9): 1216-1235.

Cooper, M.A. and V.T. Singleton, 2007. A survey of the 2001 to 2005 quartz crystal microbalance biosensor literature: Applications of acoustic physics to the analysis of biomolecular interactions. Journal of Molecular Recognition, 20(3): 154-184.

Coulter, L., M.A. Landree and T.A. Cooper, 1997. Identification of a new class of exonic splicing enhancers by in vivo selection. Mol. Cell. Biol., 17(4): 2143-2150.

Cruz-Aguado, J.A. and G. Penner, 2008. Determination of ochratoxin a with a DNA aptamer. Journal of agricultural and food chemistry, 56(22): 10456-10461.

Darmostuk, M., S. Rimpelová, H. Gbelcová and T. Ruml, 2015. Current approaches in selex: An update to aptamer selection technology. Biotechnology advances. DOI 10.1016/j.biotechadv.2015.02.008.

Davlieva, M., J. Donarski, J. Wang, Y. Shamoo and E.P. Nikonowicz, 2014. Structure analysis of free and bound states of an rna aptamer against ribosomal protein s8 from bacillus anthracis. Nucleic acids research: gku743.

Deng, Q., I. German, D. Buchanan and R.T. Kennedy, 2001. Retention and separation of adenosine and analogues by affinity chromatography with an aptamer stationary phase. Analytical chemistry, 73(22): 5415-5421. DOI 10.1021/ac0105437.

Di Primo, C., E. Dausse and J.-J. Toulmé, 2011. Surface plasmon resonance investigation of rna aptamer–rna ligand interactions. In: Therapeutic oligonucleotides. Springer: pp: 279-300.

Dobbelstein, M. and T. Shenk, 1995. In-vitro selection of rna ligands for the ribosomal l22 protein associated with epstein-barr virus-expressed rna by using randomized and cdna-derived rna libraries. J. Virol., 69(12): 8027-8034.

Dong, Y., Y. Xu, W. Yong, X. Chu and D. Wang, 2014. Aptamer and its potential applications for food safety. Critical reviews in food science and nutrition, 54(12): 1548-1561.

Ellington, A.D. and J.W. Szostak, 1990. In vitro selection of rna molecules that bind specific ligands. Nature, 346(6287): 818-822.

Entzian, C. and T. Schubert, 2015. Studying small molecule–aptamer interactions using microscale thermophoresis (mst). Methods.

Esposito, V., M. Scuotto, A. Capuozzo, R. Santamaria, M. Varra, L. Mayol, A. Virgilio and A. Galeone, 2014. A straightforward modification in the thrombin binding aptamer improving the stability, affinity to thrombin and nuclease resistance. Org. Biomol. Chem., 12(44): 8840-8843.

Girardot, M., P. Gareil and A. Varenne, 2010. Interaction study of a lysozyme-binding aptamer with mono- and divalent cations by ace. Electrophoresis, 31(3): 546-555. DOI 10.1002/elps.200900387.

Gold, L., D. Ayers, J. Bertino, C. Bock, A. Bock, E. Brody, J. Carter, A. Dalby, B. Eaton, T. Fitzwater, D. Flather, A. Forbes, T. Foreman, C. Fowler, B. Gawande, M. Goss, M. Gunn, S. Gupta, D. Halladay, J. Heil, J. Heilig, B. Hicke, G. Husar, N. Janjic, T. Jarvis, S. Jennings, E. Katilius, T. Keeney, N. Kim, T. Koch, S. Kraemer, L. Kroiss, N. Le, D. Levine, W. Lindsey, B. Lollo, W. Mayfield, M. Mehan, R. Mehler, S. Nelson, M. Nelson, D. Nieuwlandt, M. Nikrad, U. Ochsner, R. Ostroff, M. Otis, T. Parker, S. Pietrasiewicz, D. Resnicow, J. Rohloff, G. Sanders, S. Sattin, D. Schneider, B. Singer, M. Stanton, A. Sterkel, A. Stewart, S. Stratford, J. Vaught, M. Vrkljan, J. Walker, M. Watrobka, S. Waugh, A. Weiss, S. Wilcox, A. Wolfson, S. Wolk, C. Zhang and D. Zichi, 2010. Aptamer-based multiplexed proteomic technology for biomarker discovery. PloS one, 5(12). DOI 10.1371/journal.pone.0015004.

Gong, Q., J.P. Wang, K. Ahmad, A. Csordas, J. Zhou, J. Nie, R. Stewart, J. Thomson, J. Rossi and H. Soh, 2012. Selection strategy to generate aptamer pairs that bind to distinct sites on protein targets. Anal. Chem., 84(12): 5365-5371. DOI 10.1021/ac300873p.

Graham, J.C. and H. Zarbl, 2012. Use of cell-selex to generate DNA aptamers as molecular probes of hpv-associated cervical cancer cells. PloS one, 7(4): e36103.

Guo, K., A. Paul, C. Schichor, G. Ziemer and H.P. Wendel, 2008. Cell-selex: Novel perspectives of aptamer-based therapeutics. . Int. J. Mol. Sci. , 9: 668-678.

Han, S.R., 2013. In vitro selection of rna aptamer specific to salmonella typhimurium. Journal of microbiology and biotechnology, 23(6): 878-884.

Hermann, T. and D.J. Patel, 2000. Adaptive recognition by nucleic acid aptamers. Science, 287(5454): 820-825. DOI 10.1126/science.287.5454.820.

Heydari, S., Gholam Hossein Haghayegh, 2014. Application of nanoparticles in quartz crystal microbalance biosensors. Journal of sensor technology, 4: 81-100. Available from http://dx.doi.org/10.4236/jst.2014.42009.

Hianik, T., V. Ostatna, M. Sonlajtnerova and I. Grman, 2007. Influence of ionic strength, ph and aptamer configuration for binding affinity to thrombin. Bioelectrochemistry, 70(1): 127-133. Available from

http://www.ncbi.nlm.nih.gov/pubmed/16725379. DOI 10.1016/j.bioelechem.2006.03.012.

Homann, M. and H. Goeringer, 1999. Combinatorial selection of high affinity rna ligands to live african trypanosomes. Nucleic acids research, 27(9): 2006-2014.

Hu, J. and C.J. Easley, 2011. A simple and rapid approach for measurement of dissociation constants of DNA aptamers against proteins and small molecules via automated microchip electrophoresis. The Analyst, 136(17): 3461-3468.

Huang, C.J., H. Lin, S.C. Shiesh and G.B. Lee, 2010. Integrated microfluidic system for rapid screening of crp aptamers utilizing systematic evolution of ligands by exponential enrichment (selex). Biosens. Bioelectron., 25(7): 1761-1766. DOI 10.1016/j.bios.2009.12.029.

Huang, Y., X. Chen, N. Duan, S. Wu, Z. Wang, X. Wei and Y. Wang, 2015. Selection and characterization of DNA aptamers against staphylococcus aureus enterotoxin c1. Food chemistry, 166: 623-629. DOI 10.1016/j.foodchem.2014.06.039.

Jayasena, S.D., 1999. Aptamers: An emerging class of molecules that rival antibodies in diagnostics. Clin. Chem., 45(9): 1628-1650.

Jenison, R.D., S.C. Gill, A. Pardi and B. Polisky, 1994. High-resolution molecular discrimination by rna. Science, 263(5152): 1425-1429.

Jensen, K., B. Atkinson, M.C. Willis, T. Koch and L. Gold, 1995. Using in vitro selection to direct the covalent attachment of human immunodeficiency virus type 1 rev protein to high-affinity rna ligands. Proc. Natl. Acad. Sci. U. S. A., 92(26): 12220-12224.

Jerabek-Willemsen, M., T. André, R. Wanner, H.M. Roth, S. Duhr, P. Baaske and D. Breitsprecher, 2014. Microscale thermophoresis: Interaction analysis and beyond. Journal of Molecular Structure, 1077: 101-113.

Jiang, L., A. Majumdar, W. Hu, T. Jaishree, W. Xu and D.J. Patel, 1999. Saccharide–rna recognition in a complex formed between neomycin b and an rna aptamer. Structure, 7(7): 817-S817.

Jing, M. and M.T. Bowser, 2011. Methods for measuring aptamer-protein equilibria: A review. Analytica chimica acta, 686(1): 9-18.

Kailas, L., E. Ratcliffe, E. Hayhurst, M. Walker, S. Foster and J. Hobbs, 2009. Immobilizing live bacteria for afm imaging of cellular processes. Ultramicroscopy, 109(7): 775-780.

Kang, D., J. Wang, W. Zhang, Y. Song, X.L. Li, Y. Zou, M. Zhu, Z. Zhu, F.Y. Chen and C.J. Yang, 2012. Selection of DNA aptamers against glioblastoma cells with high affinity and specificity. PloS one, 7(10). DOI 10.1371/journal.pone.0042731.

Kaul, M., C.M. Barbieri, J.E. Kerrigan and D.S. Pilch, 2003. Coupling of drug protonation to the specific binding of aminoglycosides to the a site of 16s rrna: Elucidation of the number of drug amino groups involved and their identities. Journal of molecular biology, 326(5): 1373-1387.

Kawakami, J., H. Imanaka, Y. Yokota and N. Sugimoto, 2000. In vitro selection of aptamers that act with zn2+. J. Inorg. Biochem., 82(1-4): 197-206.

Kawano, R., T. Osaki, H. Sasaki, M. Takinoue, S. Yoshizawa and S. Takeuchi, 2011. Rapid detection of a cocaine-binding aptamer using biological nanopores on a chip. Journal of the American Chemical Society, 133(22): 8474-8477.

Konopsky, V.N. and E.V. Alieva, 2009. Optical biosensors based on photonic crystal surface waves. Biosensors and Biodetection: 49-64.

Krishnan, A., E. Vogler, B.A. Sullenger and R.C. Becker, 2013. The effect of surface contact activation and temperature on plasma coagulation with an rna aptamer directed against factor ixa. J. Thromb. Thrombolysis, 35(1): 48-56. DOI 10.1007/s11239-012-0778-7.

Kwon, M., S.-M. Chun, S. Jeong and J. Yu, 2001. In vitro selection of rna against kanamycin b. Molecules and cells, 11(3): 303-311.

Latham, M.P., G.R. Zimmermann and A. Pardi, 2009. Nmr chemical exchange as a probe for ligand-binding kinetics in a theophylline-binding rna aptamer. Journal of the American Chemical Society, 131(14): 5052-5053.

Le, X.C., V. Pavski and H. Wang, 2005. 2002 wae mcbryde award lecture affinity recognition, capillary electrophoresis, and laser-induced fluorescence polarization for ultrasensitive bioanalysis. Canadian journal of chemistry, 83(3): 185-194.

Li, L., D. Xiang, S. Shigdar, W. Yang, Q. Li, J. Lin, K. Liu and W. Duan, 2014. Epithelial cell adhesion molecule aptamer functionalized plga-lecithin-curcumin-peg nanoparticles for targeted drug delivery to human colorectal adenocarcinoma cells. International Journal of Nanomedicine, 9: 1083-1096. DOI 10.2147/IJN.S59779.

Li, Y., L. Guo, F. Zhang, Z. Zhang, J. Tang and J. Xie, 2008. High-sensitive determination of human α-thrombin by its 29-mer aptamer in affinity probe capillary electrophoresis. Electrophoresis, 29(12): 2570-2577. DOI 10.1002/elps.200700798.

Lin, P.-H., R.-H. Chen, C.-H. Lee, Y. Chang, C.-S. Chen and W.-Y. Chen, 2011. Studies of the binding mechanism between aptamers and thrombin by circular dichroism, surface plasmon resonance and isothermal titration calorimetry. Colloids and Surfaces B: Biointerfaces, 88(2): 552-558.

Lin, P., R.H. Chen, C. Lee, Y. Chang, C.S. Chen and W. Chen, 2011. Studies of the binding mechanism between aptamers and thrombin by circular dichroism, surface plasmon resonance and isothermal titration calorimetry. Colloid Surf. B-Biointerfaces, 88(2): 552-558. DOI 10.1016/j.colsurfb.2011.07.032.

Lonergan, N., L. Britt and C. Sullivan, 2014. Immobilizing live escherichia coli for afm studies of surface dynamics. Ultramicroscopy, 137: 30-39.

Long, S.B., M.B. Long, R.R. White and B.A. Sullenger, 2008. Crystal structure of an rna aptamer bound to thrombin. Rna, 14(12): 2504-2512.

Lou, X., J. Qian, Y. Xiao, L. Viel, A.E. Gerdon, E.T. Lagally, P. Atzberger, T.M. Tarasow, A.J. Heeger and H.T. Soh, 2009. Micromagnetic selection of aptamers in microfluidic channels. Proceedings of the National Academy of Sciences of the United States of America, 106(9): 2989-2994. DOI 10.1073/pnas.0813135106.

Lu, B., J. Wang, J. Zhang, X. Zhang, D. Yang, L. Wu, Z. Luo, Y. Ma, Q. Zhang, Y. Ma, X. Pei, H. Yu and J. Liu, 2014. Screening and verification of ssdna aptamers targeting human hepatocellular carcinoma. Acta Biochim. Biophys. Sin., 46(2): 128-135. DOI 10.1093/abbs/gmt130.

Luscombe, N.M., R.A. Laskowski and J.M. Thornton, 2001. Amino acid–base interactions: A three-dimensional analysis of protein–DNA interactions at an atomic level. Nucleic acids research, 29(13): 2860-2874.

Macaya, R.F., P. Schultze, F.W. Smith, J.A. Roe and J. Feigon, 1993. Thrombin-binding DNA aptamer forms a unimolecular quadruplex structure in solution. Proceedings of the National Academy of Sciences, 90(8): 3745-3749.

McKeague, M. and M.C. Derosa, 2012. Challenges and opportunities for small molecule aptamer development. Journal of Nucleic Acids, 2012. DOI 10.1155/2012/748913.

McKeague, M. and M.C. Derosa, 2012. Challenges and opportunities for small molecule aptamer development. J Nucleic Acids, 2012: 748913. Available from http://www.ncbi.nlm.nih.gov/pubmed/23150810. DOI 10.1155/2012/748913.

McKeague, M., E. McConnell, J. Cruz-Toledo, E. Bernard, A. Pach, E. Mastronardi, X. Zhang, M. Beking, T. Francis, A. Giamberardino, A. Cabecinha, A. Ruscito, R. Aranda-Rodriguez, M. Dumontier and M. DeRosa, 2015. Analysis of in vitro aptamer selection parameters. Journal of Molecular Evolution, 81(5): 150-161. DOI 10.1007/s00239-015-9708-6.

Meyer, C., U. Hahn and A. Rentmeister, 2011. Cell-specific aptamers as emerging therapeutics. Journal of nucleic acids, 2011.

Min, K., M. Cho, S.Y. Han, Y.B. Shim, J. Ku and C. Ban, 2008. A simple and direct electrochemical detection of interferon-gamma using its rna and DNA aptamers. Biosensors & bioelectronics, 23(12): 1819-1824. Available from http://www.ncbi.nlm.nih.gov/pubmed/18406597. DOI 10.1016/j.bios.2008.02.021.

Miyachi, Y., N. Shimizu, C. Ogino and A. Kondo, 2009. Selection of DNA aptamers using atomic force microscopy. Nucleic acids research: gkp1101.

Musafia, B., R. Oren-Banaroya and S. Noiman, 2014. Designing anti-influenza aptamers: Novel quantitative structure activity relationship approach gives insights into aptamer–virus interaction.

Musumeci, D. and D. Montesarchio, 2012. Polyvalent nucleic acid aptamers and modulation of their activity: A focus on the thrombin binding aptamer. Pharmacology & therapeutics, 136(2): 202-215.

Nagatoishi, S., Y. Tanaka and K. Tsumoto, 2007. Circular dichroism spectra demonstrate formation of the thrombin-binding DNA aptamer g-quadruplex under stabilizing-cation-deficient conditions. Biochemical and biophysical research communications, 352(3): 812-817.

Ngubane, N.A.C., L. Gresh, A. Pym, E. Rubin and M. Khati, 2014. Selection of rna aptamers against the m. Tuberculosis esxg protein using surface plasmon resonance-based selex. Biochem. Biophys. Res. Commun., 449(1): 114-119. DOI 10.1016/j.bbrc.2014.04.163.

Nguyen, B., J. Stanek and W.D. Wilson, 2006. Binding-linked protonation of a DNA minor-groove agent. Biophysical journal, 90(4): 1319-1328.

Nguyen, T.H.M. and V.H. Vu, 2012. Bioethanol production from marine algae biomass: Prospect and troubles. SLUB Dresden.

Ninomiya, K., K. Kaneda, S. Kawashima, Y. Miyachi, C. Ogino and N. Shimizu, 2013. Cell-selex based selection and characterization of DNA aptamer recognizing human hepatocarcinoma. Bioorganic & medicinal chemistry letters, 23(6): 1797-1802.

Nishikawa, F., H. Arakawa and S. Nishikawa, 2006. Application of microchip electrophoresis in the analysis of rna aptamer-protein interactions. Nucleosides, Nucleotides, and Nucleic Acids, 25(4-6): 369-382.

Nitsche, A., A. Kurth, A. Dunkhorst, O. Panke, H. Sielaff, W. Junge, D. Muth, F. Scheller, W. Stocklein, C. Dahmen, G. Pauli and A. Kage, 2007. One-step selection of

vaccinia virus-binding DNA aptamers by monolex. BMC Biotechnol., 7. DOI 10.1186/1472-6750-7-48.

Ouellet, E., J.H. Foley, E.M. Conway and C. Haynes, 2015. Hi-fi selex: A high-fidelity digital-pcr based therapeutic aptamer discovery platform. Biotechnology and bioengineering.

Peng, L., B. Stephens, K. Bonin, R. Cubicciotti and M. Guthold, 2007. A combined atomic force/fluorescence microscopy technique to select aptamers in a single cycle from a small pool of random oligonucleotides. Microsc. Res. Tech., 70(4): 372-381. DOI 10.1002/jemt.20421.

Pilch, D.S., M. Kaul, C.M. Barbieri and J.E. Kerrigan, 2003. Thermodynamics of aminoglycoside–rrna recognition. Biopolymers, 70(1): 58-79.

Pinto, A., P.N. Polo, O. Henry, M.C. Redondo, M. Svobodova and C.K. O'Sullivan, 2014. Label-free detection of gliadin food allergen mediated by real-time apta-pcr. Analytical and bioanalytical chemistry, 406(2): 515-524. Available from http://www.ncbi.nlm.nih.gov/pubmed/24247552. DOI 10.1007/s00216-013-7475-z.

Radom, F., P.M. Jurek, M.P. Mazurek, J. Otlewski and F. Jelen, 2013. Aptamers: Molecules of great potential. Biotechnology advances, 31(8): 1260-1274. Available from http://www.ncbi.nlm.nih.gov/pubmed/23632375. DOI 10.1016/j.biotechadv.2013.04.007.

Rebekah, W., R. Christopher, S. Elizabeth, W. Alisa, L. Jeffrey, H. Maureane and S. Bruce, 2001. Generation of species cross-reactive aptamers using "toggle" selex. Molecular Therapy, 4(6): 567. DOI 10.1006/mthe.2001.0495.

Robertson, D.L. and G.F. Joyce, 1990. Selection in vitro of an rna enzyme that specifically cleaves single-stranded DNA. Nature, 344(6265): 467-468.

Rodriguez-Mozaz, S., M.J.L. de Alda and D. Barceló, 2006. Biosensors as useful tools for environmental analysis and monitoring. Analytical and bioanalytical chemistry, 386(4): 1025-1041.

Roulet, E., S. Busso, A.A. Camargo, A.J.G. Simpson, N. Mermod and P. Bucher, 2002. High-throughput selex sage method for quantitative modeling of transcription-factor binding sites. Nature biotechnology, 20(8): 831.

Ruigrok, V.J., M. Levisson, J. Hekelaar, H. Smidt, B.W. Dijkstra and J. Van Der Oost, 2012. Characterization of aptamer-protein complexes by x-ray crystallography and alternative approaches. International journal of molecular sciences, 13(8): 10537-10552.

Sakamoto, T., A. Oguro, G. Kawai, T. Ohtsu and Y. Nakamura, 2005. Nmr structures of double loops of an rna aptamer against mammalian initiation factor 4a. Nucleic acids research, 33(2): 745-754.

Santosh, B. and P.K. Yadava, 2014. Nucleic acid aptamers: Research tools in disease diagnostics and therapeutics. BioMed research international, 2014: 540451. Available from http://www.ncbi.nlm.nih.gov/pubmed/25050359. DOI 10.1155/2014/540451.

Seferos, D.S., A.E. Prigodich, D.A. Giljohann, P.C. Patel and C.A. Mirkin, 2008. Polyvalent DNA nanoparticle conjugates stabilize nucleic acids. Nano letters, 9(1): 308-311.

Shangguan, D., Y. Li, Z. Tang, Z.C. Cao, H.W. Chen, P. Mallikaratchy, K. Sefah, C.J. Yang and W. Tan, 2006. Aptamers evolved from live cells as effective molecular

probes for cancer study. Proceedings of the National Academy of Sciences, 103(32): 11838-11843.

Shangguan, D., L. Meng, Z.C. Cao, Z. Xiao, X. Fang, Y. Li, D. Cardona, R.P. Witek, C. Liu and W. Tan, 2008. Identification of liver cancer-specific aptamers using whole live cells. Analytical chemistry, 80(3): 721-728.

Shi, H., G. Zhao, M. Liu, L. Fan and T. Cao, 2013. Aptamer-based colorimetric sensing of acetamiprid in soil samples: Sensitivity, selectivity and mechanism. Journal of hazardous materials, 260: 754-761.

Smestad, J. and L.J. Maher, 2012. Ion-dependent conformational switching by a DNA aptamer that induces remyelination in a mouse model of multiple sclerosis. Nucleic acids research: gks1093.

Smirnov, I. and R.H. Shafer, 2000. Effect of loop sequence and size on DNA aptamer stability. Biochemistry, 39(6): 1462-1468.

Song, K.M., S. Lee and C. Ban, 2012. Aptamers and their biological applications. Sensors, 12(1): 612-631. Available from http://www.ncbi.nlm.nih.gov/pubmed/22368488. DOI 10.3390/s120100612.

Stoltenburg, R., C. Reinemann and B. Strehlitz, 2005. Flumag-selex as an advantageous method for DNA aptamer selection. Anal. Bioanal. Chem., 383(1): 83-91. DOI 10.1007/s00216-005-3388-9.

Stoltenburg, R., C. Reinemann and B. Strehlitz, 2007. Selex—a (r)evolutionary method to generate high-affinity nucleic acid ligands. Biomolecular Engineering, 24(4): 381-403. Available from http://www.sciencedirect.com/science/article/pii/S1389034407000664. DOI http://dx.doi.org/10.1016/j.bioeng.2007.06.001.

Stoltenburg, R., T. Schubert and B. Strehlitz, 2015. In vitro selection and interaction studies of a DNA aptamer targeting protein a. PloS one, 10(7): e0134403.

Stratis-Cullum, D.N., S. McMasters and P.M. Pellegrino, 2009. Affinity probe capillary electrophoresis evaluation of aptamer binding to campylobacter jejuni bacteria. DTIC Document.

Strehlitz, B., C. Reinemann, S. Linkorn and R. Stoltenburg, 2012. Aptamers for pharmaceuticals and their application in environmental analytics. Bioanalytical Reviews, 4(1): 1-30. DOI 10.1007/s12566-011-0026-1.

Suh, S., H. Dwivedi, S.J. Choi and L. Jaykus, 2014. Selection and characterization of DNA aptamers specific for listeria species. Anal. Biochem., 459: 39-45. DOI 10.1016/j.ab.2014.05.006.

Sultan, Y., R. Walsh, C. Monreal and M.C. DeRosa, 2009. Preparation of functional aptamer films using layer-by-layer self-assembly. Biomacromolecules, 10(5): 1149-1154.

Sun, H. and Y. Zu, 2015. A highlight of recent advances in aptamer technology and its application. Molecules (Basel, Switzerland), 20(7): 11959. DOI 10.3390/molecules200711959.

Sundaresan, N. and C.H. Suresh, 2007. A base-sugar-phosphate three-layer oniom model for cation binding: Relative binding affinities of alkali metal ions for phosphate anion in DNA. Journal of chemical theory and computation, 3(3): 1172-1182.

Tan, Y., Q. Guo, Q. Xie, K. Wang, B. Yuan, Y. Zhou, J. Liu, J. Huang, X.X. He, X. Yang, C.M. He and X. Zhao, 2014. Single-walled carbon nanotubes (swcnts)-assisted cell-systematic evolution of ligands by exponential enrichment (cell-selex) for

improving screening efficiency. Anal. Chem., 86(19): 9466-9472. DOI 10.1021/ac502166b.

Tatarinova, O., V. Tsvetkov, D. Basmanov, N. Barinov, I. Smirnov, E. Timofeev, D. Kaluzhny, A. Chuvilin, D. Klinov and A. Varizhuk, 2014. Comparison of the 'chemical'and 'structural'approaches to the optimization of the thrombin-binding aptamer. PloS one, 9(2): e89383.

Thirunavukarasu, D. and H. Shi, 2015. An rna aptamer specific to hsp70-atp conformation inhibits its atpase activity independent of hsp40. Nucleic acid therapeutics, 25(2): 103-112.

Tuerk, C. and L. Gold, 1990. Systematic evolution of ligands by exponential enrichment: Rna ligands to bacteriophage t4 DNA polymerase. Science, 249(4968): 505-510.

Van Simaeys, D., D. López-Colón, K. Sefah, R. Sutphen, E. Jimenez and W. Tan, 2010. Study of the molecular recognition of aptamers selected through ovarian cancer cell-selex. PloS one, 5(11): e13770.

Vater, A., F. Jarosch, K. Buchner and S. Klussmann, 2003. Short bioactive spiegelmers to migraine-associated calcitonin gene-related peptide rapidly identified by a novel approach: Tailored-selex. Nucleic Acids Res., 31(21). DOI 10.1093/nar/gng130.

Vater, A., S. Sell, P. Kaczmarek, C. Maasch, K. Buchner, E. Pruszynska-Oszmalek, P. Kolodziejski, W. Purschke, K. Nowak, M. Strowski and S. Klussmann, 2013. A mixed mirror-image DNA/rna aptamer inhibits glucagon and acutely improves glucose tolerance in models of type 1 and type 2 diabetes. J. Biol. Chem., 288(29): 21136-21147. DOI 10.1074/jbc.M112.444414.

Velazquez-Campoy, A., M.J. Todd and E. Freire, 2000. Hiv-1 protease inhibitors: Enthalpic versus entropic optimization of the binding affinity. Biochemistry, 39(9): 2201-2207.

Venczel, E.A. and D. Sen, 1993. Parallel and antiparallel g-DNA structures from a complex telomeric sequence. Biochemistry, 32(24): 6220.

Wang, B., F. Huang, T. Nguyen, Y. Xu and Q. Lin, 2013. Microcantilever-based label-free characterization of temperature-dependent biomolecular affinity binding. Sensors and Actuators B: Chemical, 176: 653-659.

Wang, K., L. Gan, L. Jiang, X. Zhang, X. Yang, M. Chen and X. Lan, 2015. Neutralization of staphylococcal enterotoxin b by an aptamer antagonist. Antimicrobial agents and chemotherapy, 59(4): 2072. DOI 10.1128/AAC.04414-14.

Wen, J.D. and D.M. Gray, 2004. Selection of genomic sequences that bind tightly to ff gene 5 protein: Primer-free genomic selex. Nucleic Acids Res., 32(22). DOI 10.1093/nar/gnh179.

Wickiser, J.K., M.T. Cheah, R.R. Breaker and D.M. Crothers, 2005. The kinetics of ligand binding by an adenine-sensing riboswitch. Biochemistry, 44(40): 13404-13414.

Win, M.N., J.S. Klein and C.D. Smolke, 2006. Codeine-binding rna aptamers and rapid determination of their binding constants using a direct coupling surface plasmon resonance assay. Nucleic acids research, 34(19): 5670-5682.

Wong, A. and G. Wu, 2003. Selective binding of monovalent cations to the stacking g-quartet structure formed by guanosine 5'-monophosphate: A solid-state nmr study. Journal of the American Chemical Society, 125(45): 13895-13905. Available from http://dx.doi.org/10.1021/ja0302174. DOI 10.1021/ja0302174.

Wu, L.H. and J. Curran, 1999. An allosteric synthetic DNA. Nucleic Acids Res., 27(6): 1512-1516.

Yang, M., Z. Peng, Y. Ning, Y. Chen, Q. Zhou and L. Deng, 2013. Highly specific and cost-efficient detection of salmonella paratyphi a combining aptamers with single-walled carbon nanotubes. Sensors, 13(5): 6865-6881. DOI 10.3390/s130506865.

Yang, Y., D. Yang, H.J. Schluesener and Z. Zhang, 2007. Advances in selex and application of aptamers in the central nervous system. Biomolecular engineering, 24(6): 583-592.

Zhang, Y., Y. Chen, D. Han, I. Ocsoy and W. Tan, 2010. Aptamers selected by cell-selex for application in cancer studies. Bioanalysis, 2(5): 907-918.

Zhao, N., S.-n. Pei, P. Parekh, E. Salazar and Y. Zu, 2014. Blocking interaction of viral gp120 and cd4-expressing t cells by single-stranded DNA aptamers. International Journal of Biochemistry and Cell Biology, 51: 10-18. DOI 10.1016/j.biocel.2014.03.008.

Zimbres, F.M., A. Tárnok, H. Ulrich and C. Wrenger, 2013. Aptamers: Novel molecules as diagnostic markers in bacterial and viral infections? BioMed research international, 2013.

Zykovich, A., I. Korf and D. Segal, 2009. Bind-n-seq: High-throughput analysis of in vitro protein-DNA interactions using massively parallel sequencing. Nucleic acids research, 37(22): e151-e151. DOI 10.1605/01.301-0011889293.2010.

SECTION 2.3

A review on immobilised aptamers for high throughput biomolecular detection and screening

Caleb Acquah, Michael K. Danquah, Lau Sie Yon, Amandeep Sidhu, Clarence M. Ongkudon

DECLARATION FOR THESIS SECTION 2.3

A review on immobilised aptamers for high throughput biomolecular detection and screening.

The candidate will like to declare that there is no conflict of interests involved in this work and that my extent of contribution as candidate is as shown below:

Contribution of Candidate	Conceptualisation, initiation and write-up	75%

The following co-authors were involved in the development of this publication and attest to the candidate's contribution to a joint publication as part of his thesis. Permission by co-authors are as follows:

Name	Signature	Date
Michael K. Danquah		13.07.2017
Lau Sie Yon		13.07.2017
Charles K.S. Moy		13.07.2017
Amandeep Sidhu		18.07.2017
Clarence M. Ongkudon		13.07.2017

ABSTRACT

The discovery of Systematic Evolution of Ligands by Exponential Enrichment (SELEX) assay has led to the generation of aptamers from libraries of nucleic acids. Concomitantly, aptamer-target recognition and its potential biomedical applications have become a major research endeavour. Aptamers possess unique properties that make them superior biological receptors to antibodies with a plethora of target molecules. Some specific areas of opportunities explored for aptamer-target interactions include biochemical analysis, cell signalling and targeting, biomolecular purification processes, pathogen detection and, clinical diagnosis and therapy. Most of these potential applications rely on the effective immobilisation of aptamers on support systems to probe target species. Hence, recent research focus is geared towards immobilising aptamers as oligosorbents for biodetection and bioscreening. This article seeks to review advances in immobilised aptameric binding with associated successful milestones and respective limitations. A proposal for high throughput bioscreening using continuous polymeric adsorbents is also presented.

Keywords: Aptamers; Biosensing; Screening; Immobilisation; Oligosorbents

1.   INTRODUCTION

Nucleic acids are thread-like polynucleotides contained in all living and non-living cells, and are essential to all known forms of life. Since the pioneering of nucleic acid research by Friedrisch Meister in 1868, there has been an ever-growing development and understanding of nucleic acids and their applications. One of such developments is the discovery of aptamers from synthetic sequence of nucleotide linkages (Famulok and Mayer, 2011; Radom *et al.*, 2013).

Aptamers are *in vitro* chemically synthesised oligonucleotides with high specificity and sensitivity towards a specific target. The length of aptamers is usually in the region of 35-100 nucleotides, with a unit size being equal to the size of its base (Famulok and Mayer, 2011). The advent of aptamers began in the year 1990 when three different laboratories of G. F. Joyce, J.W. Szostack and L. Gold reported independently on a novel *in vitro* selection technique in successive months (Andrew and Jack, 1990; Robertson and Joyce, 1990; Tuerk and Gold, 1990). The technique allows for the selection of a specific sequence of nucleic acids from a large pool of different sequences of DNA and RNA against any target, and was termed as the systematic evolution of ligands by exponential enrichment, SELEX (Tuerk and Gold, 1990). An infinite array of targets exists for specific binding to aptamers. Some of the aptamer binding targets reported in literature include numerous variant molecular apatopes (binding site of a target by an aptamer) of small organic molecules such as ethanolamine, protein molecules, whole cells, metal ions such as K^+, lipids and sugar moieties (Mann *et al.*, 2005; Radom *et al.*, 2013; Sharma and Sharma, 2013). Also, aptamers can be biomolecularly engineered to improve their bioavailability and biostability (Mann *et al.*, 2005; Bunka and Stockley, 2006). The biostability of aptamers has been reportedly achieved by engineering 2′-amino-modified, 2′-fluoro-modified pyrimidines, 2′-methyl pyrimidines, 4′-thio pyrimidines or 3′–3′ linked dinucleotide caps into the aptamer (Bunka and Stockley, 2006). Notably, the chemical structure of an aptamer is made up of 4 bases of nucleotides whereas protein markers such as antibodies are made up of 20 bases of amino acids. Antibodies have a vast number of combinatorial parings which allows for specific molecular recognition of targets (Hermann and Patel, 2000; McKeague and Derosa, 2012). However, aptamers are highly

specific due to their singular function of binding to their cognate molecules (Jayasena, 1999; Hermann and Patel, 2000; McKeague and Derosa, 2012).

Over the past decade, there have been interesting developments in the application of immobilised aptamers as biomolecular devices for binding of target molecules. These new applications, unlike conventional technologies, such as protein nanopores (Ding *et al.*, 2009; Gao *et al.*, 2009), solid phase extraction (Zhao *et al.*, 2012), and liquid chromatography (van Den Ouweland and Kema, 2012), have several advantages. These advantages include higher sensitivity, longer life span, absence of matrix effect, higher throughput, and absence of sample pre-treatment. This is attributed to the molecular recognition ability of aptamers to selectively bind to their specified targets and differentiate between enantiomeric targets (Madru *et al.*, 2011). One of such new aptamer-based chromatographic application has been referenced to as oligosorbents (Madru *et al.*, 2011).

Protein nanopores are useful for biosensing, single molecule recognition and detection of nucleic acids. Through structure-directed genetic engineering and chemical modifications, the characteristics of protein nanopore can be enhanced (Gao *et al.*, 2009). Protein nanopores have fixed pore sizes which are mostly invariable for different target sizes, and possess fragile lipid bilayers (Gao *et al.*, 2009). Several attempts to circumvent these setbacks have led to the fabrication of synthetic nanopores in micropipettes with immobilised antibodies and subsequently with aptamers as probes (Ding *et al.*, 2009). Several extensive reviews existing on the use of surface based aptasensors for target detection cover aptazymes, acoustic, optical, molecular beacon aptasensors, electrochemical, cantilever-based, signalling aptamers, proximity ligation and extension, and nanoparticle-conjugated aptasensors (Tombelli *et al.*, 2005; Mairal *et al.*, 2008; Song *et al.*, 2008; Hamula *et al.*, 2011). Also, Deng *et al.* (2014) reported a review on the use of thrombin targets as models for the development of aptameric assays, which included various affinity separation and screening assays. In addition, the development of oligosorbents and applications as superior assays over conventional immunosorbents has also been critically discussed recently (Pichon *et al.*, 2015). All these reviews have only focussed on the application of aptameric binding as a form of biomarking for target

detection. There have been no comprehensive review reports on the application of aptameric binding for high throughput bio-separation and screening of molecular/cellular species by convective mass transport using macroporous continuous polymers (called monoliths). Macroporous continuous polymers can possess convective mass transfer ability to enable rapid target adsorption. Also, there are limited reports discussing the inherent limitations for oligosorbents in the literature. Current oligosorbent formats have only relied on the immobilisation of aptamers on particulate adsorbents. These adsorbents are disadvantaged with slow diffusive mass transport mechanism due to their small particle pores, thus hindering the achievement of high throughput screening.

Herein, this article reports on recent advances in the application of immobilised aptamers as polymeric aptasensors for biomolecular detection and screening including milestones covered and their associated limitations. A theoretical insight into modifiable features and constraints of both oligosorbents and aptamer-monoliths to enhance performance is presented. A proposal for enhanced bioscreening technology using monolithic supports with convective mass transport mechanism for high throughput applications is also presented.

2. AN OVERVIEW OF APTAMER-TARGET INTERACTION MECHANISMS

Aptamers are readily generated from SELEX for a specific target. The main idea behind SELEX is to simulate the evolution of synthetic oligonucleotides as the natural process of evolution is slow and complex (Radom *et al.*, 2013). SELEX, which is an *in vitro* selection process, is very rapid and can be modified for different targets. The entire SELEX process is simplified to be an iterative cycle of partitioning and amplification (Pinto *et al.*, 2014). A library of nucleic acids with defined sequences is randomised and incubated against a specified target for binding and selection. Nucleic acid molecules that do not bind to the target are eluted by employing techniques such as magnetic separation, filtration and affinity chromatography. Selected nucleic acids are amplified and enriched several times by adjusting binding parameters such as pH and buffer composition until the best binding ligand dominates the population of sequences. The selected and most specific binding ligand amongst the pool of sequences usually has the smallest dissociation constant, K_d,

often in the millimolar-picomolar range or even less (Stoltenburg *et al.*, 2007; Mairal *et al.*, 2008; Zhu *et al.*, 2012; Pinto *et al.*, 2014).

Aptamers possess the inherent ability to form secondary structures which enables them to detect and bind onto specific targets (Chang *et al.*, 2014). Aptamers, with the aid of their secondary structural conformation, are able to distinguish between variant targets or enantiomers based on the conformational differences in the structures of target molecules (O'Sullivan, 2002; Ulrich and Wrenger, 2009; Mascini *et al.*, 2012). Some of these structural differences include the presence or absence of a hydroxy group, a methyl group or the D- enantiomeric configuration against the L- enantiomeric configuration (O'Sullivan, 2002). Rationally, aptamers can be modified to conformational switching with their ligand binding abilities preserved. In the absence of a target, the thermodynamically stable conformation of the aptamer is maintained (Chang *et al.*, 2014). In the presence of the target, the affinity between the duo induces binding to form an aptamer-target complex. After binding, an adaptive trapping of the target by the aptamer occurs. This results in the formation of stabilised tertiary structures from the secondary structures of the aptamer (Pinto *et al.*, 2014). Such structural changes in the conformations of aptamers can be characterised through the use of circular dichroism, quartz crystal microbalance, interferometer and isothermal titration calorimetry (Ozalp *et al.*, 2013). Hianik *et al.* (2007) studied the effect of immobilisation, ionic concentration, aptamer configuration, and pH on the interactions between thrombin and its binding aptamer with an electrochemical indicator and a quartz crystal microbalance. It was observed that the linear aptamer had a faster change in frequency and a higher steady state frequency value than their molecular beacon aptamers. This observation was linked to the bulky structure of the molecular beacons and their high molecular weights of 10576 Da and 6791 Da (Hianik *et al.*, 2007).

Aptamer-target interactions are based on affinity binding. The binding between the aptamer and the target molecule existing within the tertiary structure (aptamer-target complex) is non-covalent. The concept of aptamer-target binding and the existence of non-covalent bonding is illustrated in Figure 1. The non-covalent interactions can be as a result of hydrogen bonding, hydrophobic interaction, aromatic stacking, electrostatic interactions, and van der Waals interactions (Mascini *et al.*, 2012; Pinto *et al.*, 2014;

Santosh and Yadava, 2014). Aptamers either fold around small molecules such as ethanolamine into their nucleic acid structures or are encapsulated into the structures of large molecules such as proteins (Rhouati *et al.*, 2011). Research advancements have led to the development of aptamers for multiple variant target binding. With such multi-targeted aptamers, the interactions between the aptamer and the targets can be any of the above-mentioned non-covalent bonding types, or a combination, depending on the interacting moieties (Jayasena, 1999; Zhu *et al.*, 2014). It has been reported that aptamers do not only bind to their cognate molecules, but also inhibit their biological functions by interfering with the catalytic site of the molecule, ligand-receptor recognition sites, or through the induction of allosteric effects (Ulrich and Wrenger, 2009; Anthony *et al.*, 2010; Dun, 2010). In terms of binding performance and specificity, no distinguishing features have been reported for RNA and DNA aptamers to date. However, RNA aptamers are easily expressed within the same cell, whereas DNA molecules are much more stable (Radom *et al.*, 2013). RNA and DNA aptamers have different sequences and patterns of folding towards the same target molecule (Song *et al.*, 2012).
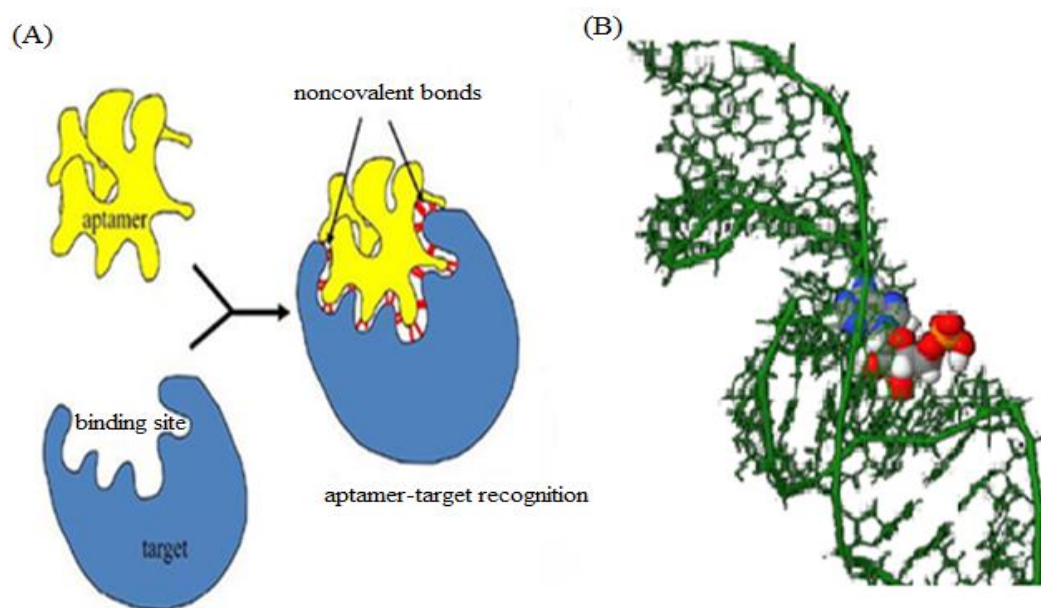
Figure 1. (A) A simplified diagram of an aptamer-target interaction showing non-covalent bonding between the aptamer and the target binding site (Finch et al., 2013). (B) An arbitrary aptameric molecule binding onto a target; figure available online.

3.   APTAMER IMMOBILISATION

Aptamer based biosensors are referred to as aptasensors. The application of immobilised aptamers as bio-receptors in the development of biosensors has several benefits. Generally, aptamers are immobilised on solid surfaces to enhance their structural stability, prolong the life span of the sensor, and for real-time recognition applications (Banerjee and Nilsen-Hamilton, 2013).

3.1   Development of Immobilised Aptamers for Biodetection and Screening

Centi *et al*. (2008) reported using the thrombin aptamer as a model to study the detection limit for binding immobilised and free aptamers towards a single protein target. Immobilised aptamers detected the target proteins in solution with a detection limit of 430 nM (Centi *et al.*, 2008). Free aptamers in solution could not detect at this limit, and this was attributed to steric hindrance (Centi *et al.*, 2008). However, a further improvement in detection (175 nM) was achieved with an immobilised aptamer in a sandwich assay format. Binding studies were carried out with a surface plasmon resonance technique (Centi *et al.*, 2008).

Aptamer immobilisation is significant to explore different applications of aptameric binding with targets. Aptamers immobilise at high densities owing to their small molecular size, thus enhancing their ability to probe target molecules (Zhao *et al.*, 2012). Various methods of immobilising aptamers on solid supports have been recently reported. These include physical adsorption, covalent bonding immobilisation, self-assembly, immobilisation by polymerization, coupling by affinity reactions immobilisation, and polynucleotides–nanoparticles hybrids (Bănică, 2012). The afore-mentioned immobilisation chemistries are chiefly achieved through modifications of the 3' and/or 5' ends of the aptamer with an appropriate functional group (de-los-Santos-Álvarez *et al.*, 2008). However, the binding characteristics of aptamers under immobilised conditions could vastly be affected by the physicochemical properties of the binding surface, resulting from a possible induced structural dislocation of active and/or binding sites of the aptameric molecule, and this may affect the K_d value. K_d is the fundamental parameter characterising the binding strength, hence K_d for an immobilised aptamer may be different from that of the same aptamer in free solution. Under immobilised conditions, K_d might

increase because of restricted mobility towards the formation of unique secondary structures for access to active group on the aptamer, or decrease as a result of enhanced molecular interaction between the aptamer and the target. However, research report investigating the possible biophysical differences between the binding features of immobilised and free aptamers are minimal.

Conspicuously, the key design criteria essential for the development of an effective immobilised aptameric sensor for high throughput screening applications include: (i) real-time rapid detection with high sensitivity and selectivity through the achievement of high ligand density immobilisation of aptamers on adsorbents with convective mass transport; (ii) engineering of the immobilisation chemistry through the introduction of spacers and/or surface modifying agents to maintain the binding performance of aptamer under immobilised conditions; (iii) capacity to withstand complex environment as with field samples such as water bodies, food matrices, agricultural soil and plants, and human or animal samples; (iv) capacity for multiple bioaffinity interactions and simultaneously monitor different molecular species; (v) a wide range of possibilities for developing signal transduction and amplification mechanisms; (vi) ability to regenerate to enable routine and repeated use. Techniques for target elution and regeneration are dependent on the type of stationary support and the immobilisation chemistry. This is important to maintain the physicochemical properties of the adsorbent and the maximum ligand density. Common regeneration methods include the use of chaotropic reagents, temperature effect or DNA enzyme digestion (Zhao *et al.*, 2012). Peyrin *et al*., (2009) discussed the selection of operating conditions for bioseparation of targets in a chromatographic context based on differences in binding association and dissociation constants. They classified aptameric assays as type 1 and type 2 where the former represents aptamers with moderate to high affinity constant, and the latter for aptamers with low affinity constants. Key operating conditions affecting aptamer conformations for optimal throughput in type 1 and 2 assays include ionic concentration, pH of the mobile phase, addition of organic modifiers and operating temperatures (Peyrin, 2009; Pichon *et al.*, 2015).

The development of porous polymeric biosensors with immobilised aptamers has proven to be more effective than antibody formats. By flanking aptamers with two primer

sequences, they are able to report the detection of targets without being labelled, unlike antibodies (Svobodova *et al.*, 2014). Two main assay configurations for aptamers are in existence and are a function of the size of the target, namely, single site binding and double sites binding (Song *et al.*, 2008; Mascini *et al.*, 2012). The single site binding configuration is often employed for molecules small in size, whereas double sites binding is employed for large molecules (Song *et al.*, 2008).

4.   CURRENT APPLICATIONS OF APTAMERS

The multifarious applications of aptamers is as a result of the ability to form stable three-dimensional structures, have a low dissociation constant (k_d), and undergo chemical modifications of its sugar backbone with amino/fluoro groups when necessary. Modifications of the sugar backbone extend the aptameric half-life and project other functionalities. Prior to chemical modifications, aptamers usually last for less than 10mins in biological fluids (O'Sullivan, 2002; Ulrich and Wrenger, 2009; Santosh and Yadava, 2014). Table 1 shows some advantageous properties of aptamers for different process parameters.

Table 1. List of demonstrated advantages of aptamers for biomedical applications.

Parameter	Advantage of aptamers	Reference(s)
Cost of manufacture	Less expensive and readily produced scalable methods compared to the production of monoclonal antibodies.	(Jayasena, 1999; Hu *et al.*, 2014; Santosh and Yadava, 2014)
Product variation	Largely consistent performance. Batch-to-batch variations exist with antibodies.	(Jayasena, 1999; Tombelli *et al.*, 2007)
Duration	Short duration to biochemically synthesis aptamers. Takes weeks instead of the usual months for antibodies.	(Rhouati *et al.*, 2011; Santosh and Yadava, 2014)
Medium/suitable environments	Aptamers show a wider range of stability towards different residing media of the target.	(Jayasena, 1999; Tombelli *et al.*, 2007; Dun, 2010)
Biopurity	The selection process of aptamers is not prone to viral or bacterial contamination.	(Santosh and Yadava, 2014)

Immunogenicity or toxicity	Aptamers are synthesised *in vitro* hence are mostly void of biotoxins.	(Jayasena, 1999; Ulrich and Wrenger, 2009)
Target space	Aptamers virtually have an infinite array of targets.	(Ulrich and Wrenger, 2009; Radom *et al.*, 2013; Santosh and Yadava, 2014)
Shelf life	Aptamers are stable and have a long shelf life. They can be regenerated even after denaturation.	(Jayasena, 1999; Zhao *et al.*, 2012; Hu *et al.*, 2014)

4.1 Aptamers for Medical Applications

Sensors for clinical diagnosis are expected to be highly specific, easy to read, sensitive, accurate, have good performance under varying physiological conditions, stable and fast. These requirements are achievable with aptamers as probes for detection (Soontornworajit and Wang, 2011; Radom *et al.*, 2013). For example, in generating aptamers for a target protein, it is not significant to know the molecular signature (number or type) of the protein pre-generation (Fang and Tan, 2010; Zhu *et al.*, 2012). This makes it easier to probe new pathogenic species with minimal knowledge of their biomolecular framework. Several methods of generating aptamers against protein targets exist. Some of these methods are Primer-free SELEX, Toggle SELEX, *In vivo* SELEX, Cell SELEX and Genomic SELEX (Aquino-Jarquin and Toscano-Garibay, 2011; McKeague and Derosa, 2012; Radom *et al.*, 2013). Pathogenic processes have a unique protein or enzymatic synthesis and activity that can be detected with the use of aptameric probes with high specificity. Fang *et al.* (2010) elaborated on the significance of aptamer generation by cell-SELEX for the molecular recognition of cancerous cells. An aptamer-modified microfluidic device for cell enrichment has also been developed to separate viable and non-viable cells from a large cellular environment with little or no sample pre-treatment (Fang and Tan, 2010; Soontornworajit and Wang, 2011). Other promising approaches reported in literature for cell detection are flow cytometry analysis, aptamer-functionalized nanoparticles for biosensing, and histological examination.

Application of aptasensors is essential in the detection of food and water-borne diseases in complex matrices (Leonard *et al.*, 2003; Kärkkäinen *et al.*, 2011; Sonia *et al.*, 2013).

Several other successes have been notably achieved by the application of aptameric recognition for the detection of toxins in the lectin family (Sharma and Sharma, 2013), Lup-an-1 food allergen (Nadal *et al.*, 2012), prions (Takemura *et al.*, 2006), variant strains of *Escherichia coli* (Kim *et al.*, 2013), and Trypanosomes (Kim *et al.*, 2013). Mann *et al.* (2005) reported the successful identification of an immobilised aptamer suitable for binding ethanolamine; one of the smallest compounds ever detected by an aptamer. Ethanolamines are of clinical and environmental concerns due to their disease causing effects (Mann *et al.*, 2005). Minunni *et al.* (2004) demonstrated the reproducibility, specificity and reusability of aptasensors through the use of an RNA^{TAT} aptamer for the detection of HIV-Tat protein.

The success of therapeutic analysis is measured by the capacity to target specific infected cells amongst healthy cells (Guo *et al.*, 2008; Dun, 2010). This synchronises with the aims of modern molecular therapy, which seeks to avoid conventional trial-and-error targeting with low specificity (Fang and Tan, 2010). Aptameric binding of targets is a significant component of modern molecular therapies in the development of high sensitivity and rapid molecular or cellular targeting systems for disease treatment. The following features make aptamers effective therapeutic markers: high specificity and efficiency, non-immunogenic, non-toxic, and non-recalcitrance after being tested at high dosages of 10 mg/kg daily for 90 days in rats; administration through intravenous or subcutaneous injection; and economical to develop (Santosh and Yadava, 2014). Therapeutic aptamers function by either inhibiting target molecules or as receptor agonists (Radom *et al.*, 2013). Advances in modern therapeutic research have led to the invention and acceptance of Macugen, which is a vascular endothelial growth factor binding aptamer (Guo *et al.*, 2008; Banerjee and Nilsen-Hamilton, 2013) with the potential of providing new therapeutic pathways to prevent cardiovascular diseases. Other successful work carried out include: ARC1779 which has an antithrombotic activity and currently undergoing clinical trials(Ulrich and Wrenger, 2009); AS1411, formerly known as AGRO100, which is a cancer aptamer and undergoing clinical trials (Guo *et al.*, 2008), NOX-E36, an aptamer for diabetes (Guo *et al.*, 2008), and significant findings made in preclinical studies against cancer targets by modulating apoptosis in organisms (Guo *et al.*, 2008).

Suggestions are being made to improve healthcare delivery through the establishment of Point-of-Care Testing (POCT) approach (Cass and Zhang, 2011). The use of aptasensors for POCT will help save time, increase productivity, and avoid huge capital investments required for establishing several fixed structures for lab diagnosis. Alternatively, aptasensors can be routinely applied in door-to-door domestic testing, mass screening of infectious and contagious diseases, clinical diagnosis, and border chemo/bio-security programs. This is because immobilised aptamers can be engineered to develop miniaturised sensors with a high surface density as compared to immunoassay sensors (Mairal *et al.*, 2008; Song *et al.*, 2008). This will certainly be of much importance during pandemics in offering a rapid and easy-to-use detection system capable of breaking the mode of transmissions. Medical diagnostic and therapeutic applications of aptamers are receiving much attention from researchers, and this is pivotal to improve the detection of pathogenic entities rapidly and accurately from human samples (Anthony *et al.*, 2010; Zhu *et al.*, 2012; Deng *et al.*, 2014). Some of the interesting developments in the application of immobilised aptamers include immobilisation on engineered glass nanopores, sepharose, magnetic beads, silica, and also as oligosorbents. Table 2 shows different applications of aptasensors.

Table 2. Identified immobilised aptameric supports and applications.

Type of aptamer	Type of support	Application	Reference
IgE aptamer; Ricin aptamer	Glass	To detect and screen IgE, Ricin toxin.	(Ding *et al.*, 2009)
AptC.1	Silica	To immobilise Chymotrypsin in the construction of an enzymatic reactor for protein digestion.	(Xiao *et al.*, 2012)
Amino modified cocaine aptamer	Cyanogen Bromide - activated sepharose	Selective detection and extraction of cocaine	(Madru *et al.*, 2011)
Amino modified cocaine aptamer	Streptavidin-activated agarose	Selective detection and extraction of cocaine	(Madru *et al.*, 2011)
Ochratoxin A aptamer	Magnetic nanospheres	Detection and extraction of ochratoxin A from food samples	(Wu *et al.*, 2011)
Ochratoxin A aptamer	Cyanogen Bromide -	Detection and extraction of ochratoxin A	(Rhouati *et al.*, 2011)

	activated Sepharose		
A10 RNA aptamer	Quantum Dot	Targeting of cells and sensing delivery of drug for cancer treatment	(Bagalkot *et al.*, 2007)
β-conglutin aptamer	Microtiter plate	Detecting of β-conglutin food allergen	(Svobodova *et al.*, 2014)

5.   POLYMERIC APTASENSORS FOR BIOSCREENING OF TARGETS

5.1   Immobilisation of aptamers on a single glass nanopore

Immobilisation of aptamers on a glass nanopore of a pipette for the detection of IgE and ricin, the third most toxic substance and a potential bio-threat, has been successfully performed and reported (Ding *et al.*, 2009). This follows the successful work done by Gao *et al.* (2009) in fabricating a synthetic nanopore at the tip of a micropipette. Prior to that, protein nanopores with attached receptors were used for single molecule detection. However, this method lacked the capacity for real-time detection and possessed fragile lipid membranes. The aftermath of the development of synthetic glass nanopores led to modifications with antibodies. However, antibodies, unlike aptamers, are mostly limited to non-toxic targets, present difficulty during immobilization, and are relatively difficult to synthesise. Aptamer-embedded nanopores are very robust, specific and effective for molecular detection of pathogens with nano sizes (Ding *et al.*, 2009). Future applications of this immobilised aptameric system could be multiple target biosensing. Significant challenges of single glass nano-pores include prolong recognition time, low binding frequency and clogging by DNA targets (Ding *et al.*, 2009). These are attributed to the diffusion-collision rate and the binding activation energy (Zhao *et al.*, 2012).

5.2   Application of immobilised aptamers as oligosorbents

Another unique development of immobilised aptamers is the synthesis of oligosorbents. Oligosorbents are produced by immobilising aptamers on solid supports. They are able to detect and screen targets with high affinity and specificity from complex matrixes by employing the established biomolecular recognition mechanisms of aptamers (Ali and Pichon, 2014). Oligosorbents can be applied in purification processes for specific detection and screening of target molecules from complex samples. Prior to the advent of

aptamer-based oligosorbents, molecular screening and purification of target species relied on several unit steps such as ion-exchange or hydrophobic interaction liquid chromatography, and solid phase extraction with either hydrophobic supports or immunoaffinity columns. Table 3 compares the characteristics of various molecular screening and purification techniques with oligosorbents.

Table 3. Characteristic features of various purification techniques in juxtaposition with oligosorbents.

Detection and Screening Method	Characteristic feature(s) for binding and screening			Reference(s)
Liquid chromatography	Pre-treatment of sample is required	Time-consuming	Problem of matrix effect	(Chapuis-Hugon *et al.*, 2011; Madru *et al.*, 2011; Wu *et al.*, 2011)
Conventional solid phase extraction	Large quantity of organic solvent required	Time-consuming	Not specific	(Madru *et al.*, 2011; Wu *et al.*, 2011)
Immunoaffinity columns	Expensive to operate due to the use of antibodies	Exhibit variations from different batches of antibodies	Have a short life cycle and not suitable for high temperature and harsh solvents	(Chapuis-Hugon *et al.*, 2011; Madru *et al.*, 2011; Wu *et al.*, 2011)
Aptamer-based biomolecular recognition mechanism	Less expensive relative to the above methods	Specific and have a high affinity for target	Have a long-life span	(Chapuis-Hugon *et al.*, 2011; Madru *et al.*, 2011; Wu *et al.*, 2011)

Efficient immobilisation of aptamers on supporting systems depends on the following factors: the type of immobilisation support, the functional groups of the support, pore framework of the matrix, the type of bonding between the supporting system and the aptamer, and the length of the spacer arm if required. By studying these characteristics of a known support system, an optimal immobilised aptameric sensor can be developed for detecting and screening of target molecules. Research reports indicate that high throughput recovery efficiencies within the range of 67% to 96% were achieved with

oligosorbents for different analyses of food samples (Bagalkot *et al.*, 2007; Madru *et al.*, 2009; Chapuis-Hugon *et al.*, 2011; Madru *et al.*, 2011; De Girolamo *et al.*, 2012; Ali and Pichon, 2014). Current aptamer applications as oligosorbents have mostly been devoted to the detection of cocaine samples and ochratoxin A in food, drinks and blood plasma. The challenge, however, now lies in the application of this approach or modified versions for enhanced bio/chemical detection and screening of other target molecules. Nonetheless, this can be achieved by generating and characterising specific aptamers for the chosen targets of interest.

Even though chemo-physical modifications have led to improvements in throughput, there are two inherent setbacks in the use of polymeric beads, such as silica, in their particulate form as supports for aptamers. In Figure 2, the pore size and transport mechanism of particulate oligosorbent system is shown. The configuration for solid phase extraction using oligosorbent packing usually results in small pore sizes. Due to the small pore size and the distribution of empty spaces between the oligosorbent particles, the mechanism of mass transfer of solutes is by diffusion through the interstitial voids. The experimental void fraction (ε) between particles in the stationary phase of a packed column is estimated to be between 30-50% of the entire volume of the column for smooth diffusion to take place without channelling (Benitez, 2009).
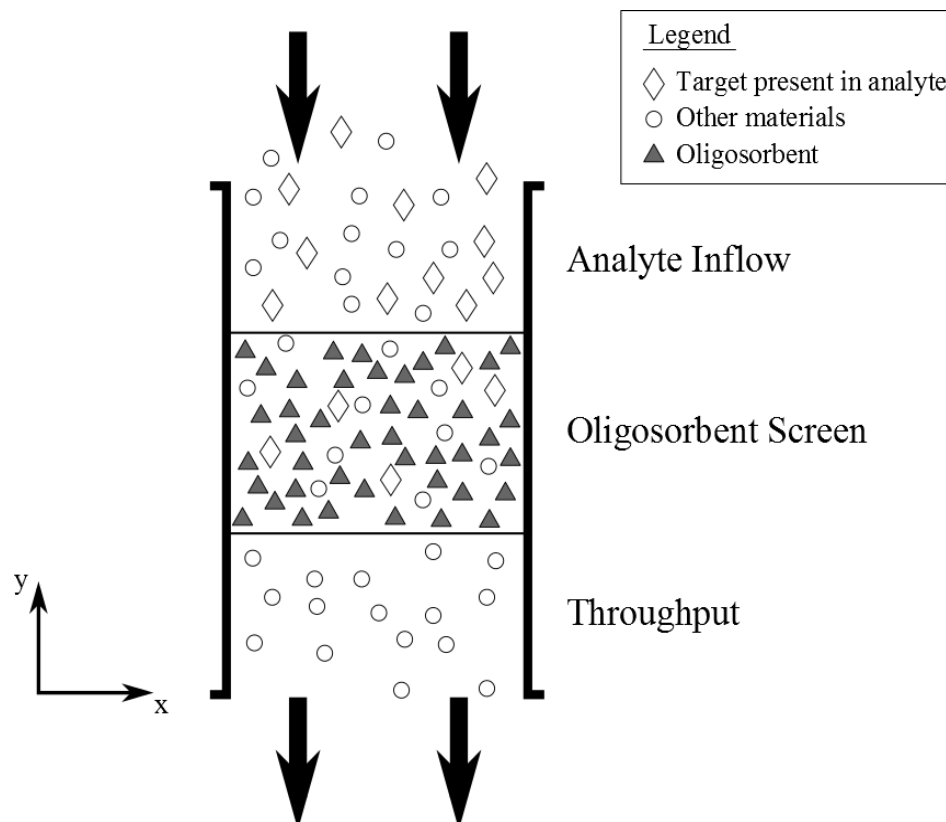
Figure 2. Process configuration of an oligosorbent chromatographic column for screening analytes.

A classic expression relating the void fraction and effective diffusivity (D_{AB}) of solutes in the liquid analyte is shown by equation (1). It must be emphasized that the rate determining step of the solid phase extraction of targets with oligosorbents is the rate of diffusion. Solutes such as proteins and DNA with large hydrodynamic sizes, will take a longer time to diffuse through the matrix.

$$\varepsilon = \frac{void\ volume\ (V)}{total\ volume\ of\ the\ column(V_T)} \qquad (1)$$

Considering the configuration of an oligosorbent system and molecular diffusion as the means of mass transfer, Fick's law can be used to estimate the effective diffusivity as:

$$D_{AB,eff} = \frac{\varepsilon D_{AB}}{\tau} \qquad (2)$$

Diffusivity of a solute A in a liquid solvent B can be theoretically estimated from Stokes-Einstein equation. This expression is given as:

$$D_{AB} = \frac{kT}{6\pi r_A \mu_B} \tag{3}$$

where τ is the tortuosity of the pore-path, r_A is the radius of the solute in the solvent, T is the operating temperature in K, k is the Boltzmann's constant and μ_B is the viscosity of the liquid solvent B. From the above equations, it becomes clear that the effective diffusion of particles is a function of the void fraction, the radius (size) of the solute, which in this sense is the target and in other terms the viscosity of the solvent as well. This can be expressed as:

$$D_{AB,eff} = f(\varepsilon, r_A, \mu_B) \tag{4}$$

The first parameter of the function, ε, is a design parameter which can be controlled and improved by considering other adsorbents such as engineered macroporous continuous polymers.

5.3   High throughput immobilised systems

Considering the drawbacks of oligosorbent systems as discussed earlier, a more effective approach will be the use of a continuous adsorbent system as the stationary support. Such supports have been demonstrated to be effective for high throughput results. Zhao *et al.*, (2008a) were the first group to successfully host aptamers on the monolithic polymer (glycidyl methacrylate-co-trimethylolpropanetrimethacrylate). They used 61mer G-quartet DNA aptamer-monolith system for the detection and separation of thrombin and cytochrome c in diluted serum samples. The density of immobilised aptamers on the column was ~164 pmol/μL. The estimated K_d ~150 μM after aptamer immobilisation was about 30 times more than the reported SELEX value of ~4.6 μM (Zhao *et al.*, 2008). The reduction in binding affinity could be because of some of the factors explained earlier for K_d.

In another experiment by Zhao *et al.*, (2008b), they used a similar polymeric monolith to host 15mer and 29mer DNA aptamers and obtained K_d values of ~100 nM and ~0.5 nM respectively. The detection limit of thrombin were observed to decrease from 4 nM to 0.1 nM for both aptamers (Zhao *et al.*, 2008). The improvement was attributed to the increase in pre-concentration duration of thrombin from 0.5 min to 5 min, and the increase in the

immobilisation density of aptamer to 250 pmol/μL (Zhao *et al.*, 2008). Han *et al.*, (2012) demonstrated an online screening of lysozyme from a protein mixture by covalently immobilising an anti-Lys DNA aptamer on a poly (glycidyl methacrylate-co-ethylene dimethacrylate) monolithic rod. They attained a low back pressure of 1.0 MPa at a volumetric flow rate of 0.8 mL/min, an aptamer immobilisation density of 290 pmol/μL compared to 204 pmol/μL for microbeads, and a high precision, functionality, stability and reproducibility for 20 experimental runs using the monolithic rod (Han *et al.*, 2012). Hybrid silica monolithic rod with immobilised amino-modified apt-29 was used to screen thrombin at a detection limit of 3.4 nM (Deng *et al.*, 2012). They achieved an immobilisation density of 568 pmol/μL and a binding capacity of 1.95×10^{-24} mol/nm^2 compared to 1.4×10^{-25} mol/nm^2 for open tubular capillaries (Deng *et al.*, 2012). Brothier *et al.*, (2014) demonstrated the design and application of a miniaturised hybrid silica monolith for the extraction of ochratoxin A and cocaine. The monolith was characterised in terms of its stability, reproducibility, permeability and morphology. Back pressures of ~4.8 bars and ~12.1 bars at flow rates of 200 nL/min and 500 nL/min were observed for aqueous buffer and acetonitrile/water respectively. Also, the density of aptamer immobilisation was ~6.27 nmol/μL and ~5.14 nmol/μL for ochratoxin A and cocaine extraction (Pichon *et al.*, 2015). Figure 3 shows an illustrative scheme for the immobilisation of an aptamer on a macroporous polymeric support and Table 4 reports a comparison between aptamer immobilised continuous polymer systems and particulate oligosorbent systems.
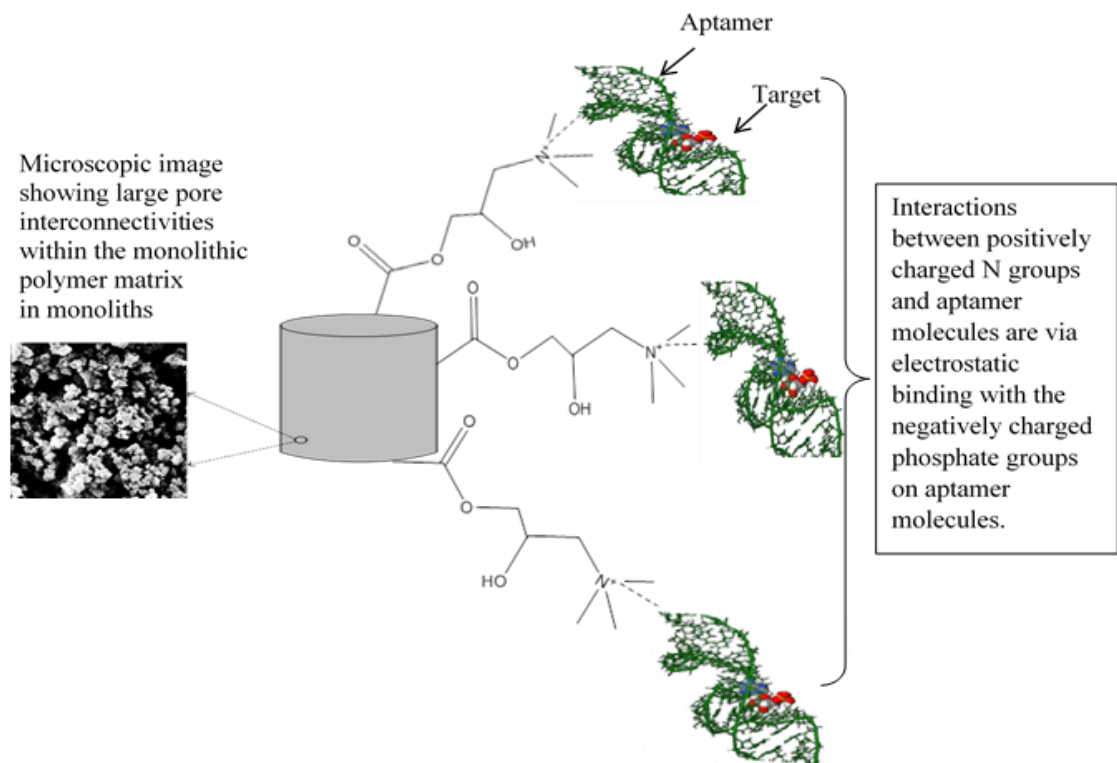
Figure 3. Aptameric immobilisation of a continuous polymeric support with non-uniform large-pore interconnectivities for molecular probing of a target molecule.

6.   CHALLENGES TO APTAMERIC BINDING AND APPLICATION

Challenges relating to aptameric binding and application can be classified as follows: (i) Technological gap between aptamer research and practical applications (ii) Limitations to aptamer generation by SELEX and, (iii) Limitation to molecular recognition of some specific targets. With all the aforementioned benefits of aptameric binding and applications, only the Macugen aptamer has been accepted for clinical application. So what is hindering the progress of aptameric binding applications through the clinical phases? First and foremost, Baird (2010) highlighted that since aptamers are aimed at replacing antibody-systems for molecular binding, it is natural for practitioners to resist the change. There still exists a knowledge gap between researchers and practitioners concerning the benefit of aptamers over antibodies in all application spheres (Baird, 2010). Moreover, it generally takes about fifteen to twenty years for new scientific discoveries to be implemented and accepted. As a result, applications of aptamers for diagnosis, therapeutic, and environmental analysis will take some time.

Radom *et al*., (2013) also discussed three different challenges that the SELEX approach brings to bear despite its' simplicity and significance in aptamer selection. One possibility is the hybridization between the primers and random regions. This leads to a destruction of the secondary and tertiary structures of the aptamer responsible for binding the target. As a result, significant attention is required in designing the primers in order to circumvent the problem of sequence overlapping during SELEX. The second challenge SELEX poses are the post-amplification steps in each round of aptamer selection (Radom *et al.*, 2013). This step involves separation of strands to ensure that only the appropriate strands are left for the next cycle. The techniques for the separation of nucleic acid aptamers have their own advantages and disadvantages. For RNA aptamers, separation is achieved by transcripting ssDNA templates into ssRNA and later digesting the DNA template. However, the separation process for DNA aptamers is achieved by eliminating the negative strands by employing either lambda-exonuclease digestion of the negative dephosphorylated strand, asymmetric PCR, denaturing polyacrylamide gel electrophoresis, or with streptavidin-coated magnetic beads. The third challenge identified by Radom *et al.*, (2013) is the susceptible formation of incomplete complementary dimers. This can lead to the formation of concatamers, which are aptamers of undesired sizes. This problem can be circumvented by carefully monitoring the number of cycles of amplification for selected nucleic acids.

Another peculiar problem facing aptameric binding is the selection of aptamers against hydrophobic targets such as steroids and alkaloids, as well as negatively charged molecules (Stoltenburg *et al.*, 2007; Pinto *et al.*, 2014). Efforts to resolve this challenge include the attachment of non-polar functional groups and the exploitation of non-stacked base pairs (Pinto *et al.*, 2014).

7.   CONCLUSION

Aptamers have a wide range of applications and this has triggered significant research interests. Immobilising aptamers on surfaces for target detection has the potential to achieve high throughput screening with high accuracy, sensitivity and specificity at a relatively low cost. Immobilised aptamers have been used in solid phase extraction units/columns, in the development of biosensors and in the fabrication of glass nanopore

sensors. Potential applications exist in the health sector for mass screening during disease outbreaks, and also for the food and beverage industry, pharmaceutical industry, defence and domestic use. Immobilisation of aptamers in glass nanopore and solid phase extraction media have some challenges relating to low pore sizes, high back pressure and the limited capacity for high throughput screening. This can be resolved by applying continuous adsorbent systems. Such adsorbents, unlike the oligosorbents, are macroporous and possess significant longitudinal permeability with aptamers functionalised in their pore surfaces. These can be engineered to have minimal void fractions and a convective mass transfer mechanism. Application of continuous adsorbents will further strengthen the development of immobilised aptameric binding for full-scale application in a chromatographic format. However, it must be noted that the binding characteristics of aptamers under immobilised conditions can be significantly affected by controlled spatial mobility at the point of attachment and its' performance. Also, research into various polymeric supports with the capacity to enhance convective fluid transport for high throughput screening is essential.

8.   ACKNOWLEDGMENT

9.   REFERENCES

Ali, W.H. and V. Pichon, 2014. Characterization of oligosorbents and application to the purification of ochratoxin a from wheat extracts. Analytical and bioanalytical chemistry, 406(4): 1233. DOI 10.1007/s00216-013-7509-6.
Andrew, D.E. and W.S. Jack, 1990. In vitro selection of rna molecules that bind specific ligands. Nature, 346(6287): 818. DOI 10.1038/346818a0.
Anthony, D.K., P. Supriya and E. Andrew, 2010. Aptamers as therapeutics. Nature Reviews Drug Discovery, 9(8): 660. DOI 10.1038/nrd3249.

Aquino-Jarquin, G. and J.D. Toscano-Garibay, 2011. Rna aptamer evolution: Two decades of selection. International journal of molecular sciences, 12(12): 9155-9171. DOI 10.3390/ijms12129155.

Bagalkot, V., L. Zhang, E. Levy-Nissenbaum, S. Jon, P.W. Kantoff, R. Langer and O.C. Farokhzad, 2007. Quantum dot-aptamer conjugates for synchronous cancer imaging, therapy, and sensing of drug delivery based on bi-fluorescence resonance energy transfer. Nano letters, 7(10): 3065.

Baird, G.S., 2010. Where are all the aptamers? American journal of clinical pathology, 134(4): 529-531. Available from http://www.ncbi.nlm.nih.gov/pubmed/20855632. DOI 10.1309/AJCPFU4CG2WGJJKS.

Banerjee, J. and M. Nilsen-Hamilton, 2013. Aptamers: Multifunctional molecules for biomedical research. Journal of molecular medicine, 91(12): 1333-1342. Available from http://www.ncbi.nlm.nih.gov/pubmed/24045702. DOI 10.1007/s00109-013-1085-2.

Bănică, F.G., 2012. Nucleic acids in chemical sensors. In: Chemical sensors and biosensors: Fundamentals and applications. John Wiley & Sons Inc, West Sussex, U.K: pp: 118-134.

Benitez, J., 2009. Fundamentals of mass transfer. In: Principles and modem applications of mass transfer operations. John Wiley & Sons, Canada: pp: 17-64.

Brothier, F. and V. Pichon, 2014. Miniaturized DNA aptamer-based monolithic sorbent for selective extraction of a target analyte coupled on-line to nanolc. Analytical and bioanalytical chemistry, 406(30): 7875-7886. Available from http://www.ncbi.nlm.nih.gov/pubmed/25335821. DOI 10.1007/s00216-014-8256-z.

Bunka, D.H. and P.G. Stockley, 2006. Aptamers come of age - at last. Nature reviews. Microbiology, 4(8): 588-596. Available from http://www.ncbi.nlm.nih.gov/pubmed/16845429. DOI 10.1038/nrmicro1458.

Cass, A.E.G. and Y. Zhang, 2011. Nucleic acid aptamers: Ideal reagents for point-of-care diagnostics? Faraday Discussions, 149: 49. DOI 10.1039/c005487a.

Centi, S., G. Messina, S. Tombelli, I. Palchetti and M. Mascini, 2008. Different approaches for the detection of thrombin by an electrochemical aptamer-based assay coupled to magnetic beads. Biosensors & bioelectronics, 23(11): 1602-1609. Available from http://www.ncbi.nlm.nih.gov/pubmed/18313283. DOI 10.1016/j.bios.2008.01.020.

Chang, C.C., C.Y. Chen, X. Zhao, T.H. Wu, S.C. Wei and C.W. Lin, 2014. Label-free colorimetric aptasensor for ige using DNA pseudoknot probe. The Analyst, 139(13): 3347-3351. Available from http://www.ncbi.nlm.nih.gov/pubmed/24821053. DOI 10.1039/c4an00253a.

Chapuis-Hugon, F., A. du Boisbaudry, B. Madru and V. Pichon, 2011. New extraction sorbent based on aptamers for the determination of ochratoxin a in red wine. Analytical and bioanalytical chemistry, 400(5): 1199-1207. Available from http://www.ncbi.nlm.nih.gov/pubmed/21221554. DOI 10.1007/s00216-010-4574-y.

de-los-Santos-Álvarez, N., M.a.J. Lobo-Castañón, A.J. Miranda-Ordieres and P. Tuñón-Blanco, 2008. Aptamers as recognition elements for label-free analytical devices.

TrAC Trends in Analytical Chemistry, 27(5): 437-446. DOI 10.1016/j.trac.2008.03.003.

De Girolamo, A., L. Le, G. Penner, R. Schena and A. Visconti, 2012. Analytical performances of a DNA-ligand system using time-resolved fluorescence for the determination of ochratoxin a in wheat. Analytical and bioanalytical chemistry, 403(9): 2627-2634. Available from http://www.ncbi.nlm.nih.gov/pubmed/22576657. DOI 10.1007/s00216-012-6076-6.

Deng, B., Y. Lin, C. Wang, F. Li, Z. Wang, H. Zhang, X.F. Li and X.C. Le, 2014. Aptamer binding assays for proteins: The thrombin example--a review. Analytica chimica acta, 837: 1-15. Available from http://www.ncbi.nlm.nih.gov/pubmed/25000852. DOI 10.1016/j.aca.2014.04.055.

Deng, N., Z. Liang, Y. Liang, Z. Sui, L. Zhang, Q. Wu, K. Yang, L. Zhang and Y. Zhang, 2012. Aptamer modified organic-inorganic hybrid silica monolithic capillary columns for highly selective recognition of thrombin. Analytical chemistry, 84(23): 10186-10190. Available from http://www.ncbi.nlm.nih.gov/pubmed/23137349. DOI 10.1021/ac302779u.

Ding, S., C. Gao and L.-Q. Gu, 2009. Capturing single molecules of immunoglobulin and ricin with an aptamer-encoded glass nanopore. Analytical chemistry, 18(16): 6649.

Dun, S.I., 2010. Searching for molecular solutions: Empirical discovery and its future In: The blind shaper of nucleic acids. John Wiley & Sons, USA.

Famulok, M. and G. Mayer, 2011. Aptamer modules as sensors and detectors. Accounts of chemical research, 44(12): 1349. DOI 10.1021/ar2000293.

Fang, X. and W. Tan, 2010. Aptamers generated from cell-selex for molecular medicine: A chemical biology approach. Accounts of chemical research, 43(1): 48. DOI 10.1021/ar900101s.

Finch, A.S. and D.N. Stratis-Cullum, 2013. Biomedical applications of aptamers, In: J.G.Bruno, editor. Aptamer Based Detection of Hazardous Materials for Defense and Security.

Gao, C., S. Ding, Q. Tan and L. Gu, 2009. Method of creating a nanopore-terminated probe for single-molecule enantiomer discrimination. Anal. Chem., 81(1): 80-86. DOI 10.1021/ac802348r.

Guo, K., A. Paul, C. Schichor, G. Ziemer and H.P. Wendel, 2008. Cell-selex: Novel perspectives of aptamer-based therapeutics. . Int. J. Mol. Sci. , 9: 668-678.

Hamula, C., H.Q. Zhang, F. Li, Z. Wang, X.C. Le and X. Li, 2011. Selection and analytical applications of aptamers binding microbial pathogens. Trac-Trends Anal. Chem., 30(10): 1587-1597. DOI 10.1016/j.trac.2011.08.006.

Han, B., C. Zhao, J. Yin and H.L. Wang, 2012. High performance aptamer affinity chromatography for single-step selective extraction and screening of basic protein lysozyme. J. Chromatogr. B, 903: 112-117. DOI 10.1016/j.jchromb.2012.07.003.

Hermann, T. and D.J. Patel, 2000. Adaptive recognition by nucleic acid aptamers. Science, 287(5454): 820-825. DOI 10.1126/science.287.5454.820.

Hianik, T., V. Ostatna, M. Sonlajtnerova and I. Grman, 2007. Influence of ionic strength, ph and aptamer configuration for binding affinity to thrombin. Bioelectrochemistry, 70(1): 127-133. Available from

http://www.ncbi.nlm.nih.gov/pubmed/16725379. DOI 10.1016/j.bioelechem.2006.03.012.

Jayasena, S.D., 1999. Aptamers: An emerging class of molecules that rival antibodies in diagnostics. Clin. Chem., 45(9): 1628-1650.

Kärkkäinen, R.M., M.R. Drasbek, I. McDowall, C.J. Smith, N.W.G. Young and G.A. Bonwick, 2011. Aptamers for safety and quality assurance in the food industry: Detection of pathogens. International Journal of Food Science & Technology, 46(3): 445-454. DOI 10.1111/j.1365-2621.2010.02470.x.

Kim, Y.S., M.Y. Song, J. Jurng and B.C. Kim, 2013. Isolation and characterization of DNA aptamers against escherichia coli using a bacterial cell-systematic evolution of ligands by exponential enrichment approach. Analytical biochemistry, 436(1): 22-28. Available from http://www.ncbi.nlm.nih.gov/pubmed/23357235. DOI 10.1016/j.ab.2013.01.014.

Kim, Y.S., M.Y. Song, J. Jurng and B.C. Kim, 2013. Isolation and characterization of DNA aptamers against escherichia coli using a bacterial cell–systematic evolution of ligands by exponential enrichment approach. Analytical biochemistry, 436(1): 22-28.

Leonard, P., S. Hearty, J. Brennan, L. Dunne, J. Quinn, T. Chakraborty and R. O'Kennedy, 2003. Advances in biosensors for detection of pathogens in food and water. Enzyme and Microbial Technology, 32(1): 3-13. Available from http://www.sciencedirect.com/science/article/pii/S0141022902002326. DOI http://dx.doi.org/10.1016/S0141-0229(02)00232-6.

Madru, B., F. Chapuis-Hugon and V. Pichon, 2011. Novel extraction supports based on immobilised aptamers: Evaluation for the selective extraction of cocaine. Talanta, 85(1): 616-624. Available from http://www.ncbi.nlm.nih.gov/pubmed/21645749. DOI 10.1016/j.talanta.2011.04.016.

Madru, B., F. Chapuis-Hugon, V. Pichon and E. Peyrin, 2009. Determination of cocaine in human plasma by selective solid-phase extraction using an aptamer-based sorbent. Analytical chemistry, 81(16): 7081-7086. DOI 10.1021/ac9006667.

Mairal, T., V. Cengiz Özalp, P. Lozano Sánchez, M. Mir, I. Katakis and C. O'Sullivan, 2008. Aptamers: Molecular tools for analytical applications. Analytical and bioanalytical chemistry, 390(4): 989-1007. DOI 10.1007/s00216-007-1346-4.

Mairal, T., V.C. Ozalp, P. Lozano Sanchez, M. Mir, I. Katakis and C.K. O'Sullivan, 2008. Aptamers: Molecular tools for analytical applications. Analytical and bioanalytical chemistry, 390(4): 989-1007. Available from http://www.ncbi.nlm.nih.gov/pubmed/17581746. DOI 10.1007/s00216-007-1346-4.

Mann, D., C. Reinemann, R. Stoltenburg and B. Strehlitz, 2005. In vitro selection of DNA aptamers binding ethanolamine. Biochemical and biophysical research communications, 338(4): 1928-1934. Available from http://www.ncbi.nlm.nih.gov/pubmed/16289104. DOI 10.1016/j.bbrc.2005.10.172.

Mascini, M., I. Palchetti and S. Tombelli, 2012. Nucleic acid and peptide aptamers: Fundamentals and bioanalytical aspects. Weinheim: pp: 1316-1332.

McKeague, M. and M.C. Derosa, 2012. Challenges and opportunities for small molecule aptamer development. Journal of Nucleic Acids, 2012. DOI 10.1155/2012/748913.

Minunni, M., S. Tombelli, A. Gullotto, E. Luzi and M. Mascini, 2004. Development of biosensors with aptamers as bio-recognition element: The case of hiv-1 tat protein. Biosensors & bioelectronics, 20(6): 1149-1156. Available from http://www.ncbi.nlm.nih.gov/pubmed/15556361. DOI 10.1016/j.bios.2004.03.037.

Nadal, P., A. Pinto, M. Svobodova, N. Canela and C.K. O'Sullivan, 2012. DNA aptamers against the lup an 1 food allergen (lupin aptamers). PloS one, 7(4): e35253. DOI 10.1371/journal.pone.0035253.

O'Sullivan, C.K., 2002. Aptasensors--the future of biosensing? Analytical and bioanalytical chemistry, 372(1): 44-48. Available from http://www.ncbi.nlm.nih.gov/pubmed/11939212. DOI 10.1007/s00216-001-1189-3.

Ozalp, V.C., M.B. Serrano-Santos and T. Schafer, 2013. Responsive membranes and materials. John Wiley & Sons, Canada.

Peyrin, E., 2009. Nucleic acid aptamer molecular recognition principles and application in liquid chromatography and capillary electrophoresis. Journal of separation science, 32(10): 1531-1536. DOI 10.1002/jssc.200900061.

Pichon, V., F. Brothier and A. Combes, 2015. Aptamer-based-sorbents for sample treatment-a review. In: Anal. Bioanal. Chem. pp: 681-698.

Pinto, A., P.N. Polo, O. Henry, M.C. Redondo, M. Svobodova and C.K. O'Sullivan, 2014. Label-free detection of gliadin food allergen mediated by real-time apta-pcr. Analytical and bioanalytical chemistry, 406(2): 515-524. Available from http://www.ncbi.nlm.nih.gov/pubmed/24247552. DOI 10.1007/s00216-013-7475-z.

Radom, F., P.M. Jurek, M.P. Mazurek, J. Otlewski and F. Jelen, 2013. Aptamers: Molecules of great potential. Biotechnology advances, 31(8): 1260-1274. Available from http://www.ncbi.nlm.nih.gov/pubmed/23632375. DOI 10.1016/j.biotechadv.2013.04.007.

Rhouati, A., N. Paniel, Z. Meraihi and J.-L. Marty, 2011. Development of an oligosorbent for detection of ochratoxin a. Food Control, 22(11): 1790-1796. DOI 10.1016/j.foodcont.2011.04.021.

Robertson, D.L. and G.F. Joyce, 1990. Selection in vitro of an rna enzyme that specifically cleaves single-stranded DNA. Nature, 344(6265): 467-468. DOI 10.1038/344467a0.

Santosh, B. and P.K. Yadava, 2014. Nucleic acid aptamers: Research tools in disease diagnostics and therapeutics. BioMed research international, 2014: 540451. Available from http://www.ncbi.nlm.nih.gov/pubmed/25050359. DOI 10.1155/2014/540451.

Sharma, A. and R.K. Sharma, 2013. Aptamers—a promising approach for sensing of biothreats using different bioinformatics tools. Soft Nanoscience Letters, 03(04): 1-5. DOI 10.4236/snl.2013.34A001.

Song, K.M., S. Lee and C. Ban, 2012. Aptamers and their biological applications. Sensors, 12(1): 612-631. Available from http://www.ncbi.nlm.nih.gov/pubmed/22368488. DOI 10.3390/s120100612.

Song, S., L. Wang, J. Li, C. Fan and J. Zhao, 2008. Aptamer-based biosensors. TrAC Trends in Analytical Chemistry, 27(2): 108-117. DOI 10.1016/j.trac.2007.12.004.

Sonia, A.-G., D.-L.-S.-Á. Noemí, J.M.-O. Arturo and L.-C. María Jesús, 2013. Aptamer-based analysis: A promising alternative for food safety control. Sensors, Vol 13, Iss 12, Pp 16292-16311 (2013).

Soontornworajit, B. and Y. Wang, 2011. Nucleic acid aptamers for clinical diagnosis: Cell detection and molecular imaging. Analytical and bioanalytical chemistry, 399(4): 1591-1599. Available from http://www.ncbi.nlm.nih.gov/pubmed/21161512. DOI 10.1007/s00216-010-4559-x.

Stoltenburg, R., C. Reinemann and B. Strehlitz, 2007. Selex—a (r)evolutionary method to generate high-affinity nucleic acid ligands. Biomolecular Engineering, 24(4): 381-403. Available from http://www.sciencedirect.com/science/article/pii/S1389034407000664. DOI http://dx.doi.org/10.1016/j.bioeng.2007.06.001.

Svobodova, M., T. Mairal, P. Nadal, M.C. Bermudo and C.K. O'Sullivan, 2014. Ultrasensitive aptamer based detection of beta-conglutin food allergen. Food chemistry, 165: 419-423. Available from http://www.ncbi.nlm.nih.gov/pubmed/25038695. DOI 10.1016/j.foodchem.2014.05.128.

Takemura, K., P. Wang, I. Vorberg, W. Surewicz, S.A. Priola, A. Kanthasamy, R. Pottathil, S.G. Chen and S. Sreevatsan, 2006. DNA aptamers that bind to prpc and not prpsc show sequence and structure specificity. Experimental Biology and Medicine, 231(2): 204-214.

Tombelli, S., M. Minunni and M. Mascini, 2005. Analytical applications of aptamers. Biosensors & bioelectronics, 20(12): 2424-2434. Available from http://www.ncbi.nlm.nih.gov/pubmed/15854817. DOI 10.1016/j.bios.2004.11.006.

Tuerk, C. and L. Gold, 1990. Systematic evolution of ligands by exponential enrichment: Rna ligands to bacteriophage t4 DNA polymerase. Science, 249(4968): 505-510.

Ulrich, H. and C. Wrenger, 2009. Disease-specific biomarker discovery by aptamers. Cytometry. Part A : the journal of the International Society for Analytical Cytology, 75(9): 727-733. Available from http://www.ncbi.nlm.nih.gov/pubmed/19565638. DOI 10.1002/cyto.a.20766.

van Den Ouweland, J. and I. Kema, 2012. The role of liquid chromatography-tandem mass spectrometry in the clinical laboratory. In: J. Chromatogr. B. pp: 18-32.

Zhao, Q., X.-F. Li and X.C. Le, 2008. Aptamer-modified monolithic capillary chromatography for protein separation and detection. Analytical chemistry, 80(10): 3915-3920. DOI 10.1021/ac702567x.

Zhao, Q., X. Li, Y. Shao and X.C. Le, 2008. Aptamer-based affinity chromatographic assays for thrombin. Anal. Chem., 80(19): 7586-7593. DOI 10.1021/ac801206s.

Zhao, Q., M. Wu, X. Chris Le and X.-F. Li, 2012. Applications of aptamer affinity chromatography. TrAC Trends in Analytical Chemistry, 41: 46-57. DOI 10.1016/j.trac.2012.08.005.

Zhu, G., M. Ye, M. Donovan, E. Song, Z. Zhao and W. Tan, 2012. Nucleic acid aptamers: An emerging frontier in cancer therapy. Chem. Commun., 48(85): 10472-10480. DOI 10.1039/c2cc35042d.

Zhu, J., Q. Lin, J. Shang, Y. Jia, M. Stojanovic and R. Pei, 2014. Spatially selective release of aptamer-captured cells by temperature mediation. IET Nanobiotechnology, 8(1): 2-9. DOI 10.1049/iet-nbt.2013.0028.

CHAPTER THREE

SYNTHESIS AND THERMOCHEMICAL CHARACTERISATION OF POLYMETHACRYLATE MONOLITHS

SECTION 3.1

In-process thermochemical analysis of in situ poly (ethylene glycol methacrylate-co-glycidyl methacrylate) monolithic adsorbent synthesis

Caleb Acquah, Michael K. Danquah, Charles K.S. Moy, Clarence M. Ongkudon

DECLARATION FOR THESIS SECTION 3.1

In-process thermochemical analysis of in situ poly (ethylene glycol methacrylate-co-glycidyl methacrylate) monolithic adsorbent synthesis

The candidate will like to declare that there is no conflict of interests involved in this work and that my extent of contribution as candidate is as shown below:

Contribution of Candidate	Conceptualisation, initiation and write-up	85%

The following co-authors were involved in the development of this publication and attest to the candidate's contribution to a joint publication as part of his thesis. Permission by co-authors are as follows:

Name	Signature	Date
Michael K. Danquah		13.07.2017
Charles K.S. Moy		13.07.2017
Clarence M. Ongkudon		13.07.2017

ABSTRACT

Thermo-molecular mechanisms associated with the synthesis of polymethacrylate monoliths are critical in controlling the physicochemical and binding characteristics of the adsorbent. Notwithstanding, there is limited reported work focused on probing the underlining synthesis mechanism essential to establish the relationship between in-process polymerization characteristics and the physicochemical properties of the monolith for tailored applications. This work presents a real-time thermochemical analysis of polymethacrylate monolith synthesis by free radical polymerization to probe effects on the physicochemical characteristics of the adsorbent. Experimental results showed that an increase in the cross-linker monomer concentration from 30% to 70% resulted in a peak temperature increase from 96.3 ºC to 114.3 ºC. Also, an increase in initiator concentration from 1% w/v Benzoyl peroxide (BPO) to 3% w/v resulted in a temperature increase from 90.7 ºC to 106.3 ºC. Temperature build up increases the kinetic rate of intermolecular collision associated with microglobular formation and inter-globular interactions. This reduces the structural homogeneity and macroporosity of the polymer matrix. A 2-phase reactive crystallisation model was used to characterise the rate of monomeric reaction post-initiation and microglobular formation from the liquid monomeric phase in order to formulate the theoretical framework essential to evaluate the kinetics of the polymer formation process.

Keywords: Polymethacrylate; Monolith; Polymerisation; Thermochemical; Kinetics

1.   INTRODUCTION

Conventional chromatographic supports for bioseparation and purification in life sciences are generally particulate in nature with small particle pores that present significant bioprocess challenges especially for large molecule applications including plasmid DNA (pDNA), viral particles and cellular targets. The mode of mass transfer in particulate adsorbents is mostly by diffusion, and this significantly slows down the flow hydrodynamics, reducing the mass velocity and capacity of matter into and out of the adsorbent. In addition, the random packing assembly of particulate adsorbents in chromatographic columns make it challenging to fine-tune its physical features for high throughput and rapid bioseparation applications.

Monolithic adsorbents are regarded as relatively new chromatographic stationary supports synthesised by various chemo-molecular techniques to form a single piece of continuous sorbents in an unstirred mould (Svec, 2004; Danquah and Forde, 2007; Wang *et al.*, 2014). Monoliths have the trademark of offering convective mass transport of fluids and low column backpressure as a result of their macroporous nature (Nischang, 2013). Their pore characteristics and surface functionalities can also be molecularly engineered to target analytes with varying physicochemical properties such as hydrodynamic size, charge and active moieties (Svec, 2012; Pfaunmiller *et al.*, 2013; Podgornik *et al.*, 2013). There are three main types of monoliths; organic, inorganic and hybrid organic-inorganic monoliths. Organic monoliths, especially polymethacrylates, represent one of the most utilised monolithic adsorbents for chromatographic applications. They are largely pH resistant and biocompatible with easily tailored pore characteristics and readily available reactive moiety, such as epoxy group, for functionalization (Roberts *et al.*, 2009; Ongkudon and Danquah, 2010; Podgornik *et al.*, 2013). Polymethacrylate monoliths are synthesised via free radical copolymerization of cross-linker and functional methacrylate-based monomers either initiated thermally or by radiation (Schlemmer *et al.*, 2009; Svec, 2010; Vonk *et al.*, 2015). Thermal initiation approach is commonly used, as it is cheap and primarily requiring the use of an isothermal water bath (Szumski and Buszewski, 2009; Alves *et al.*, 2013). The synthesis process includes various steps of thermo-molecular mechanisms involving the monomers and the initiator. These steps are (i) sensible heat transfer from the heating medium to the polymerization mixture; (ii) Decomposition of

138

initiator at temperature T_i (where T_i is the decomposition temperature of the initiator) resulting in the release of exotherms and temperature shoot; (iii) Reactive monomeric interactions driven by the released free radicals to form a nucleic complex in the liquid phase and; (iv) Formation of the solid polymer out of the liquid phase through microglobule development from the nuclei. In each of these steps, the control of the physicochemical characteristics is important, hence, an in-depth understanding of the phenomenon is important to develop well-characterised monoliths for targeted applications. However, current research efforts have mostly focussed on bulk synthesis, characterisation, functionalization and chromatographic application (Jandera *et al.*, 2012; Zhang *et al.*, 2013; Aydoğan, 2015; Yang *et al.*, 2015) with limited focus on understanding the molecular mechanisms governing the monolith formation process. This limits opportunities to fully exploit adsorbent properties to enhance chromatographic performance indicators. Both in-process and post polymerization characterisations are essential in tailoring the physicochemical properties of the adsorbent in order to widen the scope of application and also tackle common challenges relating to structural stability, pore homogeneity and wall channelling.

Various in-process synthesis conditions such as mass ratio of monomers, polymerization time, concentration of initiator, porogen type and composition, temperature affect the molecular arrangement of microglobules and cluster of globules during polymer formation, conferring unique physicochemical characteristics which affect the functions of the polymer in the molecular or nanoscale level (Danquah and Forde, 2008; Kim *et al.*, 2013; Chen *et al.*, 2015). Polymerization temperature is critical to control the molecular organisation of microglobules during synthesis. Hence, it is an essential parameter to manipulate the structural and physical characteristics of polymethacrylate monoliths (Danquah and Forde, 2008; Szumski and Buszewski, 2009). Mihelic *et al.* (2001) studied the kinetics of polymerization for methacrylate monolith synthesis as well as the overall heat of reaction using differential scanning calorimetry (DSC). They reported the presence of two heating effects during polymerization; endothermic heat from porogen evaporation, and exothermic heat from monomer polymerization with the initiator. However, the endothermic heat of porogen evaporation had minimal effects on the peak temperature of the polymerization process. In addition, it was demonstrated that thermal polymerization

of monomer-porogen mixture without an initiator can occur but at temperatures above 110 °C (Mihelic *et al.*, 2001). Danquah *et al.* (2008) also demonstrated that the mechanism of homogenous pore formation during polymethacrylate synthesis can be controlled by minimizing the extent of release of exothermic heat into the polymerization mixture. They accomplished this by expelling the heat of decomposition from the initiator and isothermally pumping free radicals into the monomer mixture for the commencement of monolith synthesis. However, correlations existing between thermo-molecular mechanisms of the synthesis process and the structural and pore characteristics of the polymer are not well understood and this represents a major research gap. In contrast to the breadth of bioseparation applications of polymethacrylate monoliths reported, there has been limited work investigating in-process characteristics, such as temperature distribution, and its impacts on the structural properties of the polymer under varying compositional scenarios. This work attempts to develop the theoretical framework essential to understand temperature-induced behaviours of the polymerization process, and the effects of in-process synthesis mechanisms on the physicochemical characteristics of the polymer. It formulates an understanding of the polymerization kinetics and evaluates effects on the rate of polymerization as well as temperature control. Thermochemical analyses were performed using a real-time technique for *in situ* parametric characterisation of the monolith synthesised by thermal free radical copolymerization. In addition, a mathematical approach based on reaction kinetics and Avrami's isothermal model is used to establish and monitor the rates of monomeric reaction post-initiation and polymer formation out of the liquid phase.

2.   EXPERIMENTAL

2.1   Materials

Glycidyl methacrylate (GMA) (MW 142.15, 97%), ethylene glycol dimethacrylate (EDMA) (MW 198.22, 98%), benzoyl peroxide (BPO) (MW 242.23, 70%), methanol (HPLC grade, MW 32.04, 99.93%), 1-dodecanol (MW 186.33, 98%), cyclohexanol (MW 100.16, 99%), were purchased from Sigma–Aldrich (USA). 12 cm x 15 cm rimless test tubes (Borosil, India) were applied for *in situ* thermo-molecular characterisation of monoliths in a water bath (Memmert, Germany). Thermo-molecular characterisation of

the synthesis processes was carried out with a real-time midi logger GL220 thermocouple probe (Graphtec, USA).

2.2   Methods

2.2.1   Polymethacrylate monolith synthesis

Polymethacrylate resin was produced after the mixture of monomers (GMA and EDMA), porogens (1-dodecanol and cyclohexanol) and initiator (BPO) for each set of experiment was sonicated for 10 mins, sparged with N_2 for 5 min, to deoxygenate the mixture and prevent any side reactions that may occur due to the presence of oxygen gas, and held at a constant temperature above the decomposition temperature of the initiator. Thermal free-radical copolymerization was achieved using an isothermal water bath reactor. Since porogens are mostly non-reactive and are mainly responsible for the solvation of monomers as well as the medium for pore formation, a fixed ratio (70%:30%) of total porogen to total monomer was maintained throughout the study. Also, the porogenic ratio of cyclohexanol to 1-dodecanol was maintained at 70%:30%. Hence, the polymerization conditions that we changed to represent each set of experiment were the following: temperature, the concentration ratio of functional monomer (GMA) to cross-linking monomer (EDMA), and the concentration of initiator. Polymerization temperatures investigated for *in situ* characterisation of the synthesis process were 61 ^{o}C, 65 ^{o}C, 75 ^{o}C and 85 ^{o}C at a constant GMA to EDMA ratio of 70%:30% and an initiator of 1% w/v of total monomers. The ratio of GMA to EDMA was investigated over the range 30%:70% to 70%:30% at a constant temperature of 85 ^{o}C and an initiator of 1% w/v of total monomers. Variations in the concentration of initiator from 1-3% was also studied at a constant temperature of 85 ^{o}C and a GMA to EDMA ratio of 70%:30%.

2.2.2   Temperature monitoring

15 mL solution of the above-described mixtures were pipetted into labelled glass test tubes and were securely clamped. The clamped test tubes containing the mixture were then inserted into the water bath while the temperature was monitored in real-time using midi Logger GL220 thermocouple. Monitoring of results was terminated after the peak temperature was obtained and thermal equilibrium with the water bath was reached.

Polymeric monoliths are poor conductors of heat; hence, a continual dip in temperature could be observed once the thermal probe continues to be in the monolith after the thermal equilibrium point.

2.2.3 SEM analysis

With the exception of monoliths utilised for *in situ* characterisation studies, all other monoliths were washed with methanol in a soxhlet extractor for a period of about 5 hours and air dried for 7 days for pores characterisation. The morphology of monolithic pores was probed with a variable pressure scanning electron microscope (SEM) (S-3400N Hitachi model, Japan) with the average pore size being estimated with an imageJ software of the probing device. Sputter coating was applied on the monoliths using gold, a sputter current of 20 mA for 30 s to ensure the conduction of signals during probing.

2.2.4 Mathematical analysis of rate of polymerization

Matlab and Simulink R 2014b were used to model the polymerization of monoliths based on a 2-phase mechanistic approach deduced from the established Avrami's model for crystallisation. The choice of this approach was based on the fact that the formation of bulk monoliths is preceded by nucleation and reaction of these nuclei with the monomers. The first phase involved the post-initiation monomeric reaction stage to an intermediate liquid polyresin. The second phase involves the transformational processes leading to the formation of the solid polymer from the liquid intermediate phase. Varied conditions of monomer ratios of 1, 1.5, 2, 2.5 and 3 were therefore modelled with 2 different hypothetically selected rate constants of 0.5 s^{-1} and 0.3 s^{-1}.

3. RESULTS AND DISCUSSION
3.1 Effect of polymerization temperature

The lowest polymerization temperature was selected with reference to the decomposition temperature of the initiator (60 $^{\circ}$C). As shown in SEM images in Figure 1, increasing the polymerization temperature resulted in decreasing pore size as follows: 65 $^{\circ}$C (x 4700, 10 µm), 75 $^{\circ}$C (x 5000, 10 µm) and 85 $^{\circ}$C (x 6000, 5 µm) and increasing surface area of the adsorbent monolith. In addition, the kinetics of molecular collision increases at elevated

temperatures and this enhances the energy levels of reactant species to achieve activation complex. Under such high frequency collision conditions, the formation rate of microglobules and its aggregation to globule are hindered by thermo-molecular instability existing in the monomeric phase. The images indicate decreasing size of the globular assembly with increasing temperature, and this affects the intra-globular and inter-cluster pore sizes. This observation is in line with previously reported findings (Svec and Fréchet, 1995; Danquah and Forde, 2008; Szumski and Buszewski, 2009).

Temp 65 °C **Temp 75 °C** **Temp 85°C**
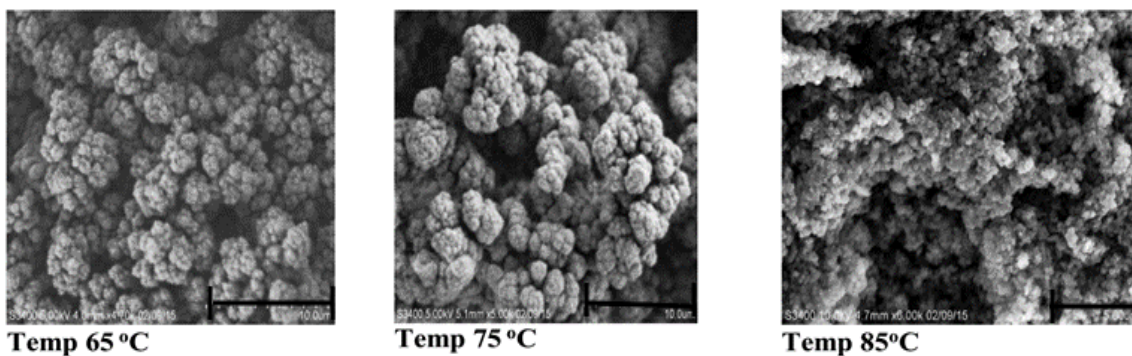
Figure 1. SEM images of polymethacrylate monoliths at a magnification of x 4700 (10 µm), x 5000 (10 µm) and x 6000 (5 µm) all at a voltage of about 5 kV.

An increase in polymerization temperature leads to rapid decomposition of the initiator into free radicals to form a large number of nuclei per second for a unit volume of polymerization mixture. From equation (1), it can be deduced that an increase in temperature results in an exponential increase in the rate of change of the reaction which has a direct effect on the amount of free radicals released.

$$\frac{d\xi}{dt} = (1 - \xi)^n A exp^{(-\frac{E_a}{RT_s})} \tag{1}$$

where ξ is the extent of the reaction; A is the pre-exponential factor; n is the order of the reaction; E_a is the activation energy; R is the gas constant; n is the order of the reaction, and T_s is the polymerization temperature for the synthesis reaction (Mihelic *et al.*, 2001). Notably, the rate of decomposition of the initiator is directly affected by the polymerization temperature. Owing to the rapid increase in the rate of decomposition of the initiator, large amounts of monomers are successively converted in a chain reaction per unit time for every temperature rise. This stepwise conversion and addition of monomeric units lead to gradual agglomeration and cross-linking of large amounts of nuclei layer-by-layer until the entire monomeric substrates convert and polymerise out of

the porogenic phase as illustrated in Figure 2. Also, the rate at which the solid polymer phase crystallises out of the porogenic phase is faster with increasing temperature. This indicates that temperature is a critical parameter affecting stage-wise molecular mechanisms controlling the overall polymerization process, thus, sensible heat transfer into the polymerization mixture; initiator decomposition rate for the formation of free radicals; rate of monomeric interactions in the presence of free radicals to form nuclei and microglobules; aggregation of microglobules to form globules and clusters; and the rate
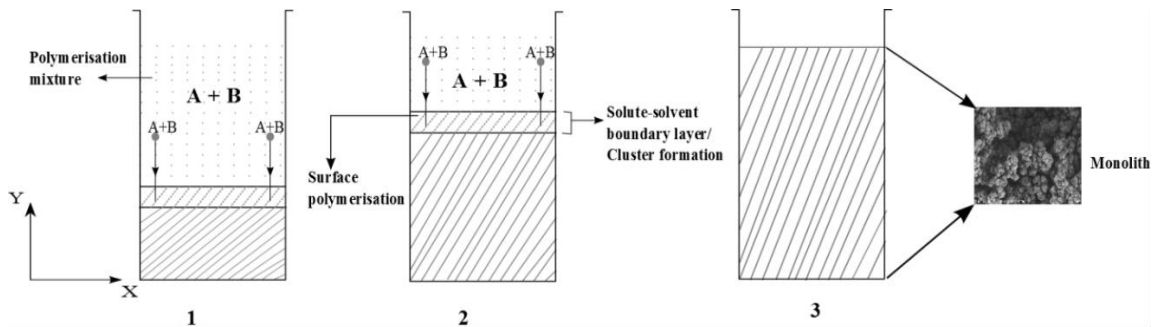
of crystallisation of the polymer out of the porogenic phase.

Figure 2. A mechanistic scheme for polymethacrylate monolith formation from reacting monomers A and B from the bottom to the top of the mould in a stepwise direction (stages 1-3).
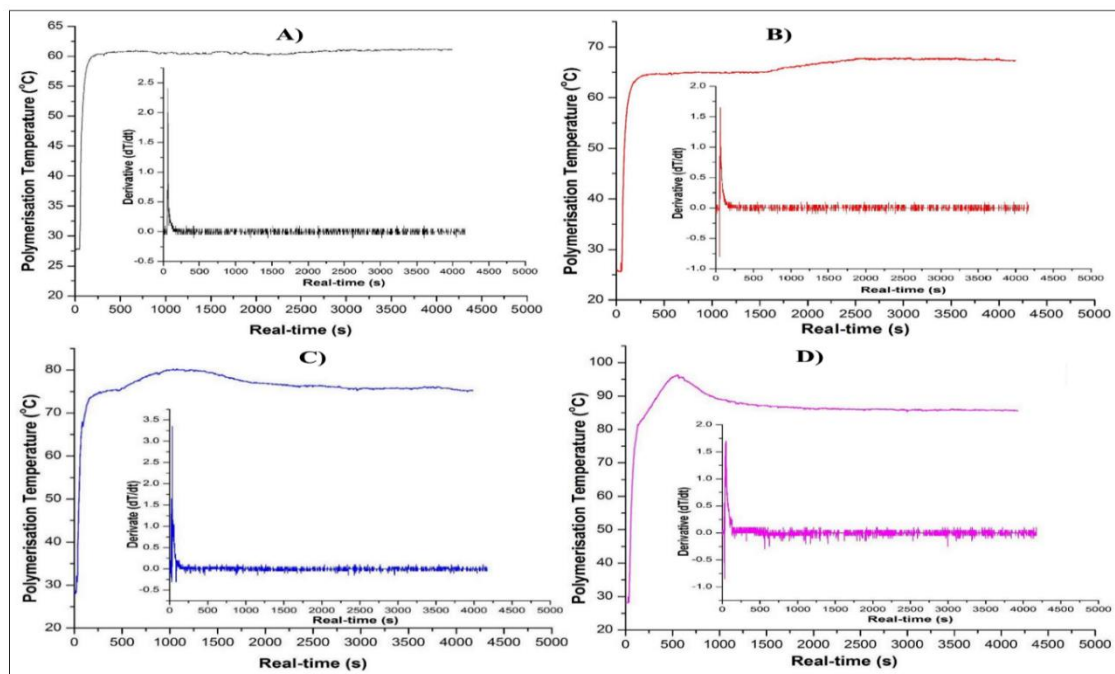
Figure 3. Real time polymerization temperature profiles for polymethacrylate monolith synthesis of volume 15 mL at different temperatures of: A) 61 $^{\circ}$C; B) 65 $^{\circ}$C; C) 75 $^{\circ}$C; D) 85 $^{\circ}$C.

Real-time temperature profiles recorded during polymerization at 61 ºC, 65 ºC, 75 ºC and 85 ºC presented in Figure 3 show comparable thermal paths before polymerization time (t) ≤ 250 s. The thermal effects of the process during this period corresponds to sensible heat transfer from the heating medium to the monomeric mixture thus resulting in a warming-up phase until sufficient heat energy is accumulated to commence initiator decomposition into free radicals. The rate of sensible heat dispatch into the monomer medium is a function of the polymerization temperature. The amount of free radicals released after initiator decomposition and consequently the rate of formation of nuclei increases per unit time for each increase in polymerization temperature. High temperature conditions result in fast kinetic interactions between the reacting molecules with a high probability of nuclei formation driven by the availability of free radicals. The amount of heat energy required by the reactant molecules to achieve activation complex is augmented by exotherms released from initiator decomposition. The release of exotherms results in a rapid increase in the polymerization temperature before declining and stabilising in the process of polymer formation. This is shown in Figure 3 indicating the real-time temperature profiles and the corresponding differential profiles. In addition, as the temperature within the mould approaches the set polymerization temperature, there is gradual decline in the rate of change to the value before the peak temperature. The polymerization temperature declines afterwards before equilibrating at the set-point temperature. A further decline in the polymerization temperature below the set point was observed after polymer formation, and this was attributed to the poor thermal conductivity of the polymer, which obstructs conductive heat transfer from the heating medium to the thermocouple sensor surface. The respective peak polymerization temperatures, T_p, recorded were 61.3 ºC (for $T_s = 61$ ºC), 67.3 ºC (for $T_s = 65$ ºC), 80.2 ºC (for $T_s = 75$ ºC) and 96.3 ºC (for $T_s = 85$ ºC). Set point temperatures of 61 ºC and 65 ºC resulted in small changes in peak temperature as the amount of exotherms released post-initiation was not large enough to cause a significant upsurge in the polymerization temperature. The temperature and overall heat within the monolithic mould during polymerization can be expressed as:

$$T_p = T_s + \Delta T \tag{2}$$

$$\Delta H_p = \Delta H_i + \Delta H_{mi} + \Delta H_m \tag{3}$$

where T_s is the set point temperature; ΔT is the temperature rise at any time after initiator decomposition and reactions; ΔH_p is the enthalpy change of the polymerization reaction; ΔH_i is the enthalpy change during initiation; ΔH_m is the enthalpy change as the monomers react; ΔH_{mi} is the enthalpy change as the initiator interacts with the monomers. Porogens are usually non-reactive during the polymerization process. A previously investigated mixture of porogens (cyclohexanol 48%, dodecanol 12%) and monomers (glycidyl methacrylate 24%, ethylene dimethacrylate 16%) was carried out with a DSC Mettler Toledo by Mihelic *et al.* (2001). The estimated heat of polymerization, apparent activation energy and the pre-exponential factor according to Mihelic *et al.* (2001) for the said composition were 190 J/g ± 5%; 1.681×10^9 s^{-1} and 81.5 kJ/mol. From the aforementioned equations (2-3), the heat of polymerization is dependent on (i) the set-point temperature, (ii) composition of the polymerization mixture, and (iii) the thermochemical properties of the monomers since their enthalpies are dependent on specific heat capacities.

Once the temperature of the reaction mixture reaches 60 °C and above, the initiators undergo complete decomposition to form radicals and release a quantum of energy termed as ΔH_i. These radicals react sporadically with the subunits of monomers to form monomer radicals which also reacts with each other to form smaller chains of polymer units leading to the formation of monoliths and their associated energies ΔH_{mi} and ΔH_m, respectively. Fundamentally, the formation of these monomer radicals and monomer chains through their molecular interactions causes an increase in the energy of the mixture as well as temperature rise.

3.2   Effect of monomer variation

Two types of monomers were employed in the synthesis of the polymethacrylate monolith at a constant temperature of 85 °C: EDMA as the cross-linking monomer and GMA as the functional monomer harbouring the epoxy moiety. An increase in the concentration of the cross-linking monomer results in the formation of a higher number of interconnectivities between globules and clusters of globules. Nevertheless, it must be noted that excessive amounts of total monomers to total porogen in the non-solvating mixture could lead to the

formation of gel-like monoliths irrespective of the temperature of polymerisation and polymerisation time. This is made evident in Figure 4 below with 30% total porogen and 70% total monomers synthesised at: (A) 85 ºC and (B) 80 ºC respectively.

(A) (B)
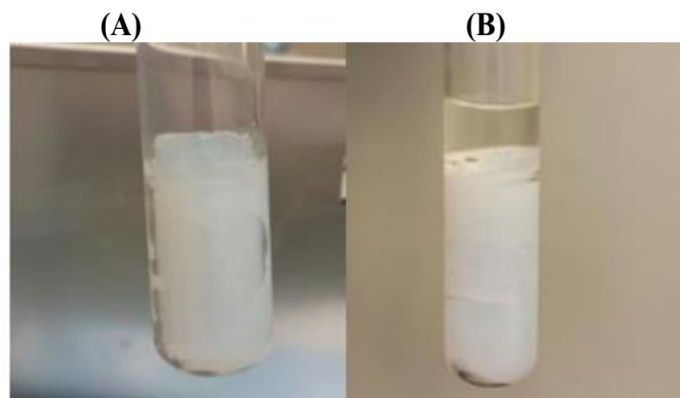
Figure 4. The effect of excessive concentration of monomers in porogenic mixture on polymer formation.

The type and concentration of the cross-linking monomer define the network structure of the monolith, affecting physical properties such as the mechanical strength and porosity. High cross-linker concentrations commensurate with the formation of large surface areas, less pores and high tensile strength of the polymer. Figure 5 shows the SEM images of polymethacrylate monoliths synthesised at 40% (x 6000, 5 µm), 60% (x 6000, 5 µm) and 70% EDMA (x 7000, 5 µm) concentrations.

EDMA 40% EDMA 60% EDMA 70%
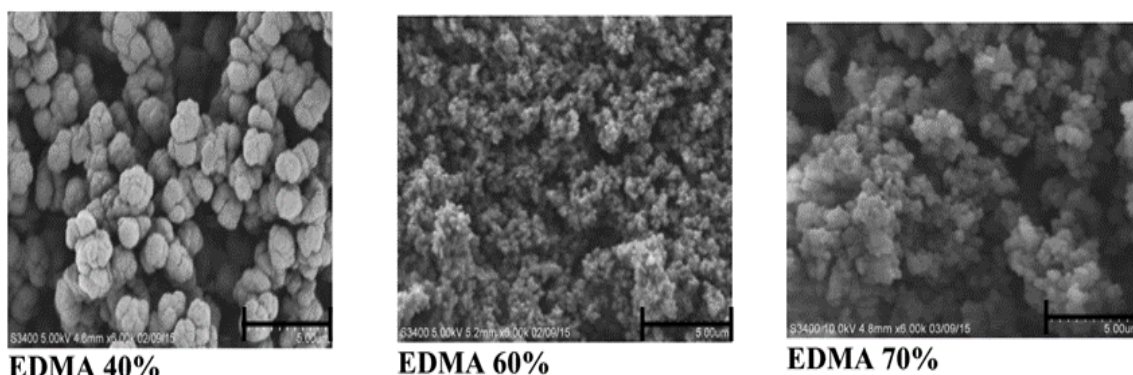
Figure 5. SEM images of polymethacrylate adsorbents synthesised at 40% (5 µm), 60% (5 µm) and 70% (5 µm) EDMA concentrations. SEM analysis were conducted at 5 kV, 5 kV and 10 kV with magnifications of 4.6 mm x 6000, 5.2 mm x 6000 and 4.3 mm x 7000, respectively.

During thermochemical analysis of the polymerization reaction, the ratio of EDMA to GMA was varied from 30% to 70%. The boundary ratios (30% – 70%) were selected as polymethacrylate monoliths require reactive epoxy groups in the polymer architecture

147

from the GMA for adsorbent functionalisation. From Figure 6, it can be inferred that an increase in the EDMA/GMA ratio resulted in an increase in the temperature build-up during polymerization. The peak temperature increased from 96.3 $^{\circ}$C at EDMA 30% to 114.3 $^{\circ}$C at EDMA 70%. Increasing the EDMA concentration creates an additional thermal evolution from the interactions between generated free radicals and the monomer. Aside the increased interconnectivities associated with high EDMA concentrations, the increasing peak temperatures further buttress the point that elevated EDMA concentrations lead to early formation of nuclei, reduction in pore size and pore volume (Danquah and Forde, 2008). The polymerization systems with varying EDMA concentrations generated similar thermal effects as observed for increasing the polymerization set-point temperature. However, because the polymerization temperature was kept constant at 85 $^{\circ}$C, the thermal paths of the reactions in the sensible heat transfer region appeared to be similar until post initiator decomposition where the temperature peaks after traversing the polymerization set-point temperature. Under high EDMA conditions, more methylene units are available to react with the free radicals present in the same volume of polymerization mixture. Due to the associated increase in temperature, which is proportional to the concentration of EDMA, the rate of initiation is also directly affected and this results in late phase separation.
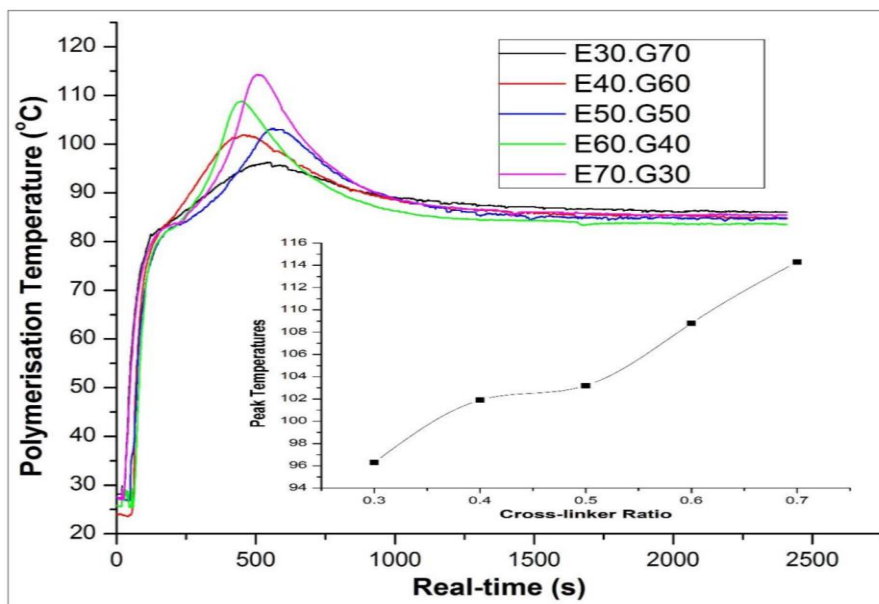
Figure 6. Real-time polymerization temperature profiles for varying EDMA/GMA concentration ratio.

3.3   Effect of initiator concentration

Although it has been experimentally determined by Mihelic *et al.* (2001) using a differential scanning calorimeter, that synthesis of poly(GMA-co-EDMA) monoliths can occur at high temperatures >110 °C without an initiator, the latter serves as a catalyst to speed up molecular interactions between the monomers thus, enhancing the rate of nucleation. The initiator decomposes at the initiation temperature to form free radicals, which interact with the monomers to induce nucleation. The free radicals induced nucleation step requires a lesser amount of heat to generate significant exotherms after decomposition. The effects of five varied initiator concentrations on the polymerization kinetics and temperature build up were investigated at a constant monomer ratio of EDMA/GMA (30%:70%), temperature of 85 °C and a total porogen concentration of 70% (cyclohexanol 70% : dodecanol 30%). As shown in Figure 7 the thermal reaction paths pre-initiation were comparable with an increase in peak temperatures for higher initiator concentrations. The peak temperatures increased from 90.7 °C for 1% w/v BPO to 106.3 °C for 3% w/v BPO. In addition, increasing the initiator concentration resulted in a rapid rate of nuclei formation since more free radicals are released per unit quantum of energy to cause the formation of a large number of nuclei in the polymerization mixture. The increase in peak temperatures together with rapid polymerization rates are a result of an increase in the initiator decomposition to produce more radicals, which also reacts with the monomers to produce heat.

The significantly large amount of exotherms released as a result of increasing the concentration of initiators in the reacting mixture leads to a faster frequency of nucleation formation, thereby forming more intra-globules, inter-clusters of globules and smaller pore sizes. Large amounts of initiators also render the polymeric monolith highly brittle.
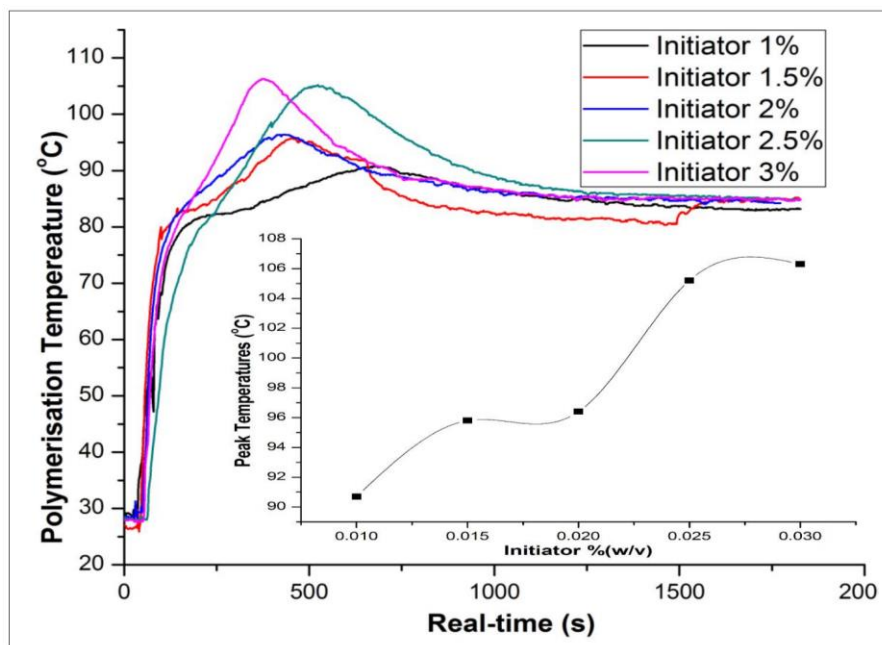
Figure 7. Real-time polymerization temperature profiles for varying initiator concentrations.

3.4 Effect of Polymerization time

Polymerization time is another important tool to engineer the structural characteristics of the monolithic adsorbent without changing the synthesis conditions. In this study, different post-initiation polymerization times were investigated for the synthesis of poly(EDMA-co-GMA). These durations were based on the time during which the polymerization mixture changes from pale white to opaque. It was observed that with an increase in polymerization time, from 5 h to 9 h, the average pore size reduced from 40 µm to 30 µm as shown in Figure 8. The reduction in pore size is due to the continuous conversion of the cross-linker monomers to form more nuclei units, which increased the surface area of the polymer and cause a reduction in the pore size. Internal heat effects within the mould can also cause further reductions in the pore size as a result of the low thermal diffusivity of the polymer to the external environment (water bath) after formation. It has previously been reported that extending the polymerization time causes a decrease in the porosity, height of the monolith and pore size distribution (Svec and Fréchet, 1995). It can also be inferred that the polymerization time coupled with temperature build-up from the bottom of the mould can cause a variation in the axial pore size distribution with smaller pores below the monolith length. Though not investigated

150

in this present work, it is anticipated that there is an optimum time above which there is no reduction in the pore size of the monolith, and this optimum time is a function of the concentration of the cross-linker monomer present in the polymerization mixture.

5hours   7hours   9hours
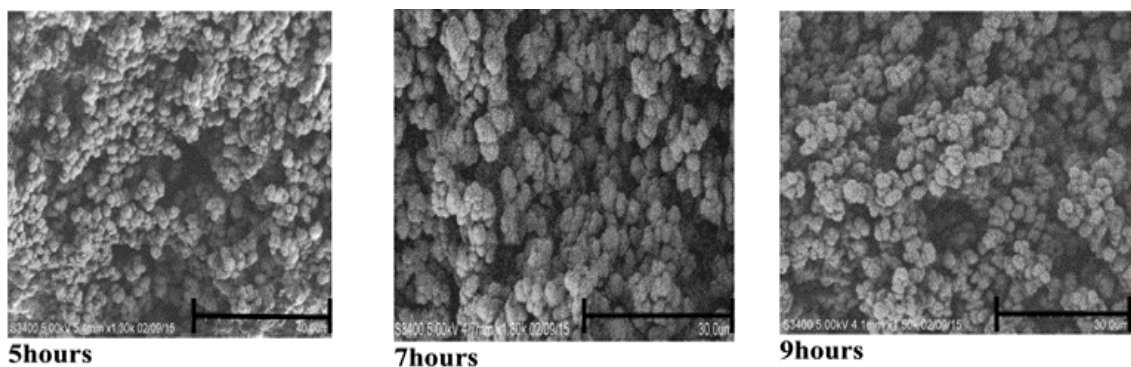
Figure 8. SEM images of polymethacrylate adsorbents synthesised for 5 h (40 µm), 7 h (30 µm) and 9 h (30 µm). Analysis were carried out at resolutions of 5.4 mm x 1300, 4.2 mm x 1900 and 4.1 mm x 1500, all at about 5 kV.

## 4.	Kinetics of Polymerization

Synthesis of polymethacrylate monoliths by free radical polymerization is often governed by the reactivity of two monomers (cross-linkers and functional monomers) in a mixture containing an initiator to commence the formation of nuclei after the initiator decomposition temperature is reached. The polymer formation is characterised by two key processes: chemical reaction between the monomers, and the growth of nuclei. Until the sporadic formation of nuclei, no solid phase evolves within the polymerization mixture. The randomised combinations of nuclei to form microglobules and subsequent combinations to form globules and clusters result in the heterogeneous nature of polymethacrylate monoliths and dictate the pore size distribution of the monolith. The degree of randomness can be controlled via synthesis conditions such as temperature and the initiator concentration. The nuclei serve as the seed crystal to induce polymer growth. To elucidate the polymer growth process, a crystallisation rate model is applied and the resistance to the formation of the bulk solid polymer phase is factored through the kinetics of the reaction. The two monomers [GMA (*A*) and EDMA (*B*)] react post-initiation when subjected to suitable thermochemical conditions. Instantaneous reaction of *A* and *B* post-initiation results in the formation of a viscous liquid intermediary stage, containing nuclei subunits, that dictates the propagation of chain molecules in the polymerization process. The extent of GMA-co-EDMA chains influences the rate of formation of the solid

151

polymer. Figure 9 shows a mechanistic view of the polymer formation process incorporating the reactivity stage and the polymer growth stage. The monomeric reaction stage can be represented by the following chemical reaction.
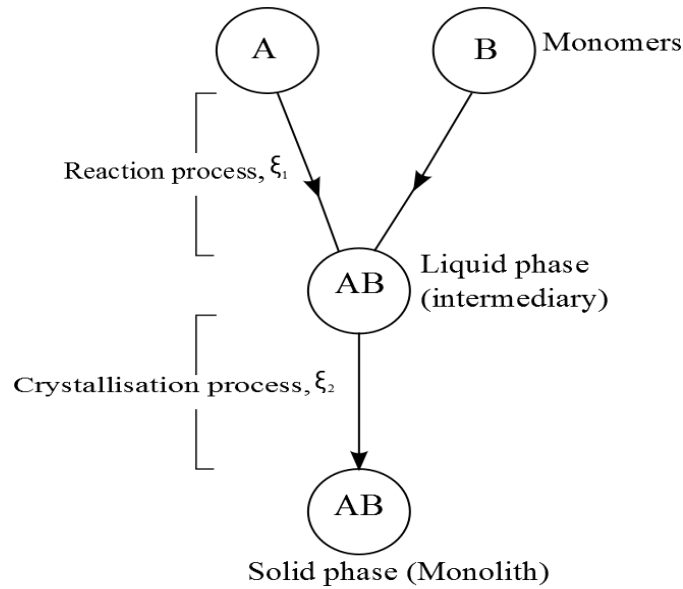
Figure 9. A mechanistic view of polymethacrylate monolith formation showing the monomeric reaction stage and the polymer growth phase. The reaction stage is characterised by the extent, ξ_1, and the polymer growth stage is characterised by the extent, ξ_2.

$$\begin{matrix} A & & B & \xrightarrow{Z} & AB \\ (GMA) & + & (EDMA) & & (Polymer) \end{matrix} \tag{4}$$
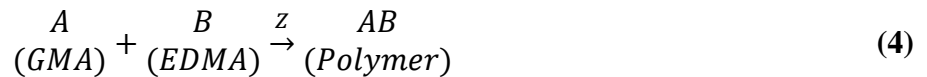
where Z represents the totality of suitable reaction conditions. A_o and B_o are the initial concentrations of the reactants whiles A and B are the concentrations at time (t). From equation (1), Mihelic *et al.* (2001) experimentally determined the reaction order for the synthesis of polymethacrylate monoliths as first order. Hence, the reaction rate equation can be written as follows.

$$\frac{d\xi_1}{dt} = k_1(A_o - \xi_1)(B_o - \xi_1) \tag{5}$$

Assuming the monomer ratio B_o/A_o is x and A is the limiting reactant, equation (5) can be written in terms of the limiting reactant as follows.

$$\frac{d\xi_1}{dt} = k_1(A_o - \xi_1)(xA_o - \xi_1) \tag{6}$$

The polymer growth phase occurs gradually in a layer-by-layer format from the bottom of the mould after the formation of the first nuclei to form globules, clusters of globules with pore interconnectivities to yield a single continuous piece. Avrami's isothermal crystallisation equation is used to model the polymer growth phase owing to its ability to predict the kinetics of polymer formation in a finite volume, isothermal and non-isothermal conditions as follows (Avrami, 1941; Foreman and Blaine, 1995; Piorkowska and Galeski, 2003):

$$\frac{d\xi_2}{dt} = k_2(T)f(\xi_2) \tag{7}$$

$$f(\xi_2) = r(1 - \xi_2)[-In(1 - \xi_2)]^{1-\frac{1}{r}} \tag{8}$$

where $f(\xi_2)$ governs the kinetics of polymer growth; $k_2(T)$ is the specific rate constant; and r is the Avrami's constant which typically ranges from 1 to 4. A value of $r = 4$ is chosen since the mechanism of polymethacrylate monolith formation is based on sporadic formation of nuclei. An isothermal model is used as the polymerization temperature rapidly equilibrates to the set-point temperature post-initiation. Considering the two stages, monomer reactivity and polymer growth, during the polymerization process, it can be inferred that the extent of formation (ξ_1) of AB_l liquid in the intermediate region is dependent on the rate at which the monomers react. Also, the extent of AB_l liquid transforming into the bulk-solid polymer (ξ_2) is dependent on the amount of AB_s solid present in the mould.

Various conditions were selected for modelling with MATLAB using different hypothetical conditions based on experimental observations. The ratios of monomers (*B/A*) were varied from 1:1 to 3:1 using Avrami's model. Different hypothetical rate constants are also shown in Figure 10 for the two stages leading to the formation of monoliths.
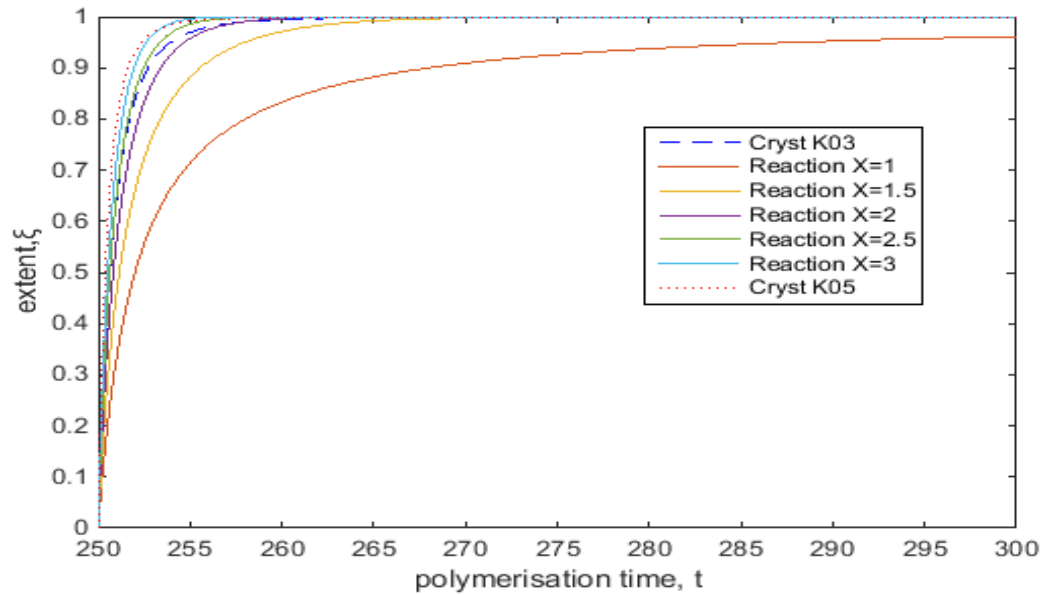
Figure 10. The effects of polymer growth rate constant and varying monomer concentration ratio on the extent of polymerization within the mould.

If k_1 represents the rate constant for the monomeric reaction stage, and k_2 represents the rate constant for the polymer growth phase, theoretically, three scenarios can occur between the monomer reactivity and the polymer growth rates. These scenarios are $k_1 > k_2$, $k_1 = k_2$ and $k_1 < k_2$. Scenario 1 ($k_1 > k_2$) shows the condition where the rate constant of AB_l (liquid) formation is higher than AB_s (solid) formation. Scenario 2 ($k_1 = k_2$) shows the condition where the rate of AB_l (liquid) formation is equal to that of AB_s (solid) formation. Scenario 3 ($k_1 < k_2$) shows the condition where the rate of AB_l (liquid) formation is slower than AB_s (solid) formation.

In scenario 1, $k_1 > k_2$ was modelled with hypothetical values of 0.5 s^{-1} and 0.3 s^{-1} for k_1 and k_2 respectively, and it was observed that the rate at which the monomers react to form the intermediary phase is much slower than the rate at which the bulk solid begins to form under the same conditions. However, the extent to which the monomers react to form the intermediary phase is higher at the early phase of the reaction than that of the formation of the solid phase. Apparently, this section of the Avrami's model is in keeping with the polymerization of monoliths. Thus, the magnitude of their rate constants at either phase dictates the extent to which the reaction proceeded. The higher the rate constant for the first stage (monomeric reaction to form the intermediary AB_l), the higher the amount of AB_l that can be produced for the second stage simultaneously. According to Avrami's

154

equation (7), the formation of the bulk solid phase in the second phase is governed by a function of the extent of reaction $f(\xi_2)$, implying that the rate constants directly affected the extent of the reactions.

In scenario 2 where k_1 (0.3 s^{-1}) = k_2 (0.3 s^{-1}), it was observed that the rate at which the monomers react to form the intermediary phase was faster than that of the formation of the solid phase but with a lower extent of reaction as evident in comparing the reaction curve x=1 to that of Avrami's crystallisation model (k = 0.3). From the analysis, an increase in the ratio of monomers from x=1 to x=3 yielded in a corresponding increase in the extent of the reaction. This can be comparable to mixtures with low concentrations of monomers in the porogenic system. The implication is that, in the formation of monoliths based on the crystallisation model, the rate at which the solid phase forms is mainly temperature dependent since the rate constant is a function of temperature. In addition, given the same conditions, the transformation rate of the liquid phase into solid phase to form the bulk polymer is faster. Lastly, the third scenario, $k_1 < k_2$, is the reverse of the first scenario. Inference from analysis (graph not shown) indicates that once the rate constant of phase 1 is less than that of phase 2, then the extent of the reaction for phase 1 will be lower than that of the second phase.

5.   CONCLUSION

In summary, varied conditions for the synthesis of monoliths were probed to elucidate their *in situ* thermochemical effect during polymerization. Inferences from our parameteric analysis further proves the fact that the key parameter to the control of pore size and rate of formation hinges on the overall impact of the contribution of temperature in the polymerization mould. The higher the amount of exotherm released during polymerization, the smaller the size of pores. Online observations from the illustrated data indicates that an increase in the amount of cross-linkers (EDMA) from 30% to 70% correlates with an increase in polymerization peak temperatures from 96.3 °C to 114.3°C and a reduction in pore size as revealed by the SEM analysis. Similarly, an increase in the concentration of initiators (BPO) from 1% w/v to 3% w/v resulted in a temperature increase from 90.7°C to 106.3°C. In addition, the different set point temperatures for the water bath resulted in different thermal path for polymerization mixtures of the same

compositions and a corresponding increase in peak temperatures. Consequently, the overall internal thermal path for the reactive mixture is a function of the amount of cross-linker and initiator present as well as the set point temperature for the water bath.

The moderation of time as an in-process parameter whiles maintaining mixture compositions constant for EDMA-co-GMA polymeric monoliths also proved to be essential in reducing the pore sizes. An attempt to model the polymerization of monoliths based on the established Avrami's isothermal model was in keeping with known experimental observations. The rate of monolith formation was observed to intensify with increasing amount of monomers. Essentially, results from the experiment show that the thermochemical processes leading to the formation of monoliths are very sensitive and could potentially cause variation in pore sizes, porosity, rate of formation and their mechanical strength when altered slightly. In addition, the extents of reactions in each phase of the proposed model are directly dependent on their rate constant.

6.   ACKNOWLEDGMENT

Authors wish to declare that there is no conflict of interest or commercial with respect to

the publication.

7.   REFERENCES

Alves, F., P. Scholder and I. Nischang, 2013. Conceptual design of large surface area porous polymeric hybrid media based on polyhedral oligomeric silsesquioxane precursors: Preparation, tailoring of porous properties, and internal surface functionalization. ACS applied materials & interfaces, 5(7): 2517-2526. Available from http://www.ncbi.nlm.nih.gov/pmc/articles/PMC3624795/. DOI 10.1021/am303048y.

Avrami, M., 1941. Granulation, phase change, and microstructure kinetics of phase change. Iii. The Journal of chemical physics, 9(2): 177-184.

Aydoğan, C., 2015. A new anion-exchange/hydrophobic monolith as stationary phase for nano liquid chromatography of small organic molecules and inorganic anions. Journal of Chromatography A, 1392: 63-68. Available from http://www.sciencedirect.com/science/article/pii/S0021967315003970. DOI http://dx.doi.org/10.1016/j.chroma.2015.03.014.

Chen, L., J. Ou, Z. Liu, H. Lin, H. Wang, J. Dong and H. Zou, 2015. Fast preparation of a highly efficient organic monolith via photo-initiated thiol-ene click polymerization for capillary liquid chromatography. Journal of Chromatography A, 1394: 103-110. DOI 10.1016/j.chroma.2015.03.054.

Danquah, M.K. and G.M. Forde, 2007. Towards the design of a scalable and commercially viable technique for plasmid purification using a methacrylate monolithic stationary phase. Journal of Chemical Technology & Biotechnology, 82(8): 752-757. DOI 10.1002/jctb.1733.

Danquah, M.K. and G.M. Forde, 2008. Preparation of macroporous methacrylate monolithic material with convective flow properties for bioseparation: Investigating the kinetics of pore formation and hydrodynamic performance. Chemical Engineering Journal, 140(1-3): 593-599. DOI 10.1016/j.cej.2008.02.012.

Danquah, M.K., J. Ho and G.M. Forde, 2008. A thermal expulsion approach to homogeneous large-volume methacrylate monolith preparation; enabling large-scale rapid purification of biomolecules. Journal of Applied Polymer Science, 109(4): 2426-2433. DOI 10.1002/app.28346.

Foreman, J. and R. Blaine, 1995. Isothermal crystallization made easy: A simple model and modest cooling rates. ANTEC'95., 2: 2409-2412.

Jandera, P., M. Staňková, V. Škeříková and J. Urban, 2012. Cross-linker effects on the separation efficiency on (poly)methacrylate capillary monolithic columns. Part i. Reversed-phase liquid chromatography. Journal of Chromatography A. DOI 10.1016/j.chroma.2012.12.003.

Kim, N.-j., J.-h. Kwon and M. Kim, 2013. Highly oriented self-assembly of conducting polymer chains: Extended-chain crystallization during long-range polymerization. The Journal of Physical Chemistry C, 117(29): 15402-15408. DOI 10.1021/jp404566n.

Mihelic, I., M. Krajnc, T. Koloini and A. Podgornik, 2001. Kinetic model of a methacrylate-based monolith polymerization. Ind. Eng. Chem. Res., 40(16): 3495-3501.

Nischang, I., 2013. Porous polymer monoliths: Morphology, porous properties, polymer nanoscale gel structure and their impact on chromatographic performance. Porous polymer monoliths: Morphology, porous properties, polymer nanoscale gel structure and their impact on chromatographic performance, 1287: 39-58.

Ongkudon, C.M. and M.K. Danquah, 2010. Process optimisation for anion exchange monolithic chromatography of 4.2 kbp plasmid vaccine (pcdna3f). Journal of Chromatography B, 878(28): 2719-2725. DOI 10.1016/j.jchromb.2010.08.011.

Pfaunmiller, E., M. Paulemond, C. Dupper and D. Hage, 2013. Affinity monolith chromatography: A review of principles and recent analytical applications. Analytical and bioanalytical chemistry, 405(7): 2133-2145. DOI 10.1007/s00216-012-6568-4.

Piorkowska, E. and A. Galeski, 2003. New possibilities in the description of overall crystallization of polymers. Physics, 42(3-4): 773-792. DOI 10.1081/MB-120021606.

Podgornik, A., V. Smrekar, P. Krajnc and A. Strancar, 2013. Estimation of methacrylate monolith binding capacity from pressure drop data. Journal of chromatography. A,

1272: 50-55. Available from http://www.ncbi.nlm.nih.gov/pubmed/23261298. DOI 10.1016/j.chroma.2012.11.057.

Podgornik, A., S. Yamamoto, M. Peterka and N.L. Krajnc, 2013. Fast separation of large biomolecules using short monolithic columns. Journal of chromatography. B, Analytical technologies in the biomedical and life sciences, 927: 80-89. Available from http://www.ncbi.nlm.nih.gov/pubmed/23465515. DOI 10.1016/j.jchromb.2013.02.004.

Roberts, M.W., C.M. Ongkudon, G.M. Forde and M.K. Danquah, 2009. Versatility of polymethacrylate monoliths for chromatographic purification of biomolecules. Journal of separation science, 32(15-16): 2485-2494. Available from http://www.ncbi.nlm.nih.gov/pubmed/19603394. DOI 10.1002/jssc.200900309.

Schlemmer, B., R. Bandari, L. Rosenkranz and M.R. Buchmeiser, 2009. Electron beam triggered, free radical polymerization-derived monolithic capillary columns for high-performance liquid chromatography. Electron beam triggered, free radical polymerization-derived monolithic capillary columns for high-performance liquid chromatography, 1216(13): 2664-2670.

Svec, F., 2004. Preparation and hplc applications of rigid macroporous organic polymer monoliths. Journal of separation science, 27(10-11): 747-766. DOI 10.1002/jssc.200401721.

Svec, F., 2010. Porous polymer monoliths: Amazingly wide variety of techniques enabling their preparation. Journal of Chromatography A, 1217(6): 902-924.

Svec, F., 2012. Quest for organic polymer-based monolithic columns affording enhanced efficiency in high performance liquid chromatography separations of small molecules in isocratic mode. Journal of Chromatography A, 1228: 250-262.

Svec, F. and J.M.J. Fréchet, 1995. Kinetic control of pore formation in macroporous polymers. Formation of "molded" porous materials with high flow characteristics for separations or catalysis. Chemistry of Materials, 7(4): 707-715.

Svec, F. and J.M.J. Fréchet, 1995. Temperature, a simple and efficient tool for the control of pore size distribution in macroporous polymers. Macromolecules, 28(22): 7580-7582.

Szumski, M. and B. Buszewski, 2009. Effect of temperature during photopolymerization of capillary monolithic columns. Journal of separation science, 32(15-16): 2574-2581. DOI 10.1002/jssc.200900220.

Vonk, R., S. Wouters, A. Barcaru, G. Vivó-Truyols, S. Eeltink, L. Koning and P. Schoenmakers, 2015. Post-polymerization photografting on methacrylate-based monoliths for separation of intact proteins and protein digests with comprehensive two-dimensional liquid chromatography hyphenated with high-resolution mass spectrometry. Analytical and bioanalytical chemistry, 407(13): 3817-3829. DOI 10.1007/s00216-015-8615-4.

Wang, H., J. Ou, H. Lin, Z. Liu, G. Huang, J. Dong and H. Zou, 2014. Chromatographic assessment of two hybrid monoliths prepared via epoxy-amine ring-opening polymerization and methacrylate-based free radical polymerization using methacrylate epoxy cyclosiloxane as functional monomer. Journal of Chromatography A, 1367: 131-140. DOI 10.1016/j.chroma.2014.09.072.

Yang, R., J. Pagaduan, M. Yu and A. Woolley, 2015. On chip preconcentration and fluorescence labeling of model proteins by use of monolithic columns: Device

fabrication, optimization, and automation. Analytical and bioanalytical chemistry, 407(3): 737-747. DOI 10.1007/s00216-014-7988-0.

Zhang, A., F. Ye, J. Lu and S. Zhao, 2013. Screening α-glucosidase inhibitor from natural products by capillary electrophoresis with immobilised enzyme onto polymer monolith modified by gold nanoparticles. Food chemistry, 141(3): 1854-1859. DOI 10.1016/j.foodchem.2013.04.100.

CHAPTER FOUR

THERMAL STABILITY AND KINETIC MODELLING OF POLYMETHACRYLATE MONOLITHS VIA THERMOGRAVIMETRIC ANALYSIS

SECTION 4.1

Parametric investigation of polymethacrylate monolith synthesis and stability via thermogravimetric characterization

Caleb Acquah, Michael K. Danquah, Charles K.S. Moy, Mahmood Anwar, Clarence M. Ongkudon

DECLARATION FOR THESIS SECTION 4.1

Parametric investigation of polymethacrylate monolith synthesis and stability via thermogravimetric characterization

The candidate will like to declare that there is no conflict of interests involved in this work and that my extent of contribution as candidate is as shown below:

Contribution of Candidate	Conceptualisation, initiation and write-up	80%

The following co-authors were involved in the development of this publication and attest to the candidate's contribution to a joint publication as part of his thesis. Permission by co-authors are as follows:

Name	Signature	Date
Michael K. Danquah		13.07.2017
Charles K.S. Moy		13.07.2017
Clarence M. Ongkudon		13.07.2017
Mahmood Anwar		18.07.2017

ABSTRACT

Polymethacrylate monoliths are synthetic adsorbents with macroporous and mesoporous interconnected channels that can be engineered to target the hydrodynamic features of a wide range of cells, biomolecules and viruses. However, rigorous study into the effect of synthesis conditions on their thermal stability is limited. This work attempts to characterise the influence of key synthesis process variables on the stability of polymethacrylate monoliths using thermogravimetric analysis at a heating rate of 10 ℃/min. Experimental results showed that the thermal stability of polymethacrylate monoliths increased with decreasing polymerisation temperature from 85 ℃ to 65 ℃. Increasing the total porogen (P) to monomer (M) ratio increased the thermal stability of the monolith by >62% and >50% for P40/M60-P60/M40 and P60/M40-P80/M20, respectively. The impact of the initiator concentration, monomer variation, biporogen ratio, washing and activation of the monoliths were also investigated. NMR analyses conducted confirmed the hydrolysis of epoxy moieties on the monolith.

Keywords: Polymerisation; Polymethacrylate monoliths; Thermogravimetry; Polymer Degradation; Thermal stability

1. INTRODUCTION

Advances in bio-separation and purification technologies based on liquid chromatography have resulted in the development of macroporous polymeric stationary phase adsorbents for rapid and high throughput separation of cells and biomolecules. One of such stationary adsorbents is monolithic polymers such as polymethacrylates which have demonstrated to offer convective mass transport for rapid bio-separation compared to particulate adsorbents with diffusive mass transfer mechanisms (Svec and Fréchet, 1995).

Polymeric monoliths are continuous solo-phase adsorbents with interconnected meso- and/or macro-pores synthesised within a mould. Polymethacrylate monoliths, for example, have gained significant interest in bioseparation due to their ease of synthesis, ability to engineer their pore sizes to enhance convective transport and prevent clogging, ease of ligand coupling for functionalisation, as well as the ability to retain ligand density and binding performance after multiple runs (Danquah and Forde, 2007). Monoliths assume the shape of their mould during synthesis and this results in varied architectural structures, size and bed morphology (Ongkudon *et al.*, 2014). Monoliths can be synthesized using techniques such as sol–gel, polyemulsions, living polymerisation, polycondensations, click reactions and free radical polymerisation (Acquah *et al.*, 2016; Liu *et al.*, 2016). Polymethacrylate monoliths have largely been synthesised via free radical co-polymerisation to introduce epoxy functional groups for easy reactive functionalisation whilst being resistant to a wide pH range (Roberts *et al.*, 2009; Podgornik *et al.*, 2013). The synthesis of polymethacrylate monoliths is performed using various precursors in the form of cross-linker monomer, functional monomer, porogen and initiator under defined synthesis conditions.

Mihelič *et al.* (2001) demonstrated using differential scanning calorimetry (DSC) that the initiator decomposes to provide significant energy and temperature to meet the activation complex of the polymerisation reaction in order to trigger the formation of nuclei. The cross-linking and functional monomers in a copolymeric format enable the formation of cross-linked polymeric core with reactive functional groups for easy immobilisation of suitable ligands. It has been previously demonstrated that an increase in the proportion of cross-linker monomer generates a high temperature build-up, resulting in the formation of

small size nucleic points that coalesce to form polymeric core with small pores (Danquah and Forde, 2008; Jandera *et al.*, 2012; Acquah *et al.*, 2016). Other reported studies have discussed the effects of polymerisation temperature and type of porogen on the pore structure and morphology of polymethacrylate monoliths (Cooper, 2000; Chen *et al.*, 2015). The type and concentration of porogen is dictated by the type of monomers with a demonstrated effect on the mechanical strength of the monolith (Danquah and Forde, 2008; Wang *et al.*, 2012; Liu *et al.*, 2013; Iacono *et al.*, 2016).

Thermal stability is a major challenge with polymeric monoliths, and this has obstructed applications involving elevated temperature conditions (Hayes *et al.*, 2014; Acquah *et al.*, 2016). The thermal stability of polymeric monoliths has previously been demonstrated to be under 210 ℃ for methacrylate monolith HMA-co-EDMA (Yusuf *et al.*, 2016), 380 ℃ for poly(divinylbenzene) monolith (Sýkora *et al.*, 2000), and 300 ℃ for the hybrid synthesised monolith, POSS-epoxy–TPTM (Lin *et al.*, 2015). These characteristic temperature ranges represent the safe region beyond which the respective polymers will lose their molecular and structural properties. Thus, indicating striking features of the synthesised monolith for prolonged biotechnological applications involving heat or in the dry state (Park *et al.*, 2014). To date, no research studies have comprehensively investigated the effects of synthesis conditions on the thermal stability of polymeric monoliths in general. Understanding the effects of polymerisation conditions on the thermal stability of polymethacrylate monolith provides an opportunity to develop them with predetermined stability for tailored thermophilic applications. Hence, the aim of this study is to conduct a parametric investigation of various *in situ* and *ex situ* process conditions relevant to polymeric monolith synthesis and establish effects on the thermal stability of the polymer. In addition, emphasis is placed on the first degradation stage beyond which the polymer will lose its molecular properties.

2. EXPERIMENTAL

2.1 Materials

Glycidyl methacrylate (GMA, MW 142.15, 97%), ethylene glycol dimethacrylate (EDMA, MW 198.22, 98%), hydrochloric acid (HCl, MW 36.5, 37%), 1-dodecanol (MW 186.33, 98%), cyclohexanol (MW 100.16, 99%), benzoyl peroxide or initiator (BPO, MW

242.23, 70%), and methanol (HPLC grade, MW 32.04, 99.93%) were purchased from Sigma–Aldrich. Polymerisation was performed using rimless cylindrical test-tubes (1.5 x 12 cm, Borosil, India) as moulds in an isothermal water bath reactor acquired from Memmert (WNB 14, Germany).

2.2   Method

The method of synthesis of polymethacrylate monolith, as shown in the reaction scheme in Figure 1, is as reported in our previous publications (Danquah and Forde, 2008; Acquah *et al.*, 2016) based on a free radical polymerisation technique in an isothermal water bath. Process conditions investigated include porogen to monomers ratio, porogen type and concentration, initiator concentration, polymerisation temperature, porogen dissolution method, and epoxy activation mechanism. All sample mixtures were purged with N_2 for 5 min and washed with methanol for 6 h. To ensure consistency, parameters to simplify the analysis of TGA, DTG and isothermal data are defined as follows: T_{onset} is the temperature at which the TGA curves commence, R_1 is the rate of degradation before depolymerisation, R_2 is the rate of degradation during the second stage of depolymerisation, R_3 is the rate of degradation during the third stage of depolymerisation, T_p is the maximum temperature during each stage of degradation and T_f is the final temperature for each stage. Each sample was synthesised thrice to ensure repeatability. The average of the replicates was normalised for each sample with the associated relative standard error to assess the extent of deviation owing to the random nature of free radical polymerisation processes. Morphological analyses of dried monoliths were conducted with a variable pressure scanning electron microscope (model S-3400N, Hitachi, Japan) at a voltage of 5 kV.
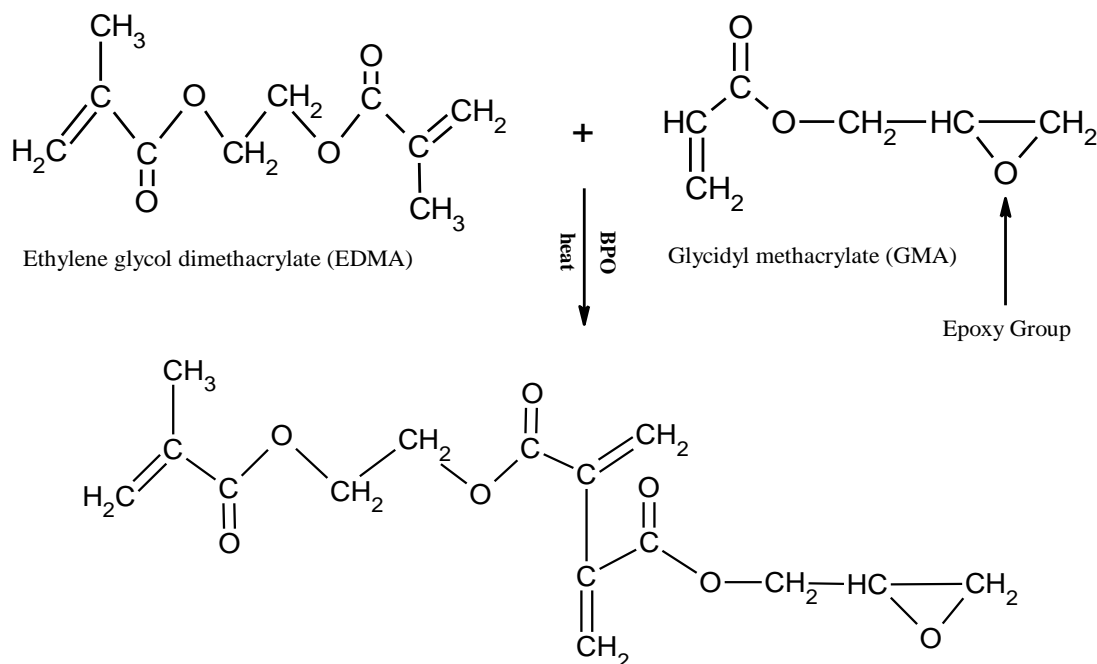
Figure 1. Reaction schematics for the synthesis of polymethacrylate monolith by free radical polymerisation

2.2.1 EDMA-GMA (E/G) Effect

The thermal effect of EDMA to GMA ratio was investigated based on the following variations: E40/G60, E60/G40 and E80/G20 on a v/v basis. The polymerisation process occurred at 85 ^{o}C for 4 h with the following material compositions: Porogen-Monomer ratio (60%/40%, v/v); BPO composition (1%, w/v of total monomer); Cyclohexanol-Dodecanol ratio (60%:40%, v/v).

2.2.2 Porogen-Monomer (P/M) Effect

The ratio of porogen to monomer was varied as follows: P40/M60, P60/M40 and P80/M20 on v/v basis. Other parameters were made constant as follows: Cyclohexanol-Dodecanol ratio (60%:40%, v/v); BPO composition (1%, w/v of total monomer); EDMA-GMA ratio (40%:60%, v/v). The polymerisation temperature was set at 85 ^{o}C for 4 h.

2.2.3 Temperature Effect

Water bath set point temperatures for polymerisation were varied as follows: 61 ^{o}C, 65 ^{o}C, 75 ^{o}C and 85 ^{o}C. For each aforementioned temperature condition, 5 ml of polymerisation mixture was prepared with the following compositions: Porogen-

Monomer ratio (60%/40%, v/v); Cyclohexanol-Dodecanol ratio (60%:40%, v/v); BPO composition (1%, w/v of total monomer); EDMA-GMA ratio (40%:60%, v/v). The polymerisation mould was immersed in the water bath at the set point temperature, and polymerisation proceeded for 4 h.

2.2.4 Cyclohexanol-Dodecanol (C/D) Effect

The effect of cyclohexanol to dodecanol ratio was investigated based on the following variations: C40/D60, C60/D40 and C80/D20 on a v/v basis. The polymerisation temperature was set as 85 °C for 4 h as other parameters were also left constant as follows: Porogen-Monomer ratio (60%/40%, v/v); BPO composition (1%, w/v of total monomer); EDMA-GMA ratio (40%:60%, v/v).

2.2.5 Initiator concentration Effect

Three different concentrations of the initiator (BPO) were applied: BPO (0.5%, w/v), BPO (1%, w/v) and BPO (1.5%, w/v). The ratios were calculated relative to the total volume of monomer. The polymerisation temperature was set as 85 °C for 4 h as other parameters were also kept constant as follows: Porogen-Monomer ratio (60%/40%, v/v); EDMA-GMA ratio (40%:60%, v/v).

2.2.6 Effect of methanol washing and acid activation

10 ml of polymerisation mixture was prepared based on the composition: Porogen-Monomer ratio (60%/40%, v/v); cyclohexanol-dodecanol ratio (60%:40%, v/v); BPO composition (1%, w/v of total monomer); EDMA-GMA ratio (40%:60%, v/v) and pipetted equally into two different test tubes for polymerisation at a temperature of 85 °C. The synthesised polymer samples were divided to compare the effect of methanol washing to an unwashed sample and also the impact of acidic activation on polymer stability using 1 M HCl at 60 °C for 6 h.

2.3 Thermogravimetric Characterisation of Monoliths

Thermogravimetric characterisations of polymethacrylate monoliths were carried out using a TGA/DSC 1 system (Mettler Toledo, USA). The polymers from different

experiments were crushed with 20 mg sampled out for thermogravimetric analysis in 70 µL aluminium oxide pans. Thermogravimetric (TG) and differential thermogravimetric (DTG) analyses were mainly conducted at 10 $^{\circ}$C/min over a temperature range of 50 – 450 $^{\circ}$C and nitrogen flow rate of 25 mL/min. The Mettler Toledo system was frequently purged with nitrogen gas at a flow rate of 100 mL/min and a heat flow of 20 $^{\circ}$C/min for equilibration. In addition, isothermal degradation of the samples was measured at 150 $^{\circ}$C for 120 min.

3. RESULTS AND DISCUSSION

3.1 Synthesis of Polymethacrylate Monolith

Polymethacrylate monoliths were thermally synthesised by means of free radical polymerisation of the two monomers (GMA and EDMA) in an interfacial layer after decomposition of the initiator (BPO); hence, their thermal stability characteristics were analysed based on chemistries for heterogeneous solids. The presence of nuclei caused scissions of monomeric units in the sonicated mixture to form monomer radicals which subsequently lead to reaction between the methacrylate monomers. Formation of the polymer occurs stage wise from the bottom of the column to the apex of the reagents. The final polymer formed has a dual phase in the mould- a solid phase being the polymer and a liquid phase being the unreacted monomers, inert porogens (cyclohexanol and dodecanol) and formed droplets of water molecules. Thus, necessitating the need for rigorous washing of the formed polymers with non-destructive chaotropic reagents such as methanol.

3.2 Thermogravimetric analysis

3.2.1 Effect of EDMA/GMA (E/G) ratio on thermal stability

The impact of varying the concentration of monomers on the thermal stability of monoliths using the TG and DTG curves is shown in Figures 2a and 2b, respectively, for a heat flow rate of 10 $^{\circ}$C/min. It was conspicuously observed that irrespective of monomer variation, the monoliths possessed three (3) main degradation stages but with different characteristic temperatures. The selected concentrations studied for the EDMA-co-GMA polymeric monoliths were: E40/G60; E60/G40 and E80/G20. The occurrence of the second and third stage, referred to as depolymerisation in the current analysis, of the

monolith could be attributed to the fact that the polymer synthesis proceeded with two homopolymeric compounds as monomers. This observation is in good agreement with the previous experiment by Vlad *et al.* (2003) where they confirmed the impact of different cross-linkers on the thermal stability and degradation of acrylamide copolymers.
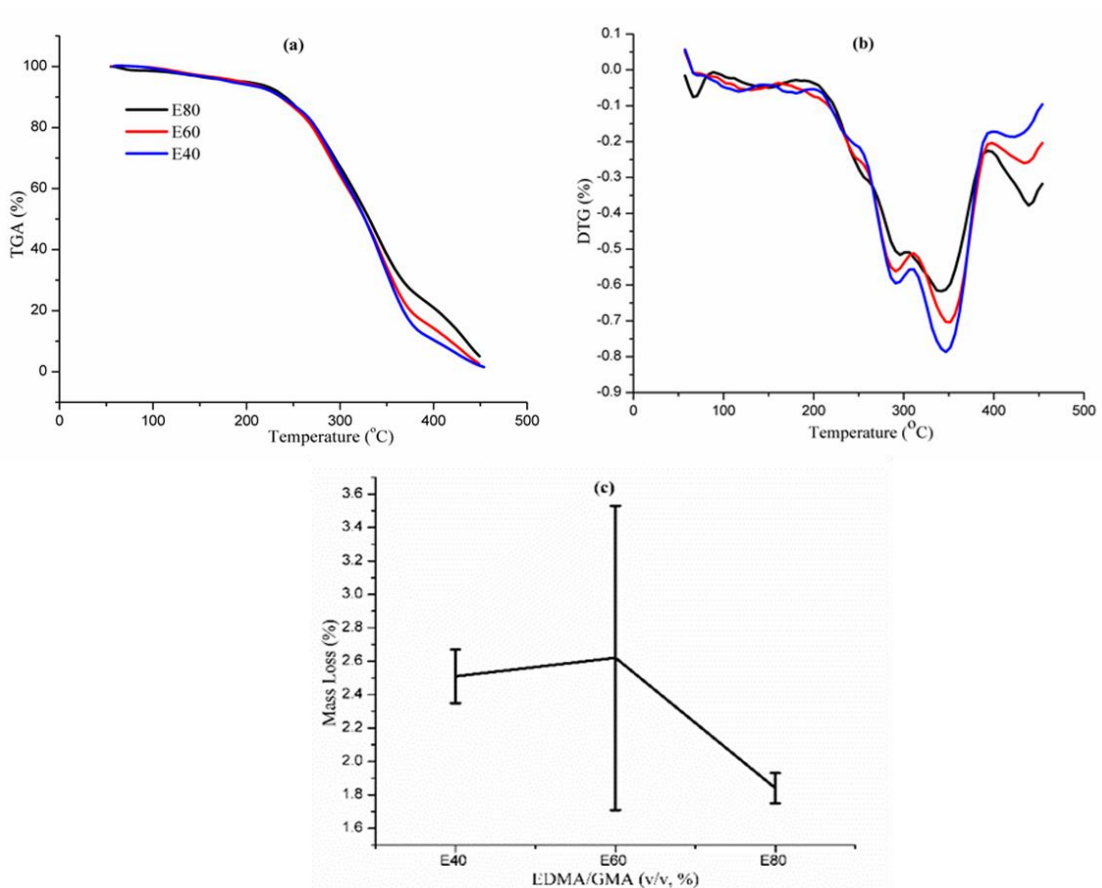
Figure 2. a) TGA, b) DTG and c) total mass loss curves obtained under isothermal conditions for varied monomer ratios during the formation of EDMA-co-GMA polymethacrylate monoliths synthesised at 85 °C for 4 h.

Generally, the first degradation of the varied samples under this condition occurred with minimal rate of mass loss R_1 <6% and low associated standard errors ranging from 0.81– 1.43% as indicated in Table 1. It was observed that an increase in the amount of EDMA could cause a corresponding decrease in the rate of degradation R_1 (% of mass loss/min) in the first stage. The reduction in mass loss is due to the fact that high amount of EDMA correlates with the formation of large amounts of interconnected networks to form a hard and robust monolith as previously reported by the seminal work of Svec and Fréchet

(1995) and by other recent groups such as Jandera *et al.* (2012) utilising different kinds of cross-linking reagents to vary pore sizes.

Table 1. Characteristic temperatures and rate of mass loss for polymethacrylate monoliths with different monomer ratios

First Stage				
EDMA/GMA (%v/v)	T_{onset} (^{o}C)	T_p	T_{final} (^{o}C)	R_1 (% min^{-1})
E40/G60	57.36±0.12	164.61±27.17	206.44±2.26	5.96±0.81
E60/G40	56.19±0.55	156.37±25.87	188.78±9.67	4.82±1.43
E80/G20	55.15±0.44	118.90±27.88	191.88±1.02	4.30±1.00
Second Stage (Depolymerisation)				
E40/G60	206.44±2.26	296.02±5.78	307.99±0.87	26.81±2.30
E60/G40	188.78±9.67	288.27±1.44	304.72±2.33	47.29±3.87
E80/G20	191.88±1.02	292.50±2.56	298.84±4.42	24.73±3.85
Third Stage (Depolymerisation)				
E40/G60	307.99±0.87	345.61±1.80	393.50±2.52	47.29±3.87
E60/G40	304.72±2.33	345.87±0.41	389.57±0.33	43.49±4.30
E80/G20	298.84±4.42	338.39±4.56	388.48±0.73	39.00±2.65
Isothermal Mass Loss for 120 mins				
E40/G60	2.51±0.16			
E60/G40	2.62±0.91			
E80/G20	1.84±0.09			

Owing to the sensitive applications of monoliths for thermophilic targets and chromatographic operations, their corresponding characteristic temperatures in the first stage represents the safe range within which monoliths can be operated without having significant consequential damage on their surface chemistry and mechanical properties. The cause of mass loss within this range is mainly due to the chemical dehydration of any absorbed moisture and extraction solvent (methanol). The mass loss of the second

degradation stage was observed to be significantly higher than the first stage as expected due to the commencement of depolymerisation process in the monolith. This results in the polymer losing its chemical nomenclature which could be attributed to the breakdown of bonds in the acrylate group of compounds in reference to the temperature ranges in the TG/DTG curves. The highest rate of mass loss was observed in the composition E60/G40. In addition, the third stage of degradation signified the final depolymerisation of the monolith. The trend in the third stage of degradation indicates that degradation of the epoxy-bond in monoliths could occur within the characteristic temperatures of ~298 – 308 ^{o}C for the selected samples. In addition, the characteristic temperatures for depolymerisation of the monolith also increased with increasing amount of GMA as previously remarked by Carioscia *et al.* (2007), Allaoui and El Bounia, (2009) for other epoxy-based materials.

To further elucidate the pattern of thermal stability, isothermal mass loss analyses were also conducted for each E/G sample at a temperature of 150 ^{o}C. The selected temperature was to ensure the polymer warm sufficiently to evaporate (at >100 ^{o}C) any moisture present as well as being within the first stage of degradation, thus; giving a good depiction of the thermal stability of the samples. In coherence with the dynamic temperature test at 10 ^{o}C/min, E80/G20 had the minimal mass loss indicating the robust nature of the interconnected networks among bonds, as shown in Figure 2c. Nevertheless, E60/G40 unexpectedly had a slightly higher mass loss than E40/G60. Although the variation observed between both samples were small under the said condition, it indicates the relatively weak nature of the van der Waals bonds in the former. However, much analytical studies maybe necessary to further expound their chemistries.

3.2.2 Effect of polymerisation temperature on thermal stability

Another fundamental parameter applicable in the engineering of monolithic pores is their temperature of polymerisation. As the thermal decomposition temperature of BPO is ~ 60 ^{o}C, the effect of polymerisation temperature in the current analyses were investigated at 61 ^{o}C, 65 ^{o}C, 75 ^{o}C and 85 ^{o}C. Our group have previously demonstrated that increasing polymerisation temperature results in an increase in temperature build-up during polymerisation, causing a rapid decomposition of the initiator to generate large quantities

of nuclei zones that coalesce to form small pore size monoliths (Danquah *et al.*, 2008; Acquah *et al.*, 2016). TGA, DTG and Isothermal degradation curves from the current analyses reveal the consequential impact of this mechanism on the thermal stability of polymethacrylate monoliths as seen in Figure 3.
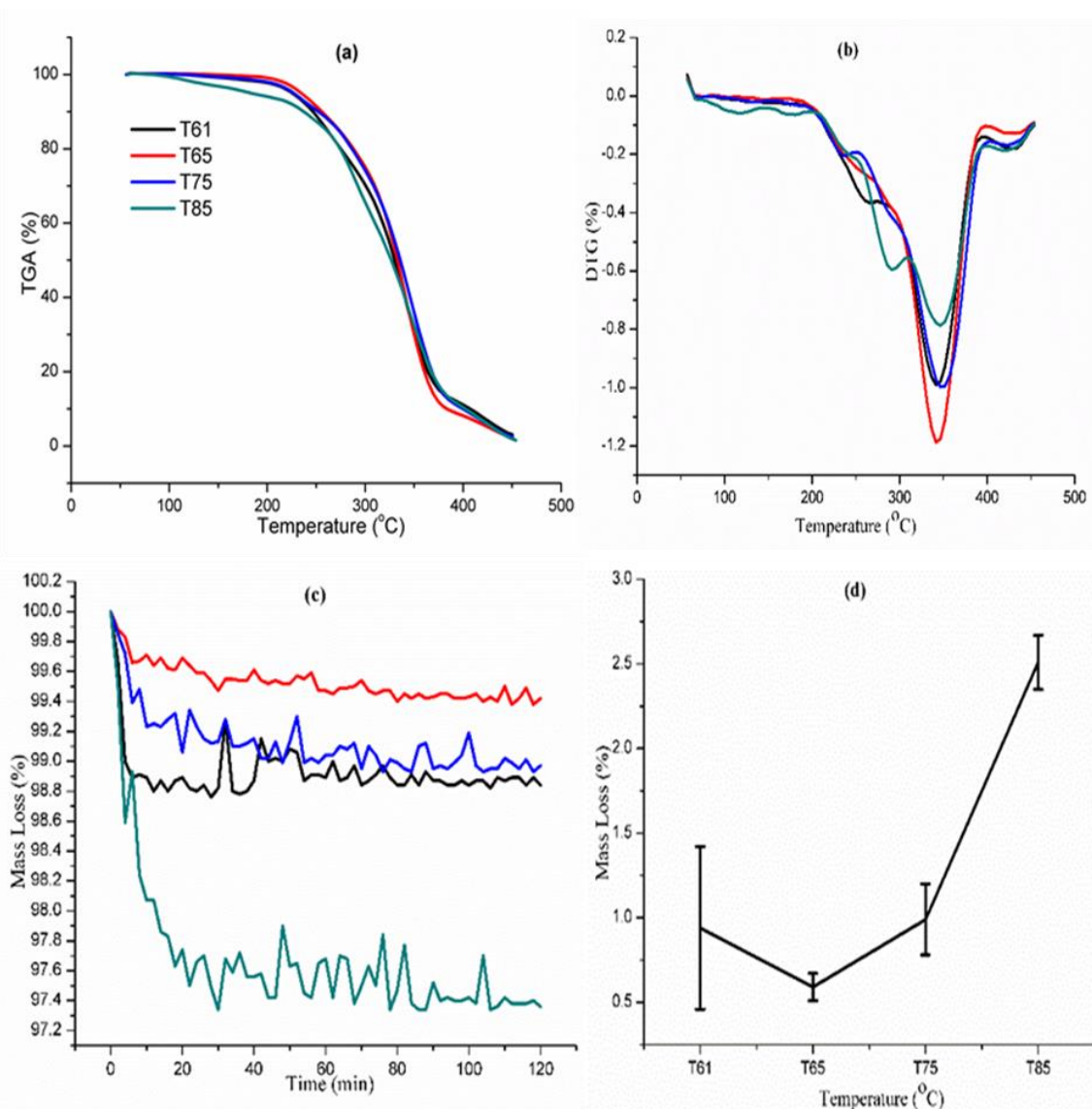
Figure 3 (a) TGA, (b) DTG, (c) average isothermal curves and (d) standard error of isothermal mass loss, under varied monomer ratios in the formation of EDMA-co-GMA polymethacrylate monoliths synthesised at E40/G60 for 4 h. Dynamic heating rate of 10 °C/min and isothermal temperature of 150 °C were applied for samples synthesised at 61°C, 65°C, 75°C and 85°C to investigate the effect of temperature on thermal stability.

It can be observed that the number of degradation stages remained unchanged despite the variation of polymerisation temperature which results in different rate of reaction. In

addition, the pattern of degradation as seen in the TG and DTG curves of Figures 3a and 3b, respectively were similar despite the differences in their corresponding characteristic temperatures. It was observed in the first stage that an increase in the polymerisation temperature resulted in an increase in the rate of mass loss, R_1, although they were generally <6% per min with a low standard error ranging from 0.10-8.81% as indicated in Table 2. This shows the suitable extent of thermal stability of organic polymethacrylate monoliths. Nevertheless, there was also a corresponding increase in the characteristic temperatures necessary for safe operation of monoliths for relatively high temperature processes. Monolithic samples synthesised at 61 ^{o}C were observed to be outliers in the trend due to the incomplete conversion of significant amount of monomers under the selected time duration of 4 h. The unconverted monomers therefore reduced the formation of more interconnected chains serving as the backbone of the polymer. The trend is further supported clearly by the isothermal curve shown in Figure 3c and the corresponding average mass loss in Figure 3d.

Table 2. Effect of polymerisation temperature on the thermal stability of polymethacrylate monoliths.

First Stage				
Temp. Samples	T_{onset} (^{o}C)	T_p	T_{final} (^{o}C)	R_1 (% min^{-1})
T 61 ^{o}C Sample	56.15±0.57	191.94±13.99	201.34±5.96	2.20±0.59
T 65 ^{o}C Sample	56.21±0.61	200.96±2.35	200.96±2.35	0.95±0.10
T 75 ^{o}C Sample	56.15±0.66	202.04±1.67	202.04±1.67	2.16±0.49
T 85 ^{o}C Sample	57.36±0.12	164.61±27.17	206.44±2.26	5.96±8.81
Second Stage (Depolymerisation)				
T 61 ^{o}C Sample	201.34±5.96	283.98±11.80	294.67±1.99	25.37±0.93
T 65 ^{o}C Sample	200.96±2.35	268.38±14.82	281.71±8.01	17.24±2.54
T 75 ^{o}C Sample	202.04±1.67	300.55±1.02	300.55±1.02	23.71±2.28
T 85 ^{o}C Sample	206.44±2.26	296.02±5.78	307.99±0.87	31.07±4.56
Third Stage (Depolymerisation)				
T 61 ^{o}C Sample	294.67±1.99	341.17±0.91	388.34±1.48	56.25±9.92

T 65 ºC Sample	281.71±8.01	341.99±1.48	389.72±3.30	72.61±1.63
T 75 ºC Sample	300.55±1.02	347.70±0.90	394.00±1.05	62.63±2.80
T 85 ºC Sample	307.99±0.87	345.61±1.80	393.50±2.52	47.29±3.87
Isothermal Mass Loss for 120 mins				
T 61 ºC Sample	0.94±0.48			
T 65 ºC Sample	0.59±0.08			
T 75 ºC Sample	0.99±0.21			
T 85 ºC Sample	2.51±0.16			

The outcome correlates with the fact that each selected condition possess an optimum time of polymerisation to convert monomers into the polymer (Greiderer *et al.*, 2009; Acquah *et al.*, 2016). Under relatively low polymerisation temperature conditions, given the same polymerisation time and synthesis conditions, the generation of free radicals and the kinetic velocity of active monomeric and porogenic molecules is slower. This confers a lower entropy associated with molecular arrangements of reduced amounts of nuclei points within the polymerisation system, thus, creating a more porous sub-polymeric structure that interrupts heat transfer gradient within the polymer matrix. In addition, prolonged exposure of monoliths in the mould to high heating conditions could result in gradual oxidation of bonds resulting in hydrolysis of acrylate chains which leads to the high rate of mass loss in the first stage. In the work reported by Geiser *et al.* (2007) on the performance stability and repeatability of poly(butyl methacrylate-co-ethylene dimethacrylate) synthesised by means of photo- and thermal initiation, they reported that polymerisation temperatures at relatively lower set-points are more effective to improve the solvency and viscosity of the porogenic medium of polymerisation. This increased the performance stability of the polymer during application (Geiser *et al.*, 2007), which is also in keeping with our current findings. This implies that lower polymerisation temperatures favour the formation of thermally stable methacrylate polymers.

3.2.3 Effect of Porogen-Monomer (P/M) ratio on thermal stability

Previous experiments have shown that an increase in porogen concentration relative to monomer concentration leads to increases in pore size and porosity of the polymer (Danquah and Forde, 2008) with a decrease in mechanical strength. That notwithstanding, there has been no research reports investigating the effects of porogen to monomer ratio on the thermal stability of polymethacrylate monoliths. From the thermogravimetric curves of Figures 4a – 4c, it was observed that increasing the ratio of porogen to monomer does not only increase the pore size but also increases the thermal stability of the monoliths. P40/M60 had the highest safe characteristic temperature range ending at ~233 ^{o}C for safe operation without losing the chemical signature of the polymer as indicated in Table 3. However, this required compromising on the rate of mass loss which will eventually affect the performance stability of the monolith in operations. For instance, the rate of degradation in the first stage was drastically reduced by >62% per min when the volume concentration of porogen was increased from P40/M60 to P60/M40, and by >50% per min for an increase in porogen from P60/M40 to P80/M20. The relative standard errors to the average mass losses, as illustrated in Figure 4d, were also minimal within close ranges of 0.81-1.24%.
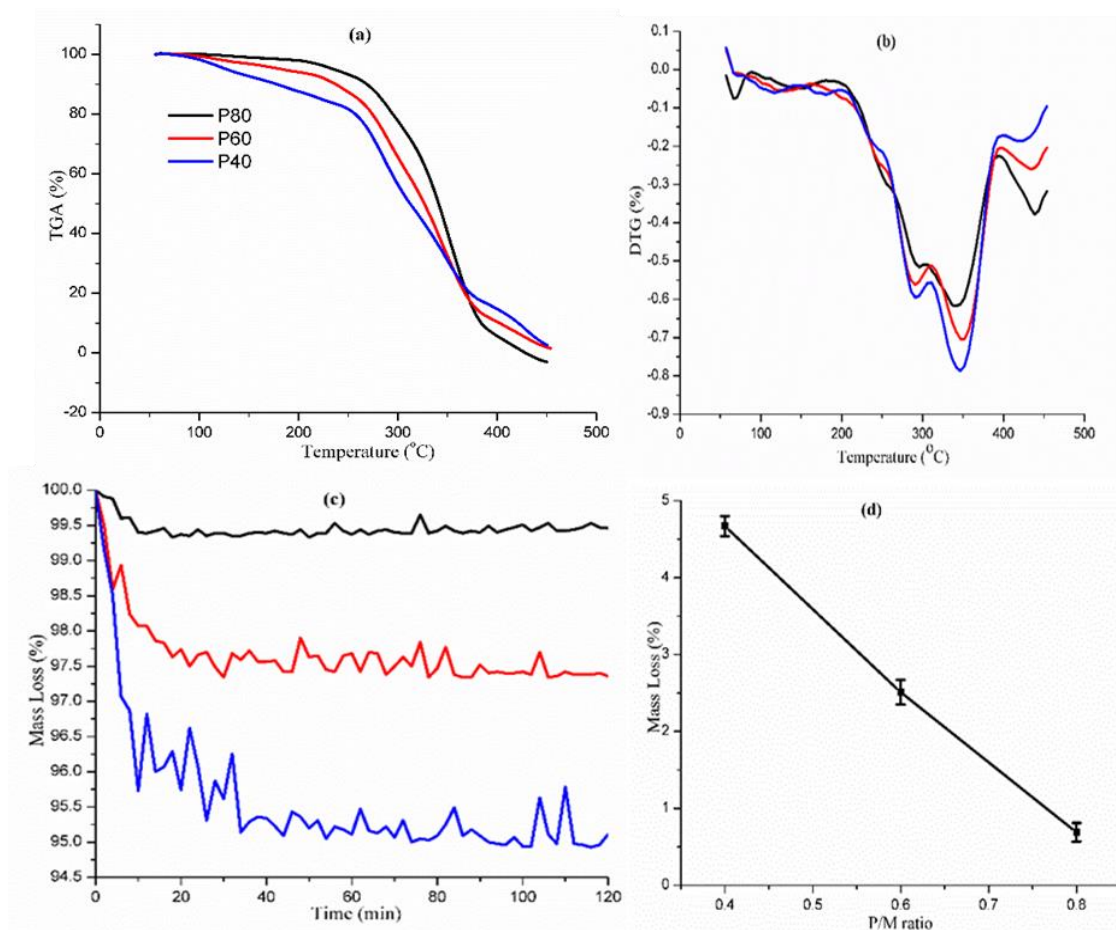
Figure 4. (a) TGA, (b) DTG, (c) Isothermal condition curves and (d) average mass loss for varied monomer ratios in the formation of EDMA-co-GMA polymethacrylate monoliths synthesised at E40/G60 for 4 h. Dynamic heating rate of 10 ^{o}C/min and isothermal temperature of 150 ^{o}C were applied for samples P40/M60, P60/M40 and P80/M20 to investigate the effect of temperature on thermal stability.

Table 3. Effect of porogen to monomer ratio on the thermal stability of polymethacrylate monoliths

First Stage				
Porogen/monomer (%v/v)	T_{onset} (^{o}C)	T_p	T_{final} (^{o}C)	R_1 (% min^{-1})
P40/ M60	56.14±0.54	226.00±7.16	233.98±3.91	16.04±0.95
P60/ M40	57.36±0.12	164.61±27.17	206.44±2.26	5.96±0.81
P80/ M20	56.48±0.65	216.08±12.92	216.08±12.92	2.93±1.24
Second Stage (Depolymerisation)				
P40/ M60	233.98±3.91	286.15±1.14	315.51±0.71	34.68±0.37

P60/ M40	206.44±2.26	296.02±5.78	307.99±0.87	26.81±2.30
P80/ M20	216.08±12.92	295.72±2.5	298.95±3.49	17.79±3.06
Third Stage (Depolymerisation)				
P40/ M60	315.51±0.71	349.49±1.15	387.52±0.60	31.29±0.74
P60/ M40	307.99±0.87	345.61±1.80	393.50±2.52	47.29±3.87
P80/ M20	17.79±3.06	354.20±0.28	399.22±2.76	68.09±2.09
Isothermal Mass Loss for 120 mins				
P40/ M60	4.67±0.13			
P60/ M40	2.51±0.16			
P80/ M20	0.69±0.13			

According to Svec and Fréchet (1995), the void fraction within the formed polymer is a function of the volume fraction of porogens. High porogen concentrations relative to monomer reduce nuclei formation points within the polymerisation system thus creating a more porous polymeric structure that resists heat transfer within the polymer as shown in Figure 5. For a given composition of monomer ratio, an increase in porogen concentration results in increasing solvation within the swollen nuclei. The isothermal curves further affirm the impact of the ratio of porogen to monomer on the thermal stability of polymethacrylate monoliths.
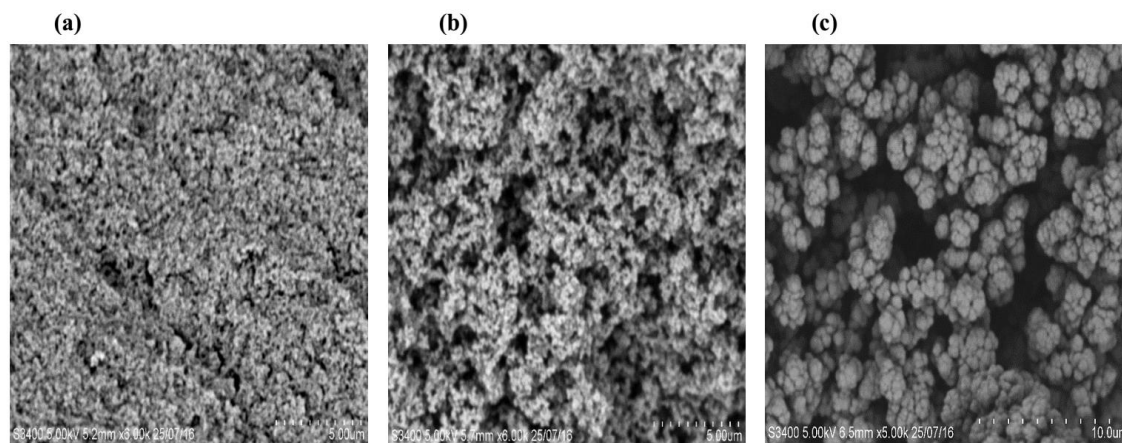
Figure 5. SEM images showing the morphological effect of increasing pore size with varying porogen to monomer ratio: (A) P40/M60 v/v%; (B) P60/M40 v/v%; and (C) P80/M20 v/v%

3.2.4 Effect of Cyclohexanol-Dodecanol (C/D) ratio on thermal stability

Different classes of porogens including microporogens, macroporogens, supercritical carbon dioxide, solid porogens and polymer porogens exist for the synthesis of polymethacrylate monoliths (Svec, 2010). Cyclohexanol and/or dodecanol are one of the most commonly used inert diluent solvents for the synthesis of polymethacrylate monoliths (Buchmeiser, 2007). Due to their relative characteristic effects on the pore and surface structures of the polymer, cyclohexanol and dodecanol are often used in combination to explore synergistic impacts on pore formation (Gunasena and El Rassi, 2013; Carrasco-Correa *et al.*, 2015; Aydoğan and El Rassi, 2016). Dodecanol, which is a poor porogenic solvent, has been shown to increase the pore size of the polymer when paired with cyclohexanol at relatively high temperatures of polymerisation (Danquah and Forde, 2008). The effect of cyclohexanol to dodecanol ratio on the thermal stability of polymethacrylate monolith was therefore investigated in this work.

From the thermogravimetric results in Figure 6a - 6c there was minimal correlation between the thermal stability of the samples with respect to the proportion of the biporogen mixtures. From Table 4, the rate of mass loss R_1 was higher for C60/D40 contrary to our expectations of a decrease in mass loss as the amount of dodecanol is increased due to the resultant increase in pore size interrupting with the resultant heat transfer gradient when the proportion of dodecanol is increased. To annihilate the possibility of the occurrence of any systematic error leading to the results in C60/D40 mass loss, TGA and isothermal tests were conducted multiple times with multiple synthesised samples of C60/D40. However, the results were still within the same region. By inference, the thermal stability data suggests that the use of excessive amount of microporogens may not be suitable for the solvency of monomers under thermally initiated free radical polymerisation, as observed in our case.
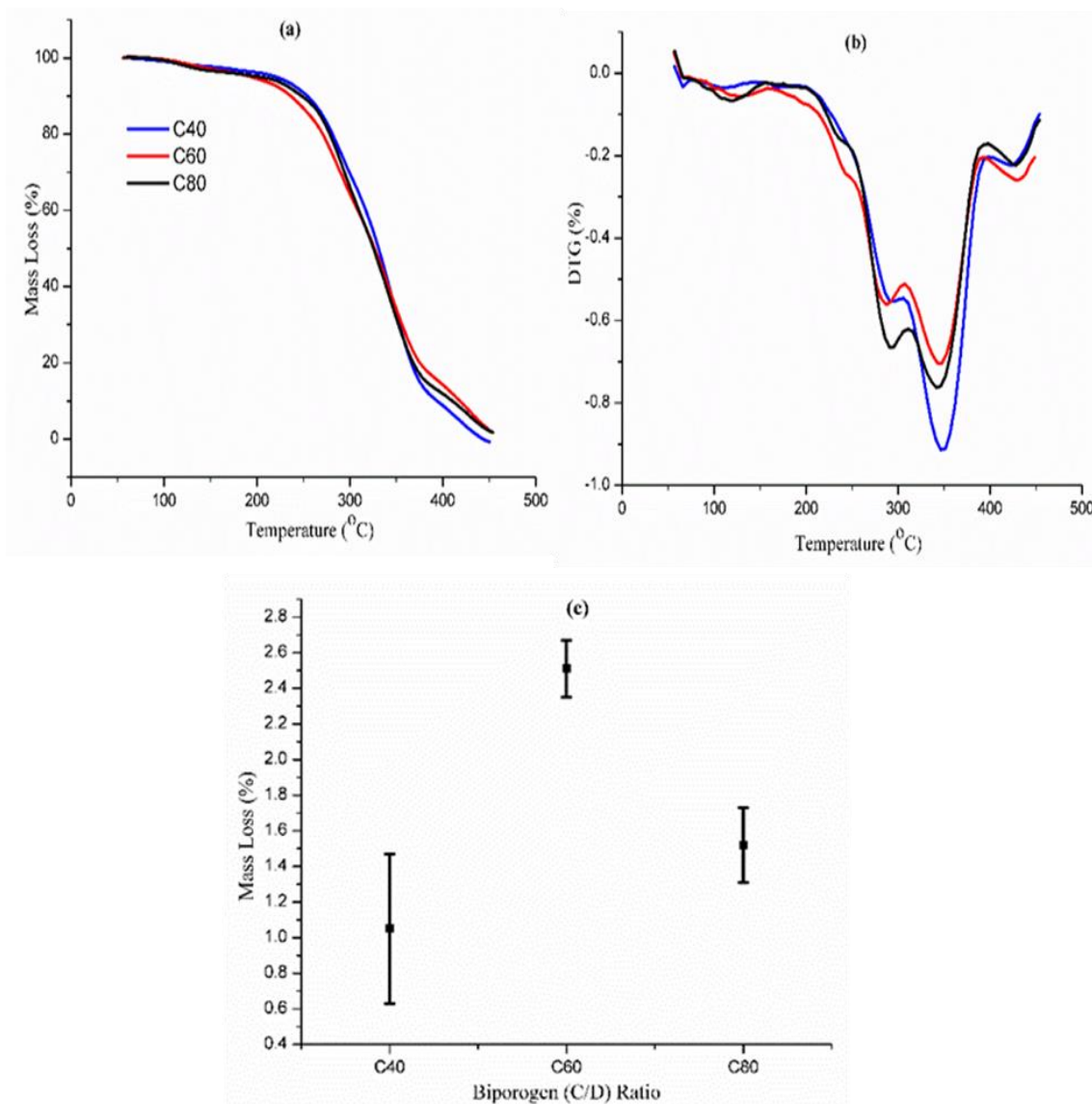
Figure 6. (a) TGA, (b) DTG, (c) average mass loss for varied biporogen mixture of cyclohexanol to dodecanol concentration ratios of C40 / D60; C60 / D40; and C80 / D20 ratios in the formation of polymethacrylate monoliths synthesised for 4 h. Dynamic heating rate of 10 °C/min and isothermal temperature of 150 °C were applied to investigate the effect of temperature on thermal stability.

Table 4. Effect of varied ratios of microporogen to macroporogen on thermal stability of methacrylate monoliths.

First Stage				
Cyclo/Dodecanol (%v/v)	T_{onset} (°C)	T_p	T_{final} (°C)	R_1 (% min^{-1})
C40/ D60	57.03±0.25	125.28±42.49	204.12±1.78	3.7±2.76
C60/ D40	57.36±0.12	164.61±27.17	206.44±2.26	5.96±0.81
C80/ D20	57.22±0.06	120.76±0.79	205.76±0.62	5.13±0.36
Second Stage (Depolymerisation)				
C40/ D60	204.12±1.78	296.46±4.13	304.74±3.89	26.18±5.69
C60/ D40	206.44±2.26	296.02±5.78	307.99±0.87	26.81±2.30
C80/ D20	205.76±0.62	294.61±4.42	310.15±3.72	35.58±5.63
Third Stage (Depolymerisation)				
C40/ D60	304.74±3.89	348.69±2.32	394.54±1.07	53.82±8.55
C60/ D40	307.99±0.87	345.61±1.80	393.50±2.52	47.29±3.87
C80/ D20	310.15±3.72	344.11±2.49	391.79±2.14	47.30±5.58
Isothermal Mass Loss for 120 mins				
C40/ D60	1.05±0.42			
C60/ D40	2.51±0.16			
C80/ D20	1.52±0.21			

3.2.5   Effect of initiator concentration on thermal stability

The impact of initiator concentration has previously been shown to minimise the pore size of polymethacrylate monoliths, as confirmed in the SEM images of Figure 7, and increased the degree of thermal build-up during monolith synthesis (Danquah and Forde, 2008; Acquah *et al.*, 2016).
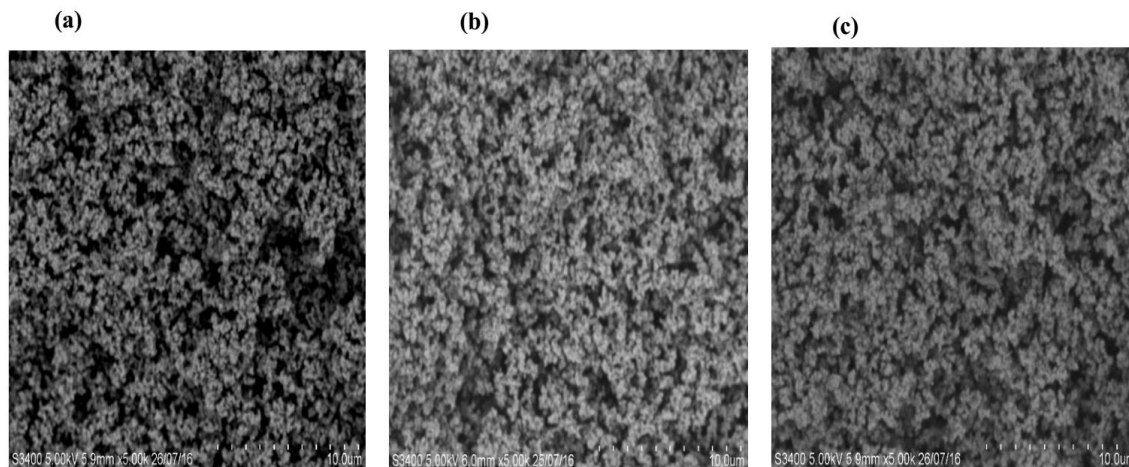
Figure 7. SEM images showing the morphological effect of decreasing pore size with varying concentration of initiator (BPO): (A) BPO 0.5 w/v%; (B) 1 w/v%; and (C) 1.5 w/v%

From the thermogravimetric results shown in Figures 8a-8c, concentration of free radicals generated by the decomposition of varied BPO amount had minimal effect on the thermal stability of the monoliths. This could be since only a fixed quantity of free radical is required per unit monomeric composition for complete polymerisation initiation. That notwithstanding, samples synthesised with 1% w/v of initiator consistently had a lesser stability but with an improved characteristic end temperature as evident in Table 5. Notably, initiator concentrations of 0.5-1% w/v of total monomer remains the most utilised proportion to date.
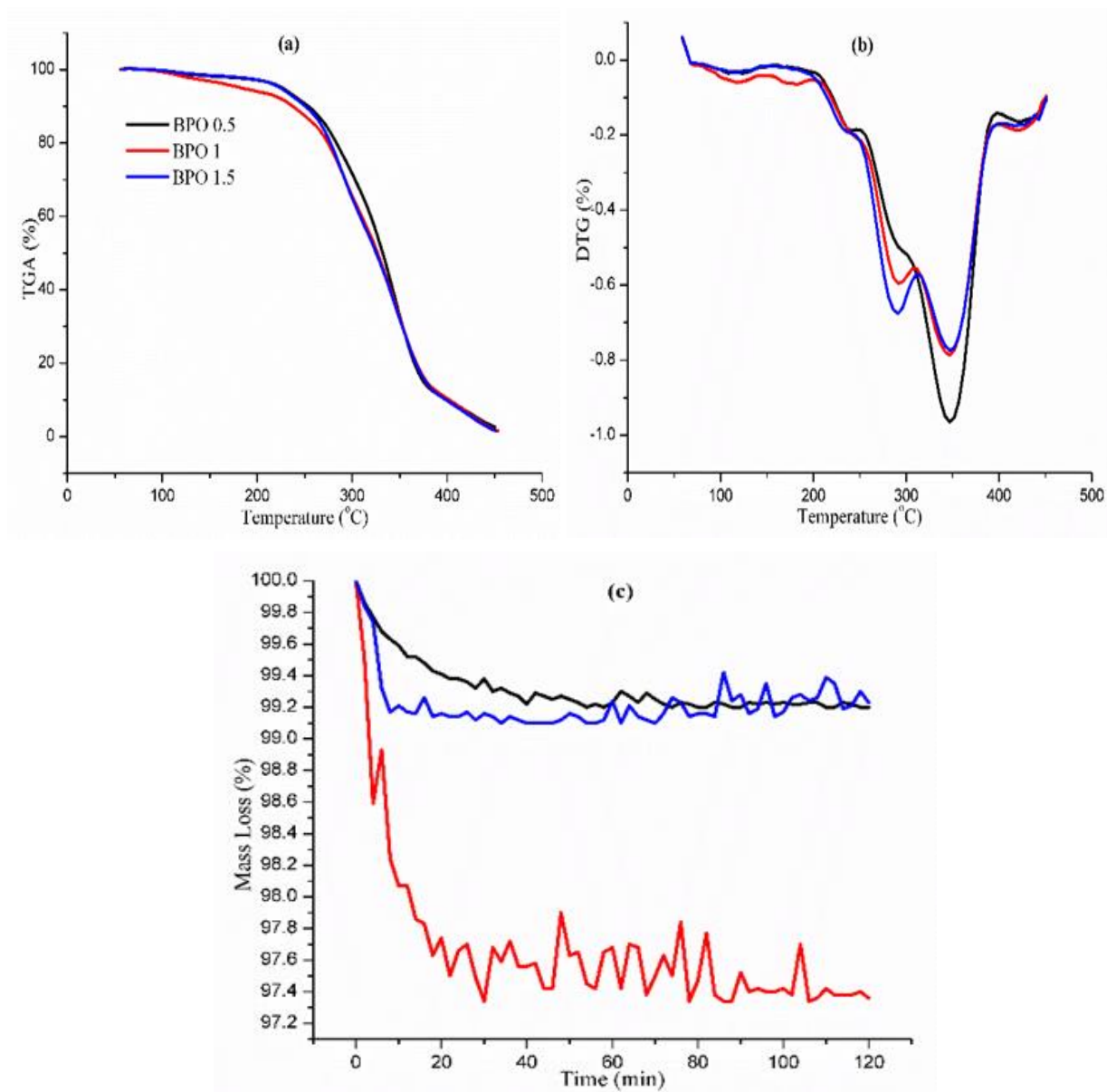
Figure 8. (A) TGA, (B) DTG, (C) average mass loss for varied initiator concentration ratios of 0.5%; 1%; and 1.5% w/v in the formation of polymethacrylate monoliths synthesised for 4 h. Dynamic heating rate of 10 °C/min and isothermal temperature of 150 °C were applied to investigate the effect of temperature on thermal stability.

Table 5. Effect of initiator concentrations on the thermal stability of polymethacrylate monoliths

First Stage				
Initiator (%w/v)	T_{onset} (^{o}C)	T_p	T_{final} (^{o}C)	R_1 (% min^{-1})
0.5	55.98±0.60	165.88±27.22	197.03±7.25	2.87±2.05
1	57.36±0.12	164.61±27.17	206.44±2.26	5.96±0.81
1.5	58.75±2.42	165.27±26.52	193.39±1.96	2.51±1.90
Second Stage (Depolymerisation)				
0.5	197.03±7.25	294.02±3.13	294.02±3.13	22.05±0.19
1	206.44±2.26	296.02±5.78	307.99±0.87	26.81±2.30
1.5	193.39±1.96	290.33±0.97	310.72±1.76	38.02±2.22
Third Stage (Depolymerisation)				
0.5	294.02±3.13	345.12±1.81	397.06±2.91	62.82±2.34
1	307.99±0.87	345.61±1.80	393.50±2.52	47.29±3.87
1.5	310.72±1.76	348.54±0.59	397.56±1.39	47.48±3.78
Isothermal Mass Loss for 120 mins				
0.5	0.76±0.42			
1	2.51±0.16			
1.5	0.90±0.41			

3.2.6 Effect of methanol washing and activation on thermal stability

Polymethacrylate monoliths possess a two-phase system within the mould after polymerisation; (i) the solid-phase polymer and (ii) liquid phase containing the inert porogen, unreacted monomeric reagents and droplets of condensed water. As a result, polymethacrylate monoliths require washing with a suitable chaotropic reagent, mostly methanol, without causing chemical and physical damage to the polymer. Figure 9 reveals the presence of unwanted materials (dry porogenic crust) within the cross-section of polymeric monoliths as compared to washed monoliths.
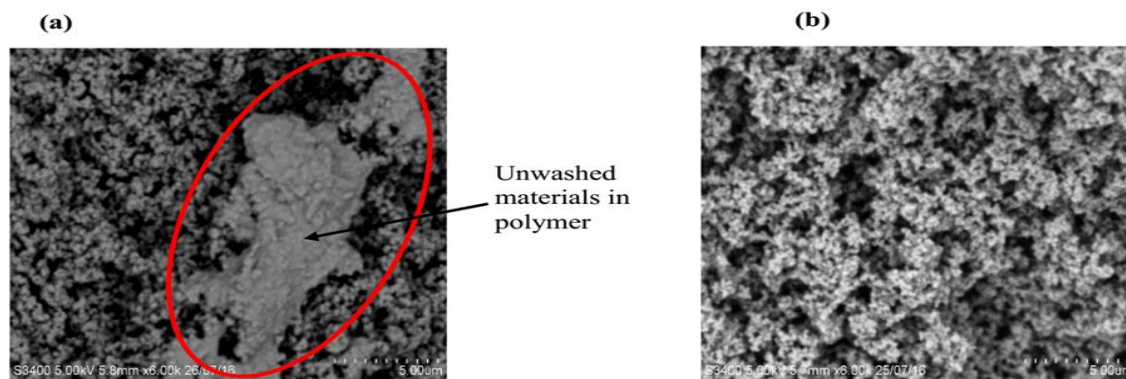
Figure 9. SEM images showing the presence and absence of a dry porogenic crust in (A) an unwashed and (B) washed EDMA-co-GMA monolith with composition C60%, D40%, E60%, G40% v/v and BPO 1% w/v.

To ensure immobilisation of functional ligands onto polymethacrylate monoliths, epoxy moieties are often activated in several ways including the facile epoxy method which involves acid activation with HCl. This results in the hydrolysis of the epoxy moiety for ligand immobilisation. Nuclear magnetic resonance (NMR) results in Figure 10 further confirms the reduction in intensity of epoxy moiety from 3.342 to 2.380 ppm, thus, signifying the hydrolysis of epoxy functional groups in the backbone of the monolith.
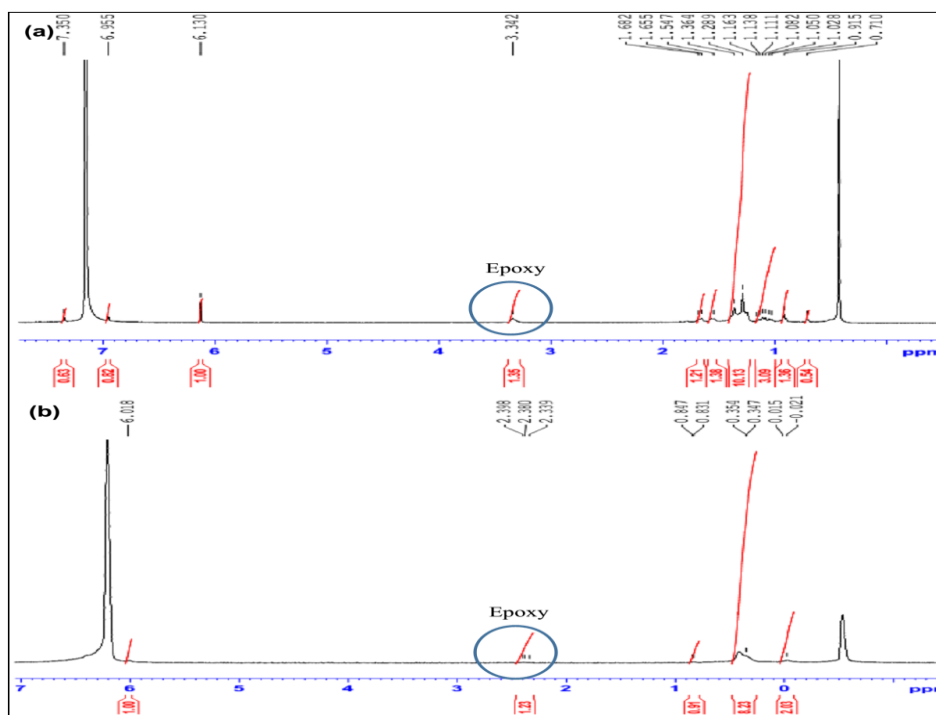
Figure 10. ^{1}H and ^{13}C NMR spectra of polymethacrylate monoliths with emphasis on the hydrolysis of epoxy functional groups from (A) inactivated or washed monoliths (3.342 ppm) to (B) activated monoliths (2.380 ppm).

185

Figures 11a and 11b show that unwashed polymethacrylate monoliths are thermally unstable and reactive and this leads to degradation in the presence of heat. Unwashed monoliths were observed to have a constant decline in mass loss from the onset of decomposition, T_{onset}, 57.18 ^{o}C to ~ 195 ^{o}C with ~45.67% mass loss and two degradation peaks; in reference to the corresponding DTG curve. This renders it unreliable for any applications. The rapid mass loss is due to the presence of residual organic methacrylate reagents, alcoholic groups – cyclohexanol and dodecanol, and condensed water droplets volatilising and decomposing. The temperature ranges from 195 – 252 ^{o}C resulting in ~ 4.96% mass loss could be attributed to the decomposition of lighter molecular weight residues held together by van der Waals forces in the aliphatic chains. Depolymerisation of the unwashed samples occurred between ~252 ^{o}C – 390 ^{o}C, accounting for ~34.15% mass loss, since the bulk of the polymer had already been lost in relatively lower temperature conditions in the earlier stages of the monolith.
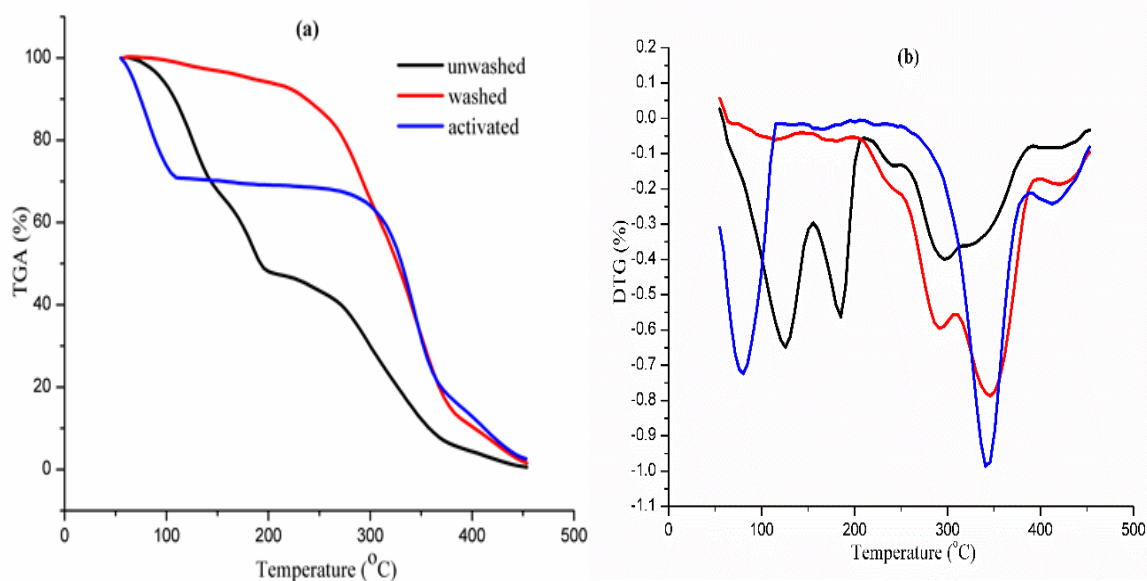
Figure 11. (A) TGA, (B) DTG of unwashed, washed and activated monoliths synthesised for 4 h. Dynamic heating rate of 10 ^{o}C/min and isothermal temperature of 150 ^{o}C were applied to investigate the effect of temperature on thermal stability.

Relative to the unwashed sample, methanol-washed portion of the same polymer sample resulted in thermally stable results from the onset temperature, T_{onset}, 57.42 ^{o}C to ~206 ^{o}C resulting in ~5.5% in mass loss despite the wider temperature range. Signifying the improvement in the characteristic features of the washed monolith for safe operation over an unwashed monolith. Consequently, depolymerisation of the washed monolithic sample

occurred between 206 ºC – 393 ºC, accounting for a bulk mass loss of 78.02%. Activation with HCl also caused an obvious change in the pattern of degradation. For HCl activated polymer, there was a sharp decrease in mass loss (~24.77%) from 55.15 ºC - 108 ºC. The temperature range with reference to the TG and DTG curves clearly shows that the mass loss was mainly due to dehydration of the hydrolysed epoxy groups successfully done with HCl. After this temperature range, analogous to the washed sample, the sample became thermally stable with a mass loss of only 2.24% until the depolymerisation stage (~250 ºC – 385 ºC) where the mass loss was 44.88%. The R_1 values indicating the thermal stability with respect to rate of mass loss per min were 50.63%; 27.02% and 5.52% for unwashed, activated and washed samples, respectively.

4.   CONCLUSION

Polymethacrylate monoliths have become essential stationary adsorbents for diverse chromatographic applications. Research into this adsorbent material and potential applications thereof has gained much popularity over the past two decades. However, an area that has received limited research attention has been the relationship between polymer synthesis conditions and thermal stability. This work investigated the thermo-molecular mechanisms associated with polymer synthesis and its relationship with thermal stability. The thermal stability of polymethacrylate monoliths was investigated by varying *in situ* and *ex situ* synthesis conditions. Porogen to monomer ratio and polymerisation temperature demonstrated to be the most influential parameters affecting the thermal stability of the monolith. In addition, an increase in cross-linker monomer resulted in the enhancement of thermal stability within the first degradation stage in reference to their TG and DTG curves. Minimal differences were observed for the variation of initiator (BPO) concentration. Nevertheless, monoliths prepared with 1% w/v of BPO demonstrated a lower thermal stability compared to those synthesised with 0.5 % w/v BPO and 1.5 % w/v BPO. In addition, TGA curves can be utilised as a destructive technique for low resourced labs in assessing the extent of polymer washing and preliminary post modification processes.

5.   ACKNOWLEDGEMENT

6.   REFERENCES

Acquah, C., M.K. Danquah, C.K.S. Moy and C.M. Ongkudon, 2016. In-process thermochemical analysis of in situ poly(ethylene glycol methacrylate-co-glycidyl methacrylate) monolithic adsorbent synthesis. Journal of Applied Polymer Science, 133: 1-9. Available from http://dx.doi.org/10.1002/app.43507. DOI 10.1002/app.43507.

Acquah, C., C.K.S. Moy, M.K. Danquah and C.M. Ongkudon, 2016. Development and characteristics of polymer monoliths for advanced lc bioscreening applications: A review. Journal of Chromatography B, 1015–1016: 121-134. Available from http://www.sciencedirect.com/science/article/pii/S1570023216300976. DOI http://dx.doi.org/10.1016/j.jchromb.2016.02.016.

Allaoui, A. and N. El Bounia, 2009. How carbon nanotubes affect the cure kinetics and glass transition temperature of their epoxy composites?–a review. EXPRESS Polymer Letters, 3: 588-594. DOI 10.3144/expresspolymlett.2009.73.

Aydoğan, C. and Z. El Rassi, 2016. Monolithic stationary phases with incorporated fumed silica nanoparticles. Part ii. Polymethacrylate-based monolithic column with "covalently" incorporated modified octadecyl fumed silica nanoparticles for reversed-phase chromatography. Journal of Chromatography A, 1445: 62-67. Available from http://www.sciencedirect.com/science/article/pii/S0021967316303995. DOI http://dx.doi.org/10.1016/j.chroma.2016.03.083.

Buchmeiser, M.R., 2007. Polymeric monolithic materials: Syntheses, properties, functionalization and applications. Polymer, 48(8): 2187-2198.

Carioscia, J.A., J.W. Stansbury and C.N. Bowman, 2007. Evaluation and control of thiol–ene/thiol–epoxy hybrid networks. Polymer, 48(6): 1526-1532.

Carrasco-Correa, E.J., G. Ramis-Ramos and J.M. Herrero-Martínez, 2015. Hybrid methacrylate monolithic columns containing magnetic nanoparticles for capillary electrochromatography. Journal of Chromatography A, 1385: 77-84.

Chen, L., J. Ou, Z. Liu, H. Lin, H. Wang, J. Dong and H. Zou, 2015. Fast preparation of a highly efficient organic monolith via photo-initiated thiol-ene click polymerization for capillary liquid chromatography. Journal of Chromatography A, 1394: 103-110. DOI 10.1016/j.chroma.2015.03.054.

Cooper, A.I., 2000. Polymer synthesis and processing using supercritical carbon dioxide. Journal of Materials Chemistry, 10(2): 207-234.

Danquah, M.K. and G.M. Forde, 2007. The suitability of deae-cl active groups on customized poly(gma-co-edma) continuous stationary phase for fast enzyme-free isolation of plasmid DNA. Journal of chromatography. B, Analytical technologies

in the biomedical and life sciences, 853(1-2): 38-46. Available from http://www.ncbi.nlm.nih.gov/pubmed/17400523. DOI 10.1016/j.jchromb.2007.02.050.

Danquah, M.K. and G.M. Forde, 2008. Preparation of macroporous methacrylate monolithic material with convective flow properties for bioseparation: Investigating the kinetics of pore formation and hydrodynamic performance. Chemical Engineering Journal, 140(1-3): 593-599. DOI 10.1016/j.cej.2008.02.012.

Danquah, M.K., J. Ho and G.M. Forde, 2008. A thermal expulsion approach to homogeneous large-volume methacrylate monolith preparation; enabling large-scale rapid purification of biomolecules. Journal of Applied Polymer Science, 109(4): 2426-2433. DOI 10.1002/app.28346.

Geiser, L., S. Eeltink, F. Svec and J.M. Fréchet, 2007. Stability and repeatability of capillary columns based on porous monoliths of poly (butyl methacrylate-co-ethylene dimethacrylate). Journal of Chromatography A, 1140(1): 140-146.

Greiderer, A., L. Trojer, C.W. Huck and G.K. Bonn, 2009. Influence of the polymerisation time on the porous and chromatographic properties of monolithic poly (1, 2-bis (p-vinylphenyl)) ethane capillary columns. Journal of Chromatography A, 1216(45): 7747-7754.

Gunasena, D.N. and Z. El Rassi, 2013. Neutral, charged and stratified polar monoliths for hydrophilic interaction capillary electrochromatography. Journal of Chromatography A, 1317: 77-84.

Hayes, R., A. Ahmed, T. Edge and H. Zhang, 2014. Core–shell particles: Preparation, fundamentals and applications in high performance liquid chromatography. Journal of Chromatography A, 1357: 36-52. Available from http://www.sciencedirect.com/science/article/pii/S0021967314007304. DOI http://dx.doi.org/10.1016/j.chroma.2014.05.010.

Iacono, M., D. Connolly and A. Heise, 2016. Fabrication of a gma-co-edma monolith in a 2.0 mm id polypropylene housing. Materials, 9(4): 263.

Jandera, P., M. Staňková, V. Škeříková and J. Urban, 2012. Cross-linker effects on the separation efficiency on (poly)methacrylate capillary monolithic columns. Part i. Reversed-phase liquid chromatography. Journal of Chromatography A. DOI 10.1016/j.chroma.2012.12.003.

Lin, H., L. Chen, J. Ou, Z. Liu, H. Wang, J. Dong and H. Zou, 2015. Preparation of well-controlled three-dimensional skeletal hybrid monoliths via thiol–epoxy click polymerization for highly efficient separation of small molecules in capillary liquid chromatography. Journal of Chromatography A, 1416: 74-82.

Liu, C.-C., Q.-L. Deng, G.-Z. Fang, H.-L. Liu, J.-H. Wu, M.-F. Pan and S. Wang, 2013. Ionic liquids monolithic columns for protein separation in capillary electrochromatography. Analytica chimica acta, 804: 313-320.

Liu, Z., J. Ou and H. Zou, 2016. Click polymerization for preparation of monolithic columns for liquid chromatography. TrAC Trends in Analytical Chemistry, 82: 89-99.

Mihelič, I., M. Krajnc, T. Koloini and A. Podgornik, 2001. Kinetic model of a methacrylate-based monolith polymerization. Industrial & engineering chemistry research, 40(16): 3495-3501.

Ongkudon, C.M., T. Kansil and C. Wong, 2014. Challenges and strategies in the preparation of large-volume polymer-based monolithic chromatography adsorbents. Journal of separation science, 37(5): 455-464.

Park, S.-B., J. Sakamoto, M.-H. Sung and H. Uyama, 2014. Ph-controlled degradation and thermal stability of a porous poly (γ-glutamic acid) monolith crosslinked with an oxazoline-functionalized polymer. Polymer Degradation and Stability, 99: 99-104.

Podgornik, A., V. Smrekar, P. Krajnc and A. Strancar, 2013. Estimation of methacrylate monolith binding capacity from pressure drop data. Journal of chromatography. A, 1272: 50-55. Available from http://www.ncbi.nlm.nih.gov/pubmed/23261298. DOI 10.1016/j.chroma.2012.11.057.

Roberts, M.W., C.M. Ongkudon, G.M. Forde and M.K. Danquah, 2009. Versatility of polymethacrylate monoliths for chromatographic purification of biomolecules. Journal of separation science, 32(15-16): 2485-2494. Available from http://www.ncbi.nlm.nih.gov/pubmed/19603394. DOI 10.1002/jssc.200900309.

Svec, F., 2010. Porous polymer monoliths: Amazingly wide variety of techniques enabling their preparation. Journal of Chromatography A, 1217(6): 902-924.

Svec, F. and J.M.J. Fréchet, 1995. Kinetic control of pore formation in macroporous polymers. Formation of "molded" porous materials with high flow characteristics for separations or catalysis. Chemistry of Materials, 7(4): 707-715.

Sýkora, D., E.C. Peters, F. Svec and J.M.J. Fréchet, 2000. "Molded" porous polymer monoliths: A novel format for capillary gas chromatography stationary phases. Macromolecular Materials and Engineering, 275(1): 42-47. Available from http://dx.doi.org/10.1002/(SICI)1439-2054(20000201)275:1<42::AID-MAME42>3.0.CO;2-X. DOI 10.1002/(SICI)1439-2054(20000201)275:1<42::AID-MAME42>3.0.CO;2-X.

Vlad, C.D., M.V. Dinu and S. Dragan, 2003. Thermogravimetric analysis of some crosslinked acrylamide copolymers and ion exchangers. Polymer degradation and stability, 79(1): 153-159.

Wang, Y., Q.-L. Deng, G.-Z. Fang, M.-F. Pan, Y. Yu and S. Wang, 2012. A novel ionic liquid monolithic column and its separation properties in capillary electrochromatography. Analytica chimica acta, 712: 1-8.

Yusuf, K., A.Y. Badjah-Hadj-Ahmed, A. Aqel and Z.A. Alothman, 2016. Monolithic metal–organic framework mil-53(al)-polymethacrylate composite column for the reversed-phase capillary liquid chromatography separation of small aromatics. Journal of separation science, 39(5): 880-888. DOI 10.1002/jssc.201501289.

SECTION 4.2

Thermogravimetric characterization of ex situ polymethacrylate (EDMA-co-GMA) monoliths

Caleb Acquah, Michael K. Danquah, Charles K.S. Moy, Mahmood Anwar, Clarence M. Ongkudon

DECLARATION FOR THESIS SECTION 4.2

Thermogravimetric characterization of ex situ polymethacrylate (EDMA-co-GMA) monoliths

The candidate will like to declare that there is no conflict of interests involved in this work and that my extent of contribution as candidate is as shown below:

Contribution of Candidate	Conceptualisation, initiation and write-up	80%

The following co-authors were involved in the development of this publication and attest to the candidate's contribution to a joint publication as part of his thesis. Permission by co-authors are as follows:

Name	Signature	Date
Michael K. Danquah		13.07.2017
Charles K.S. Moy		13.07.2017
Clarence M. Ongkudon		13.07.2017
Mahmood Anwar		18.07.2017

ABSTRACT

The thermo-molecular mechanisms associated with free radical synthesis of polymethacrylate monoliths offers an effective pathway to tune their pore characteristics. In this work, thermogravimetric analyses were used for *ex situ* characterisation of polymethacrylate monoliths synthesised from ethylene glycol dimethacrylate (EDMA) and glycidyl methacrylate (GMA). Apparent activation energies of the polymeric monoliths were determined by using Ozawa-Flynn-Wall (OFW) and Kissinger–Akahira–Sunose (KAS) iso-conversional method. The number of degradation stages for the polymers were observed to be as follows: homopolymeric GMA and EDMA (2 degradation stages each) and polymeric EDMA-co-GMA monoliths (3 degradation stages). The relationship between apparent activation energy and extent of conversion showed that the degradation of monoliths is based on a complex multistep reaction rather than a single reaction model. Kinetic parameters showed that an increase in the composition of EDMA and GMA above 20% significantly enhances the thermal stability of polymeric EDMA-co-GMA monoliths under elevated non-isothermal conditions. E40/G60 and E60/G40 monoliths were identified as the most thermally stable monoliths from the kinetic analyses.

Keywords: Monoliths; Polymethacrylate; Apparent Activation Energy; Thermogravimetric Analyses; Isoconvensional Methods.

1.   INTRODUCTION

Monoliths are continuous unit of porous adsorbents with the propensity to provide convective mass transport for fluids. Active research into the synthesis of monoliths commenced over two decades ago with organic gel-like monoliths (Hjertén *et al.*, 1989; Hjertén *et al.*, 1993); blocks of methacrylate monoliths (Svec and Fréchet, 1995; Svec and Fréchet, 1995) and silica-based monoliths (Minakuchi *et al.*, 1996). In contrast to particulate beds; the pores, surface areas, interstitial voids and pore size distribution of monoliths can be tailored to improve upon their efficiency depending on the target size (Roberts *et al.*, 2009; Acquah *et al.*, 2016).

Different varieties of monoliths exist in the form of polystyrenes, polymethacrylates, cryogels, silica monolith and hybrid silica monoliths mainly depending on their monomeric units. However, polymethacrylate monoliths are the most utilised owing to their ease of synthesis, wide pH range, presence of epoxy ends, mechanical and chemical stability (Ongkudon and Danquah, 2010; Podgornik *et al.*, 2013). Numerous innovative research into the advancement of monoliths through their formation processes (Danquah *et al.*, 2008; Jandera *et al.*, 2013; Alshitari *et al.*, 2015), up-scaling (Podgornik *et al.*, 2000; Urthaler *et al.*, 2005; Danquah and Forde, 2008), non-invasive characterisation techniques (Lendero *et al.*, 2005; Podgornik *et al.*, 2005), *in situ* analysis (Mihelič *et al.*, 2001; Acquah *et al.*, 2016), and tackling of wall-channelling (Greiderer *et al.*, 2009; Ongkudon *et al.*, 2013) have sprang up into the scene. These have maximised the usefulness of monoliths for bioscreening applications such as chromatographic separations, biosensors, catalytic bioreactors, purification and concentration processes (Acquah *et al.*, 2016). These processes are often carried out at room temperatures but could also be designed for specific applications requiring process conditions above room temperature. For instance; Peters *et al.* (1997) demonstrated the application of thermally reversible gates grafted into a poly GMA-co-EDMA monolithic polymer using poly(N-isopropylacrylamide). At temperatures of 40 °C the GMA-co-EDMA modified polymer allowed the free flow of fluids whereas a high back pressure ensued at 25 °C to restrain the flow for protein separations. Similar thermally reversible gate monolithic devices have also been demonstrated for microfluidic chips (Luo *et al.*, 2003; Yu *et al.*, 2003) and molecularly

imprinted polymers (Wen *et al.*, 2016). In addition, monolithic columns have been successfully used for isothermal separations at high temperatures (Sýkora *et al.*, 2000; Korolev *et al.*, 2006).

The synthesis of polymethacrylate monoliths often requires the reaction between a functional monomer such as Glycidyl methacrylate (GMA), crosslinking monomer such as Ethylene glycol dimethacrylate (EDMA) and an initiator, all in a suitable porogenic solvent such as dodecanol and cyclohexanol. The polymerisation reaction is mostly initiated thermally by means of a free radical process leading to the formation of a cross-linked polymer with pores. Thorough analysis into the physicochemical effect of process parameters such as monomer concentration and ratio; porogen concentration and ratio; temperature; initiator amount; polymerisation time and diverse types of monomers with different repeating non-polar ends on the pore size and porosity have previously been documented (Svec and Fréchet, 1995; Danquah and Forde, 2008; Jandera *et al.*, 2013). An increase in cross-linker concentration is well known to result in the formation of large surface areas as well as an enhancement in the interconnectivities.

The quintessence of monitoring the kinetics of thermally initiated processes is to establish a mathematical relationship between the process rate, extent of conversion and the temperature (Vyazovkin *et al.*, 2011). Kinetic and thermal analysis of polymers can be investigated via any of the following thermal analysis techniques: dynamic mechanical analysis, infrared spectroscopy, differential scanning calorimetry (DSC), dilatometry and thermogravimetric analysis (TGA) (Vyazovkin, 2015; Carrasco-Hernandez *et al.*, 2016). The most utilised amongst the aforementioned techniques are the DSC and TGA (Vyazovkin, 2015). Major challenges in the synthesis and application of monoliths pertains to the control of internal temperature build-up, prevention of cracks, thermal and mechanical stability, especially for large scale (Danquah *et al.*, 2008; Deng *et al.*, 2012; Ongkudon *et al.*, 2014). In order to understand these impacts, Mihelič *et al.* (2001) previously probed into the impact of monomers (24% GMA and 16% EDMA), porogens (12% dodecanol and 48% cyclohexanol) and benzoyl peroxide as an initiator on the kinetics of polymerising monoliths. Their analysis was done based on the use of a DSC equipment with five (5) dynamic scans and an Ozawa-Flynn-Wall (OFW) model. The

OFW model is generally known to be of essence for multiple reaction mechanisms without knowledge of their reaction mechanism by assuming a linear correlation. However, according to the International confederation for thermal analysis and calorimetry (ICTAC) kinetics committee, a much accurate estimation can be obtained when the Kissinger–Akahira–Sunose (KAS) model is applied (Vyazovkin, 2015).

Recently, Göbel *et al.* (2010) also demonstrated the use of DSC analysis, IR spectroscopy, acid–base titration and other biophysical techniques to characterise the phase behaviour of some ionic liquids in silica modified monoliths. Vlad *et al.* (2003) also performed a pre- and post-effects of functionalising various cross-linked acrylamide copolymers with ion-exchangers and its impact on their thermal stability and kinetics. It was observed that the degradation of the acrylamide copolymers where dependent on the type of monomers and their moiety. Likewise, various characteristic temperatures have been observed as the thermally stable point beyond which depolymerisation occurs leading to the loss of chemical signature for the following types of monoliths: HMA-co-EDMA methacrylate monolith, 210 $^{\circ}$C (Yusuf *et al.*, 2016); poly(divinylbenzene) monolith, 380 $^{\circ}$C (Sýkora *et al.*, 2000); poly(g-glutamic acid) monolith, ~230 $^{\circ}$C (Park *et al.*, 2014); and POSS-epoxy–TPTM hybrid monolith, 300 $^{\circ}$C (Lin *et al.*, 2015).

In-depth thermal and kinetic studies of several polymers have been done by means of thermogravimetric (TGA/DTG/DSC) analysis (Jeske *et al.*, 2012; Jakić *et al.*, 2013; Nabinejad *et al.*, 2015) but lacking for polymethacrylate monoliths contrary to its significance as a stationary phase for bioseparation. Some of these polymers such as cross-linked polystyrenes (Wang *et al.*, 1999) have shown that the thermal stability of polymers are mainly determined by the amount of cross-linking. Generally, epoxy resins are also thought of to enhance crosslinking with co-monomers which could aid in the thermal, chemical and mechanical stability of polymers (Carioscia *et al.*, 2007). Nevertheless, they have also been shown to lead to the production of brittle polymers when cured with a co-monomer (Vabrik *et al.*, 1998). To the best of our knowledge there has been no thorough thermally initiated kinetic study into the thermal stability of synthesised polymethacrylate monoliths.

Hence, the aim of this work is to present an in-depth *ex situ* kinetic analysis probing into the thermal stability of poly EDMA-co-GMA monoliths through thermogravimetric analysis using a Mettler Toledo thermogravimetric (TG) equipment. The thermal stability analyses of the polymer were based on chemistries for heterogeneous solids. It was hypothesised that variation in the concentration of GMA could dictate the thermal stability of monoliths. The apparent/global activation energy of different compositions of monoliths were ascertained and compared using both the OFW and KAS isoconversional method.

2.   EXPERIMENTAL

2.1   Materials

Ethylene glycol dimethacrylate (EDMA, MW 198.22, 98%), glycidyl methacrylate (GMA, MW 142.15, 97%), 1-dodecanol (MW 186.33, 98%), cyclohexanol (MW 100.16, 99%), benzoyl peroxide (BPO, MW 242.23, 70%), and methanol (HPLC grade, MW 32.04, 99.93%) were acquired from Sigma–Aldrich. EDMA and GMA are the two monomers serving as the cross-linker and functional monomer, respectively.

2.2   Method

Methacrylate monoliths were synthesised by adapting our previous protocol (Danquah and Forde, 2008; Danquah *et al.*, 2008). Different samples of methacrylate monoliths were prepared by means of thermal free radical polymerisation in a water bath. Monoliths were synthesised having varied EDMA-GMA volume ratio as follows: 0/100; 20/80; 40/60; 60/40; 80/20; and 100/0%, L/L. Other conditions for adsorbent synthesis were maintained constant at a reacting temperature of 85 °C for 4 hours, an overall porogen (Cyclohexanol 60%: Dodecanol 40%, L/L) to monomers ratio of 60%:40% and 1% w/v of initiator. Washing of monoliths was done for 6 hours by using methanol in a soxhlet extractor to remove any unreacted monomers and porogens present in the monolith after polymerisation. Monoliths were air dried for a period of 7 days. The morphology of a selected monolith was investigated using a variable pressure scanning electron microscope, SEM, (S-3400N Hitachi model, Japan). Monoliths were sputter coated with gold to increase the conduction during SEM analysis.

2.3 Thermogravimetric Characterisation of Monoliths

Thermal analyses of the polymer were preceded with purging of the system (Mettler Toledo equipment) at 20 °C/min under a nitrogen gas flow of 100 mL/min. This is to ensure the analysis is free of external contaminants in the furnace capable of negatively influencing the results. Thermogravimetric characterisation of polymethacrylate monoliths were performed by using multiple heating rates of 5, 10, 15, 20 and 25 °C/min in a temperature range of 50 °C – 450 °C under constant N_2 flow rates of 25 mL/min. Portions of each sample weighing 20 mg was used after being pulverized and thoroughly shaken.

2.4 Non-isothermal Kinetic Analysis

Ozawa-Flynn-Walls (OFW) and Kissinger–Akahira–Sunose (KAS) isoconversional models were applied to calculate the kinetic properties based on the experimental results without fore knowledge of the reaction model, $f(\alpha)$. Parameters obtained are presented in their respective tables where; T_{max} is the maximum/peak temperature (K) and E_a is the "apparent" activation energy. Data pairs generated from OFW and KAS isoconversional models were matched with trend lines for the multiple heating rates.

3. RESULTS AND DISCUSSION

3.1 Polymerisation of Polymethacrylate Monolith

Polymethacrylate monoliths were thermally synthesised by means of free radical polymerisation of the two monomers (GMA and EDMA) in an interfacial layer after decomposition of the initiator (BPO); hence, their thermal characteristics were analysed based on chemistries for heterogeneous solids. The presence of nuclei caused scission of monomeric units in the cured mixture to form monomer radicals which subsequently led to reaction between the methacrylate monomers. EDMA-co-GMA monolithic adsorbents can be easily tailored to meet the hydrodynamic size of biomolecular targets. An increase in the concentration of EDMA resulted in smaller pores and larger surface areas, whist an increment in the amount of GMA corresponded to an upsurge in the functional groups for

ligand immobilisation (Danquah and Forde, 2008). An example of the morphology of pores in monoliths at a specified condition is shown in Figure 1. Epoxy moieties on the functional monomer also enhanced the formation of chemical crosslinking networks with EDMA in the formation of the polymer. This was confirmed subsequently with the TG data.
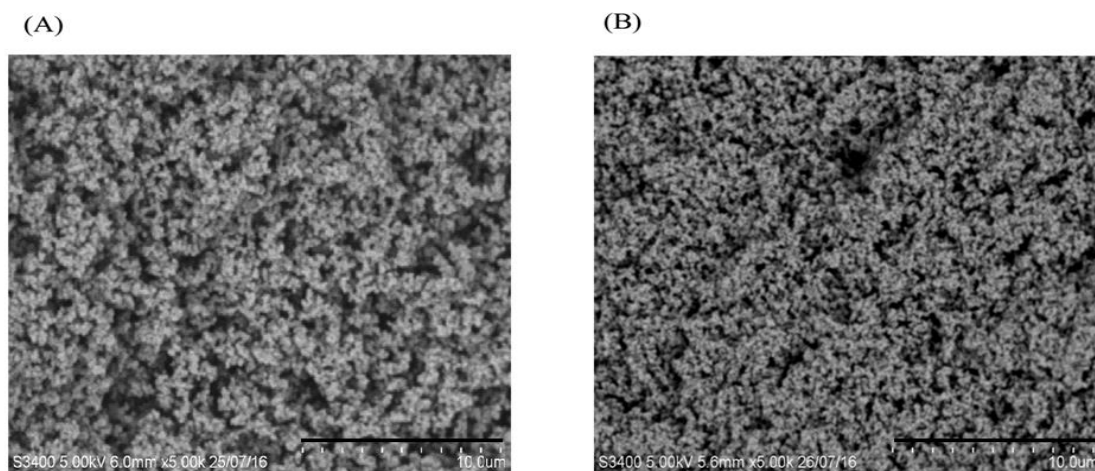
Figure 1. Scanning electron micrograph of EDMA-co-GMA polymeric monolith showing the morphology with varied compositions (a) E40/G60 and (b) E80/G20; thus, an increase in their respective surface areas and reduction in pore sizes.

3.2   Thermogravimetric analysis

The principal steps for the degradation of heterogeneous solids include: (i) transfer of heat and reactants to separation surfaces of each interphase; (ii) consumption of solid reactants and migration of separation surface interphase; and (iii) transport of volatile products from the reaction space (Vlad *et al.*, 2003). The impact of varying the concentration of monomers on the thermal degradability of monoliths using the TG and DTG curves is shown in Figures 2a and 2b, respectively, for a heat flow rate of 5 $^{\circ}$C/min on selected monomer variations (E/G): 0/100; 20/80; 40/60; 60/40/; 80/20; and 100/0.
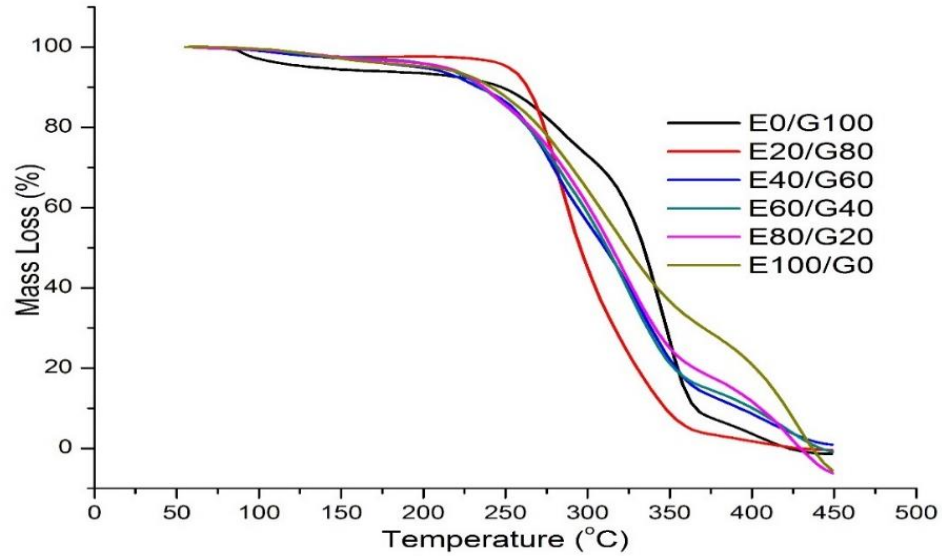
Figure 2a. TG curves illustrating the thermal degradation of varied EDMA-co-GMA polymethacrylate monoliths at heating rates of 5 °C/min to assess their thermal stability effects.
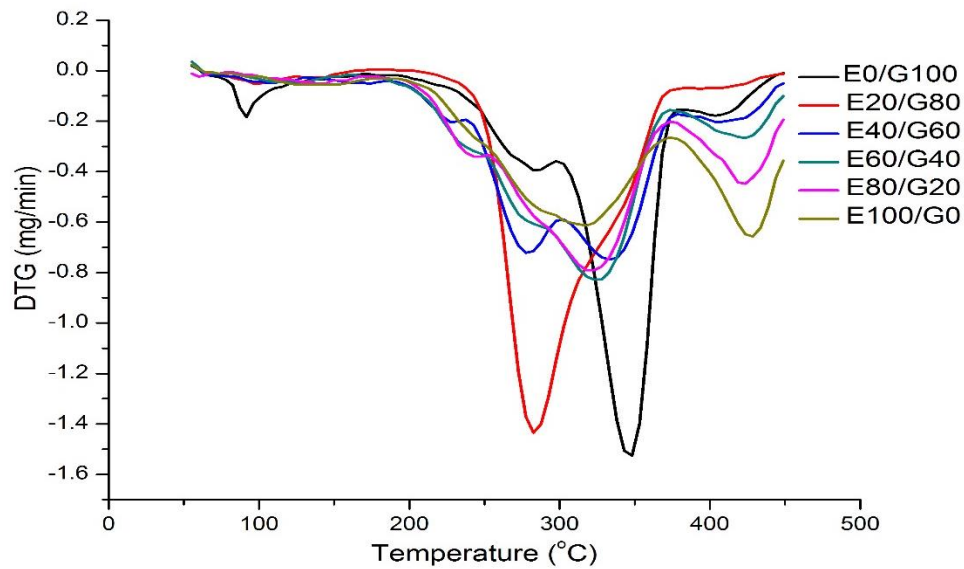
Figure 2b. DTG curves illustrating the thermal degradation of varied EDMA-co-GMA polymethacrylate monoliths at heating rates of 5 °C/min to assess their thermal stability effects.

Homopolymer resins, E0/G100 and E100/G0 when polymerised with the initiator (BPO) to form solid homopolymers were seen to undergo 2 stages of degradation as evident in the TG/DTG curves. These degradations were within the temperature ranges of about 55.2 - 223.3 °C with a mass loss rate of 7.0% and 223.3 – 381.9 °C with a mass loss of 79.7% for the first and second stages of E0/G100, respectively, with a heating rate of 5 °C/min.

On the other hand, E100/G0, homopolymer of EDMA had the following characteristic temperature ranges of about 55.4 – 195.8 °C with a corresponding mass loss rate of 4.3% and 195.8 – 372.7 °C with a mass loss rate of 61.8 %, for the first and second respective stages of degradation. The first stage of degradation for each homopolymer and monoliths were marked to be the characteristic point beyond which the polymer loses its chemical signature. The narrow characteristic temperature range in the first stage for E100/G0 as compared to E0/G100 is indicative of the fact that the presence of epoxy moiety in resins or polymers enhances their thermal stability (Carioscia *et al.*, 2007; Allaoui and El Bounia, 2009).

Unlike the homopolymers, the thermal degradation of monoliths were all observed to have three stages of degradation. The first stage being the point beyond which the monoliths loses their chemical and mechanical properties, similar to the homopolymers. The mass loss in this stage is mainly due to dehydration. The second (2) and third (3) stages are depolymerisation stages resulting in the chemical decomposition of the polymer, mainly attributed to the loss of the two polymer chains EDMA and GMA forming the monolith. In reference to the DTG curves and the respective peak temperatures of the homopolymers, stage 2 of the monolith depolymerisation could be attributed to the lighter ends of the polymers (such as methacrylic acid groups) devolatilizing out of the system whereas stage 3 is mainly dictated by the concentration of the epoxy-based resin in the monolithic polymer. The application of 3-5 temperature programs is recommended as appropriate to attain more accurate kinetic values according to the ICTAC kinetics committee (Vyazovkin *et al.*, 2011). The impact of different heating rates on the mass loss of EDMA-co-GMA monolithic polymers were analysed at 5, 10, 15, 20 and 25 °C/min. As expected, an increase in the rate of heat supply for the same mass of sample caused a shorter degradation time due to the increase in instantaneous transfer of heat. This phenomenon generally resulted in the shift of peak temperatures higher (from the left to right) for each stage. Data for maximum temperature of depolymerisation (T_{max}) for each stage as a function of the five (5) heating rates are shown in Table 1. It was observed that the peak temperatures for each monolith generally shifted to higher temperatures as the heating rates were increased.

Table 1. Effect of different heating rates on depolymerisation T_{max} in stages 2 and 3 of EDMA-co-GMA monoliths.

EDMA/GMA (Depolymerisation Stage)		0/100	20/80	40/60	60/40	80/20	100/0
Stage 2	5 ºC/min		283.5	279.0	282.9	285.6	
	10 ºC/min		293.9	289.9	289.9	297.1	
	15 ºC/min		297.9	299.1	296.4	265.1	
	20 ºC/min		301.7	302.5	299.1	273.8	
	25 ºC/min		305.1	304.5	303.4	262.6	
Stage 3	5 ºC/min	347.9	315.3	335.0	326.6	322.0	314.9
	10 ºC/min	363.6	351.9	348.4	346.3	342.4	320.3
	15 ºC/min	363.1	361.1	357.2	351.1	309.0	340.8
	20 ºC/min	365.7	366.1	364.1	359.0	344.8	348.2
	25 ºC/min	368.4	371.3	363.2	363.0	357.2	353.7

3.3 Non-isothermal kinetic analysis

Kinetic analysis can be done with either disc scanning calorimetry (DSC) or TG/DTG. TG/DTG is a highly sensitive technique used to study the thermal stability and polymer degradation without the need for calibration curves, whereas; a DSC technique is used for identification based on the polymers melting point (Jeske *et al.*, 2012). Notably, isoconversional models based on integral methods are the most appropriate for thermogravimetric data interpretation (Karimian *et al.*, 2016).

Monitoring the kinetics of processes initiated thermally, such as the synthesis of EDMA-co-GMA polymers, formulates a mathematical relationship between the process rate, extent of conversion and the temperature (Vyazovkin *et al.*, 2011). This can be determined through the kinetic triplet E_a, A and $f(\alpha)$. In addition, predictions made based on these analyses are critical in estimating the life span and compositions outside the current experimental analysis (Vyazovkin *et al.*, 2011; Jakić *et al.*, 2013). Equations employed for kinetic study is fundamentally hinged on a single step equation:

$$r = \frac{d\alpha}{dt} \equiv \beta \frac{d\alpha}{dT} \qquad \qquad (1)$$

$$r = A exp\left(-\frac{E_a}{RT}\right) f(\alpha) \qquad \qquad (2)$$

where β is the heating rate, α is the extent of conversion, T is absolute temperature in K, $f(\alpha)$ is the reaction model. Isoconvensional models such as Ozawa-Flynn-Wall's (OFW) and Kissinger-Akahira-Sunose's (KAS) methods are often applied in that regard in accordance with ASTM 698 without prior knowledge of $f(\alpha)$ in the determination of the kinetic parameters (Vyazovkin *et al.*, 2011; Jeske *et al.*, 2012). The extent of conversion can be calculated based on equation (3) below:

$$\alpha = \frac{m_o - m}{m_o - m_f} \tag{3}$$

where m_o, m_f and m are the initial, final and mass at any time, respectively. The dependence of the extent of conversion for each monolith composition (E20/G80; E40/G60; E60/G40 and E80/G20) with respect to the full range degradation temperature at 5 °C/min was plotted and is shown in Figure 3. It can be observed that there are > 1 pattern in the rate of change in the conversion of mass with respect to temperature, with the steepest point coinciding with the depolymerisation stage from about 225 °C – 375 °C. This further shows the inability of a single reaction model, $f(\alpha)$ to accurately cover the full kinetics of the monolithic polymer.
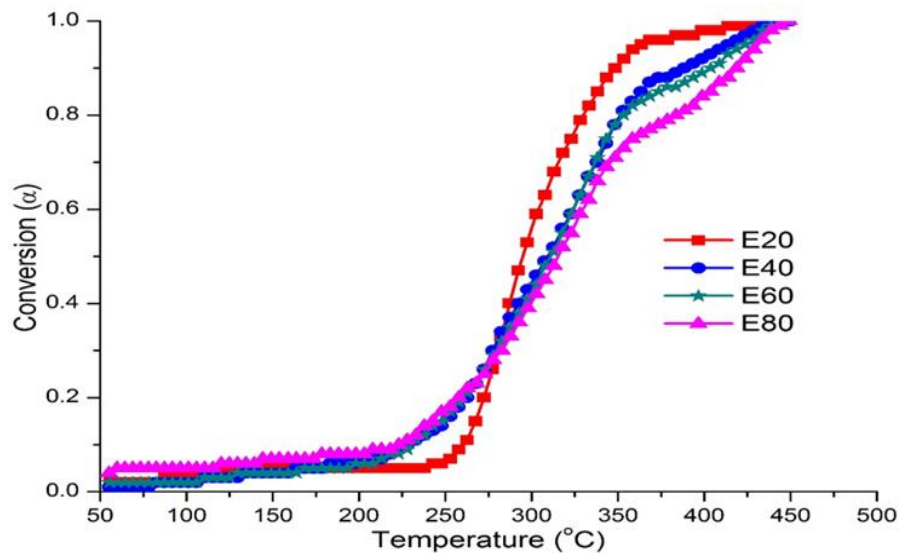
Figure 3. Trajectory of the extent of conversion as a function of temperature for monoliths at a heating rate of 5 °C/min.

OFW and KAS methods are both integral isoconversional methods, with the former seemingly being the most utilised whereas the latter has been recently remarked by the ICTAC kinetic committee (Vyazovkin *et al.*, 2011) as offering an improvement in accuracy of E_a values. OFW model in the current analysis has the basic equation:

$$logβ = log\left(\frac{AE_a}{R}\right) - 2.315 - 0.4567\left(\frac{E_a}{RT}\right) - \log f(α) \tag{4}$$

Equation (4) can be modified in terms of an equation of a straight line: $y = mx + c$ for easy analysis. Thus;

$$logβ = aT^{-1} + b \tag{5}$$

where

$$a = -0.4567\frac{E_α}{R} \tag{6}$$

$$b = log\left(\frac{AE_a}{R}\right) - 2.315 \tag{7}$$

Similarly, KAS isoconversional model is given as:

$$\ln(\frac{β}{T^2_{max}}) = \left(\frac{-E_a}{RT_{max}}\right) + \ln\frac{AE_a}{R} - \ln f(α) \tag{8}$$

Equation (4) – (8) was used to calculate the activation energies for the different compositions. Arrhenius equation can be estimated from equation (9):

$$K = A\exp\left(-\frac{E_a}{RT}\right) \tag{9}$$

where 'A' is the frequency factor (min^{-1}) which determines the frequency of molecular collision leading to polymer degradation as a function of temperature; E_a is the activation energy (kJ/mol); R is the energy gas constant (8.3145 J/mol K); T is the Temperature (K).

To accurately determine the kinetic parameters, the dependency of the apparent energy on extent of conversion from α = 0.05 - 0.9 and a step size of 0.05 was calculated for each monolith and homopolymers as shown in Figure 4a – 4f. It was demonstrated for each sample that the apparent activation energy varied with respect to extent of conversion. Thus, a single average activation energy will be inaccurate to represent all three stages of degradation/thermal stability for the monolithic samples. A similar trend in increase and decrease of E_a values as α increases is also confirmed in the analysis on modified polyvinyl copolymers by Vlad *et al.* (2003). The observed fluctuations for high α values can be attributed to either competitive processes or the depolymerisation process occurring in the polymer under dynamic heating conditions. It is also evident that the homopolymer samples had distinct chemical compositions from each other due to the vast differences in pattern in their respective E_a curves. Similarities also exists for the monolithic (E20/G80; E40/G60; E60/G40 and E80/G20) samples due to the presence of the same reactive chemical constituents (EDMA, GMA, BPO) in different proportions.
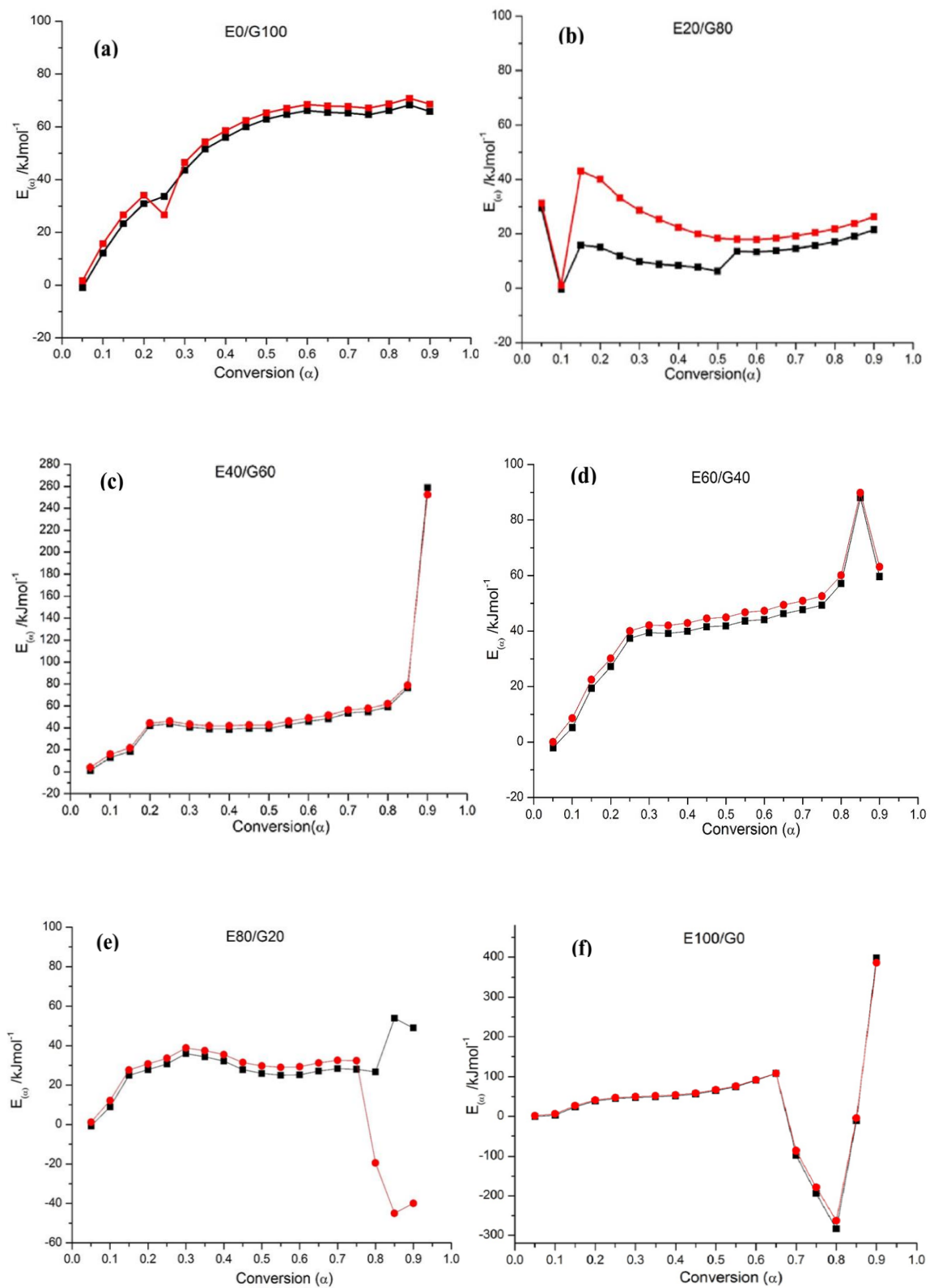
Figure 4. Relationship between apparent activation energy as a function of extent of conversion generated from two isoconversional models; KAS (red) and OFW (black), for (a) E0/G100; (b) E20/G80; (c) E40/G60; (d) E60/G40; (e) E80/G20 and; (f) E100/G0.

Activation energy in relation to the peak temperatures for each of the 3 degradation stages was calculated and presented in Table 2 based on OFW and KAS Isoconvensional models. The first stage of degradation generally had lower E_a values as compared to the second and third degradation stage for each monolith. This is due to the fact that stage 1 of monolith degradation was mainly due to dehydration process whereas stage 2 and 3 were the result of depolymerisation of the monolith. The negative activation energy values in some of the monoliths are mainly as a result of dehydration of remaining water molecules.

Table 2. Apparent activation energy (E_a) values derived from Ozawa-Flynn-Wall's (OFW) and Kissinger-Akahira-Sunose's (KAS) isoconversional method.

EDMA/ GMA	First stage, E_{a1} kJ/mol		Second stage, E_{a1} kJ/mol		Third Stage, E_{a1} kJ/mol	
	OFW	KAS	OFW	KAS	OFW	KAS
0/100	1.2	-1.1	-		74.2	72.1
20/80	-9.5	-13.5	51.6	49.4	25.1	20.7
40/60	10.5	8.0	40.2	37.4	50.	46.8
60/40	6.6	4.7	53.3	51.2	41.3	37.7
80/20	7.9	5.7	-19.4	-25.0	14.1	9.4
100/0	5.6	3.2	-		31.3	27.4

From the apparent activation energy values in the first stage of degradation, an increase in the cross-linker composition above 20% significantly enhanced the thermal stability of monoliths. With the interest of monolithic samples often in the arena of bioseparation and bioscreening, the best monomer compositions to ensure a thermally stable monolith were concluded to be E40/G60 and E60/G40 with an apparent activation energy for the first stage within 8.0 – 10.5 kJ/mol (mass loss rate from 2.7 - 5.7 % per min) and 4.7 – 6.6 kJ/mol (mass loss rate from 2.2 - 4.2 % per min). It must be emphasised that the most utilised monolith composition in bioseparation science is the E40/G60 composition. This is to ensure that there are sufficient amount of epoxy functional groups for ligand functionalisation without trading-off the amount of crosslinking, mechanical properties and permeability (Svec and Fréchet, 1995; Han *et al.*, 2012).

4.   CONCLUSIONS

An understanding of kinetic parameters for polymeric materials is essential in understanding their life span and change in material properties when subjected to elevated

temperature. Herein, various monomer mixtures were prepared as EDMA-co-GMA monolithic adsorbents and investigated for their thermal stability. Thermogravimetric curves showed that homo-GMA polymers had a better stability than homo-EDMA polymers. The kinetic parameters indicated that an increase in the composition of EDMA and GMA above 20% significantly enhances the thermal stability of monoliths under elevated non-isothermal conditions. This was due to the concurrent enhancement in the cross-linkages and amount of epoxy moiety in the monolithic polymer. E40/G60 and E60/G40 monoliths were identified as monoliths with better thermal stability amongst the synthesised samples; which happens to be consistent with literature as to the most utilised composition for monolithic applications. Nevertheless, the choice of appropriate monolithic polymer for biomolecular separations should not be purely based on the thermal stability since a number of other essential factors such as pore size for convective transfer of targets, surface area and reactive functional ends for ligand immobilisation have to be taken into consideration with a good compromise based on the user's preference. The dependence of apparent activation energy (E_a) on the extent of conversion (α) demonstrated that the degradation of monolithic polymers could not be accurately represented by a single reaction model or a single heating rate making it an example of a complex multistep reaction. Thermogravimetric analyses were therefore performed with multiple heating rates of 5, 10, 15, 20 and 25 ºC/min under N_2 atmosphere. The use of Ozawa-Flynn-Wall's and Kissinger–Akahira–Sunose isoconversional integral methods have been shown to be effective in determining the kinetic properties of EDMA-co-GMA monolithic samples. Generally, biomolecular activities with monoliths are done under temperature conditions less than 100 ºC making monoliths safe for chromatographic operations relative to their characteristic temperature ranges in the first stage of degradation.

5.   ACKNOWLEDGMENT

Authors wish to declare that there is no conflict of interest or commercial with respect to the publication.

6. REFERENCES

Acquah, C., M.K. Danquah, C.K.S. Moy and C.M. Ongkudon, 2016. In-process thermochemical analysis of in situ poly(ethylene glycol methacrylate-co-glycidyl methacrylate) monolithic adsorbent synthesis. Journal of Applied Polymer Science, 133: 1-9. Available from http://dx.doi.org/10.1002/app.43507. DOI 10.1002/app.43507.

Acquah, C., C.K.S. Moy, M.K. Danquah and C.M. Ongkudon, 2016. Development and characteristics of polymer monoliths for advanced lc bioscreening applications: A review. Journal of Chromatography B, 1015–1016: 121-134. Available from http://www.sciencedirect.com/science/article/pii/S1570023216300976. DOI http://dx.doi.org/10.1016/j.jchromb.2016.02.016.

Allaoui, A. and N. El Bounia, 2009. How carbon nanotubes affect the cure kinetics and glass transition temperature of their epoxy composites?–a review. EXPRESS Polymer Letters, 3: 588-594. DOI 10.3144/expresspolymlett.2009.73.

Alshitari, W., C.L. Quigley and N. Smith, 2015. Fabrication and evaluation of an organic monolithic column based upon the polymerisation of hexyl methacrylate with 1,6-hexanediol ethoxylate diacrylate for the separation of small molecules by capillary liquid chromatography. Talanta, 141: 103-110. DOI 10.1016/j.talanta.2015.03.064.

Carioscia, J.A., J.W. Stansbury and C.N. Bowman, 2007. Evaluation and control of thiol–ene/thiol–epoxy hybrid networks. Polymer, 48(6): 1526-1532.

Carrasco-Hernandez, S., J. Gutierrez, L. Cano and A. Tercjak, 2016. Thermal and optical behavior of poly(ethylene-b-ethylene oxide) block copolymer dispersed liquid crystals blends. European Polymer Journal, 74: 148-157. Available from http://www.sciencedirect.com/science/article/pii/S0014305715300616. DOI http://dx.doi.org/10.1016/j.eurpolymj.2015.11.019.

Danquah, M.K. and G.M. Forde, 2008. Large-volume methacrylate monolith for plasmid purification. Process engineering approach to synthesis and application. Journal of chromatography. A, 1188(2): 227-233. Available from http://www.ncbi.nlm.nih.gov/pubmed/18329651. DOI 10.1016/j.chroma.2008.02.045.

Danquah, M.K. and G.M. Forde, 2008. Preparation of macroporous methacrylate monolithic material with convective flow properties for bioseparation: Investigating the kinetics of pore formation and hydrodynamic performance. Chemical Engineering Journal, 140(1-3): 593-599. DOI 10.1016/j.cej.2008.02.012.

Danquah, M.K., J. Ho and G.M. Forde, 2008. A thermal expulsion approach to homogeneous large-volume methacrylate monolith preparation; enabling large-scale rapid purification of biomolecules. Journal of Applied Polymer Science, 109(4): 2426-2433. DOI 10.1002/app.28346.

Deng, N., Z. Liang, Y. Liang, Z. Sui, L. Zhang, Q. Wu, K. Yang, L. Zhang and Y. Zhang, 2012. Aptamer modified organic-inorganic hybrid silica monolithic capillary columns for highly selective recognition of thrombin. Analytical chemistry, 84(23): 10186-10190. Available from http://www.ncbi.nlm.nih.gov/pubmed/23137349. DOI 10.1021/ac302779u.

Göbel, R., A. Friedrich and A. Taubert, 2010. Tuning the phase behavior of ionic liquids in organically functionalized silica ionogels. Dalton Transactions, 39(2): 603-611. DOI 10.1039/b913482d.

Greiderer, A., L. Trojer, C.W. Huck and G. Bonn, 2009. Influence of the polymerisation time on the porous and chromatographic properties of monolithic poly(1,2-bis(p-vinylphenyl))ethane capillary columns. J. Chromatogr. A, 1216(45): 7747-7754. DOI 10.1016/j.chroma.2009.08.084.

Han, B., C. Zhao, J. Yin and H. Wang, 2012. High performance aptamer affinity chromatography for single-step selective extraction and screening of basic protein lysozyme. Journal of chromatography. B, Analytical technologies in the biomedical and life sciences, 903: 112-117. Available from http://www.ncbi.nlm.nih.gov/pubmed/22841745. DOI 10.1016/j.jchromb.2012.07.003.

Hjertén, S., J.-L. Liao and R. Zhang, 1989. High-performance liquid chromatography on continuous polymer beds. Journal of Chromatography A, 473: 273-275. DOI 10.1016/S0021-9673(00)91309-8.

Hjertén, S., J. Mohammad and K.i. Nakazato, 1993. Improvement in flow properties and ph stability of compressed, continuous polymer beds for high-performance liquid chromatography. Journal of Chromatography A, 646(1): 121-128. Available from http://www.sciencedirect.com/science/article/pii/S0021967399870137. DOI http://dx.doi.org/10.1016/S0021-9673(99)87013-7.

Jakić, M., N.S. Vrandečić and I. Klarić, 2013. Thermal degradation of poly (vinyl chloride)/poly (ethylene oxide) blends: Thermogravimetric analysis. Polymer degradation and stability, 98(9): 1738-1743.

Jandera, P., M. Staňková, V. Škeříková and J. Urban, 2013. Cross-linker effects on the separation efficiency on (poly)methacrylate capillary monolithic columns. Part i. Reversed-phase liquid chromatography. Journal of Chromatography A, 1274(0): 97-106. Available from http://www.sciencedirect.com/science/article/pii/S0021967312018420. DOI http://dx.doi.org/10.1016/j.chroma.2012.12.003.

Jeske, H., A. Schirp and F. Cornelius, 2012. Development of a thermogravimetric analysis (tga) method for quantitative analysis of wood flour and polypropylene in wood plastic composites (wpc). Thermochimica Acta, 543: 165-171. Available from http://www.sciencedirect.com/science/article/pii/S0040603112002535. DOI http://dx.doi.org/10.1016/j.tca.2012.05.016.

Karimian, M., M. Schaffie and M.H. Fazaelipoor, 2016. Determination of activation energy as a function of conversion for the oxidation of heavy and light crude oils in relation to in situ combustion. Journal of Thermal Analysis and Calorimetry: 1-11.

Korolev, A., T. Popova, V. Shiryaeva and A. Kurganov, 2006. Permeability, porosity, and structure of monolithic capillary columns in gas chromatography. Russian Journal of Physical Chemistry, 80(1): 120-123.

Lendero, N., J. Vidič, P. Brne, A. Podgornik and A. Štrancar, 2005. Simple method for determining the amount of ion-exchange groups on chromatographic supports. Journal of Chromatography A, 1065(1): 29-38. DOI 10.1016/j.chroma.2004.10.072.

Lin, H., L. Chen, J. Ou, Z. Liu, H. Wang, J. Dong and H. Zou, 2015. Preparation of well-controlled three-dimensional skeletal hybrid monoliths via thiol–epoxy click polymerization for highly efficient separation of small molecules in capillary liquid chromatography. Journal of Chromatography A, 1416: 74-82.

Luo, Q., S. Mutlu, Y.B. Gianchandani, F. Svec and J.M. Fréchet, 2003. Monolithic valves for microfluidic chips based on thermoresponsive polymer gels. Electrophoresis, 24(21): 3694-3702.

Mihelič, I., M. Krajnc, T. Koloini and A. Podgornik, 2001. Kinetic model of a methacrylate-based monolith polymerization. Industrial & engineering chemistry research, 40(16): 3495-3501.

Minakuchi, H., K. Nakanishi, N. Soga, N. Ishizuka and N. Tanaka, 1996. Octadecylsilylated porous silica rods as separation media for reversed-phase liquid chromatography. Anal. Chem., 68(19): 3498-3501.

Nabinejad, O., S. Debnath, M. Rahman and I. Davies, 2015. Effect of oil palm shell powder on the mechanical performance and thermal stability of polyester composites.

Ongkudon, C.M. and M.K. Danquah, 2010. Process optimisation for anion exchange monolithic chromatography of 4.2 kbp plasmid vaccine (pcdna3f). Journal of Chromatography B, 878(28): 2719-2725. DOI 10.1016/j.jchromb.2010.08.011.

Ongkudon, C.M., T. Kansil and C. Wong, 2014. Challenges and strategies in the preparation of large-volume polymer-based monolithic chromatography adsorbents. Journal of separation science, 37(5): 455-464.

Ongkudon, C.M., S. Pan and M.K. Danquah, 2013. An innovative monolithic column preparation for the isolation of 25 kilo base pairs DNA. Journal of chromatography. A, 1318: 156-162. Available from http://www.ncbi.nlm.nih.gov/pubmed/24209297. DOI 10.1016/j.chroma.2013.10.011.

Park, S.-B., J. Sakamoto, M.-H. Sung and H. Uyama, 2014. Ph-controlled degradation and thermal stability of a porous poly (γ-glutamic acid) monolith crosslinked with an oxazoline-functionalized polymer. Polymer Degradation and Stability, 99: 99-104.

Peters, E.C., F. Svec and J.M. Fréchet, 1997. Thermally responsive rigid polymer monoliths. Advanced materials, 9(8): 630-633.

Podgornik, A., M. Barut, A. Strancar, D. Josić and T. Koloini, 2000. Construction of large-volume monolithic columns. Analytical chemistry, 72(22): 5693.

Podgornik, A., V. Smrekar, P. Krajnc and A. Strancar, 2013. Estimation of methacrylate monolith binding capacity from pressure drop data. Journal of chromatography. A, 1272: 50-55. Available from http://www.ncbi.nlm.nih.gov/pubmed/23261298. DOI 10.1016/j.chroma.2012.11.057.

Podgornik, A., J. Vidic, J. Jancar, N. Lendero, V. Frankovic and A. Strancar, 2005. Noninvasive methods for characterization of large-volume monolithic chromatographic columns. Chem. Eng. Technol., 28(11): 1435-1441. DOI 10.1002/ceat.200500170.

Roberts, M.W., C.M. Ongkudon, G.M. Forde and M.K. Danquah, 2009. Versatility of polymethacrylate monoliths for chromatographic purification of biomolecules. Journal of separation science, 32(15-16): 2485-2494. Available from http://www.ncbi.nlm.nih.gov/pubmed/19603394. DOI 10.1002/jssc.200900309.

Svec, F. and J.M.J. Fréchet, 1995. Kinetic control of pore formation in macroporous polymers. Formation of "molded" porous materials with high flow characteristics for separations or catalysis. Chemistry of Materials, 7(4): 707-715.

Svec, F. and J.M.J. Fréchet, 1995. Modified poly(glycidyl metharylate-co-ethylene dimethacrylate) continuous rod columns for preparative-scale ion-exchange chromatography of proteins. Journal of Chromatography A, 702(1–2): 89-95. Available from http://www.sciencedirect.com/science/article/pii/0021967394010216. DOI http://dx.doi.org/10.1016/0021-9673(94)01021-6.

Sýkora, D., E.C. Peters, F. Svec and J.M. Fréchet, 2000. "Molded" porous polymer monoliths: A novel format for capillary gas chromatography stationary phases. Macromolecular Materials and Engineering, 275(1): 42-47.

Sýkora, D., E.C. Peters, F. Svec and J.M.J. Fréchet, 2000. "Molded" porous polymer monoliths: A novel format for capillary gas chromatography stationary phases. Macromolecular Materials and Engineering, 275(1): 42-47. Available from http://dx.doi.org/10.1002/(SICI)1439-2054(20000201)275:1<42::AID-MAME42>3.0.CO;2-X. DOI 10.1002/(SICI)1439-2054(20000201)275:1<42::AID-MAME42>3.0.CO;2-X.

Urthaler, J., R. Schlegl, A. Podgornik, A. Strancar, A. Jungbauer and R. Necina, 2005. Application of monoliths for plasmid DNA purification development and transfer to production. Journal of chromatography. A, 1065(1): 93.

Vabrik, R., I. Czajlik, G. Tury, I. Rusznak, A. Ille and A. Vig, 1998. A study of epoxy resin–acrylated polyurethane semi-interpenetrating polymer networks. Journal of applied polymer science, 68(1): 111-119.

Vlad, C.D., M.V. Dinu and S. Dragan, 2003. Thermogravimetric analysis of some crosslinked acrylamide copolymers and ion exchangers. Polymer degradation and stability, 79(1): 153-159.

Vyazovkin, S., 2015. Isoconversional kinetics of thermally stimulated processes. Springer.

Vyazovkin, S., A.K. Burnham, J.M. Criado, L.A. Pérez-Maqueda, C. Popescu and N. Sbirrazzuoli, 2011. Ictac kinetics committee recommendations for performing kinetic computations on thermal analysis data. Thermochimica Acta, 520(1–2): 1-19. Available from http://www.sciencedirect.com/science/article/pii/S0040603111002152. DOI http://dx.doi.org/10.1016/j.tca.2011.03.034.

Wang, Z., D.D. Jiang, M.A. McKinney and C.A. Wilkie, 1999. Cross-linking of polystyrene by friedel–crafts chemistry to improve thermal stability. Polymer degradation and stability, 64(3): 387-395.

Wen, L., X. Tan, Q. Sun, F. Svec and Y. Lv, 2016. "Smart" molecularly imprinted monoliths for the selective capture and easy release of proteins. Journal of separation science, 39(16): 3267-3273.

Yu, C., S. Mutlu, P. Selvaganapathy, C.H. Mastrangelo, F. Svec and J.M. Fréchet, 2003. Flow control valves for analytical microfluidic chips without mechanical parts based on thermally responsive monolithic polymers. Analytical chemistry, 75(8): 1958-1961.

Yusuf, K., A.Y. Badjah-Hadj-Ahmed, A. Aqel and Z.A. Alothman, 2016. Monolithic metal–organic framework mil-53(al)-polymethacrylate composite column for the

reversed-phase capillary liquid chromatography separation of small aromatics. Journal of separation science, 39(5): 880-888. DOI 10.1002/jssc.201501289.

CHAPTER FIVE

BIOPHYSICAL CHARACTERISATION OF APTAMER-TARGET BINDING AND APTASENSOR DEVELOPMENT

DECLARATION FOR THESIS SECTION 5.1

Characterisation of charge distribution and stability of aptamer-thrombin binding interaction

The candidate will like to declare that there is no conflict of interests involved in this work and that my extent of contribution as candidate is as shown below:

Contribution of Candidate	Conceptualisation, initiation and write-up	40%

The following co-authors were involved in the development of this publication and attest to the candidate's contribution to a joint publication as part of his thesis. Permission by co-authors are as follows:

Name	Signature	Date
Michael K. Danquah		13.07.2017
Clarence M. Ongkudon		13.07.2017
Sze Y. Tan		13.07.2017
Sing Y. Tan		13.07.2017

ABSTRACT

Aptamers are single stranded nucleic acids with specific target-binding functionalities, biophysical and biochemical properties. The binding performance of aptamers to their cognate targets is influenced by the physicochemical conditions of the binding system particularly in relation to biomolecular charge distribution and hydrodynamic conformations in solution. Herein, we report the use of zeta potential measurements to characterise the surface charge distribution, biomolecular hydrodynamic size and the binding performance of a 15-mer thrombin binding aptamer (TBA) to thrombin under various physicochemical conditions of pH, temperature, monovalent (K^+) and divalent (Mg^{2+}) cation concentrations. Charge distribution analysis demonstrated time dependence in the formation of stable TBA-thrombin and TBA-thrombin-metal ion complexes. TBA was characterised to be most stable in pH above 9. The presence of monovalent and divalent metal ions reduced the electronegativity of TBA through electrostatic interactions, and this demonstrated to improve binding characteristics. TBA-thrombin complexes generated under different physicochemical conditions showed varying surface charge distributions. The stability of TBA-thrombin complex investigated using Scatchard analysis showed that the presence of K^+ increased the binding performance by displaying a positive cooperativity relationship. The presence of Mg^{2+} showed a concave upward trend, potentially caused by heterogeneity in binding.

1. INTRODUCTION

Aptamers are single-stranded DNA/RNA ligands generated by means of an iterative process known as Systematic Evolution of Ligands by Exponential enrichment (SELEX) (Ellington and Szostak, 1990; Robertson and Joyce, 1990; Tuerk and Gold, 1990). They are a preferred class of bioprobes owing to their stability, non-immunogenicity, low cost of generation, wide spectrum of target space, minimal ethical issues, and the ability to undergo pre-/post biomodification processes (Acquah *et al.*, 2015; Nezlin, 2016). Notwithstanding, the binding performance of aptamers to their target molecules is a function of the physicochemical conditions of the binding system including pH, presence of metal ions, temperature and chemo-molecular labelling/modifications of the aptamer. This affects the kinetics of the binding process, charge and conformational distributions of the aptamer and the stability of the complex. An in-depth biophysical characterisation of aptamer-target interactions is critical to improve understanding of the binding process in order to establish optimal binding conditions for diverse applications.

The 15-mer thrombin binding aptamer (TBA) [5′-GGT TGG TGT GGT TGG-3′] is commonly used as a model aptamer to characterise aptamer-target interactions (Tasset *et al.*, 1997; Hamaguchi *et al.*, 2001; Ostatná *et al.*, 2008; Lin *et al.*, 2011). Biophysical techniques such as circular dichroism, isothermal titration and surface plasmon resonance have been used to investigate the effects of binding conditions such as the presence of metal ions and variations in thrombin concentration on the binding characteristics of 15-mer and 29-mer TBA. Lin and co-workers reported that 15-mer TBA binds to exosite I (fibrinogen recognition site) of thrombin by electrostatic interaction. They also reported that the presence of K^+ induces the formation of G-quadruplex conformations of TBA (Lin *et al.*, 2011). By using affinity capillary electrophoresis, Girardot *et al.* (2010) studied the effect of monovalent (Na^+, K^+, Cs^+) and divalent (Mg^{2+}, Ca^{2+}, Ba^{2+}) metal ions on the binding interactions of a lysozyme aptamer. A mobility swift was observed during the addition of cations to the electropheretic medium, potentially due to the interactions between aptamer molecules and cations and further inducing a conformational change of the aptamer. Girardot *et al.* (2013) employed a microchip electrophoresis technique in a frontal mode to characterise the binding behaviour of a lysozyme aptamer under different

conditions of ionic strength, divalent cations and thermal effect. The results showed that the presence of divalent metal ions improved binding affinity. Also thermal treatment of the aptamer increased conformational stability which further resulted in improved binding affinity.

In addition, the electrokinetics and binding traits of aptamers change with varying conditions of the binding medium (Hianik *et al.*, 2007; Lin *et al.*, 2011; Chang *et al.*, 2014). Zeta (ζ) potential analysis via dynamic light scattering is a useful technique in characterising interfacial distribution and electrokinetic behaviour of charged species in aqueous media (Adamczyk *et al.*, 2010; Song *et al.*, 2015), and would advance theoretical understanding of the binding behaviour of aptamers in relation to surface charge distribution, hydrodynamic mobility and binding characteristics in solution. Despite the uniqueness of ζ potential as a biophysical parameter for biomolecular characterisation and complex formation, there is limited research focused on the application of ζ potential analysis to investigate the binding characteristics of aptamers to their cognate target molecules and the stability of the emerging biomolecular complex. This study focuses on the application of ζ potential analysis as a tool to investigate the effect of varying surface charge distribution and hydrodynamic mobility on aptamer binding characteristics, and the stability of the aptamer-target complex. It contributes to building a robust theoretical understanding that underpins the binding behaviours of aptamers, providing basis to optimise binding performance for a wide range of applications including biosensor, bioseparation, cell targeting, high throughput screening, in vitro evolution, and drug delivery.

2.   MATERIALS AND METHODS

2.1   Biomolecules and reagents

15-mer thrombin aptamer 5′-GGT TGG TGT GGT TGG-3′ was purchased from First Base (Malaysia). Thrombin and Arsenazo III were purchased from Sigma-Aldrich (Malaysia). Potassium Chloride, Magnesium Chloride, Calcium Chloride and Tris-EDTA (TE) buffer were obtained from Fisher Scientific (Malaysia).

2.2 Instrumentation

Nanoplus particulate system (Nanoplus-3, USA) was used to perform zeta potential and average hydrodynamic size measurements of TBA, thrombin and thrombin-TBA complex at 25 ºC. Zeta potential analysis was performed with forward scattering optics at 15º and a voltage of 60 V. Hydrodynamic size measurement was performed with Backscatter Optics at 160°. All measurements were taken after the equilibrium time of one minute. Measurements for each analysis were triplicated, and all aqueous media were formulated with Milli-Q water purification system. An illustration of the principle of dynamic light scattering technique in characterising the zeta potential of TBA and thrombin-TBA complex is shown in Figure 1.
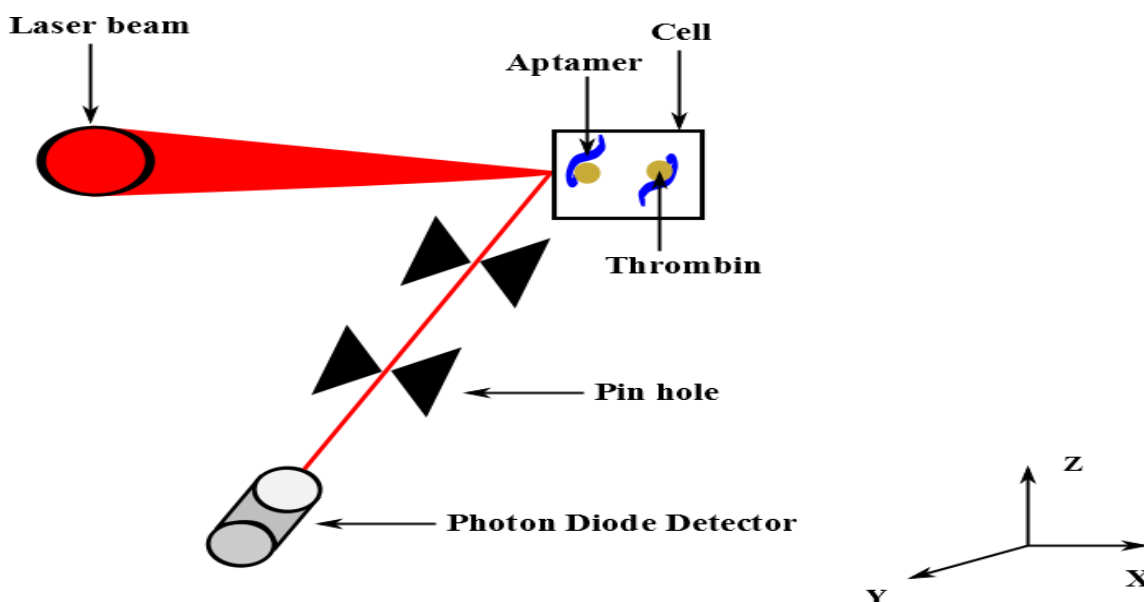
Figure 1. An illustration of the application of dynamic light scattering technique to characterise aptamer charge distribution and biophysical stability.

2.3 Zeta potential analysis of TBA and thrombin-TBA complex

2.3.1 Effect of pH

100 µM aptamer solutions were diluted in pH-adjusted TE buffers ranging from pH 4-11 to a final volume of 1 mL and incubated for 30 min at 25 °C. Zeta potential measurements were performed for each pH system. To study the effect of pH on TBA-thrombin complex, 100 µM aptamer solutions were interacted with 7.5 mg/mL thrombin solution and pH-adjusted TE buffer in a volumetric ratio of 1:1:2 to make a final volume of 1 mL. The mixtures were incubated for 30 min at 25 °C. For zeta size analysis, 1600 µM TBA

aliquots were diluted in pH-adjusted TE buffers ranging from pH 4-11 and incubated for 30 min at 25 °C. 1600 µM TBA aliquots were interacted with 7.5 mg/mL thrombin solution and pH-adjusted TE buffer in 1:1:1 volumetric ratio, followed by incubation for 30 min at 25 °C. Zeta size measurement was performed for each pH system.

2.3.2 Effect of metal ion polarity and concentrations

The effect of different metal ions on the surface charge distribution of TBA was investigated. Two different metal ions Magnesium (Mg^{2+}) and Potassium (K^+) with concentrations 0.01 M, 0.1 M, 0.5 M, 1.0 M and 1.5 M were prepared and interacted with 500 uL of TBA or Thrombin-TBA complex. The resulting solutions were then incubated for 30 min at 25 °C followed by zeta potential measurements. For zeta size measurement, TBA (1600 µM) and thrombin-TBA complex (7.5 mg/mL for thrombin) were measured after interaction with varying concentrations of metal ions in incubation for 30 min at 25 °C.

2.3.3 Effect of temperature

100 µM aptamer solution was diluted with TE at pH 8, made up to a final volume of 1 mL, and incubated for 30 min under varying temperature conditions of 20 °C, 25 °C, 30 °C, 37 °C and 45 °C. Thrombin-TBA complex was prepared by mixing 100 µM aptamer solution with 7.5 mg/mL thrombin solution, followed by incubation at the abovementioned temperatures. To understand the impact of temperature on the hydrodynamic size and zeta potential of the complex, 1600 µM aptamer solution was reacted with thrombin (7.5 mg/mL) at a volumetric ratio of 1:1 and incubated at the different temperatures.

2.4 Scatchard Analysis

Scatchard analysis was performed to investigate the binding of metal ions to TBA and Thrombin-TBA complex. Arsenazo III was used to bind free metal ions K^+ and Mg^{2+}. Arsenazo stock solution of 250 µM was prepared with 20 mL of the prepared solution aliquoted and diluted to 50 µM. This was followed by adjustment of the pH to 9 by the addition of NaOH. 20 µL of 10 µM TBA was incubated with 20 µL of metal ions with

varying concentrations 0.01, 0.1, 0.2, 0.3, 0.4, 0.5, 1.0, 1.5 and 2.0 M for 30 min. 10 μL aliquots were served into a 96 well flat bottom plate, and 250 μl of 50 μM Arsenazo was added to each well with gentle mixing. The system was allowed to incubate for 10 min before taking absorbance measurements using a microplate spectrophotometer at 610 nm wavelength. An analogous experiment was carried out using TBA-thrombin complex. The concentration of free/unbound cations in solution was determined from the absorbance readings using a standard curve. A Scatchard plots of bound/free cation concentrations versus TBA (Thrombin-TBA complex) bound cation concentrations were developed.

3.   RESULTS AND DISCUSSION

3.1   Effect of pH on the characteristics of TBA and thrombin-TBA complex

As different agents for biomarking and stabilisation may present non-isocratic conditions that can affect the binding affinity and chemical properties of aptamers, the effect of pH from 4-11 was investigated. Zeta potential analysis of TBA surface charge distribution demonstrated electronegativity over the range of pH as shown in Figure 2 (A). This was primarily due to the presence of negatively charged phosphate groups on the base DNA aptamer sequence. Also, the structure of G-quadruplex with rich guanine and centered by carbonyl oxygen increases the electronegative stability of TBA. The results indicated that the surface charge of the aptamer increased in electronegativity with increasing pH. The zeta potential of the aptamer was slightly positive at pH 4, with an isoelectric focusing (pI) point of ~4.1. The increase in aptamer electronegativity under increasing pH was as a result of deprotonation associated with increasing concentration of hydroxyl groups exposed to the aptamer. Also, high hydroxyl concentrations can result in structural conformational changes to induce redistribution of negatively charged moieties of the aptamer molecule. The positive zeta potential observed for pH < pI was due to the presence of high concentration of H^+ ions (protonation) that neutralise localised negative charges on the aptamer molecule. The aptamer was considered most stable at pH above 9 with a zeta potential of > -30 mV. The zeta potential analysis of the TBA-thrombin complex showed electronegativity within -12 mV to -22 mV over the range of pH investigated with reduced charge and molecular stability compared to free TBA. The observed lower zeta charge stability of TBA-aptamer complex compared to TBA is

because biomolecular complexation occurs at the most stable intermolecular charge activation and structural conformation, hence, variations in pH would not significantly alter the charge profile. The result further demonstrates that the biophysical charge characteristics of the complex formed from the interaction of thrombin and TBA was not significantly affected by protonation and deprotonation mechanism of pH.
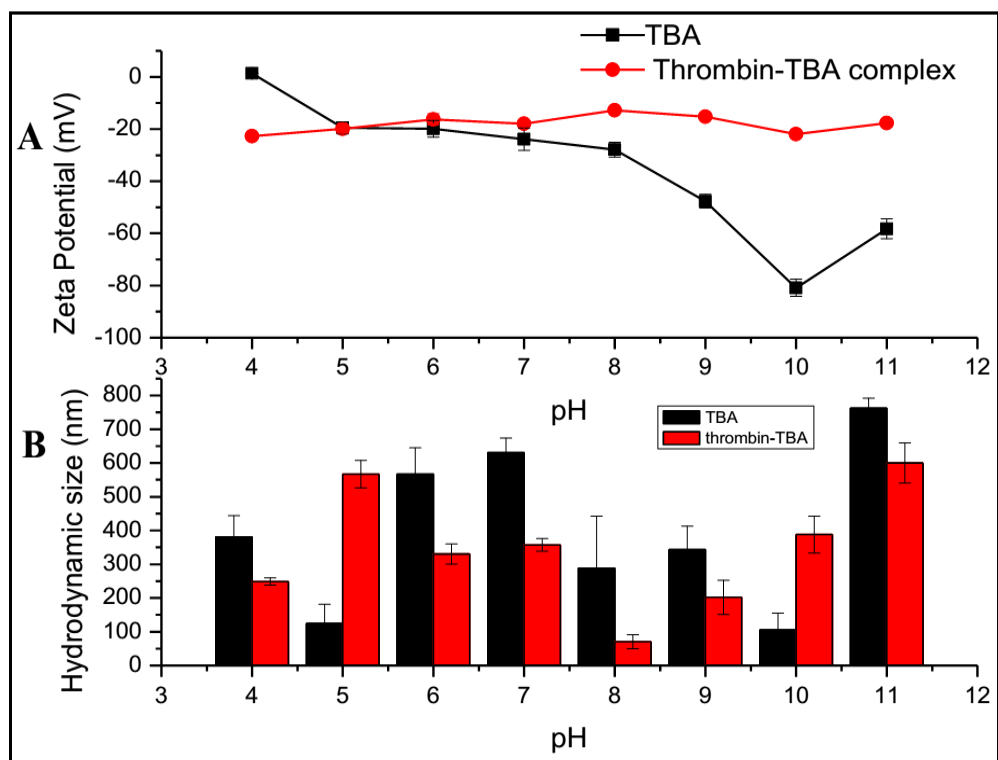
Figure 2. Effect of pH on zeta potential (A) and average hydrodynamic size (B) of TBA and thrombin-TBA complex in Tris-EDTA buffer. Buffer pH was varied from 4 to 11 (n=3 data sets).

The TBA showed a hydrodynamic size range of 100 nm to 800 nm over the pH range of 4-11. As it can be seen in Figure 2 (B), no specific trend in hydrodynamic size distribution over the pH range was observed. Variations in pH affect the polarity of charged moieties on the aptamer, as shown in the zeta potential data, and can result in intermolecular agglomeration. TBA showed the smallest average hydrodynamic size of 105.93 nm at pH 10 corresponding to the most electronegative zeta potential value of -80.9 mV. At this electronegativity, dynamic repulsive effect is significantly strong hindering agglomeration between TBA molecules. The thrombin-TBA complex showed a hydrodynamic size range of 70 nm to 600 nm over the pH range 4-11. The overall hydrodynamic size of thrombin-TBA complex was relatively smaller than TBA for most pH conditions. TBA condenses

and folds into intrinsic forms during binding with thrombin, resulting in the formation of a molecular complex with reduced hydrodynamic size. Thrombin-TBA complex showed the smallest hydrodynamic size of 70.8 nm at pH 8, and the corresponding zeta potential indicated colloidal stability. The high electrostatic repulsion at this pH reduced agglomeration and resulted in reduced particulate size of the complex.

3.1.1 Kinetic modelling of aptameric binding under varying pH conditions

The kinetic modelling was based on first order binding interaction of an aptamer ligand [A] and a target analyte [T] in a homogenous system with non-variable physicochemical conditions. It was assumed that a single monovalent analyte interacts with the aptamer and that all binding events are independent. The formation of complex [TA] follows pseudo-first order kinetics under the assumption that the reaction is not mass transfer limited. The binding between an arbitrary aptamer molecule [A] and the cognate target molecule [T] can be expressed by the reversible reaction equation (1):

$$A \ + \ T \ \underset{k_d}{\overset{k_a}{\rightleftharpoons}} \ AT \tag{1}$$

Where [AT] is the intermolecular complex formed between the aptamer and the target; and k_a and k_d are the association and dissociation rate constants respectively. The net rate at which the complex [AT] forms is defined by the difference in the rate of its formation and the rate of its dissociation into molecular entities of aptamer and target. This can be expressed by reaction equation (2):

$$\frac{d[AT]}{dt} = k_a[A][T] - k_d[AT] \tag{2}$$

The association constant, k_a, describes the rate of complex formation per unit second for one molar solution of [A] and [T]. The dissociation constant, k_d describes the stability of the complex in terms of its rate of decay into [A] and [T] per second. The concentration of aptamer in the binding system at any time can be expressed as: $[A] = [A]_{max} - [AT]$, where $[A]_{max}$ is the initial concentration of aptamer with a specified number of active

binding sites. Substituting [A] into the differential equation of AT formation (2), the formation rate of the intermolecular complex [AT] becomes:

$$\frac{d[AT]}{dt} = k_a[T]([A]_{max} - [AT]) - k_d[AT] \qquad (3)$$

Although the differential rate equation describes one-to-one binding phenomenon, it only describes the time rate of formation of [AT], thus it is not applicable in characterising absolute net concentrations of [AT]. Considering steady-state conditions and solving the differential equation (3), the intermolecular complex [AT] formation as a function of time can be expressed as equation (4):

$$[AT] = k_a[T][A]_{max}\left(\frac{1 - e^{(-k_a[T] - k_d)t}}{k_a[T] + k_d}\right) \qquad (4)$$

The generated aptamer-target binding kinetics can be correlated with biomolecular interaction analysis via surface plasmon resonance (SPR). SPR analysis generates real-time adsorption and desorption profiles of the molecular interaction between the aptamer and its target molecule displayed as a sensogram. The SPR output, resonance unit (R), is a measure of the real-time concentration of bound target on the aptamer-immobilised chip surface. The net rate of formation of the intermolecular complex (AT), expressed in R terms, is given by equation (5):

$$\frac{dR}{dt} = k_a[T][R_{max} - R] - k_d R \qquad (5)$$

The observed SPR signal R is proportional to the net concentration of [AT] complex: $R \propto [AT]$. Also, the maximum SPR signal, R_{max} is proportional to the maximum concentration of binding sites available on the aptamer immobilised on the sensing surface: $R_{max} \propto [A]_{max}$. The concentration of the intermolecular complex, R as a function of time can be obtained by integrating equation (5) to obtain equation (6):

$$R = \frac{[T]R_{max}k_a}{[T]k_a + k_d}\left(1 - e^{-([T]k_a + k_d)t}\right) \qquad (6)$$

224

The effect of pH on aptamer binding can be incorporated into the illustrated kinetic scheme through the reactive dependence of H^+ or OH^- ionic species in the binding system. In order to establish the existence of, for example, H^+ in the reactive binding system, equation (1) can be re-written as follows:

$$A^- + T^+ + H^+ \underset{k_d}{\overset{k_a}{\rightleftharpoons}} AT^*$$

(7)

With the above reactive kinetic scheme in equation (7), it is possible to predict the net binding rate in the presence of H^+ ions. Under this scenario, R_{max} would correspond to a reduced aptamer active site concentration resulting from potential inactivation of electronegative binding sites. Thus $[AT]^*$ consists of the resultant complex $[AT]$ and a second complex $[AH]$ such that $[AT]^* = [AT] + [AH]$.

The kinetic rate of $[AT]^*$ formation based on equation (7) is:

$$\frac{d[AT]^*}{dt} = k_a[T][A][H^+] - k_d[AT]^*$$

(8)

Rewriting equation (8) to reflect the effect of H^+ ions on the reactive binding scheme gives:

$$\frac{d[AT]^*}{dt} = k_a[T]([A]_{max} - [AT] - [AH])[H^+] - k_d([AT] + [AH])$$

(9)

Correlating equation (9) with SPR kinetics in terms of resonance unit (R) and assuming $R^* \propto [AT]^*, M \propto [AH]$, and $R_{max} \propto [A]_{max}$ gives:

$$\frac{dR^*}{dt} = k_a[T](R_{max} - R^*)[10^{-pH}] - k_d(R^* + M)$$

(10)

For one-to-one binding relationship, $M = 1 \times [AH] \Rightarrow [A] \times [10^{-pH}]$. Solving equation (10) for real-time resonance response unit (R_t) gives:

$$R_t = \frac{[T]k_a R_{max}}{[T]k_a + 10^{pH}k_d}\left(1 - \frac{1}{e^{(1/10^{pH}t)(10^{pH}k_d + k_a[T])}}\right) \tag{11}$$

$$\frac{[T]k_a R_{max}}{[T]k_a + 10^{pH}k_d} = R_{eq} \tag{12}$$

R_{eq} represents the equilibrium-binding signal between the aptamer and the target analyte, where there exists a steady state between the rates of association and dissociation. R_{eq} is a function of the total number of available binding sites on the aptamer, R_{max}, the kinetic rate constants, k_a and k_d, concentration of the target analyte [T], and the pH of the binding medium. This indicates that the pH of the binding medium significantly affects the equilibrium characteristics of the aptamer-target binding association and dissociation. For a given aptamer-target binding system with known kinetic constants under varying pH conditions, R_{eq} becomes a direct function of pH and the number of occupied binding sites as shown in Figure 3.
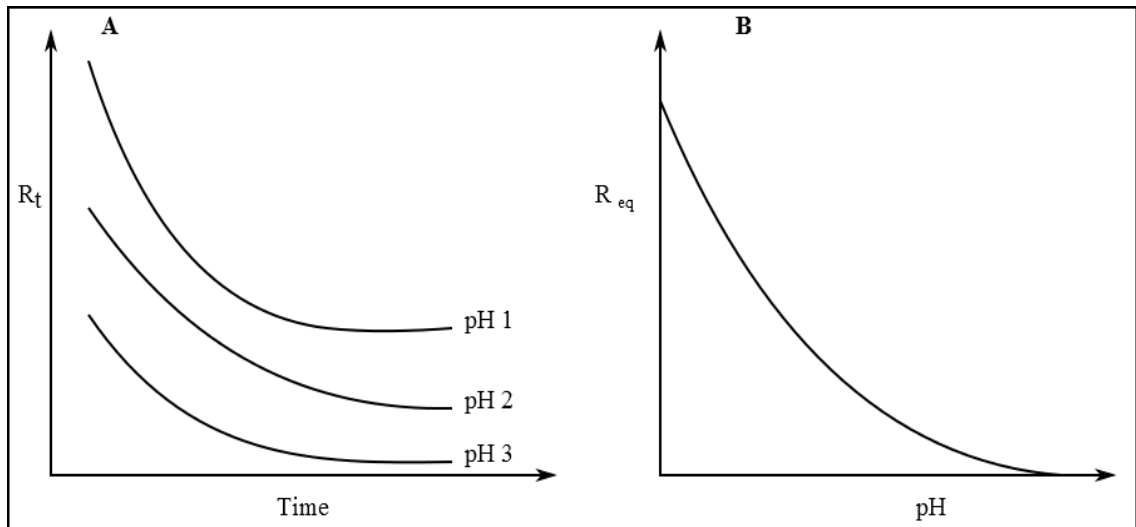
Figure 3. Effect of pH variation on (A) real-time binding signal where pH 3 > pH 2 > pH 1, and (B) equilibrium binding signal for a modelled aptamer-target binding scenario.

A sharp decrease in real-time binding is observed for signals modelled at low pH levels. Increasing the pH of the binding medium reduced the intensity of the instantaneous

binding signal. This demonstrates that pH increase results in increasing aptamer electronegativity due to deprotonation, significantly reducing electrostatic binding affinity with target molecules through intermolecular repulsion. This is in keeping with other experimentally published results showing the impact of pH on the structure of aptamer and/or target system and the resulting binding characteristics (Deng *et al.*, 2001; Hianik *et al.*, 2007). Hianik *et al.* (2007) reported that pH variation affects the structure of aptamer binding sites and obtained an optimum pH of 7.5 for 32-mer DNA aptamer-thrombin binding using a quartz crystal microbalance. It should however be noted that the choice of medium pH for optimal binding characteristics is dependent on the aptamer and target system (McKeague *et al.*, 2015). A logarithmic relationship between real-time binding signal and equilibrium binding signal was also observed in Figure 4. Thus, characteristic binding parameters can be globally fitted to provide a functional correlation for local R_{eq} kinetics.
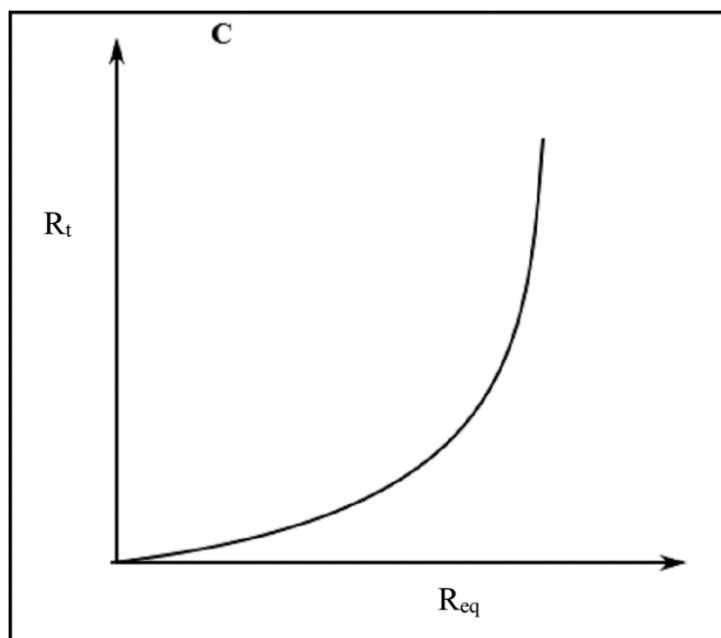
Figure 4. Relationship between equilibrium binding signal (Req) and real-time binding signal (Rt).

3.2   Stabilization effect of potassium ions (K$^+$)

To understand the effect of ionic strength on the binding features of aptamers in applications involving different buffer characteristics, the effect of ionic concentration was studied to provide a basis for optimising binding performance. Figure 5 shows that increasing concentration of K$^+$ ions results in decreasing electronegativity. The result

supports the argument that K^+ electrostatically interacts with the negative phosphate groups of the aptamer and also with free electrons at the O6 of guanine in G-quartet conformation, making the zeta potential less electronegative. The result also demonstrates that the binding effect of K^+ ions to the aptamer is not instantaneous but molecularly randomised during incubation until the spatial charge locus of binding stability is established within the system. The initial increase in electronegativity after 1 h for 1.5 M, 1.0 M and 0.01 M concentrations of K^+ ions could be due to early conformational changes of the aptamer molecule in the presence of the monovalent cation, favoring a random exposure of more anions to the surface. The zeta potential of TBA in the presence of 0.5 M and 1.0 M showed that high concentrations of K^+ ions result in increased stabilisation effect as the zeta value is highly electronegative. However, this stabilisation effect only lasted for ~ 0.5 h of binding.
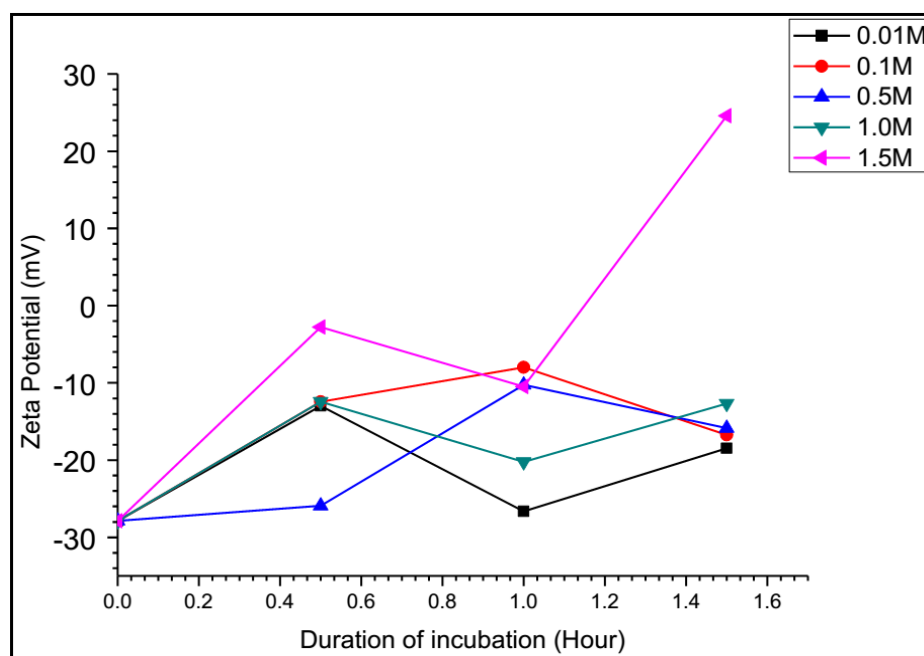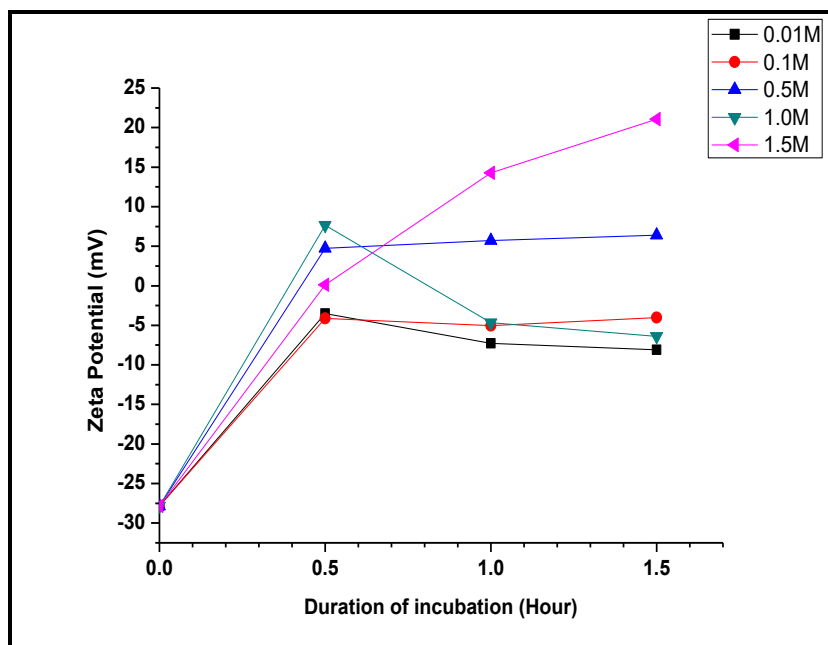

Figure 5. Effect of K^+ concentrations on the surface charge distribution of TBA after 1.5 h of incubation. Average plots for n=3 data sets.

Under high K^+ concentrations, there exists vigorous molecular interactions between the cations and the aptamer and this results in a diffusive binding mechanism. A positively charged shelter is created around the aptamer to neutralises available negative charges of the aptamer and cause the net charge to be less electronegative. The zeta potential value of TBA significantly shifted from -10.47 mV to +24.85 mV after 1.5 h of incubation with

1.5 M of K^+, indicating that high concentrations of K^+ can neutralise all the electronegative sites of the aptamer to project a positive zeta potential. High K^+ concentrations can also induce some subtle TBA structural changes. Zeta potential analysis for >1.5 M K^+ concentration was not carried out due to the formation of a large number of bubbles within the electrolytic cuvette. However, it can be predicted to be in the electropositive. TBA is most stable in potassium-induced G-quadruplex at K^+ concentration of 0.5 M after 0.5 h of incubation. The lack of uniformity in the zeta potential profiles for the different K^+ concentrations indicates conformational changes in the structure of TBA during incubation, and this is important to establish charge distribution stability after complexation.
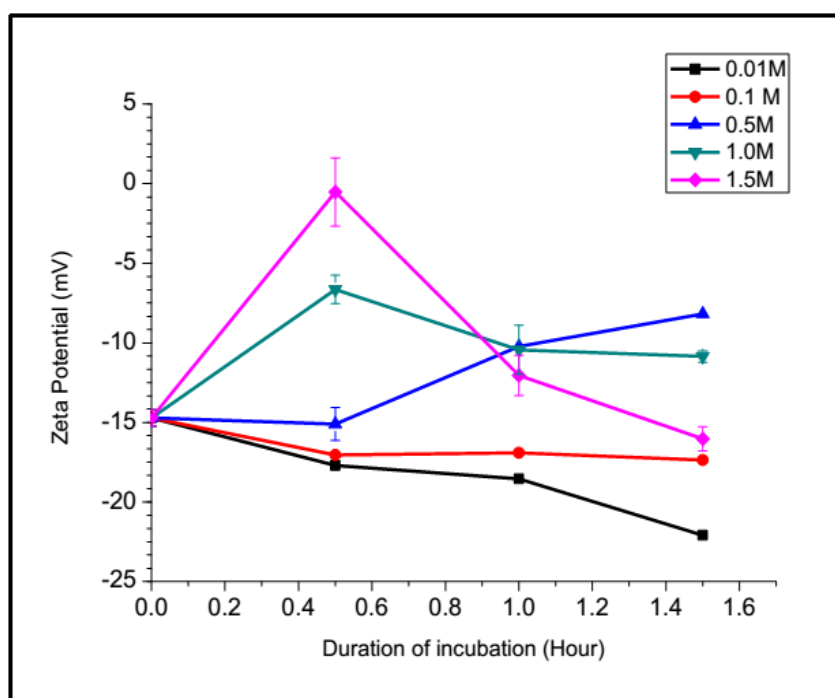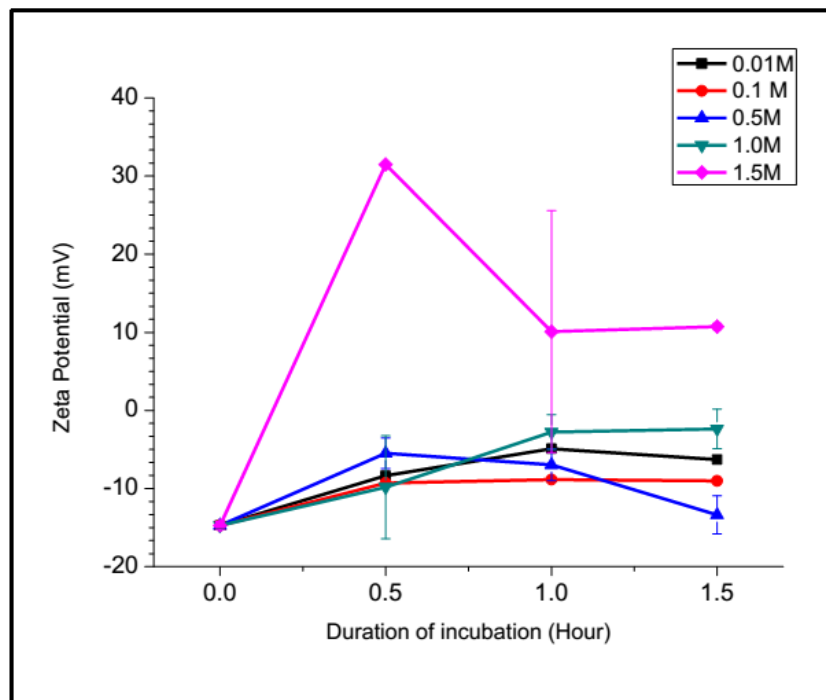

Figure 6. Effect of K^+ concentrations on the surface charge distribution of thrombin-TBA complex after 1.5 h of incubation. Average plots for n=3 data sets.

Figure 6 shows the zeta potential characterisation of thrombin-TBA complex in the presence of varying concentrations of K^+ ions. The zeta potential of thrombin-TBA complex after 0.5 h of incubation with no K^+ addition is -14.72 mV, which is comparable to -12.96 mV recorded as the zeta potential of TBA in the presence of 0.01 M K^+. This finding supports the argument that K^+-induced TBA G-quadruplex structure is similar to thrombin-induced structure in the absence of a stabilizing ion, such as K^+ ion, but with

some differences in their intramolecular configuration (Baldrich and O'Sullivan, 2005; Nagatoishi *et al.*, 2007). In the presence of thrombin, K^+ plays the role of stabilizing thrombin-TBA complex through structural changes in thrombin-TBA complex (Nagatoishi *et al.*, 2007; Russo Krauss *et al.*, 2013). The zeta potentials of thrombin-TBA complex in the presence of 0.01 M and 0.1 M K^+ ions indicate that K^+ increases the stability of the complex to a high electronegativity of -30 mV. K^+ ions are well-known as stabilizing cations of aptamer G-quadruplex structure (Nagatoishi *et al.*, 2007; Owczarzy *et al.*, 2008; Smestad and Maher, 2012).

The effect of high concentrations of K^+ became evident at 0.5 M when it resulted in reduced electronegativity. High K^+ concentrations drive non-specific interactions with the phosphate groups of TBA in a diffusive binding mechanism, causing the surface charge of the complex to be less electronegative. Compared to the effect of K^+ on TBA, the destabilizing effect of thrombin-TBA complex emerged at a higher K^+ concentration of 1.0 M. This shows that the binding of thrombin and TBA was by electrostatic interaction with thrombin and K^+ ions competing for negatively charged active sites on the TBA molecule. The destabilizing effect of thrombin-TBA complex at high K^+ concentrations was due to decreasing electronegativity from -14.72 mV in the absence of K^+ to -6.65 mV in 1.0 M K^+ and -0.52 mV in 1.5 M K^+. However, this destabilizing effect reduced after 1 h of incubation. The electronegativity increased to -10 mV and -16 mV for 1.0 M and 1.5 M K^+ respectively, and this could be due to the role of thrombin in the stabilisation of thrombin-TBA complex. Thrombin plays a key role in inducing electronegative charge distribution and stabilizing the G-quadruplex of TBA (Baldrich and O'Sullivan, 2005; Russo Krauss *et al.*, 2013).
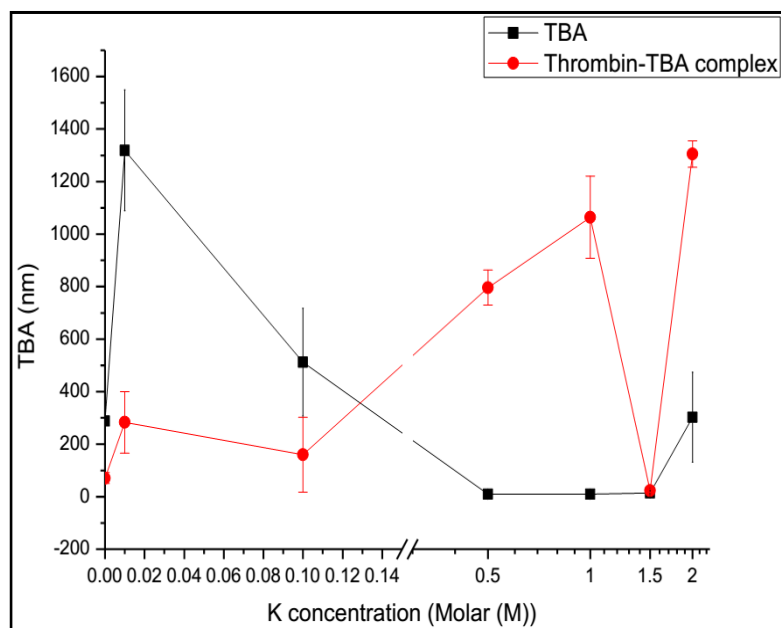
Figure 7. Effect of K$^+$ concentration on the average hydrodynamic size of TBA and thrombin-TBA complex. Average plots for n=3 data sets.

The data obtained for the effect of K$^+$ addition on the average hydrodynamic size of TBA (Figure 2) is in agreement with the zeta potential data shown in Figure 7. At low concentrations of K$^+$, the shielding effect of TBA reduces the repulsive force on the phosphate backbone and promoted intermolecular interaction, resulting in the increased hydrodynamic size of TBA at 0.01 M (1319 nm). The hydrodynamic size of TBA reduced from 9-14 nm in the presence of 0.5 M to 1.5 M K$^+$. K$^+$ ions stabilized the G-quadruplex structure of TBA by binding to the TGT loop above the G-tetrad or the one below the second G-tetrad through interactions between T4 and T13 (Mao *et al.*, 2004). The presence of K$^+$ also promotes the compaction of TBA structure, making the average hydrodynamic size small. At high K$^+$ concentrations, diffusive interactions with TBA happens, and this promotes intermolecular agglomeration to increase TBA hydrodynamic size. Marathias and Bolton (2000) reported a saturation limit of 2 M K$^+$ to stabilise the quadruplex structure of TBA (Marathias and Bolton, 2000). Extremely high K$^+$ concentrations interact non-specifically with TBA and promote molecular folding which destabilizes the G-quadruplex of TBA. The addition of K$^+$ ion increased the hydrodynamic size of thrombin-TBA complex in general. A significant size increase was observed in the presence of 0.5 M K$^+$; from 160 nm at 0.1 M K$^+$ to 796 nm at 0.5 M K$^+$. This finding was in agreement with zeta potential analysis where intermolecular repulsion reduces under high K$^+$

concentrations, leading to agglomeration of thrombin-TBA complex. This observation potentially hints that both K^+ and thrombin bind to the same binding sites on TBA, so the presence of thrombin isolates K^+ in solution minimising effective interactions necessary to cause compaction.

3.3   Effect of divalent Mg^{2+} ions on TBA and its binding activity

Figure 8 shows the charge distribution of TBA in the presence of varying concentrations of magnesium ion (Mg^{2+}). The results generally show decreasing electronegativity in the presence of Mg^{2+} due to electrostatic interactions between Mg^{2+} and the phosphate backbone of TBA via non-specific binding. This binding phenomenon results in a screening effect and neutralization of TBA negative charges. Mg^{2+} binds to TBA by inner sphere contact due to the high GC base pair structure of TBA (Noeske *et al.*, 2007). Under low Mg^{2+} concentrations, the electronegativity decreased and plateaued in the near zero region, whilst the charge distribution increased to electropositive for high Mg^{2+} concentrations. Near zero zeta potential facilitates molecular instability as a result of reduced intermolecular repulsion between TBA molecules. At 0.5 M Mg^{2+}, TBA exhibited a positive charge indicating the presence of excess Mg^{2+} residing on the structural surface of TBA to form a positive shield. The positive shielding effect results in intermolecular electrostatic repulsion of TBA molecules to form a more stable complex. The repulsive force between TBA molecules increases with increasing concentration of Mg^{2+} to 1.5 M. With further increase in Mg^{2+} concentration, molecular stability can be established in the electropositive region. The presence of Mg^{2+} facilitates the folding of TBA into different conformations with potentially different binding characteristics. Tan and Chen (2006) investigated the helix-helix interactions of a short DNA sequence (10bp) and they reported that divalent cations exhibit strong binding to DNA, inducing a self-organized correlated configuration (Tan and Chen, 2006). They also reported that intermolecular attraction between helices increases with the concentration of dication until 0.1 M. Dication concentration above 0.1 M causes repulsion between helices.

Figure 8. Effect of Mg^{2+} concentrations on the surface charge distribution of TBA after 1.5 h of incubation. Average plots for n=3 data sets.

The zeta potential of thrombin at pH 7.2 was determined to be -15.18 mV as shown in Figure 9. The presence of Mg^{2+} reduces the electronegativity of TBA. Hence, the binding of TBA to thrombin was favored in the presence of Mg^{2+}. The zeta potential of TBA in the presence of 0.01 M Mg^{2+} was -8.11 mV after 1.5 h of incubation. This value is close to the zeta potential of thrombin-TBA complex of -8.41 mV observed at the same Mg^{2+} concentration, showing that the presence of Mg^{2+} causes a conformational change in TBA for thrombin binding. The zeta potential of thrombin-TBA complex maintained electronegativity for Mg^{2+} concentrations less than 1.5 M, and this is due to the competitive binding of TBA between Mg^{2+} and thrombin. Above 1.5 M Mg^{2+} a more stable TBA-thrombin complex system can be generated.

Figure 9. Effect of Mg^{2+} concentration on the surface charge distribution of thrombin-TBA complex after 1.5 h of incubation. Average plots for n=3 data sets.

The hydrodynamic size of TBA generally increased in the presence of Mg^{2+} as shown in Figure 10. At low concentrations of Mg^{2+} (0.01 M), the size of TBA reduced significantly from 288 nm to 23.3 nm and the zeta potential data showed an electronegative profile. The pattern depicts a dose response in terms of Mg^{2+} concentration. Tan and Chen (2006) reported that the interaction of TBA with Mg^{2+} causes desolvation of Mg^{2+}, allowing small size Mg^{2+} ions to interact with TBA to cause compaction. They also discussed that the presence of high Mg^{2+} concentrations can facilitate helix-helix interactions, further affecting the degree compaction of DNA. The hydrodynamic size of TBA increased in the presence 0.1 M Mg^{2+} to 3770 nm.
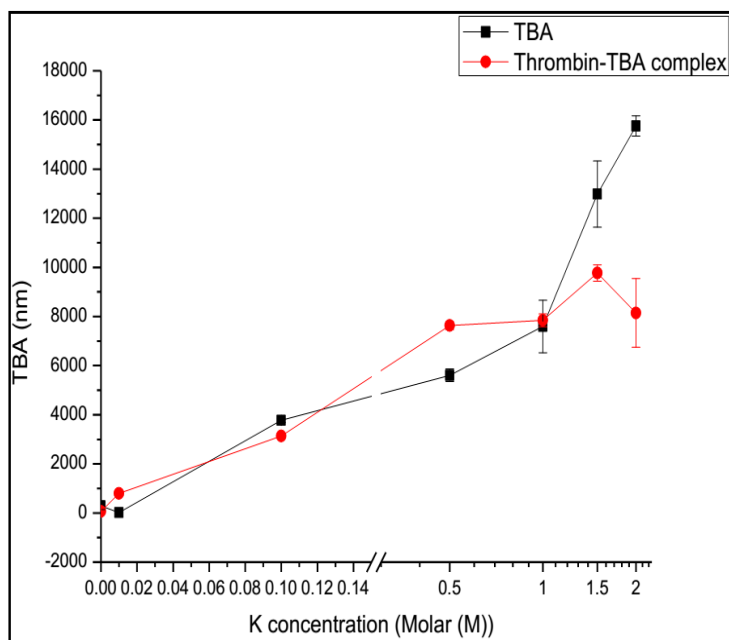
Figure 10. Mean hydrodynamic size of TBA and thrombin-TBA complex in the presence of Mg^{2+} ranging from 0.01 M to 2.0 M. Average plots for n=3 data sets.

The increase in hydrodynamic size could also be due to the screening effect of Mg^{2+} which provides outer-layer electrostatic binding sites for more negatively charged aptamers in a multi-layered pattern. The presence of Mg^{2+} can cause structural reorganization of TBA to expose negative charges of TBA to interact with Mg^{2+} ions bound to another TBA (Draper *et al.*, 2005; Tan and Chen, 2006).

The presence of Mg^{2+} increased the hydrodynamic size of thrombin-TBA complex. The size of the complex increased from 70.8 nm to 798.3 nm in the presence of 0.01 M Mg^{2+}. The size of complex further increased with increasing Mg^{2+} concentration until 0.5 M. Further increase in Mg^{2+} concentration did not demonstrate a significant effect on the hydrodynamic size of TBA-thrombin complex. From the zeta potential analysis, it was deduced that above 1.5 M Mg^{2+}, a more stable TBA-thrombin complex is formed. This is evident by the hydrodynamic size measured at 2.0 M, where the size of thrombin-TBA complex is slightly smaller compared to the size at 1.5 M.

3.4   Effect of temperature on the folding of TBA and complex

Temperature is known to affect the kinetics of binding between an aptamer and its target. However, the effect of temperature on charge and biomolecular intereaction dynamics is

not well reported. Figure 11 shows the effect of temperature on the charge and size distribution of TBA and TBA-thrombin complex. TBA was found to be most stable at ~20 °C with a zeta potential of -44.61 mV. Increase in temperature reduced the electronegativity of TBA affecting its stability. This could be due to reduced molecular enthropy which facililates condensation of TBA thereby exposing reduced surface electronegative polarity. This supports findings by Baldrich and co-workers (Baldrich and O'Sullivan, 2005). They reported that low temperatures favour the folding of TBA. TBA folds as a G-quadruplex structure at temperatures lower than 24 °C. They demonstrated through NMR analysis that the configuration of G-quadruplex formed under low temperature was intramolecularly different from G-quadruplex induced by K^+. This can be depicted from the different zeta potentials for TBA at 20 °C (-44.61 mV) and the reading obtained in the presence of K^+ (-26.65 mV to 24.59 mV). By comparing the zeta potentials, the G-quadruplex structure formed under low temperature conditions is more stable than G-quadruplex structure induced by the presence of K^+.
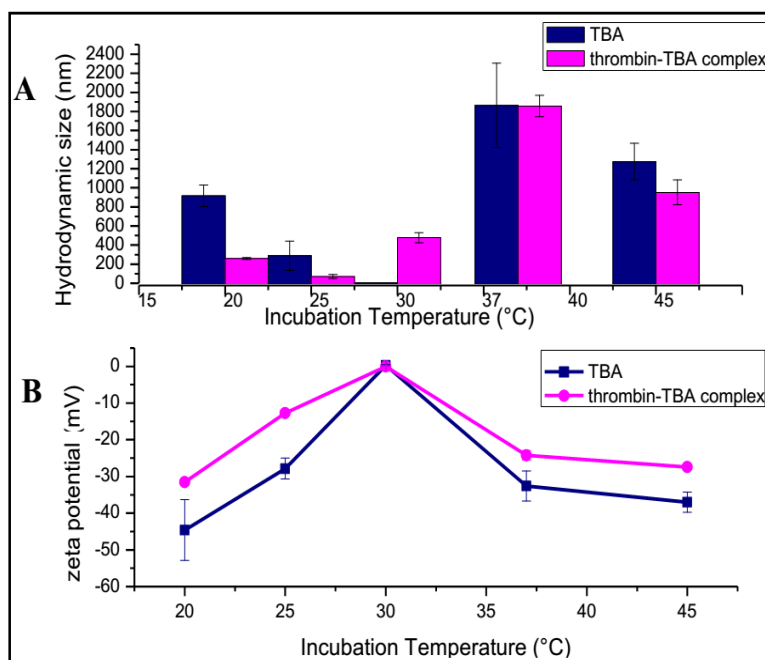
Figure 11. Effect of temperature on the zeta potential and mean hydrodynamic size of TBA and thrombin-TBA complex in Tris-EDTA buffer, pH 8. Average plots for n=3 data sets.

As shown in Figure 11 (B), zeta potential for TBA decreased to -12.76 mV at 25 °C, suggesting that temperature increase inhibits the formation of stable G-quadruplex

structure. TBA was found to be most unstable at 30 °C with a zeta potential reading of 0.29 mV. A further increase in temperature to 37 °C and 45 °C resulted in improved zeta potential readings of -32.61 mV and -37.02 mV respectively. The zeta potential at 30 °C indicates closeness to a higher temperature than the melting temperature (T_m) of G-quadruplex of TBA. Under this condition, the G-quadruplex relaxes back to the native aptamer conformation with exposed electronegative surfaces. Comparing this to findings from Nagatoishi et al., (2011), 30 °C is higher than the melting temperature of TBA G-quadruplex which is 23.1°C (Nagatoishi *et al.*, 2007).

The zeta potential profile of thrombin-TBA complex under varying temperature conditions follows the same trend as TBA. Thrombin-TBA complex established stability at 20 °C with a zeta potential of -31.54 mV. It has been reported that temperatures lower than 24 °C favour G-quadruplex formation of TBA, and folding only occurs at temperatures in the presence of K^+ (Baldrich and O'Sullivan, 2005). Between 25-30 °C incubation temperature, the formation of G-quadruplex, which facilitates stable thrombin-TBA complexation, is not favored. Above 35 °C, which is beyond the melting temperature of TBA G-quadruplex, the thrombin-TBA complex formation is stable. As explained ealier, at temperatures beyond the meting point, TBA G-quadruplex relaxes to its original conformation with more electronegative surfaces exposed. Notwithstanding, the degree of stability associated with TBA at temperatures beyond G-quadruplex melting point is higher than the stability of the TBA-thrombin complex under the same temperature conditions. Figure 11 (A) shows the hydrodynamic size distribution of both TBA and TBA-thrombin complex under various incubation temperatures. The size of TBA reduced from 20 °C to 30 °C. TBA was found to be smallest at 30 °C though the corresponding zeta potential showed the lowest stability which faciliates agglomeration. This observation hints that the cylce of formation and relaxation of G-quadruplex is over a tight temperature range between the meting point temperature T_m and the temperature commencement point for relaxation (T_r). Between the temperature range of T_m-T_r (where $T_r > T_m$), no significant change in hydrodynamic size would be expected. At higher temperatures $T > T_r$, such as 37 °C and 45 °C, the hydrodyanmic size of TBA significantly increased to 1863.6 nm and 1274.5 nm due to molecular relaxation. Thrombin-TBA complex generally demonstrated a smaller size compared to TBA except at 30 °C. This observation is due to a potential

temperature shift in the relxation cycle TBA quadruplex in the presence of thrombin, resulting in slightly increased thermal resistivity of the complex.

3.5   Scatchard analysis

Scatchard analysis is widely used to evaluate ligand-target binding parameters including association constant, number of binding sites, and ligand binding capacity (Barri *et al.*, 2008). Scatchard analysis was used in this work to study the binding characteristics of metal ions (Mg^{2+} and K^+) and TBA or TBA-complex in order to evaluate the effect of metal ions on aptamer-target binding. Figure 12 (A) shows curved Scatchard plots for Mg^{2+} and K^+ displaying an inverse cooperatively pattern. Curved Scatchard plot is attributed to cooperative binding and binding heterogeneity. For Mg^{2+}-TBA binding, a concave upward pattern was observed with the theoretical number of bound cation per molecule of TBA being ~0.07. Concave upward Scatchard pattern could be the result of negative cooperativity and/or heterogeneity in binding affinity. Negative cooperativity refers to the binding of ligands under reduced binding affinity to the receptor. Previous studies have shown that the presence of Mg^{2+} enhances the binding affinity of aptamers (Deng *et al.*, 2001; Hartwig, 2001; Cruz-Aguado and Penner, 2008; Girardot *et al.*, 2010), so the concave downwards pattern observed for Mg^{2+} treatment may only be due to heterogeneity of the binding site. This can be explained by the presence of multiple binding sites on TBA that confer different molecular interactions and binding affinities.
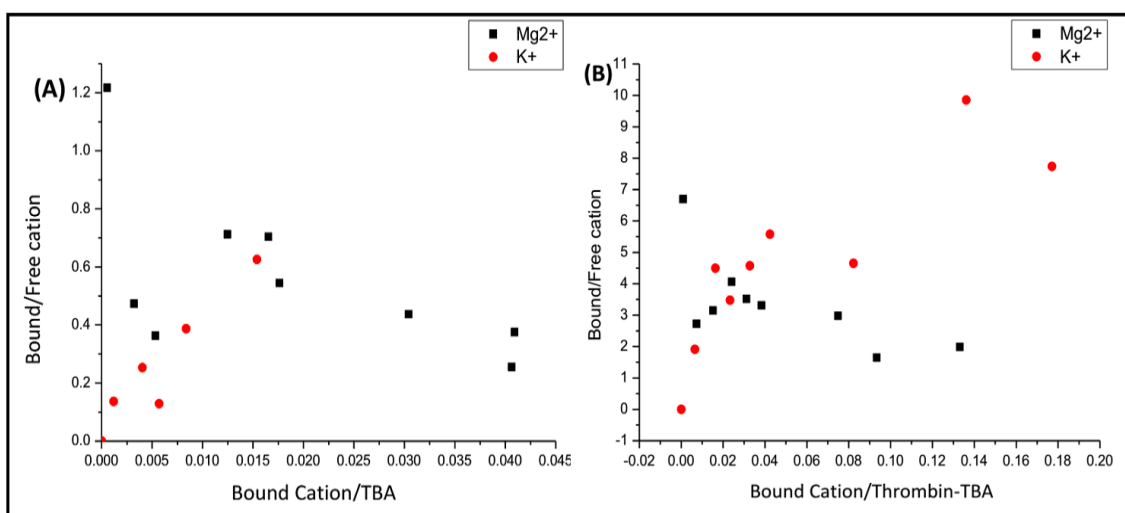
Figure 12. Scatchard plots for TBA and thrombin-TBA complex. (A) TBA was incubated with Mg^{2+} or K^+ over the concentration range: 0.01 M, 0.1 M, 0.5 M, 1 M, 1.5 M and 2

M. (B) Thrombin-TBA complex was incubated with Mg^{2+} or K^+ over the same concentration range as in (A).

Previous studies have shown that Mg^{2+} induces conformational changes in TBA (Tan and Chen, 2006; Noeske *et al.*, 2007; Girardot *et al.*, 2010), to result in the creation of heterogeneous binding sites. Heterogeneity in the binding affinity results in ligands binding to higher affinity sites first before lower affinity sites, creating the pattern of the same phenomenon as negative cooperativity. The binding of Mg^{2+} to TBA involves three types: basic binding, crosslinking and closure binding. Basic binding happens when one Mg^{2+} binds to one binding site of TBA and there is no sharing of Mg^{2+} between TBA molecules as shown in Figure 13 (A). Crosslinking interaction refers to binding of one Mg^{2+} to more than one TBA, and the TBA binding site is not saturated with Mg^{2+} (refer to Figure 13 B). As shown in Figure 13 (C), closure binding refers to the saturation binding of TBA by Mg^{2+}. There was a change of concavity observed in the Scatchard plot for Mg^{2+}-TBA binding. Change of concavity from concave down to concave up is usually observed when closure binding dominates the other binding types (Wofsy and Goldstein, 1992).
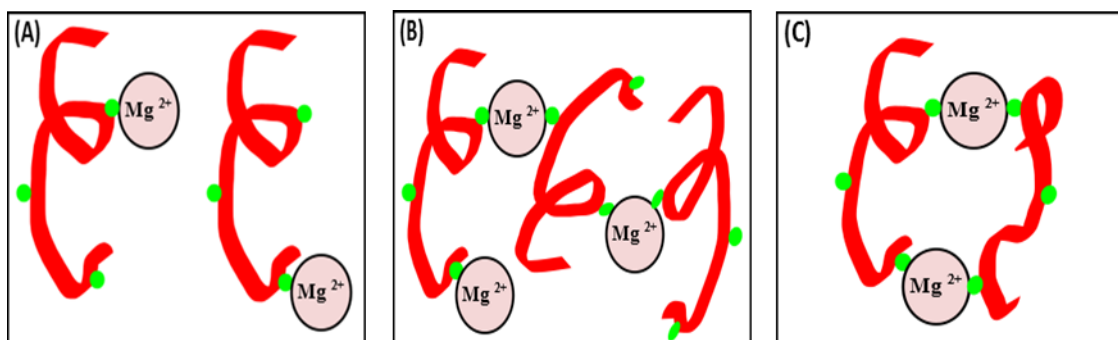
Figure 13. Illustration of Mg^{2+} and TBA binding types; (A) Basic binding, (B) crosslinking, (C) closure binding. The green circle indicates Mg^{2+} binding site of TBA.

K^+-TBA displays a positive cooperativity (increasing bound/free cation concentrations with increasing bound cation/TBA concentrations), meaning that the binding of K^+ to TBA increases the binding affinity of TBA. This is in agreement with the previous results showing that the binding of K^+ to TBA stabilizes the TBA G-quadruplex structure and enhances the binding affinity of TBA. The result indicates that K^+ confers a relatively higher binding capacity per molecule of TBA than Mg^{2+} due to the small and monovalent nature of K^+. Hence, the total charge distribution of K^+ per molecule of TBA is higher than

Mg^{2+}, and this contributes to the higher degree of aggregation of TBA. K_a values were determined with the assumption that there is only one type of binding site, and the binding affinity remains unchanged. From Table 1, the binding affinity of Mg^{2+} to TBA is 500 fold higher than that of K^+. This finding is in keeping with previously reported data by Korolev and co-workers in their competitive binding study of different metal ions to DNA. They mentioned that Mg^{2+} has a better DNA affinity compared to K^+ (Korolev *et al.*, 1999).

Table 1. Affinity binding constant (K_a) data for Mg^{2+} and K^+ from Scatchard analysis.

Binding affinity- K_a (M)	Mg^{2+}	K^+
TBA	11.25	0.02
Thrombin-TBA complex	21.90	39.73

Thrombin-TBA complex followed the same binding distribution trend as TBA upon interaction with Mg^{2+} and K^+ but at a higher gradient. Mg^{2+}-thrombin-TBA complex showed a downwards Scatchard plot whereas K^+-Thrombin-TBA complex showed a positive co-operativity. The maximum number of bound cations per Mg^{2+}-Thrombin-TBA complex was ~0.2, and this is only slightly higher than that of the binding with TBA. This supports the argument that the stability of TBA-thrombin complex reduces the effect caused by Mg^{2+} binding with neighbouring Mg^{2+}-Thrombin-TBA complex. The higher gradient slope for thrombin-TBA complex shows that both metal ions possess a relatively higher affinity towards thrombin-TBA complex as compared to TBA.

4.   CONCLUSION

The paper attempts to provide theoretical insights into the dependence of TBA and thrombin-TBA binding stability on hydrodynamic charge and size distributions in the presence of metal ions and changing physicochemical conditions. TBA was electronegative under pH > 5, and was most dispersed and stable above pH 9. It was demonstrated that pH affects the binding affinity of TBA through protonation and deprotonation mechanisms, potentially resulting in some conformational changes in TBA. Thrombin-TBA complex was determined to be electronegative, and maintained electronegativity over the pH range investigated. The presence of metal ions influenced

the formation of TBA secondary structures and the resulting thrombin-TBA complexation. K^+ induced the formation of G-quadruplex in TBA under a charge distribution stability similar to thrombin-induced G-quadruplex. The presence of K^+ also reduced the electronegativity of TBA, and at low concentrations, K^+ stabilizes the formation of TBA G-quadruplex structure. Thrombin-TBA complex is considered most dispersed and stable at 10 mM K^+ concentration. The presence of Mg^{2+} reduced the electronegativity of TBA aggressively and favoured binding to thrombin. TBA and thrombin-TBA complex are considered stable in the presence of Mg^{2+} at concentrations > 1.5 M. TBA was found to be most stable at temperature ~20 °C with reduction in electronegativity as temperature increased. TBA regained the structure flexibility at temperature above melting temperature (Tm). Scatchard plot analysis for Mg^{2+} with TBA and thrombin-TBA complex showed that the presence of Mg^{2+} gives a concave upward trend indicating binding heterogeneity. K^+ with thrombin-TBA complex displayed positive cooperativity. Whilst this work provides fundamental applications of zeta measurements to probe the binding characteristics and stability relationships between TBA, thrombin and metal ions presence under varying physicochemical conditions, it is important to mention that more sophisticated bioanalytical and stereochemical approaches are required to completely understand the spatial conformational changes of TBA and thrombin-TBA complexation during binding events.

5. ACKNOWLEDGEMENT

6. REFERENCES

Acquah, C., M.K. Danquah, J.L.S. Yon, A. Sidhu and C.M. Ongkudon, 2015. A review on immobilised aptamers for high throughput biomolecular detection and screening. Analytica chimica acta, 888: 10-18. Available from http://www.sciencedirect.com/science/article/pii/S0003267015008016. DOI http://dx.doi.org/10.1016/j.aca.2015.05.050.

Adamczyk, Z., M. Zaucha and M. Zembala, 2010. Zeta potential of mica covered by colloid particles: A streaming potential study. Langmuir : the ACS journal of surfaces and colloids, 26(12): 9368-9377.

Baldrich, E. and C.K. O'Sullivan, 2005. Ability of thrombin to act as molecular chaperone, inducing formation of quadruplex structure of thrombin-binding aptamer. Analytical biochemistry, 341(1): 194-197.

Barri, T., T. Trtić-Petrović, M. Karlsson and J.Å. Jönsson, 2008. Characterization of drug–protein binding process by employing equilibrium sampling through hollow-fiber supported liquid membrane and bjerrum and scatchard plots. Journal of pharmaceutical and biomedical analysis, 48(1): 49-56.

Chang, A.L., M. McKeague, J.C. Liang and C.D. Smolke, 2014. Kinetic and equilibrium binding characterization of aptamers to small molecules using a label-free, sensitive, and scalable platform. Analytical chemistry, 86(7): 3273-3278.

Cruz-Aguado, J.A. and G. Penner, 2008. Determination of ochratoxin a with a DNA aptamer. Journal of agricultural and food chemistry, 56(22): 10456-10461.

Deng, Q., I. German, D. Buchanan and R.T. Kennedy, 2001. Retention and separation of adenosine and analogues by affinity chromatography with an aptamer stationary phase. Analytical chemistry, 73(22): 5415-5421. DOI 10.1021/ac0105437.

Draper, D.E., D. Grilley and A.M. Soto, 2005. Ions and rna folding. Annu. Rev. Biophys. Biomol. Struct., 34: 221-243.

Ellington, A.D. and J.W. Szostak, 1990. In vitro selection of rna molecules that bind specific ligands. Nature, 346(6287): 818-822.

Girardot, M., P. Gareil and A. Varenne, 2010. Interaction study of a lysozyme-binding aptamer with mono-and divalent cations by ace. Electrophoresis, 31(3): 546-555.

Girardot, M., H. Li, S. Descroix and A. Varenne, 2013. Aptamer–target interaction: A comprehensive study by microchip electrophoresis in frontal mode. Chromatographia, 76(7-8): 305-312.

Hamaguchi, N., A. Ellington and M. Stanton, 2001. Aptamer beacons for the direct detection of proteins. Analytical biochemistry, 294(2): 126-131.

Hartwig, A., 2001. Role of magnesium in genomic stability. Mutation Research/Fundamental and Molecular Mechanisms of Mutagenesis, 475(1): 113-121.

Hianik, T., V. Ostatna, M. Sonlajtnerova and I. Grman, 2007. Influence of ionic strength, ph and aptamer configuration for binding affinity to thrombin. Bioelectrochemistry, 70(1): 127-133. Available from http://www.ncbi.nlm.nih.gov/pubmed/16725379. DOI 10.1016/j.bioelechem.2006.03.012.

Korolev, N., A.P. Lyubartsev, A. Rupprecht and L. Nordenskiöld, 1999. Competitive binding of mg 2+, ca 2+, na+, and k+ ions to DNA in oriented DNA fibers: Experimental and monte carlo simulation results. Biophysical journal, 77(5): 2736-2749.

Lin, P.-H., R.-H. Chen, C.-H. Lee, Y. Chang, C.-S. Chen and W.-Y. Chen, 2011. Studies of the binding mechanism between aptamers and thrombin by circular dichroism, surface plasmon resonance and isothermal titration calorimetry. Colloids and Surfaces B: Biointerfaces, 88(2): 552-558.

Mao, X.-a., L.A. Marky and W.H. Gmeiner, 2004. Nmr structure of the thrombin-binding DNA aptamer stabilized by sr2+. Journal of Biomolecular Structure and Dynamics, 22(1): 25-33.

Marathias, V.M. and P.H. Bolton, 2000. Structures of the potassium-saturated, 2: 1, and intermediate, 1: 1, forms of a quadruplex DNA. Nucleic acids research, 28(9): 1969-1977.

McKeague, M., E. McConnell, J. Cruz-Toledo, E. Bernard, A. Pach, E. Mastronardi, X. Zhang, M. Beking, T. Francis, A. Giamberardino, A. Cabecinha, A. Ruscito, R. Aranda-Rodriguez, M. Dumontier and M. DeRosa, 2015. Analysis of in vitro aptamer selection parameters. Journal of Molecular Evolution, 81(5): 150-161. DOI 10.1007/s00239-015-9708-6.

Nagatoishi, S., Y. Tanaka and K. Tsumoto, 2007. Circular dichroism spectra demonstrate formation of the thrombin-binding DNA aptamer g-quadruplex under stabilizing-cation-deficient conditions. Biochemical and biophysical research communications, 352(3): 812-817.

Nezlin, R., 2016. Use of aptamers in immunoassays. Molecular Immunology, 70: 149-154.

Noeske, J., H. Schwalbe and J. Wöhnert, 2007. Metal-ion binding and metal-ion induced folding of the adenine-sensing riboswitch aptamer domain. Nucleic acids research, 35(15): 5262-5273.

Ostatná, V., H. Vaisocherová, J. Homola and T. Hianik, 2008. Effect of the immobilisation of DNA aptamers on the detection of thrombin by means of surface plasmon resonance. Analytical and bioanalytical chemistry, 391(5): 1861-1869.

Owczarzy, R., B.G. Moreira, Y. You, M.A. Behlke and J.A. Walder, 2008. Predicting stability of DNA duplexes in solutions containing magnesium and monovalent cations. Biochemistry, 47(19): 5336-5353.

Robertson, D.L. and G.F. Joyce, 1990. Selection in vitro of an rna enzyme that specifically cleaves single-stranded DNA. Nature, 344(6265): 467-468.

Russo Krauss, I., A. Pica, A. Merlino, L. Mazzarella and F. Sica, 2013. Duplex-quadruplex motifs in a peculiar structural organization cooperatively contribute to thrombin binding of a DNA aptamer. Acta crystallographica. Section D, Biological crystallography, 69(Pt 12): 2403-2411. Available from http://www.ncbi.nlm.nih.gov/pubmed/24311581. DOI 10.1107/S0907444913022269.

Smestad, J. and L.J. Maher, 2012. Ion-dependent conformational switching by a DNA aptamer that induces remyelination in a mouse model of multiple sclerosis. Nucleic acids research: gks1093.

Song, Y., K. Zhao, M. Li, X. Pan and D. Li, 2015. A novel method for measuring zeta potentials of solid–liquid interfaces. Analytica chimica acta, 853: 689-695.

Tan, Z.-J. and S.-J. Chen, 2006. Ion-mediated nucleic acid helix-helix interactions. Biophysical journal, 91(2): 518-536.

Tasset, D.M., M.F. Kubik and W. Steiner, 1997. Oligonucleotide inhibitors of human thrombin that bind distinct epitopes. Journal of molecular biology, 272(5): 688-698.

Tuerk, C. and L. Gold, 1990. Systematic evolution of ligands by exponential enrichment: Rna ligands to bacteriophage t4 DNA polymerase. Science, 249(4968): 505-510.

Wofsy, C. and B. Goldstein, 1992. Interpretation of scatchard plots for aggregating receptor systems. Mathematical biosciences, 112(1): 115-154.

SECTION 5.2

Aptamer-anchored poly(EDMA-co-GMA) monolith for high throughput affinity binding

Caleb Acquah, Michael K. Danquah, Yi Wei Chan, Charles K.S. Moy, Lau Sie Yon, Clarence M. Ongkudon

'TO BE PUBLISHED'

DECLARATION FOR THESIS SECTION 5.2

Aptamer-anchored poly(EDMA-co-GMA) monolith for high throughput affinity binding

The candidate will like to declare that there is no conflict of interests involved in this work and that my extent of contribution as candidate is as shown below:

Contribution of Candidate	Conceptualisation, initiation and write-up	75%

The following co-authors were involved in the development of this publication and attest to the candidate's contribution to a joint publication as part of his thesis. Permission by co-authors are as follows:

Name	Signature	Date
Michael K. Danquah		13.07.2017
Lau Sie Yon		13.07.2017
Charles K.S. Moy		13.07.2017
Yi Wei Chan		13.07.2017
Clarence M. Ongkudon		13.07.2017

ABSTRACT

Aptamers are *in vitro* 'chemical antibodies' generated by means of an iterative process known as Systematic Evolution of Ligands by Exponential Enrichment (SELEX). They are short, single-stranded RNA or DNA sequences and have emerged as a new class of biomolecular probes. Aptamers can selectively interact with specific targets, such as proteins, cells, and biochemicals with tighter and more specific binding characteristics compared to antibodies. Aptamers are generated inexpensively, easily, reproducibly, and are simple to modify and integrate into different analytical systems. Immobilisation of aptameric ligands on solid stationary supports for effective binding of target molecules requires understanding of the relationship between aptamer-polymer interactions and the conditions governing the mass transfer of the binding process. Herein, we investigate key process parameters affecting the molecular anchoring of a thrombin-binding aptamer onto polymethacrylate monolith pore surface, and the binding characteristics of the resulting aptasensor. FT-IR spectroscopic analysis and thermogravimetric analyses were used to characterise the available functional groups and thermo-molecular stability of the immobilised polymer generated with Schiff-base activation and immobilisation scheme. The initial degradation temperature of the polymethacrylate stationary support increased with each step of the Schiff-base process: poly(EDMA-co-GMA) [196.0 $^{\circ}$C ($\pm$1.8)]; poly(EDMA-co-GMA)-EDA [235.9 $^{\circ}$C ($\pm$6.1)]; poly(EDMA-co-GMA)-EDA-GA [255.4 $^{\circ}$C ($\pm$2.7)]; and Aptasensor [273.7 $^{\circ}$C ($\pm$2.5)]. These initial temperature increments reflected in the associated endothermic energies determined with disc scanning calorimetry (DSC). The aptameric ligand density obtained after immobilisation was 480 pmol/uL. Increase in pH and ionic concentration affected the surface charge distribution and the binding characteristics of the macroporous aptasensors, resulting in the optimum binding pH and ionic concentration of pH 8 and 5 mM Mg^{2+} respectively. These results are very critical in understanding and setting parametric constraints essential to develop and enhance the performance of aptasensors.

Keywords: Aptamer; Affinity Binding; Polymethacrylate; Thermogravimetric Analysis; Biophysical Characterisation; Liquid Chromatography.

1.   INTRODUCTION

Biosensors utilise specific bioprobes to detect and analyse target molecules (Velusamy *et al.*, 2010; Kirsch *et al.*, 2013; Pakchin *et al.*, 2017). They have attracted significant attention in research and applications for medical diagnosis and prognosis, as well as the detection of environmental contaminants such as pesticides and heavy metals (Mascini and Tombelli, 2008; Lopez-Barbosa *et al.*, 2016). Unlike conventional cellular and biochemical methods, bioaffinity sensing is largely devoid of long sample processing times, offer specific and selective target binding, and can be inexpensive to develop (Acquah *et al.*, 2015).

Various kinds of bioaffinity probes exist for the development of biosensors. These include antibodies, enzymes, cells and aptamers. Antibodies are generally the most utilised bioaffinity probes in the design of biosensors, and are uniquely referred to as immunosensors. However, the development and application of antibodies as bioaffinity probes is challenged by ethical issues, high cost of production, binding specificity, bioavailability, immunogenicity, thermal stability and short shelf-life (Acquah *et al.*, 2015; Chen and Yang, 2015; Tan *et al.*, 2016).

Aptamers are short single stranded oligonucleotides that can be generated and chemically synthesised to target a wide range of proteins, cells, lipids and ions. These cognate targets are popularly known as 'apatopes'. Aptamer-target interactions are non-covalent and are based on any or a combination of the following: electrostatic, hydrogen bonding, aromatic stacking, hydrophobic, and Van der Waals interactions (Acquah *et al.*, 2015; Schulz *et al.*, 2016). Aptamers are developed through a robust iterative process known as <u>S</u>ystematic <u>E</u>volution of <u>L</u>igands by <u>Ex</u>ponential enrichment (SELEX) (Robertson and Joyce 1990; Tuerk and Gold 1990; Ellington and Szostak 1990). Owing to the rigorous iterative SELEX process, aptamers inherently possess better binding strength and specificity than antibodies. They also possess other advantageous production, biophysical and biochemical attributes including a large array of target space, low cost of production, thermal and chemical stability, low to no ethical issues, prolonged shelf-life / reusability and simple pre-/post biomodification mechanisms (Ilgu and Nilsen-Hamilton, 2016; Nezlin, 2016; Monaco *et al.*, 2017).

Molecular interactions between aptamers and their targets are affected by the physicochemical conditions of the binding environment including ionic concentration, pH, type and characteristics of the support matrix , aptamer modifications, and temperature (Hianik *et al.*, 2007; Oktem *et al.*, 2007). The immobilisation of aptamers to form aptasensors enhances their reusability through successive regeneration for continuous flow application (Jiang *et al.*, 2017; Su *et al.*, 2017). In recent times, the immobilisation of aptamers on macroporous monolithic matrices to form aptasensors with convective flow characteristics for high throughput biosensing and bioseparation applications have become a major research endeavour (Zhao *et al.*, 2008; Han *et al.*, 2012; Brothier and Pichon, 2014; Du *et al.*, 2015). Polymethacrylate monoliths, by virtue of their tunable macroporous structure, biocompatibility and simple functionalisation chemistries, have gained interest for use as the synthetic polymer core for the development of biosensors for high throughput applications (Roberts *et al.*, 2009; Acquah *et al.*, 2016). Molecular coupling of aptamers on polymethacrylate monoliths through Schiff-base chemistry ensures the formation of a covalently bonded interaction between the monolith and aptamer (Brothier and Pichon, 2014), and this reduces the likelihood of potential leaching of aptameric ligand. In addition, it incoporates a spacer-arm through amine-aldehyde linking groups to prevent the occurrence of steric hindrance. Amongst the limited number of reported studies investigating the suitability of various coupling chemistries for the developoment of macroporous aptsensors, none have focused on probing the impact of biophysical and biochemical parameters on the binding characteristics and performance of the aptasensor. This work seeks to synthesise and evaluate the chromatographic binding performance of poly(EDMA-co-GMA) macroporous disk-aptasensors under varying physicochemical conditions. The impact of key physicochemical parameters on the surface charge distribution of the aptsensor is also investigated.

2. EXPERIMENTAL

2.1 Materials

Modified 15-mer thrombin binding DNA aptamers (TBA) with the sequence 5'-/5AmMC6/GGT TGG TGT GGT TGG-3' was synthesised by Base pair biotechnologies

(Malaysia). The following chemicals were purchased from Sigma-Aldrich (USA): ethylene glycol dimethacrylate, EDMA, (MW 198.22, 98%); glycidyl methacrylate, GMA, (MW 142.15, 97%); methanol (HPLC grade, MW 32.04, 99.93%); azobisisobutyronitrile, AIBN, (MW 164.21 g/mol, 98%); cyclohexanol (MW 100.16, 99%); hydrochloric acid (HCl, MW 36.5, 37%); phosphate buffer solutions (PBS); Trizma HCl (MW 157.60, 99%); ethylenediaminetetraacetic acid (MW 292.24, 99%); sodium cyanoborohydride (MW 62.84, 95%); sodium perchlorate (MW 122.44 g/mol, 98%); ethylenediamine, EDA, (MW 60.10, 99%); glutaraldehyde, GA, (MW 100.12, 25%); and human alpha thrombin.

2.2 Methods

2.2.1 Synthesis of polymethacrylate monoliths

Disk polymethacrylate monoliths were synthesised *in situ* via free radical polymerisation as reported previously by our group (Ongkudon and Danquah, 2010; Acquah *et al.*, 2017). In brief, 0.5 mL of monoliths were prepared using 60/40 % v/v of monomer to porogen composition. The monomeric composition constituted 60% v/v GMA as the functional monomer and 40% v/v EDMA as the cross-linker. Cyclohexanol was used as the porogen, and the polymerisation mixture was sonicated for 10 min. The mixture was transferred into a 1.5 cm I.D BIORAD polypropylene column and sparged with nitrogen for about 10 min. The column was sealed and polymerisation commenced isothermally at a set point temperature of 65 ^{o}C for 16 h. The disk polymethacrylate monoliths formed were washed with methanol followed by deionised water using NGC Discover chromatography (Next Generation Chromatography Discover 100 Chromatography system, BIORAD, Melbourne, Australia) system until a constant baseline was obtained over an extended period of time. The washed monoliths were stored under wet conditions at 4 ^{o}C for activation and functionalisation.

2.2.2 Aptamer immobilisation

Prior to activation and functionalisation, the disk monoliths were incubated at 60 ^{o}C to remove bubbles trapped within the pores of the adsorbent. Thrombin binding aptamer stock solutions of 100 μM were prepared with phosphate buffer A (10 mM phosphate

buffer + 20 mM potassium chloride + 137 mM sodium chloride + 5 mM MgCl$_2$ at pH 7.4) and stored at -20 ^{o}C. Aptamer immobilisation was performed by recirculation of aptamer solution using the HPLC system through the Schiff-base activation chemistry. In the Schiff-base activation, the monoliths were interacted with 15 mL of EDA at 60 ^{o}C for 12 h, rinsed with deionised water to remove any residual EDA, and exposed to 15 mL of 10% GA solution at 25 ^{o}C. The glutaraldehyde functionalised monoliths were equilibrated with buffer A followed by 20 µM aptamer covalent immobilisation at 0.2 mL/min. Aptamer-immobilised monoliths (macroporous aptasensors) were later washed with buffer A to remove non-specifically bound aptamer molecules. 5 mg/mL NaBH$_3$CN solution was used in capping unreacted epoxy rings for 1 h followed by washing with the mobile phase buffer B, (10 mM Tris HCl + 5mM MgCl$_2$). Thrombin solution was prepared in buffer B and was used to determine the binding affinity of the monolith by chromatography.

2.2.3   FT-IR and SEM characterisation

Analysis of surface morphology was carried by Scanning Electron Microscopy (Model S-3400N, Hitachi, Japan) after drying of the polymethacrylate disk-monoliths at 60 ^{o}C for 24 h. The monolith surface was sputter-coated with gold to enable signal conduction. Fourier Transform Infra-Red spectroscopy, FTIR, (Agilent Cary 630 FTIR, USA) was used to identify newly introduced functional moieties in the polymer matrix. The FTIR analysis was conducted for both the blank and aptamer-functionalised monoliths.

2.2.3   Thermogravimetric (TG) and Disc Scanning Calorimetric (DSC) characterisation

Thermogravimetric analyses (TGA) of polymethacrylate monolith, Schiff base activated monolith, and aptamer immobilised monolith were carried out under an inert condition with a N$_2$ gas flow rate of 25 cm^3/min. The samples were exposed to a dynamic heating rate of 10 ^{o}C/min from 25 ^{o}C to 500 ^{o}C using DSC/TGA Mettler Toledo equipment. The same temperature range was used for DSC characterisation.

2.2.4 Zeta potential analysis of functionalised polymethacrylate monoliths

Different ionic concentrations of NaCl and $MgCl_2$ ranging from 0-3.5 M were prepared to investigate the effect of ionic strength on the zeta potential of the aptasensor. The aptasensor was first pulverised uniformly and conditioned with the salt concentrations for about 20 min, and the zeta potential measurements were taken. Similarly, the effect of pH on the charge distribution of the aptasensor was also studied. Zeta potential measurements were taken using Malvern Nano ZS equipped with a folded capillary cell to hold sample solutions.

2.2.5 Liquid chromatographic analysis

The HPLC system used was for the liquid chromatographic studies was an NGC Discover equipment (Next Generation Chromatography Discover 100 Chromatography system, BIORAD, Melbourne, Australia). The system is equipped with two F10 system pumps that are capable of achieving 10 mL/min at 25.2 MPa, multi-wavelength detector module, F100 sample pump for a maximum of 100 mL/min at 10 MPa, an inlet valve, mixer, column switching valve, sample inject valve, buffer blending valve, pH valve, communication adaptor, ChromLab software, and an integrated system touch screen. The chromatographic column adopted was a BIORAD polypropylene column (Econo-Pac Chromatography columns, 12 cm x 1.5 cm i.d) attached with an adjustable flow adaptor (Econo-Pac Flow Adaptor, catered for 1.5 cm column i.d).

The BIORAD polypropylene columns contained 0.5 mL of the developed aptasensor connected to an adjustable flow adaptor and configured to the HPLC system. The feed mobile phase containing thrombin was prepared using buffer B, (10 mM Tris HCl + 5 mM $MgCl_2$) under different ionic and hydrogen potential conditions. The applied flow rate for the mobile phase was 0.3 mL/min under different ionic (0, 5, 10, 15, 20 mM $MgCl_2$) and pH (4, 6, 7, 8, 10). The mobile phase was loaded for 18 mins using buffer B prior to elution. Elution of bound thrombin was done with 2 M $NaClO_4$ with subsequent washing with buffer B.

3. RESULTS AND DISCUSSION

3.1 SEM and FTIR analyses

Polymethacrylate monoliths are continuous polymers that can be synthesised into various shapes and forms depending on their mould. They enable easy functionalisation with chemical and biomolecular ligands, and possess convective mass transport characteristics. Disk monoliths have been previously demonstrated to remarkably enhance rapid hydrodynamic flow properties with minimal backpressure (Strancar *et al.*, 1998; Kramberger *et al.*, 2010; Trauner *et al.*, 2011). There is no reported work exploring the convective mass transfer and flow hydrodynamic properties of disk polymethacrylate monoliths and the high specificity binding characteristcis of aptameric ligands to develop smart biosensing formats. The present work explored molecular anchoring of a thrombin binding aptameric ligand on a disk polymethacrylate monolith and characterised it physicochemically. To achieve a covalently bonded interaction between the TBA and the monolith, a Schiff-base activation chemistry was employed as shown in the following reaction scheme as Figure 1.
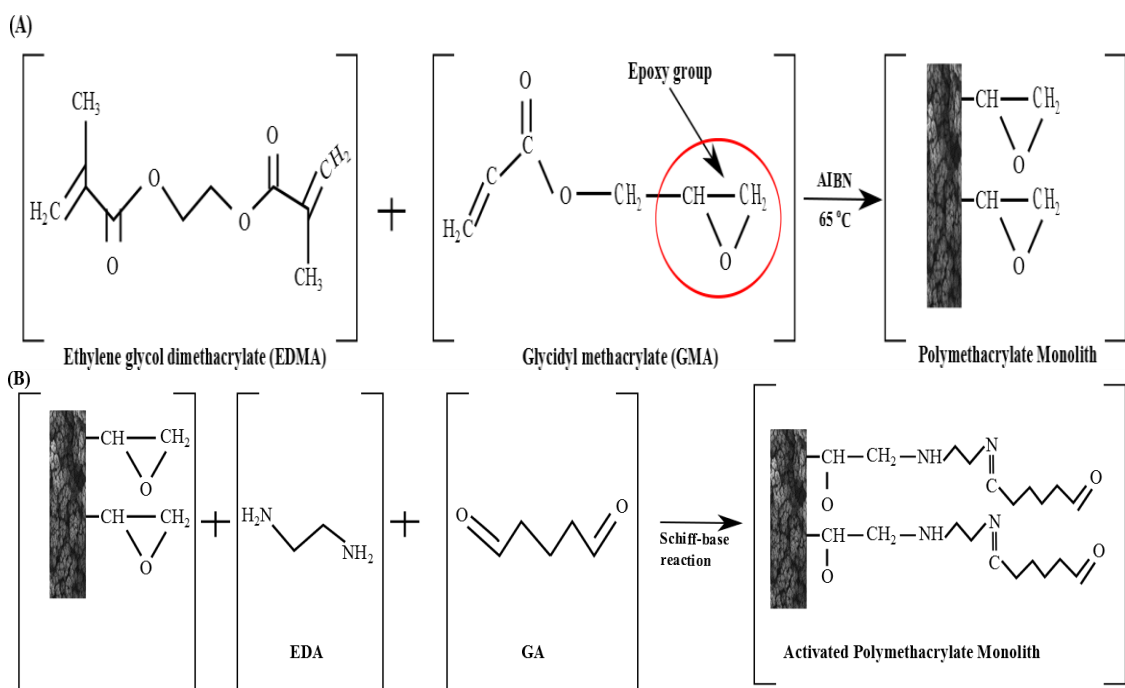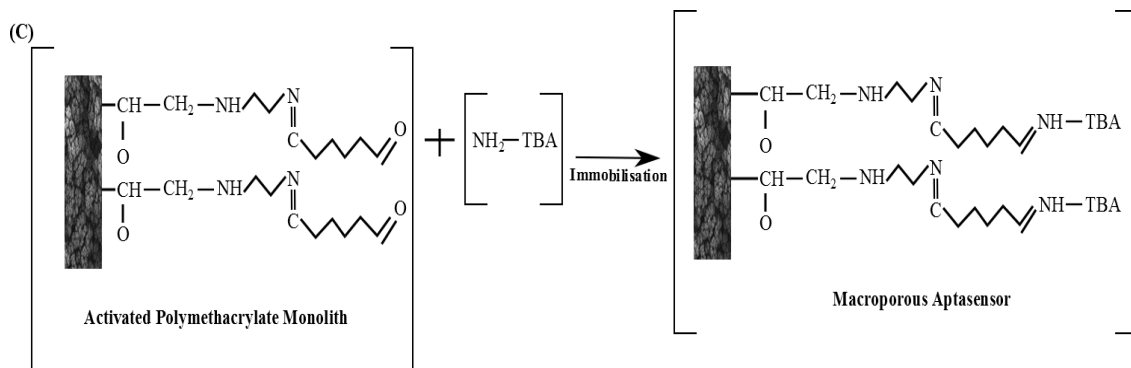
Figure 1. Schematic presentation of molecular interactions governing the development of the aptasensors. (A) Synthesis of polymethacrylate monoliths. (B) Activation of polymethacrylate monolith via Schiff-base chemistry. (C) Covalent immobilisation of amine-modified thrombin binding aptamers (TBA).

The covalent bond established between the aptamer and monolith minimizes potential leaching of aptamers during multiple applications. FTIR spectrographs of the original and aptamer-functionalised monoliths in Figure 2 show the absence of epoxy moieties in the aptamer-functionalised monolith at ~847 cm^{-1}. The original monolith showed the presence of epoxy functional groups.
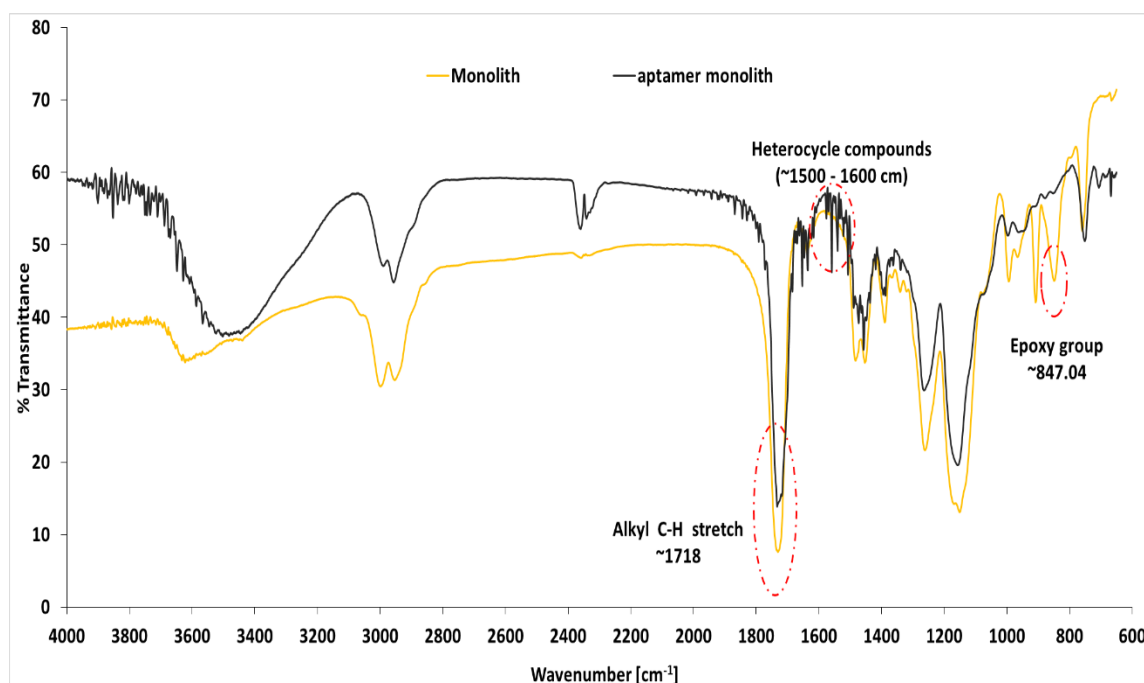
Figure 2. FTIR spectroscopic characterisation of original poly(GMA-co-EDMA) and aptamer-functionalised poly(GMA-co-EDMA) monoliths over 4000 – 600 cm^{-1} wave number.

Reaction of the epoxy moieties with ethylenediamine creates active sites for molecular interaction with glutaraldehyde. The reaction between the amine and epoxy moieties is based on a nucleophilic attack, and the subsequent reaction with glutaraldehyde leads to the introduction of a covalent linkage between the amine-activated monolith and the C6-amine-modified aptameric ligand. Since aptamers are synthetic nucleic acids, the occurrence of peaks on the spectrograph of the aptamer-functionalised monolith in the region 1500 – 1600 cm^{-1} being indicative of heterocycle compounds further demonstrate successful coupling of aptameric ligands onto the monolith. It has been reported that the nature and type of porogenic solvent affect the physiochemical characteristics and surface morphology of polymethacrylate monoliths (Danquah and Forde, 2008; Ongkudon and Danquah, 2010), and this impacts the molecular arrangement of the pore surface and the degree of ligand immobilisation. As a result, to optimise the ligand density of the disk aptasensor, a microporogen (cyclohexanol) was used to enhance permeability of the aptasensor whilst not compromising effective pore surface area for ligand immobilisation. The ligand density of the aptasensor, determined using equation (1), was 480 pmol/μL compared to previously reported ligand densities based on different techniques and porous supports; 170 pmol/μL (Zhao *et al.*, 2008), 204 pmol/μL (Deng *et al.*, 2001), 290 pmol/μL (Han *et al.*, 2012) and 568 pmol/μL (Kökpinar *et al.*, 2011). SEM images in Figure 3 show heterogeneous pore surface interconnections and morphology of the disk monolith synthesised at 65 °C in a cyclohexanol microporogen.

$$q = \frac{(C_o - C)V_s}{V_m} \tag{1}$$

where q is the ligand density of the aptamer (mol/L) covalently immobilized on the monolith; C_o and C are the initial and final concentration of aptamer solution (mol/L) respectively; and V_s and V_m are the volume (mL) of the aptamer solution and the monolith, respectively.
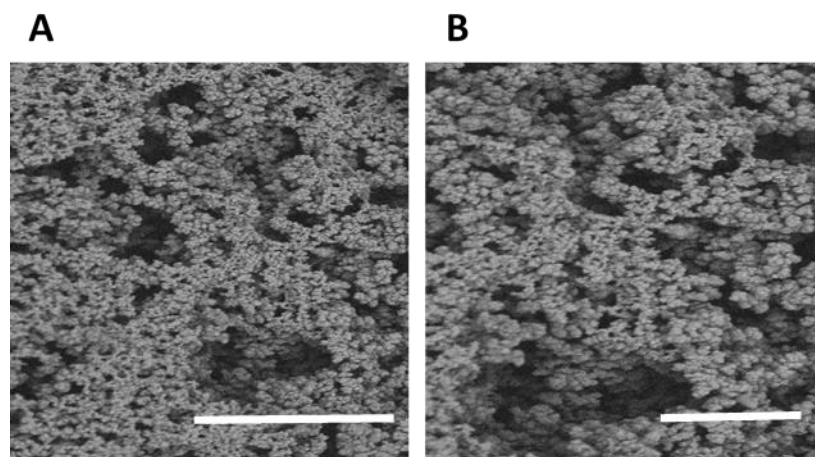
Figure 3. SEM images of polymethacrylate monoliths at magnifications of (A) 2.0 k with pore size of 20 µm and (B) 3.0 k with pore size of 10 µm.

3.2   Thermogravimetric (TG) and Differential Scanning Calorimetry (DSC) Analyses

Thermogravimetric analysis of the polymethacrylate aptasensor is important to probe the effect of temperature on the stability of the molecular interactions between the aptameric ligand and the polymer. Understanding the effect of synthesis and physicochemical conditions on the stability of polymethacrylate monoliths is critical to the development of robust aptasensors for mass and routine applications.   The synthesis of the polymethacrylate monolith was achieved by a thermally-initiated free-radical polymerisation process involving a functional monomer (GMA) and a cross-linker (EDMA) in a porogen. Mihelič *et al.* (2001) demonstrated via DSC analysis that the use of initiators reduces the activation temperature needed for polymerisation to commence.
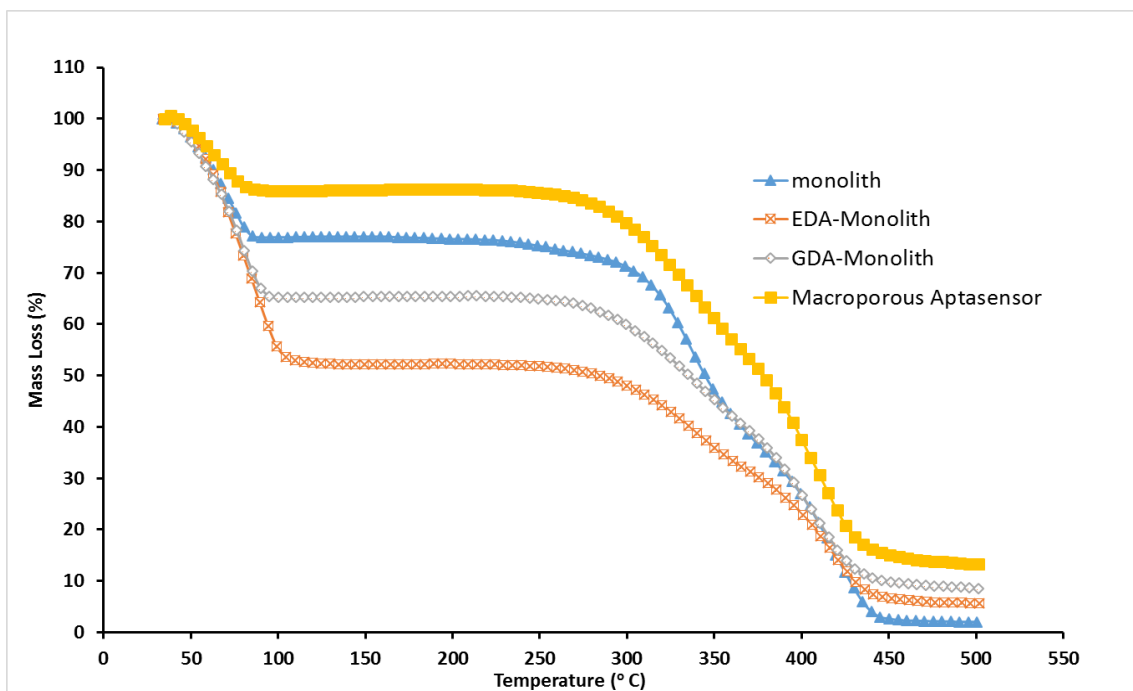
Figure 4a. Thermogravimetric analysis of (a) polymethacrylate monolith (b) EDA-activated polymethacrylate monolith (c) GDA functionalised polymethacrylate monolith and (d) C6-aptasensor.

Figure 4a and 4b show the TG and DSC patterns for each step in the development of the polymethacrylate aptasensors. The average thermal degradation curve for each process condition was observed to be similar in pattern to the original polymethacrylate monolithic adsorbent. The differences in mass loss from 25 ^{o}C – 100 ^{o}C for the polymer samples were due to differences in moisture contents after air drying. This finding is in keeping with previously reported TGA characterisations of polymers (Vlad *et al.*, 2003; Acquah *et al.*, 2017). Previous studies have shown that depending on the degree of cross-linking, polymethacrylate resin degradation commenced within the temperature range of 191 – 210 ^{o}C (Yusuf *et al.*, 2016; Acquah *et al.*, 2017; Acquah *et al.*, 2017). As shown in Table 1, there were noticeable increments in the temperature of degradation for each process step which is in conformity with findings from Awad *et al.* (2016).

Table 1. Characterisation of Schiff-base activated-monoliths via TGA for aptamer immobilisation. Results show the average of 3 replicates.

Sample	Onset of Degradation (^{o}C)	Total Residual Mass %	DSC Endothermic Peak (mW)	DSC Peak Temp (^{o}C)

Monolith	196.0 (±1.8)	0.250 (±1.82)	- 41.8 (±11.1)	200.1 (±6.5)
EDA-Monolith	235.9 (±6.1)	0.538 (±0.036)	- 25.9 (±8.4)	209.6 (±5.9)
GA-Monolith	255.4 (±2.7)	0.545 (±0.034)	- 23.7 (±4.7)	215.3 (±6.3)
Aptasensor	273.7 (±2.5)	0.653 (±0.076)	-23.05 (±1.4)	220.2 (±1.1)

This phenomenon can be attributed to the formation of covalent bonds formed from the Schiff-base activation process as well as aptamer immobilisation. Throughout this process, amine functional groups of ethylenediamine and the amine-modified C6-aptamer nucleophilically attack the epoxy functionalities of the polymethacrylate monolith. This leads to the substitution of C=O bonds of the epoxy moieties within the polymethacrylate matrix with C=N bond during the amine reductive process. Functionalisation of the monolith with covalent chemistries using ethylenediamine and glutaraldehyde activation further increases the degree of cross-linking and mechanical properties thus enhancing thermal stability (Verma *et al.*, 2013; Awad *et al.*, 2016). Also, the incorporation of stable short chain nucleotides from the aptamer onto the polymer matrix can enhance the thermal stability of the complex. The total residue for each functionalised and immobilised sample increased after complete degradation due to increase in organic content per unit sample mass. This finding demonstrates that effective activation and immobilisation of polymethacrylate resins is coupled with enhancement of thermal stability.
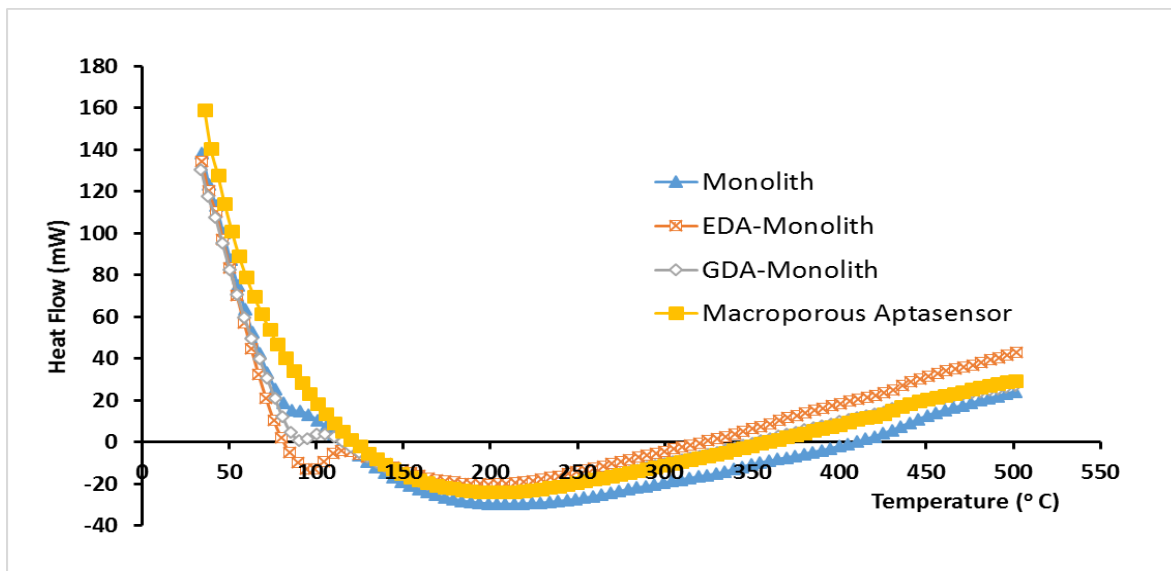
Figure 4b. Differential scanning calorimetry (DSC) curves for the aptasensor development via Schiff-base covalent chemistry. Data points represent the average of 3 replicates (n=3).

DSC curves showed significant variations in the peak heat energies of the samples, indicating the effectiveness of the grafting process. Endothermic peak heat energies increased after covalent reactions of ethylenediamine, glutaraldehyde and aptamer immobilisation due to the enhancement in the degree of cross-linking. Furthermore, there was a shift in peak temperatures towards the right in collaboration to the increase in endothermic peak heat energies.

3.3 Effect of monovalent and divalent cations on zeta potential and chromatographic performance

The secondary structure of aptamers has been shown to be affected by the presence of monovalent and divalent ions resulting in conformational changes. As the binding mechanisms of aptamers may vary with systems (Lin *et al.*, 2008), investigating the concentration of ions in a binding medium is necessary to optimise the binding kinetics and performance of aptamers to their cognate targets in a chromatographic sensor.

The zeta potentials of the aptamer-functionalised adsorbents were analysed through their electrophoretic mobility after pulverization and incubation under varying process conditions of pH and ionic strength. The thrombin binding DNA aptamers possess G-quadruplex structures with conformations and stability that can be altered by ionic

259

compositions and concentrations of their microenvironment (Nagatoishi *et al.*, 2007; Cho *et al.*, 2008). In previous reports, the effects of different cations on aptamer structural integrity were studied via circular dichroism spectroscopy (CDS), nuclear magnetic resonance (NMR), quartz crystal microbalance (QCM) and X-ray photoelectron spectroscopy (XPS) (Hianik *et al.*, 2007; Nagatoishi *et al.*, 2007; Ostatná *et al.*, 2008; Lin *et al.*, 2011). Hianik *et al.* (2007) studied the effect of Na^+ ions on immobilised aptasensors via QCM. They observed that although Na^+ had minimal effect on the stability of G-quadruplex conformation, a gradual increase in concentration resulted in a corresponding decrease in aptamer sensitivity due to shielding effects. To further understand the influence of cationic species on the charge stability and binding sensitivity of the polymer-immobilised aptamer, different concentrations of Na^+ and Mg^{2+} ions were interacted with the pulverised aptasensor and the resulting zeta potentials were analysed. As shown in Figure 5, increasing the ionic concentration of Mg^{2+} resulted in a more rapid decrease in the electronegativity of the aptamer. Mg^{2+} has a smaller ionic radius (1.5 Å) and higher electropositive charge than Na^+ (1.8 Å), and this enables it to possess a higher charge density that creates improved shedding effect at aptamer anionic interface. The isoelectric focussing points of the aptamer in the presence of Na^+ and Mg^{2+} ions were established at the concentrations 1.1 M for Mg^{2+} and 3.4 M for Na^+.
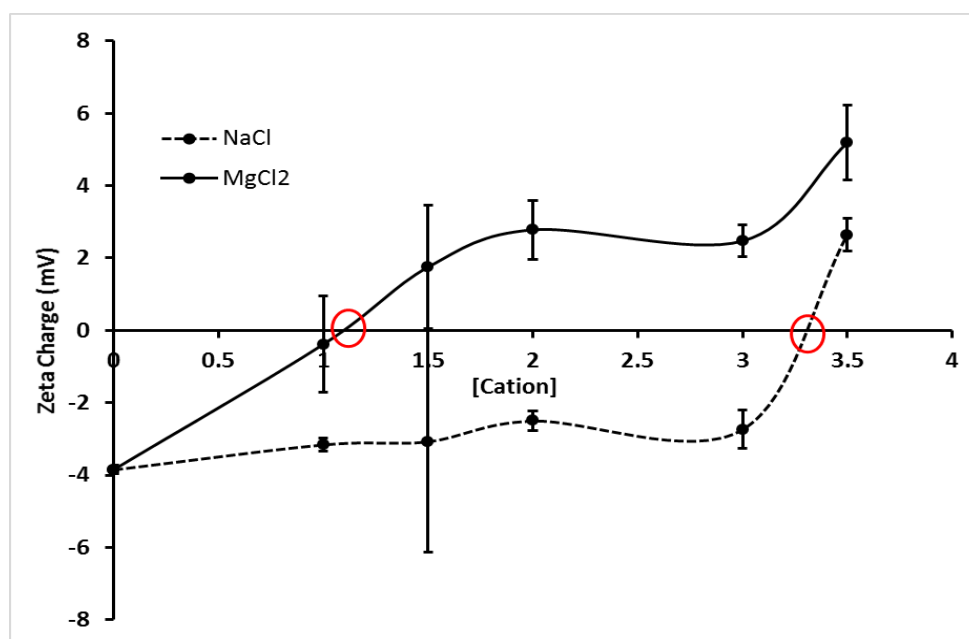
Figure 5. Effect of $[Na^+]$ and $[Mg^{2+}]$ on the zeta potential of pulverised aptasensor conducted at 25 °C using a folded capillary cell.

The effect of Mg^{2+} on the chromatographic characteristics of the aptasensor was studied over the range 0 – 20 mM in the mobile phase buffer at pH 8. Generally, raising the ionic strength of the mobile phase through $[Mg^{2+}]$ increase resulted in increasing retention time of the thrombin molecule as shown in Figure 6 as follows: 0 M (23.96 min); 5 mM (28.23 min); 10 mM (28.42 min); 15 mM (28.36 min) and 20 mM (28.32 min). This is attributed to induced formation of G-quadruplex secondary structure of the thrombin binding aptamer (TBA) and subsequent stabilisation by Mg^{2+} (Noeske *et al.*, 2007; Lin *et al.*, 2008; Tan *et al.*, 2017). Increasing concentrations of monovalent and divalent ions affects the helix-helix electrostatic interactions in the polynucleotide aptamer (Tan and Chen, 2006). The inherent polyanionic nature of aptamers due to their phosphodiester backbone renders them as negatively charged molecules with an anisotropic distribution (Noeske *et al.*, 2007). The anisotropic distribution and high electronegativity is therefore minimised by the addition of Mg^{2+} or other suitable divalent cations or high concentrations of monovalent cations to stabilise the aptamer (Noeske *et al.*, 2007; Tan *et al.*, 2017). Also, increasing Mg^{2+} introduces positive electrostatic binding sites on the aptasensor to increase thrombin molecular retention, reducing the concentration of thrombin eluted under constant elution program. Notably, the zero $[Mg^{2+}]$ mobile phase buffer showed the highest thrombin concentration in the elution with the shortest retention time, demonstrating the absence of extra positive electrostatic binding sites that increase retention. It should be noted that increasing Mg^{2+} concentration can compromise the binding specificity of the aptasensor, resulting in increasing electrostatic binding of electronegative non-targeted species. Also, Mg^{2+} ions shield active electronegative sites of the aptamer, making them unavailable or less sensitive for thrombin binding.
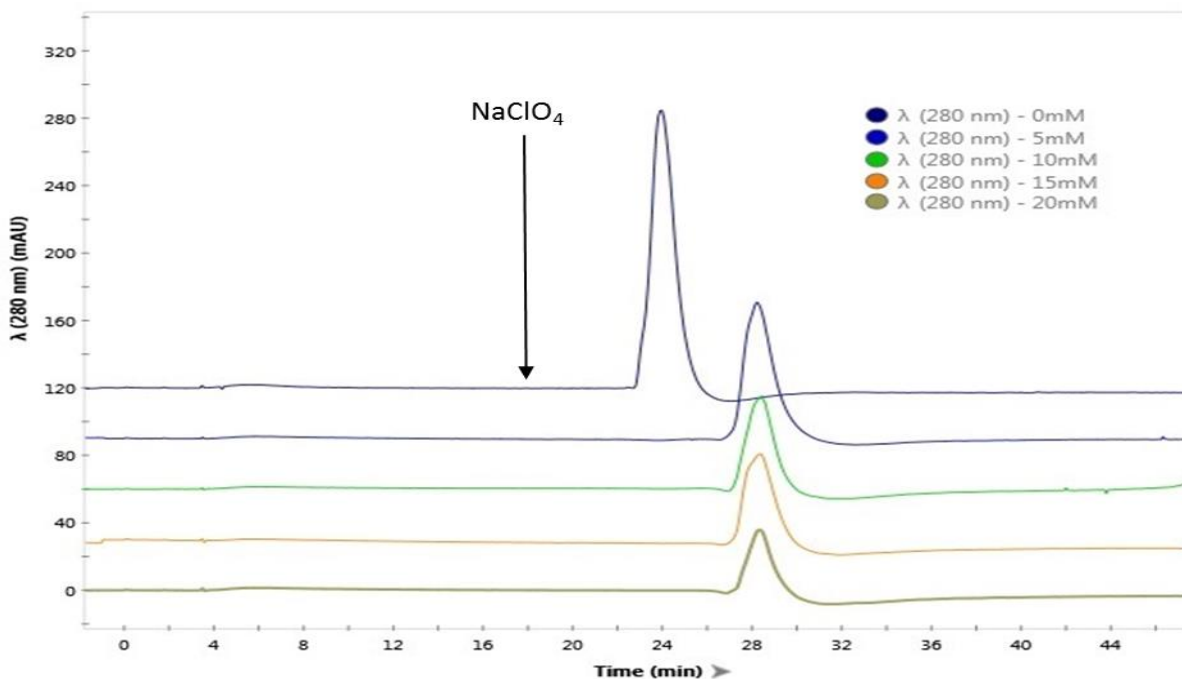
Figure 6. Effect of [Mg^{2+}] on chromatographic binding characteristics of thrombin. The chromatograph shows decreasing thrombin concentration with increasing [Mg^{2+}]. The chromatograph was generated by HPLC at a mobile phase flow rate of 0.3 mL/min and eluted with 2 M NaClO$_4$ after 18 min of sample loading.

3.3.2 Effect of pH on charge distribution and chromatographic performance

The effect of pH on the zeta potential distribution of the aptasensor was studied after pulverising the aptasensor polymer and conditioning them with different volumes of either 0.01 M HCl or 0.01 M NaOH in PBS buffer to establish a pH range. Since the monolith was immobilised with TBA in PBS buffer at pH 7.4 with an original zeta potential of -2.37 mV (±0.38), this condition was used as the baseline. Figure 7 shows the effect of pH variation on the net charge of the aptasensor.

262
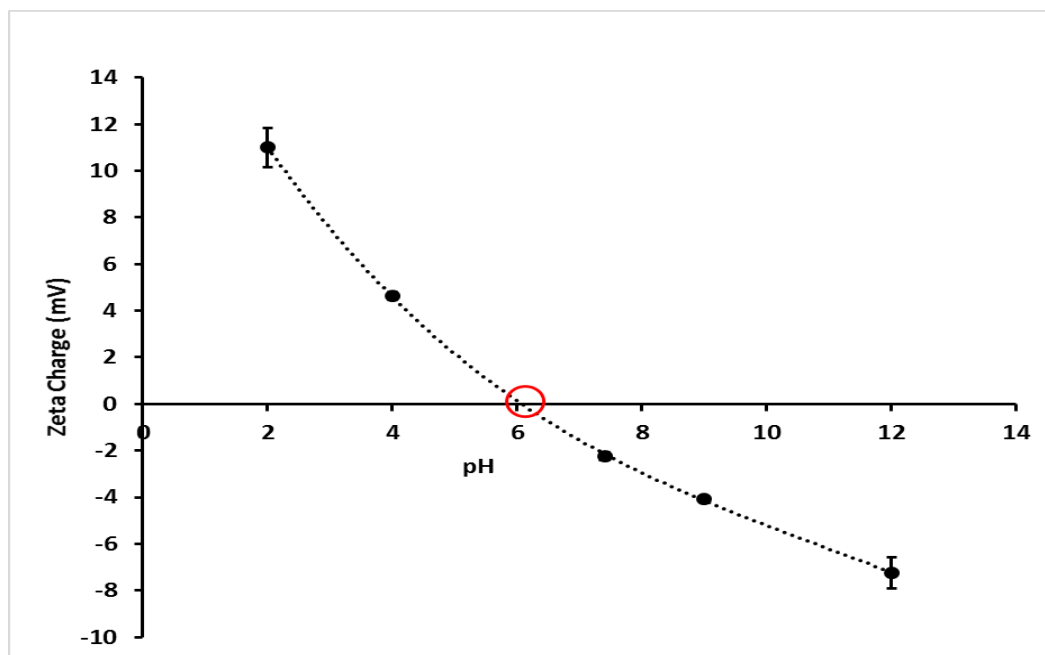
Figure 7. Effect of pH on the zeta potential of the pulverised aptasensor conducted at 25 °C using a folded capillary cell.

Generally, the zeta potential of the aptasensor decreased from 11 mV to -7.2 mV with increasing pH from 2 to 12. This trend could be attributed to two-step phenomenon: (i) adsorption of H^+ and OH^- on the surface of the aptasensor particulates, and (ii) protonation and deprotonation of aptasensor moieties under decreasing or increasing pH, respectively. Aptamers are single stranded nucleic acids; hence, they possess moieties that can undergo ionisation. Notably, carbonyl and phosphate moieties of the aptamer are known to undergo deprotonation in the presence of acids whereas pyrimidines (cytosine, thymine and uracil) are susceptible to protonation, resulting in zeta potential variation.

From the experimental data, a predictor equation with an R^2 value of 0.9986 was obtained. The predictor equation is important in determining the isoelectric focusing point, pI of the aptasensor. The pI point was estimated at 5.9. The net electronegativity of the aptasensor at pH > pI was due to the low concentration of H^+ ions and gradual increase in OH^- resulting in deprotonation of the carbonyl and phosphate moieties (Tan *et al.*, 2017). Addition of OH^- helps in the redistribution of the negative charges on the aptamer to reduce the anisotropic effect which in essence enhances the binding kinetics and performance of the aptasensor. This data is critical in developing assays for optimal operation of the aptasensor. As a result, most of the reported aptasensors operate under

pH conditions slightly above their pI point in order to maintain an electronegative charge distribution (Deng *et al.*, 2012; Han *et al.*, 2012; Du *et al.*, 2015; Marechal *et al.*, 2015). Hianik *et al.* (2007) via a quartz crystal microbalance (QCM) analysis using an anti-thrombin aptamer reported that the optimum operating pH to enhance the sensitivity of aptasensors is pH 7.4 – 7.5.

Figure 8 shows the effect of pH on retention time and absorbance areas of thrombin peaks. The pI of the target thrombin molecule is in the region of 6.35 – 7.6. The neutral operating pH showed the longest retention time with a relatively low thrombin concentration eluted. However, the alkaline regions were observed to have higher concentrations of thrombin in the eluted fraction. Consequently, the optimum operating pH of the mobile phase was determined as 8.0. The pI of the target thrombin molecule is in the region of 6.35 – 7.6. This indicates the importance of the mobile phase pH in optimising the binding characteristics of the aptasensor based on the pI of the target molecule.
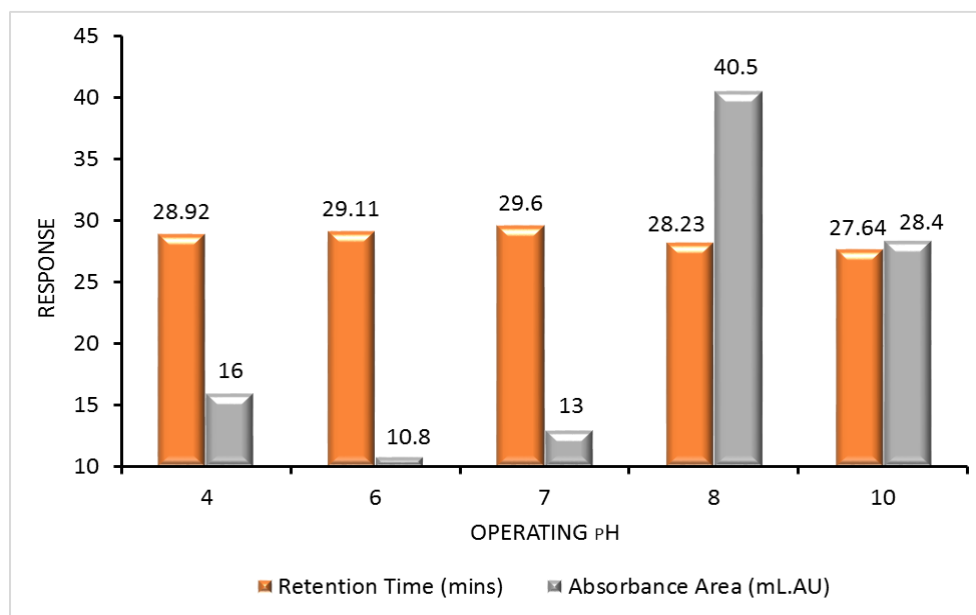
Figure 8. Effect of pH on retention time and peak absorbance area of thrombin detection. The chromatograph was generated by HPLC at a mobile phase flow rate of 0.3 mL/min and eluted with 2 M NaClO$_4$ after 18 min of sample loading.

4.   CONCLUSION

This work demonstrates that the binding performance of immobilised aptamers on polymethacrylate monoliths is affected by the physicochemical conditions in their micro-environment including ionic concentration, pH and the chemistry of the supporting system. Thermogravitmetric analysis of the polymer activation and immoblisation showed increasing initial temperatures of degradation, corresponding to an increase in the amount of endothermic energy needed to degrade samples from each modification step. The use of microporogen in the synthesis of polymethacrylate monolith enhanced the surface area, resulting in a high aptameric ligand density of 480 pmol/uL. Data for thrombin retention and elution analysis showed an optimal operating condition of pH 8 and $[Mg^{2+}]$ of 5 mM for TBA-thrombin interaction and polymeric adsorption. This body of work is critical in understanding biophysical activities governing aptamer-thrombin interactions at the polymer pore surface and the significant impacts on chromatographic performance.

5.   ACKNOWLEDGMENT

6.   REFERENCES

Acquah, C., M.K. Danquah, D. Agyei, C.K.S. Moy, A. Sidhu and C.M. Ongkudon, 2015. Deploying aptameric sensing technology for rapid pandemic monitoring. Critical reviews in biotechnology: 1-13. Available from http://dx.doi.org/10.3109/07388551.2015.1083940. DOI 10.3109/07388551.2015.1083940.

Acquah, C., M.K. Danquah, C.K. Moy, M. Anwar and C.M. Ongkudon, 2017. Thermogravimetric characterization of ex situ polymethacrylate (edma-co-gma) monoliths. The Canadian Journal of Chemical Engineering.

Acquah, C., M.K. Danquah, C.K.S. Moy, M. Anwar and C.M. Ongkudon, 2017. Parametric investigation of polymethacrylate monolith synthesis and stability via thermogravimetric characterisation. Asia-Pacific Journal of Chemical Engineering: n/a-n/a. Available from http://dx.doi.org/10.1002/apj.2077. DOI 10.1002/apj.2077.

Acquah, C., M.K. Danquah, J.L.S. Yon, A. Sidhu and C.M. Ongkudon, 2015. A review on immobilised aptamers for high throuput biomolecular detection and screening. Analytica chimica acta, 888: 10-18. Available from

http://www.sciencedirect.com/science/article/pii/S0003267015008016. DOI http://dx.doi.org/10.1016/j.aca.2015.05.050.

Acquah, C., C.K.S. Moy, M.K. Danquah and C.M. Ongkudon, 2016. Development and characteristics of polymer monoliths for advanced lc bioscreening applications: A review. Journal of Chromatography B, 1015–1016: 121-134. Available from http://www.sciencedirect.com/science/article/pii/S1570023216300976. DOI http://dx.doi.org/10.1016/j.jchromb.2016.02.016.

Awad, G.E., A.A.A. El Aty, A.N. Shehata, M.E. Hassan and M.M. Elnashar, 2016. Covalent immobilization of microbial naringinase using novel thermally stable biopolymer for hydrolysis of naringin. 3 Biotech, 6(1): 14.

Brothier, F. and V. Pichon, 2014. Miniaturized DNA aptamer-based monolithic sorbent for selective extraction of a target analyte coupled on-line to nanolc. Analytical and bioanalytical chemistry, 406(30): 7875-7886. Available from http://www.ncbi.nlm.nih.gov/pubmed/25335821. DOI 10.1007/s00216-014-8256-z.

Chen, A. and S. Yang, 2015. Replacing antibodies with aptamers in lateral flow immunoassay. Biosensors and Bioelectronics, 71: 230-242.

Cho, M.-S., Y.-W. Kim, S.-Y. Han, K.-I. Min, M. Rahman, Y.-B. Shim and C.-I. Ban, 2008. Detection for folding of the thrombin binding aptamer using label-free electrochemical methods. BMB reports, 41(2): 126-131.

Danquah, M.K. and G.M. Forde, 2008. Preparation of macroporous methacrylate monolithic material with convective flow properties for bioseparation: Investigating the kinetics of pore formation and hydrodynamic performance. Chemical Engineering Journal, 140(1-3): 593-599. DOI 10.1016/j.cej.2008.02.012.

Deng, N., Z. Liang, Y. Liang, Z. Sui, L. Zhang, Q. Wu, K. Yang, L. Zhang and Y. Zhang, 2012. Aptamer modified organic-inorganic hybrid silica monolithic capillary columns for highly selective recognition of thrombin. Analytical chemistry, 84(23): 10186-10190. Available from http://www.ncbi.nlm.nih.gov/pubmed/23137349. DOI 10.1021/ac302779u.

Deng, Q., I. German, D. Buchanan and R.T. Kennedy, 2001. Retention and separation of adenosine and analogues by affinity chromatography with an aptamer stationary phase. Analytical chemistry, 73(22): 5415-5421. DOI 10.1021/ac0105437.

Du, K., M. Yang, Q. Zhang and S. Dan, 2015. Highly porous polymer monolith immobilized with aptamer (rna) anchored grafted tentacles and its potential for the purification of lysozyme. Industrial & Engineering Chemistry Research.

Han, B., C. Zhao, J. Yin and H. Wang, 2012. High performance aptamer affinity chromatography for single-step selective extraction and screening of basic protein lysozyme. Journal of chromatography. B, Analytical technologies in the biomedical and life sciences, 903: 112-117. Available from http://www.ncbi.nlm.nih.gov/pubmed/22841745. DOI 10.1016/j.jchromb.2012.07.003.

Hianik, T., V. Ostatna, M. Sonlajtnerova and I. Grman, 2007. Influence of ionic strength, ph and aptamer configuration for binding affinity to thrombin. Bioelectrochemistry, 70(1): 127-133. Available from http://www.ncbi.nlm.nih.gov/pubmed/16725379. DOI 10.1016/j.bioelechem.2006.03.012.

Ilgu, M. and M. Nilsen-Hamilton, 2016. Aptamers in analytics. The Analyst, 141(5): 1551-1568.

Jiang, X., H. Wang, H. Wang, Y. Zhuo, R. Yuan and Y. Chai, 2017. Electrochemiluminescence biosensor based on 3-d DNA nanomachine signal probe powered by protein-aptamer binding complex for ultrasensitive mucin 1 detection. Analytical chemistry, 89(7): 4280-4286.

Kirsch, J., C. Siltanen, Q. Zhou, A. Revzin and A. Simonian, 2013. Biosensor technology: Recent advances in threat agent detection and medicine. Chemical Society Reviews, 42(22): 8733-8768.

Kökpinar, Ö., J.G. Walter, Y. Shoham, F. Stahl and T. Scheper, 2011. Aptamer-based downstream processing of his-tagged proteins utilizing magnetic beads. Biotechnology and bioengineering, 108(10): 2371-2379.

Kramberger, P., R.C. Honour, R.E. Herman, F. Smrekar and M. Peterka, 2010. Purification of the staphylococcus aureus bacteriophages vdx-10 on methacrylate monoliths. Journal of virological methods, 166(1): 60-64.

Lin, P.-H., R.-H. Chen, C.-H. Lee, Y. Chang, C.-S. Chen and W.-Y. Chen, 2011. Studies of the binding mechanism between aptamers and thrombin by circular dichroism, surface plasmon resonance and isothermal titration calorimetry. Colloids and Surfaces B: Biointerfaces, 88(2): 552-558.

Lin, P.-H., S.-L. Yen, M.-S. Lin, Y. Chang, S.R. Louis, A. Higuchi and W.-Y. Chen, 2008. Microcalorimetrics studies of the thermodynamics and binding mechanism between l-tyrosinamide and aptamer. The Journal of Physical Chemistry B, 112(21): 6665-6673.

Lopez-Barbosa, N., J.D. Gamarra and J.F. Osma, 2016. The future point-of-care detection of disease and its data capture and handling. Analytical and bioanalytical chemistry: 1-11.

Marechal, A., F. Jarrosson, J. Randon, V. Dugas and C. Demesmay, 2015. In-line coupling of an aptamer based miniaturized monolithic affinity preconcentration unit with capillary electrophoresis and laser induced fluorescence detection. Journal of Chromatography A, 1406: 109-117.

Mascini, M. and S. Tombelli, 2008. Biosensors for biomarkers in medical diagnostics. Biomarkers, 13(7-8): 637-657.

Mihelič, I., M. Krajnc, T. Koloini and A. Podgornik, 2001. Kinetic model of a methacrylate-based monolith polymerization. Industrial & engineering chemistry research, 40(16): 3495-3501.

Monaco, I., S. Camorani, D. Colecchia, E. Locatelli, P. Calandro, A. Oudin, S. Niclou, C. Arra, M. Chiariello and L. Cerchia, 2017. Aptamer functionalization of nanosystems for glioblastoma targeting through the blood-brain-barrier. Journal of Medicinal Chemistry.

Nagatoishi, S., Y. Tanaka and K. Tsumoto, 2007. Circular dichroism spectra demonstrate formation of the thrombin-binding DNA aptamer g-quadruplex under stabilizing-cation-deficient conditions. Biochemical and biophysical research communications, 352(3): 812-817.

Nezlin, R., 2016. Use of aptamers in immunoassays. Molecular Immunology, 70: 149-154.

Noeske, J., H. Schwalbe and J. Wöhnert, 2007. Metal-ion binding and metal-ion induced folding of the adenine-sensing riboswitch aptamer domain. Nucleic acids research, 35(15): 5262-5273.

Oktem, H.A., G. Bayramoglu, V.C. Ozalp and M.Y. Arica, 2007. Single-step purification of recombinant thermus aquaticus DNA polymerase using DNA-aptamer immobilized novel affinity magnetic beads. Biotechnology progress, 23(1): 146-154.

Ongkudon, C.M. and M.K. Danquah, 2010. Process optimisation for anion exchange monolithic chromatography of 4.2 kbp plasmid vaccine (pcdna3f). Journal of Chromatography B, 878(28): 2719-2725. DOI 10.1016/j.jchromb.2010.08.011.

Ostatná, V., H. Vaisocherová, J. Homola and T. Hianik, 2008. Effect of the immobilisation of DNA aptamers on the detection of thrombin by means of surface plasmon resonance. Analytical and bioanalytical chemistry, 391(5): 1861-1869.

Pakchin, P.S., S.A. Nakhjavani, R. Saber, H. Ghanbari and Y. Omidi, 2017. Recent advances in simultaneous electrochemical multi-analyte sensing platforms. TrAC Trends in Analytical Chemistry, 92: 32-41. Available from http://www.sciencedirect.com/science/article/pii/S0165993617300900. DOI https://doi.org/10.1016/j.trac.2017.04.010.

Roberts, M.W., C.M. Ongkudon, G.M. Forde and M.K. Danquah, 2009. Versatility of polymethacrylate monoliths for chromatographic purification of biomolecules. Journal of separation science, 32(15-16): 2485-2494. Available from http://www.ncbi.nlm.nih.gov/pubmed/19603394. DOI 10.1002/jssc.200900309.

Schulz, C., J. Hecht, A. Krüger-Genge, K. Kratz, F. Jung and A. Lendlein, 2016. Generating aptamers interacting with polymeric surfaces for biofunctionalization. Macromolecular Bioscience, 16(12): 1776-1791. DOI 10.1002/mabi.201600319.

Strancar, A., M. Barut, A. Podgornik, P. Koselj, D. Josic and A. Buchacher, 1998. Convective interaction media: Polymer-based supports for fast separation of biomolecules. LC-GC, 11: 660-669.

Su, Z., H. Xu, X. Xu, Y. Zhang, Y. Ma, C. Li and Q. Xie, 2017. Effective covalent immobilization of quinone and aptamer onto a gold electrode via thiol addition for sensitive and selective protein biosensing. Talanta, 164: 244-248.

Tan, S.Y., C. Acquah, A. Sidhu, C.M. Ongkudon, L.S. Yon and M.K. Danquah, 2016. Selex modifications and bioanalytical techniques for aptamer-target binding characterisation. Taylor & Francis: pp: 00-00.

Tan, S.Y., C. Acquah, S.Y. Tan, C.M. Ongkudon and M.K. Danquah, 2017. Characterisation of charge distribution and stability of aptamer-thrombin binding interaction. Process Biochemistry. Available from http://www.sciencedirect.com/science/article/pii/S135951131630887X. DOI https://doi.org/10.1016/j.procbio.2017.06.003.

Tan, Z.-J. and S.-J. Chen, 2006. Ion-mediated nucleic acid helix-helix interactions. Biophysical journal, 91(2): 518-536.

Trauner, A., M.H. Bennett and H.D. Williams, 2011. Isolation of bacterial ribosomes with monolith chromatography. PloS one, 6(2): e16273.

Velusamy, V., K. Arshak, O. Korostynska, K. Oliwa and C. Adley, 2010. An overview of foodborne pathogen detection: In the perspective of biosensors. Biotechnology advances, 28(2): 232-254. Available from

http://www.ncbi.nlm.nih.gov/pubmed/20006978.   DOI
10.1016/j.biotechadv.2009.12.004.

Verma, M.L., M. Naebe, C.J. Barrow and M. Puri, 2013. Enzyme immobilisation on amino-functionalised multi-walled carbon nanotubes: Structural and biocatalytic characterisation. PloS one, 8(9): e73642.

Vlad, C.D., M.V. Dinu and S. Dragan, 2003. Thermogravimetric analysis of some crosslinked acrylamide copolymers and ion exchangers. Polymer degradation and stability, 79(1): 153-159.

Yusuf, K., A.Y. Badjah-Hadj-Ahmed, A. Aqel and Z.A. Alothman, 2016. Monolithic metal–organic framework mil-53(al)-polymethacrylate composite column for the reversed-phase capillary liquid chromatography separation of small aromatics. Journal of separation science, 39(5): 880-888. DOI 10.1002/jssc.201501289.

Zhao, Q., X.-F. Li, Y. Shao and X.C. Le, 2008. Aptamer-based affinity chromatographic assays for thrombin. Analytical chemistry, 80(19): 7586-7593.

CHAPTER SIX

CHROMATOGRAPHIC CHARACTERISATION OF APTAMER-MODIFIED POLYMERIC DISK MONOLITH

SECTION 6.1

Chromatographic characterisation of aptamer-modified poly(EDMA-co-GMA) monolithic disk format for protein binding and separation

Caleb Acquah, Michael K. Danquah, Yi Wei Chan, Charles K. S. Moy, Clarence M. Ongkudon, Lau Sie Yon

'TO BE PUBLISHED'

DECLARATION FOR THESIS SECTION 6.1

Chromatographic characterisation of aptamer-modified poly(EDMA-co-GMA) monolithic disk format for protein binding and separation

The candidate will like to declare that there is no conflict of interests involved in this work and that my extent of contribution as candidate is as shown below:

Contribution of Candidate	Conceptualisation, initiation and write-up	75%

The following co-authors were involved in the development of this publication and attest to the candidate's contribution to a joint publication as part of his thesis. Permission by co-authors are as follows:

Name	Signature	Date
Michael K. Danquah		13.07.2017
Lau Sie Yon		13.07.2017
Charles K.S. Moy		13.07.2017
Clarence M. Ongkudon		13.07.2017
Yi Wei Chan		13.07.2017

'TO BE PUBLISHED'

ABSTRACT

Polymethacrylate monoliths are a continuous bed of porous resins with convective mass transfer characteristics. They can be synthesised into varied architectures with unique convective flow hydrodynamic characteristics. The introduction of aptamers onto monoliths could produce an effective biomedical tool for a wide range of high throughput bioscreening and bioseparation applications. In this work, a polymethacrylate disk monolith was synthesised, characterised and modified with an aptamer for chromatographic isolation and separation of thrombin from a protein mixture. Chromatographic analyses were carried out to ascertain the performance of the aptamer-modified disk monolith.

Keywords: Disk monoliths; Aptamer; Protein separation; Liquid Chromatography; Affinity binding

1.   INTRODUCTION

Over the past two decades, continuous porous sorbents known as "monoliths" with interconnected meso and/or macropores have emerged as novel supports in advancing liquid chromatographic applications (Podgornik and Krajnc, 2012; Desire *et al.*, 2017; Krajacic *et al.*, 2017). The heightened interest in monoliths is due to the high porosity, interconnected flow channels, convective transport characteristics, low buffer consumption, high binding capacity for a wide range of biomolecules, and the ease of surface modification to introduce different ligands (Bencina *et al.*, 2007; Ongkudon *et al.*, 2013; Černigoj *et al.*, 2016). The pore characteristics of monoliths can also be tailored to match the hydrodynamic metrics of the target molecule to enhance rapid bio-separation (Danquah and Forde, 2008; Podgornik *et al.*, 2013). Polymethacrylate monoliths possess unique physicochemical characteristics including ease of surface modification, resistance to pH, high ligand retention, biocompatibility, and effective convective mass transfer characteristics (Roberts *et al.*, 2009; Acquah *et al.*, 2016).

Depending on the geometry of the mould and the polymerisation conditions, polymethacrylate monoliths can be synthesised into different architectural shapes such as capillary, microfluidic columns, conical, disks, membranes and annular (Ongkudon *et al.*, 2014; Acquah *et al.*, 2017). Each of these architectural shapes present unique hydrodynamic flow characteristics within the interconnected channels of the monoliths. Short format disk monoliths have been demonstrated to enhance convective flow, flow independent chromatographic efficiency, low pressure drop, short analysis time with minimal or no compromise on peak resolution during large molecule separation (Prasanna and Vijayalakshmi, 2010; Brgles *et al.*, 2014; Isakari *et al.*, 2016). Thus, the aforementioned unique hydrodynamic flow and separation features of short format disk monoliths when incorporated into chromatographic affinity interactions as the ideal synthetic support enhances high throughput applications (Jiang *et al.*, 2005; Prasanna and Vijayalakshmi, 2010).

Owing to the high cost of affinity ligands, their reusability and efficiency are enhanced through suitable immobilisation chemistries onto solid supports. Aptamers are single-stranded oligonucleotides which are chemically synthesised by means of a stringent

iterative process known as Systematic Evolution of Ligands by Exponential Enrichment, SELEX (Robertson and Joyce 1990; Tuerk and Gold 1990; Ellington and Szostak 1990). Aptamers are heralded as "golden age" bioprobes due to their superior biophysical and chemical characteristics over antibodies. They can be developed at low costs with no batch to batch variation, possess minimal ethical issues, bind specifically to their targets with low K_D, are thermally stable and, are able to denature and renature (Acquah *et al.*, 2015; Tan *et al.*, 2016; Sharma *et al.*, 2017). Nonetheless, there have been limited successes in the development and establishment of new aptamer-based analytical techniques and assays for commercialisation. In recent times, the development of aptasensors through immobilisation of aptamers onto continuous porous supports such as monoliths has a promising area of research focus to enhance chromatographic separation of various analytes. The group of Chris Le pioneered the development of porous aptamer-modified monoliths via avidin-biotin strong non-covalent chemistries on glycidyl methacrylate-co-trimethylolpropanetrimethacrylate monoliths (Zhao *et al.*, 2008; Zhao *et al.*, 2008). However, non-covalent immobilisation of aptamers could potentially lead to loss of ligands through hydrolysis and leaching (Deng *et al.*, 2012; Brothier and Pichon, 2014). Activation chemistries such as Schiff-base, Carbonyldiimidazole, Disuccinimidylcarbonates and Azlactone chemistries result in the development of covalent bonds between aptamers and the monolithic substrate (Acquah *et al.*, 2015).

To date, there is no research report that focuses on the synthesis and chromatographic characterisation of aptamer-modified disk monoliths for enhanced biomolecular separation. This present work reports the development of an aptamer-modified disk monolith using a thrombin binding aptamer immobilised on a polymethacrylate monolith via Schiff base activation chemistry. Chromatographic investigation of performance indicators including column efficiency and dynamic binding capacity under varying mobile phase flow rates and target concentrations are presented. The selectivity of the aptamer-modified disk monolith towards the target protein molecule amongst non-targets protein molecules is investigated and presented.

2. EXPERIMENTAL

2.1 Materials

The following chemicals/reagents were purchased from Sigma-Aldrich: azobisisobutyronitrile, AIBN, (MW 164.21 g/mol, 98%); ethylene glycol dimethacrylate, EDMA, (MW 198.22, 98%); Trizma HCl (MW 157.60, 99%); glycidyl methacrylate, GMA, (MW 142.15, 97%); cyclohexanol (MW 100.16, 99%); hydrochloric acid, HCl (MW 36.5, 37%); ethylenediamine, EDA, (MW 60.10, 99%); phosphate buffer solutions (PBS); methanol (HPLC grade, MW 32.04, 99.93%); ethylenediaminetetraacetic acid (MW 292.24, 99%); glutaraldehyde, GA, (MW 100.12, 25%); and human alpha thrombin. Lysozyme egg white was purchased from Gold biotechnologies (USA). Human IgG antibody was purchased from Equitech-Bio Inc (USA). Thrombin Binding DNA aptamer (TBA) with a C-6 spacer arm having the sequence 5'-/5AmMC6/GGT TGG TGT GGT TGG-3' was synthesised and purified by Base pair biotechnologies (Malaysia).

2.2 Methods

2.2.1 Synthesis of polymethacrylate disk-monoliths

Synthesis of short format polymethacrylate disk-monolith was performed by thermal free radical polymerisation of the functional monomer (GMA) and cross-linker monomer (EDMA) in a cycohexanol microporogenic solvent. The monomer mixture (GMA/EDMA) was dissolved in the microporogen (cyclohexanol) at the ratio 24/16/60 v/v% for GMA, EDMA and cyclohexanol, respectively. 1 % w/v AIBN was added to initiate the free radical polymerisation process. The polymerisation mixture was sonicated for 10 min to obtain a homogenous mixture, and the mixture was sparged with nitrogen gas to expel dissolved oxygen. 0.5 mL of the prepared polymerisation mixture was transferred into BIORAD polypropylene columns; 120 mm×15 mm and sealed. The polymerisation was performed in an isothermal water bath (Memmert, Germany) at 65 °C for 16 h. The synthesised polymethacrylate monolith was washed with methanol using BIORAD HPLC system (Next Generation Chromatography Discover 100 Chromatography system, BIORAD, Melbourne, Australia) until a constant baseline was established followed by rinsing with ultrapure water. The washed monolith was stored at 4 °C for further *in situ* characterisation.

2.2.2 Covalent Grafting of Aptamer

Epoxy moieties present on the disk monolith were activated via a Schiff-base covalent process involving 15 mL of ethylenediamine solution (50 % v/v prepared with ultrapure water) treatment for 12 h at 60 $^{\circ}$C, washing with ultrapure water to remove any residues, and 3 h reaction with 15 mL of 10 % glutaraldehyde solution prepared with ultrapure water at room temperature. Glutaraldehyde functionalised disk-monoliths were subsequently rinsed with ultrapure water and equilibrated with buffer A (10 mM phosphate buffer + 20 mM potassium chloride + 137 mM sodium chloride + 5 mM $MgCl_2$ at pH 7.4). 20 μM TBA solution was prepared in buffer A heated at 90 $^{\circ}$C for 5 min and cooled to room temperature. TBA immobilisation was performed at 0.2 mL/min for 20 h at room temperature. Loosely bound aptamer molecules were washed with buffer A. 5 mg/mL $NaBH_3CN$ solution, which is a reducing agent, was introduced into the polypropylene column for 1 h to cap unreacted activated-epoxy rings to prevent non-specific binding. Mobile phase buffer B (10 mM Tris HCl + 5mM $MgCl_2$, pH 8.0) was used to equilibrate and store the aptamer-modified disk monolith at 4 $^{\circ}$C. Effect of temperature on the efficiency of immobilisation was also studied by statically grafting aptameric ligands at 4 $^{\circ}$C and 25 $^{\circ}$C, respectively.

2.2.3 Surface Morphology and Functional Group Characterisation

Characterisation of monolith surface morphology was performed using a variable pressure scanning electron microscope (SEM) (S-3400N Hitachi model, Japan) after oven drying of sample for 24 h at 60 $^{\circ}$C. The sample was gold sputter coated to enhance its conductivity. Fourier transform infrared (FTIR) spectroscopic analysis was conducted for the blank monolith, activated monolith and the aptasensor to investigate effective functionalisation using Agilent Cary 630 FTIR, USA with diamond attenuated reflectance.

2.2.4 Hydrodynamic Measurement and Binding Capacity Analysis

Hydrodynamic characterisation of the disk-monolith was carried out by connecting the BIORAD polypropylene column (Econo-Pac Chromatography columns) to a flow adaptor configuration and attached to the HPLC system. The Next Generation HPLC system

consisted of two F10 system pumps that can attain 10 mL/min at 25.2 MPa, F100 sample pump for a maximum flow rate of 100 mL/min at 10 MPa, multi-wavelength detector module, an inlet valve, mixer, column switching valve, sample inject valve, buffer blending valve, pH valve, communication adaptor, ChromLab software, and an integrated system touch screen. Back pressure analysis of the monolith, activated monolith and the aptamer-modified disk monolith was carried out at different flow rates using ultrapure water as the mobile phase at room temperature. Thrombin solution was prepared using mobile phase buffer B to analyse the Height Equivalent to the Theoretical Plate (HETP) under various flow conditions and the optimum linear velocity of the column. 0.4 mg/mL thrombin solution was pumped at different flow rates of 0.15, 0.2, 0.25, 0.3 mL/min to analyse the HETP of the aptamer-modified monolith.

2.2.5 Dynamic Binding Capacity Measurement (DBC$_{10\%}$)

Human alpha thrombin molecules were dissolved in the mobile phase buffer B at different concentrations (0.2, 0.3, 0.4 mg/mL) and flow rates (0.1, 0.2, 0.3 mL/min) to determine the dynamic binding capacity at 10% breakthrough. The column was regenerated using 2 M NaClO$_4$ followed by equilibration with the mobile phase buffer B.

2.2.6 Aptamer-modified monolith selectivity analysis using a multi-component mixture

The specificity and sensitivity of the aptamer-modified disk monolith towards non-targets such as lysozyme egg white (0.4 mg/mL) and Human IgG (0.4 mg/mL), and thrombin target (1 mg/mL) were analysed independently using the HPLC system, respectively. Similarly, a multi-component mixture consisting of thrombin (1 mg/mL) in the presence of lysozyme (0.4 mg/mL) was analysed via the HPLC system. Chromatographic analysis was performed at a flow rate of 0.3 mL/min using mobile phase buffer B. The elution buffer used to regenerate the column from the protein molecules was 2 M NaClO$_4$. Qualitative analysis of the eluted proteins based on their molecular size was conducted via an SDS-PAGE analysis with 6% stacking gel and 12% resolving gel.

3. RESULTS AND DISCUSSIONS

3.1 Surface Morphology and Functional Group Analysis

GMA-co-EDMA monoliths are a solitary piece of continuous polymethacrylate sorbent materials polymerised in an unstirred mould to possess interconnected channels and globules with epoxy moieties. Post-modification processes involving covalent activation of the epoxy moieties enables immobilisation of aptamers to form porous aptasensors. The surface morphology revealed in Figure 1 shows the formation of a homogenous macroporous aptamer-modified disk monolith.
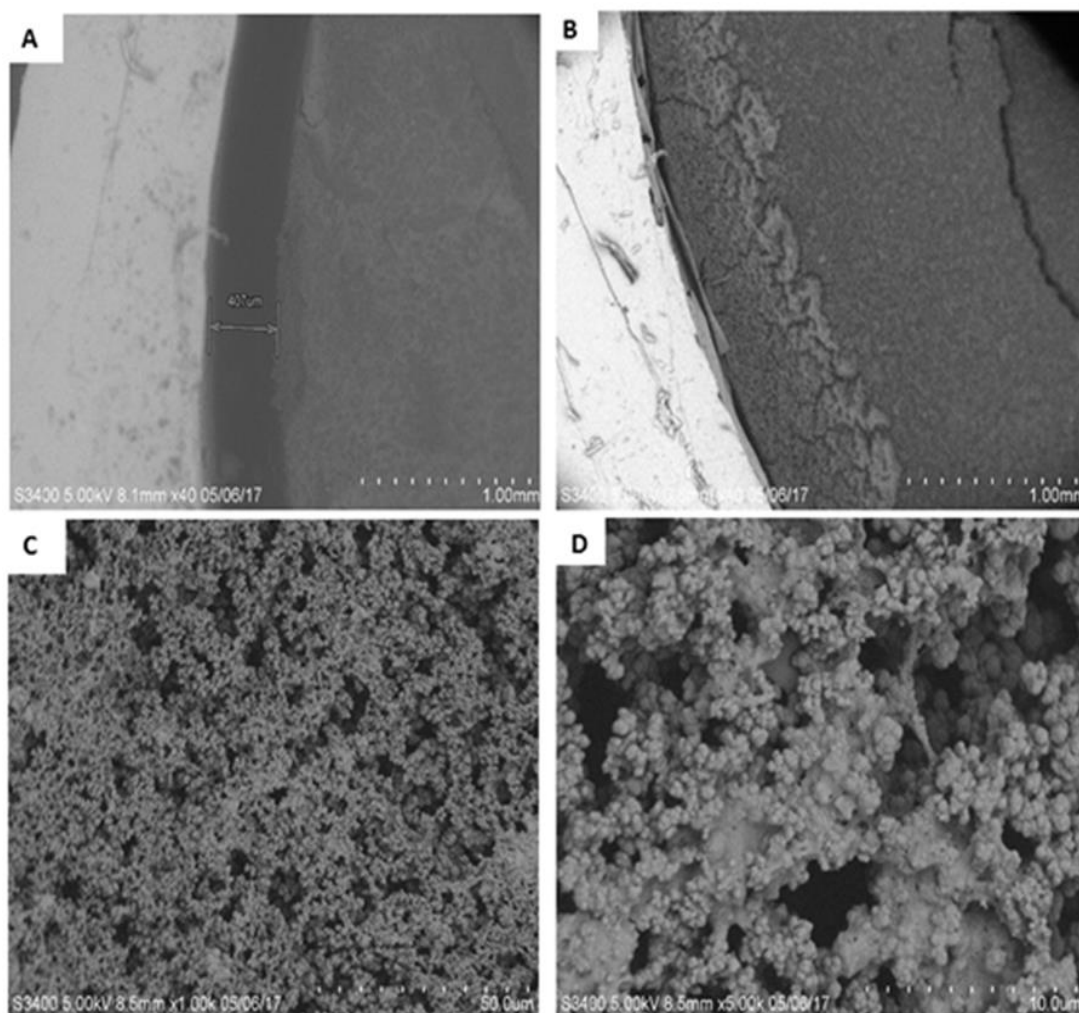
Figure 1. SEM images of disk aptasensor showing homogenous surface morphology. (A) Shows the presence of wall channel, 407 µm, between the disk monolith and the column. (B) Shows the absence of wall channel after aptamer immobilisation. (C) Shows homogenous disk aptasensor at x 5000 magnification. (D) Shows image at x 10000 magnification.

279
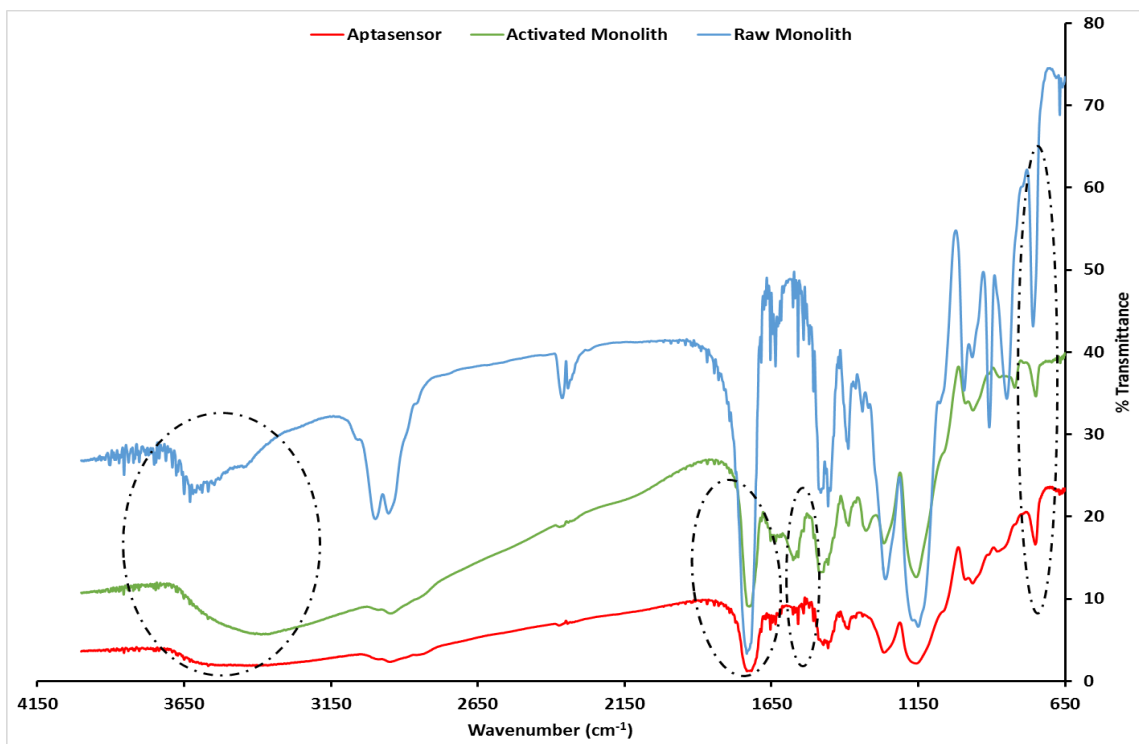
Figure 2. Fourier Transform Infrared Spectra of polymethacrylate monoliths, activated monoliths and aptasensor. Figure shows reduction in epoxy peak intensity during activation and aptamer functionalisation of the monolith.

Fourier Transform Infrared (FTIR) Spectra analysis was used to identify available functional groups in the polymer system before and after activation. Aptamer molecules were successfully immobilised on the disk monolith by pump recirculation at 0.2 mL/min for 20 h. The FTIR spectra of blank polymethacrylate monoliths, activated monoliths and the aptamer-modified disk monolith in Figure 2 shows peak changes at approximately 759, 1557, 1734 cm^{-1} wave numbers and a broad band stretch from 3348 – 3751 cm^{-1}. Peak intensity at ~759 cm^{-1} shows the presence of epoxy functional groups. The spectra shows a significant reduction in epoxy peak intensity from the blank monolith to the aptamer-modified disk monolith, supporting the conversion of epoxy moieties into active sites for aptamer coupling. Molecular rearrangements within the epoxy rings enables reaction with ethylenediamine and glutaraldehyde creating active sites for aptamer immobilisation and capping with $NaBH_3CN$. In essence, $NaBH_3CN$ reduces non-stable imine groups (-C=N-) created during the schiff base chemical reactions to more stable amine groups (-C-NH-) to prevent non-specific binding. Peak at ~ 1557 cm^{-1} on the aptamer-modified disk monolith spectra shows the presence of nucleotides in the

aptasensor, supporting the successful introduction of aptamer molecules into the monolith matrix. This peak is not present in the raw and activated monoliths. The peak at ~1734 cm⁻¹ is due to the presence of C=O bonds in the monolith. The intensity of the C=O peak reduced after activation and aptamer immobilisation, and this is potentially due to amine reductive reactions. The broad band observed for all three spectra indicates the presence of acrylate-based functionalities in the monoliths.

The effect of temperature on aptamer immobilisation onto the disk monolith was investigated under varied incubation temperature conditions of 4 °C and 25 °C. Generally, the extent of aptamer immobilisation was significantly influenced by temperature as follows: (i) before washing, 87.3 % ± 0.6 and 87.5 % ± 1.5; (ii) after washing of unbound aptamer ligands, 44.4 % ± 1.2 and 65.4 % ± 2.0, respectively. Aptamers are known to be thermodynamically stable below their melting point ($< T_m$), and under low temperature conditions their secondary structures are inherently folded (Baldrich *et al.,* 2004; Tan *et al.,* 2017). The random folding of aptamers under extremely low temperature conditions in the absence of the cognate target and unoptimised micro-conditions could affect molecular interactions and immobilisation efficiency. In addition, from Arrhenius equation (1), for the same volume of monolith and aptamer concentration, increasing temperature demonstrates improved kinetics of aptamer molecular transport from the aqueous onto the monolith phase during static grafting. Figure 3 shows increasing immobilisation efficiency with temperature increase from 4 °C to 25 °C.

$$k = A\exp\left(-\frac{E_a}{RT}\right) \qquad\qquad \textbf{(1)}$$

k is the rate constant for ligand functionalisation (mol/s); A is the pre-exponential factor between the aptamer and monolith (mol/s); R is the gas constant (8.314 J/mol/K), E_a is the apparent activation energy and T is the temperature of functionalisation, K.
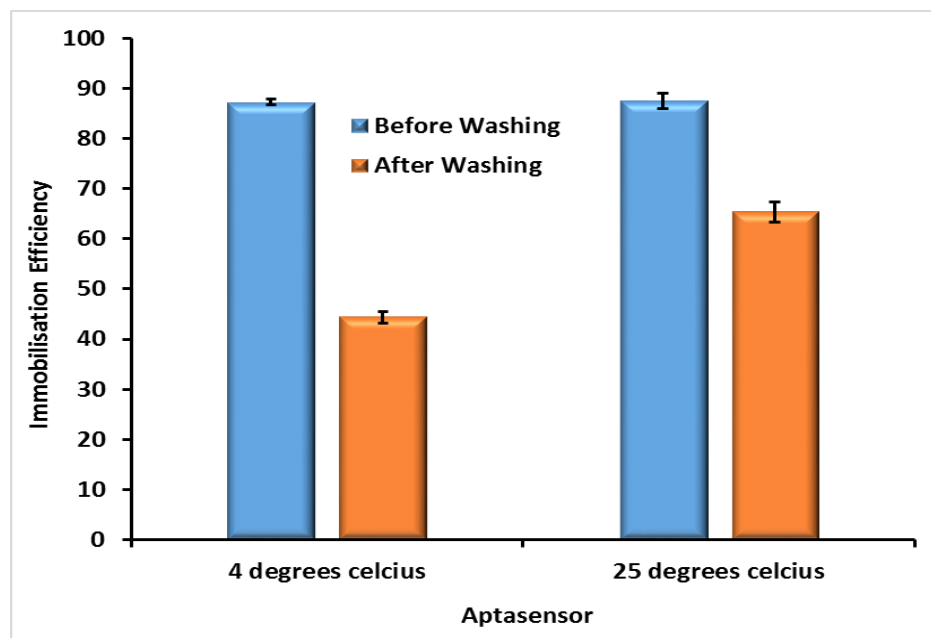
Figure 3. Effect of temperature on aptamer immobilisation efficiency at 4 ºC and 25 ºC for statically grafted disk monoliths. Data shows increasing immobilisation efficiency with temperature increase.

3.2   Effect of Flow Rate on Pressure Drop

In order to investigate the hydrodynamic characteristics of the synthesised disk monolith, the column was exposed to varying mobile phase flow rates using ultrapure water at different stages of the immobilisation process. Wall-channelling was observed for the synthesised monolith sample, leading to the requirement of higher flow rates due to the presence of side flows, as shown in Figure 4 (A). Figure 4 (B) shows that Schiff-base activation chemistry and aptamer immobilisation significantly reduces the side wall-channelling between the monolith and the polypropylene column. This was as a result of the introduction of cross-linkers through covalent amine reductive reaction between glutaraldehyde, ethylenediamine and epoxy rings of the polymethacrylate monolith. A subsequent increase in the back pressure of the aptamer-modified disk monolith relative to the activated monolith demonstrates further reduction in volume of the interconnected pores of the monolithic support. This was due to the presence of immobilised aptamers with C6-spacer arms. Nevertheless, the small mass to volume ratio of aptamers implies that a higher density of ligand coverage can be achieved without significant reduction in pore volume. The ligand density obtained for the aptamer-modified disk monolith was

480 pmol/uL; more than two folds greater than previously reported ligand densities for polymethacrylate monoliths (Zhao *et al.*, 2008; Zhao *et al.*, 2008; Han *et al.*, 2012). The use of a microporogen as the solvent for polymer synthesis introduced high density surface morphology for ligand immobilisation. It was previously demonstrated by Ongkudon and Danquah (2010) and Acquah *et al.* (2016) that the addition of macroporogens such as 1-dodecanol increases the pore size of the monolith, thus decreasing the surface area available for ligand immobilisation. A linear pressure drop – flow rate correlation was obtained for both activated and immobilised aptamer disk-monolith systems, indicating agreement with Darcy–Weisbach equation shown in equation (2). The ratio of the permeability of the activated disk-monolith, $1.88\pm0.1 \times 10^{-14}$ m^2 (RSD = 5.6%), to that of the aptamer-modified disk monolith, $1.67 \pm 0.05 \times 10^{-14}$ m^2 (RSD =3.2%) shows a marginal reduction of 1.12. This range of permeability is in keeping with data reported by Du *et al.* (2015) and Brothier and Pichon (2014) as 2.54×10^{-14} m^2 and $6.15 \pm 0.67 \times 10^{-14}$ m^2 for a polymethacrylate and a hybrid organic-silica monolith, respectively. The improvement in aptamer-modified disk monolith permeability ratio is attributed to the geometry and surface morphology of the monolith as well as the chemistry used for aptamer immobilisation.

$$\frac{\Delta P}{L} = \frac{128}{\pi} \frac{\mu Q}{d_i^{\,4}} \tag{2}$$

$$K = \frac{4\mu L}{\pi (d_i^2) \Delta P} Q \tag{3}$$

ΔP is the pressure drop (Pa); L is the length of the disk monolith (m); μ is the dynamic viscosity (Pa.S); Q is the flow rate (m^{3}s^{-1}); d_i is the internal diameter; and K is the permeability (m^2).
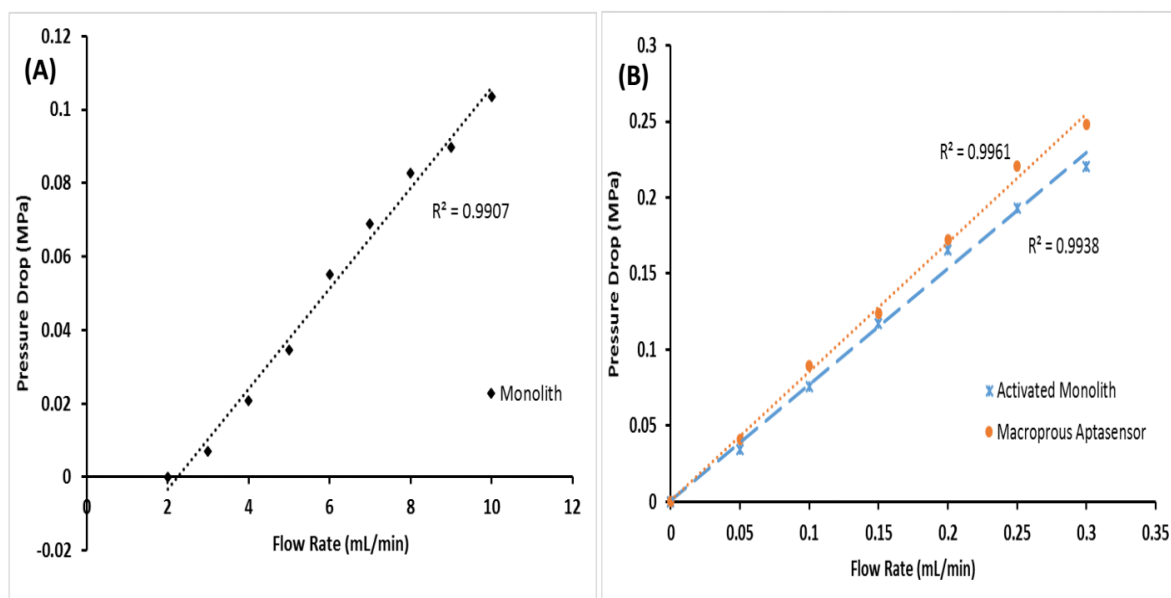
Figure 4. Effect of flow rate on pressure drop for (A) disk monolith, (B) activated disk monolith and disk-aptasensor.

3.3 Column Efficiency

The presence of interconnected pores forming a network of channels in polymethacrylate monoliths makes them efficient adsorbent matrices for convective biomolecular binding. In addition, the surface area and geometry of polymethacrylate monoliths can be engineered by incorporating specific surface modification and immobilisation chemistries and polymerisation conditions. The diffusivity of thrombin has previously been demonstrated to be in the order of 10^{-8} cm^2/s (Smith and Sefton, 1988). Due to this high diffusivity, adsorbent sensors based on convective transport phenomenon and low K_D affinity ligands yield short analysis time, flow-independent resolution, and flow-independent dynamic binding capacity (Mihelič *et al.*, 2000; Yamamoto and Kita, 2005). The efficiency of a separation column is a function of the estimated number of theoretical plates (N) and the height equivalent to the theoretical plate as given by equations (4) and (5).

$$N = 5.545 \left(\frac{t_r}{w_h}\right)^2 \tag{4}$$

$$HETP = \left(\frac{L}{N}\right) \tag{5}$$

N is the number of theoretical plates, t_r is the retention time, w_h is the peak width at half height and L is the length of the monolith. Table 1 and Figure 5 show the effect of linear velocity on the number of theoretical plates with an optimum linear velocity of 126 cm/min ($\approx$ 0.25 mL/min) at room temperature of 25 ± 2 °C.

Table 1. Effect of linear velocity on the number of theoretical plates.

Linear Velocity (cm/min)	Number of theoretical plates (N)
78	105.3
102	115.8
126	128.2
150	109.2

Under the optimum conditions, the chromatograph of the aptamer-modified disk monolith showed narrow chromatographic peaks with reduced band broadening, implying that at flow rates < 0.25 mL/min, the movement of thrombin molecules was low and resulted in reduced thrombin transfer rate. Consequently, a high mass transfer resistance was established, resulting in band broadening. Flow rates > 0.25 mL/min resulted in low retention times, compromising effective molecular affinity interactions between the immobilised aptamer and the thrombin molecules. In addition, high flow rates stretches the thrombin molecules causing them to occupy relatively large unit volumes, thus reducing the column efficiency (Bicho *et al.*, 2016).
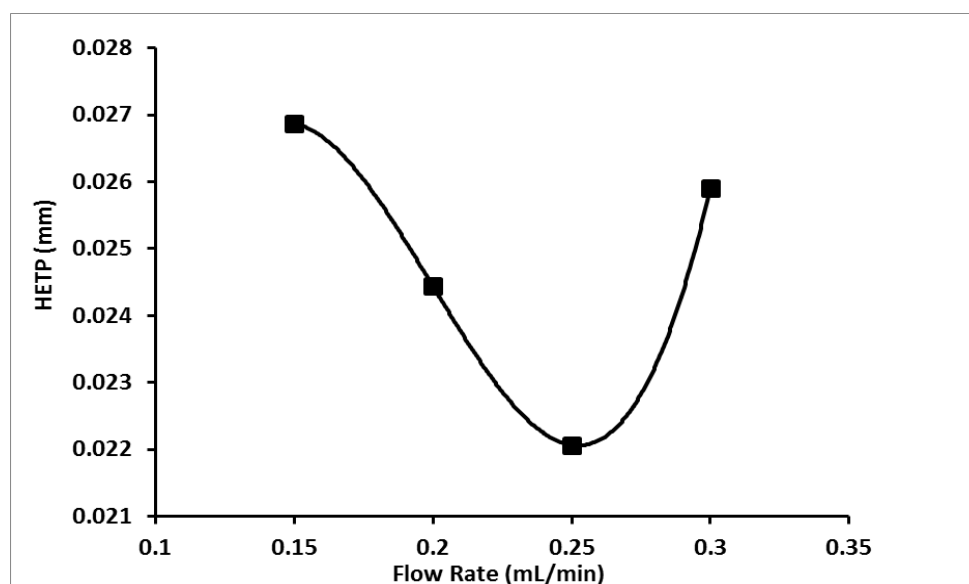
Figure 5. Van Deemter plot showing the effect of flow rate on height equivalent to the theoretical plate. Data shows an optimum ratio of 0.25 mL/min.

3.4   Dynamic Binding Capacity

The dynamic binding capacity of a polymeric aptasensor is affected by a number of factors such as the morphology of the matrix and aptamer ligand density. Engineering the synthesis conditions to increase the pore size results in increasing convective mobile phase transport. This also compromises the surface area availability for ligand binding and biomolecular adsorption (Danquah and Forde, 2007). The binding capacities for various aptamer-modified monolithic formats are presented in Table 2. The present work focuses on investigating the dynamic binding capacity of the aptamer-modified disk monolith in order to evaluate its chromatographic performance under varying flow rates and thrombin concentration. The dynamic binding capacity at 10% breakthrough was determined using equation (6):

$$DBC_{10\%} = \frac{C_o(V_{10\%} - V_o)}{V_m}$$ **(6)**

where C_o is the concentration of thrombin solution, (mg/mL); $V_{10\%}$ is the volume of thrombin solution at 10% breakthrough (mL); V_o is the void volume of the monolith (mL); and V_m is the volume of the monolith.

Table 2. Comparison of binding capacity of various macroporous aptasensors

Aptamer	Type of Monolith	DBC (mg/mL)	Reference
Anti-lysosyme	Rod column (GMA-co-EDMA)	68.22	(Du *et al.*, 2015)
Anti-ochratoxin A	Capillary column (Silica)	9.08×10^{-3}	(Brothier and Pichon, 2014)
Anti-thrombin	Capillary column (Silica)	1.15	(Deng *et al.*, 2012)
Thrombin binding	Disk (GMA-co-EDMA)	7.2±0.6	Present study

From Figure 6A and 6B, flow rate variation showed minimal differences in dynamic binding capacity with an average of 7.2 ± 0.6 (RSD = 7.9%) mg/mL of thrombin. Contrary, there were significant differences in the effect of thrombin concentration on the dynamic binding capacity of the aptamer-modified disk monolith with an average value of 6.5 ± 1.3 (RSD = 20.8%) mg/mL of thrombin. A similar effect of target concentration on dynamic binding capacity was previously reported for different monolithic applications

(Sousa *et al.*, 2007; Bicho *et al.*, 2016). The increasing dynamic binding capacity trend in thrombin concentration could be attributed to high thrombin density per unit volume of mobile carrier exposed to the matrix, resulting in higher binding titres within the binding duration at 10% breakthrough (Sousa *et al.*, 2007; Bicho *et al.*, 2016).
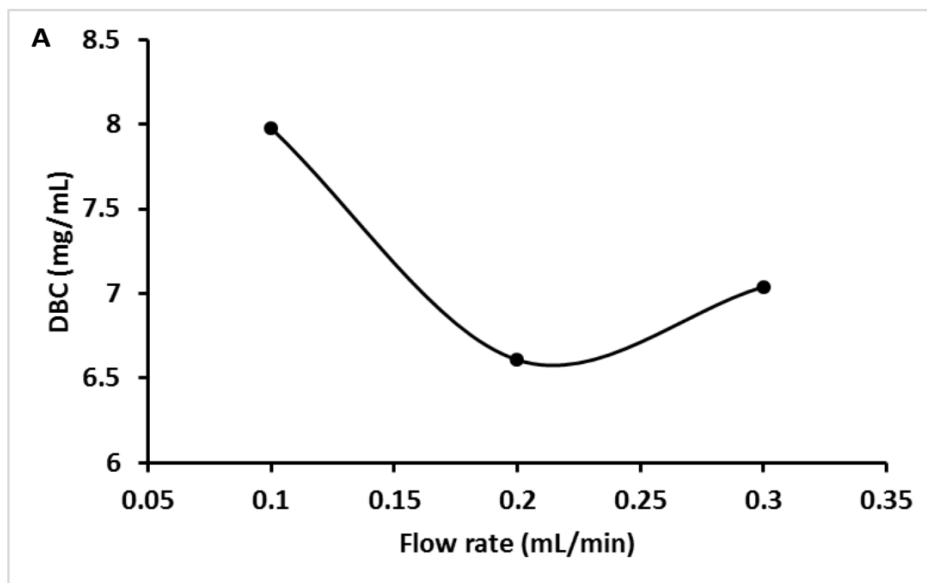
Figure 6a. Effect of flow rate on the dynamic binding capacity of the disk-aptasensor. Data shows minimal flow rate effect (RSD = 7.9%) on dynamic binding capacity.
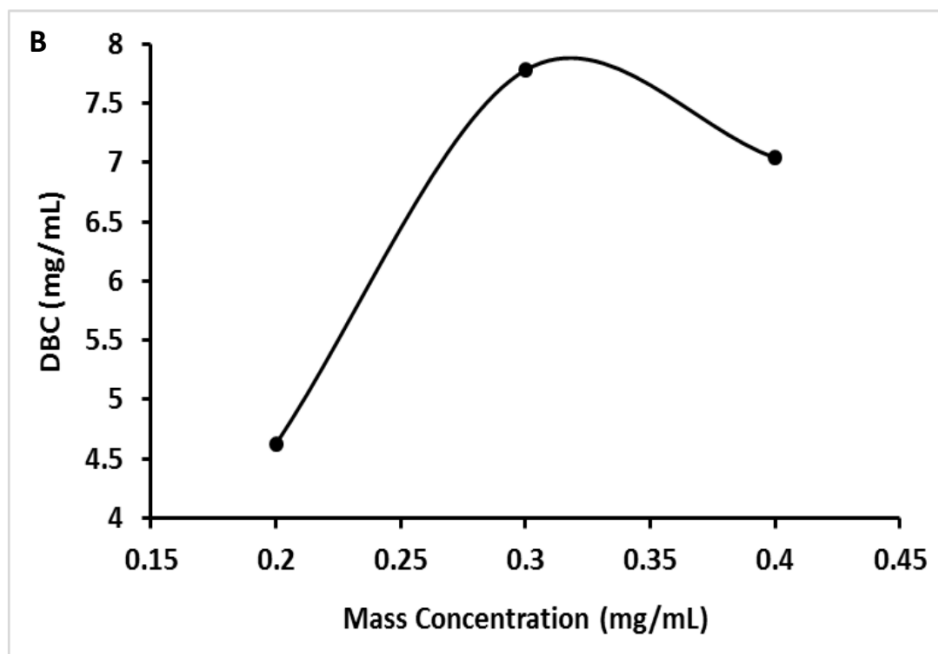
Figure 6b. Effect of thrombin concentration on dynamic binding capacity of the disk-aptasensor. Data shows optimum dynamic binding capacity of 7.78 mg/mL at a flow rate of 0.3 mL/min.

3.5   Target protein binding and selectivity analysis of the disk-aptasensor

To demonstrate the selectivity and binding performance of the aptamer-modified disk monolith towards the target thrombin protein, a protein mixture of lysosyme (0.4 mg/mL) and thrombin (1.0 mg/mL) was prepared and interacted with the aptasensor adsorbent under chromatographic conditions. The chromatographic profiles of the individual proteins in addition to human IgG were also analysed in order to determine the retention time, the binding and elution characteristics of each protein. 2 M $NaClO_4$ was used as the elution buffer and the chromatographs were generated at a wavelength of 280 nm. Figure 7 shows the chromatographs of the individual proteins. Lysosyme and human IgG molecules were recovered at retention times of 6.73 mins and 7.86 mins, respectively, during the running of each feed with mobile phase buffer B before elution with minimal interaction with the thrombin specific aptamer-modified disk monolith. The difference in retention times for the two protein molecules could be attributed to their different charge to mass ratio in the disk aptasensor. Thrombin molecules were retained and remained bound to the aptamer-modified disk monolith until elution with 2 M $NaClO_4$.
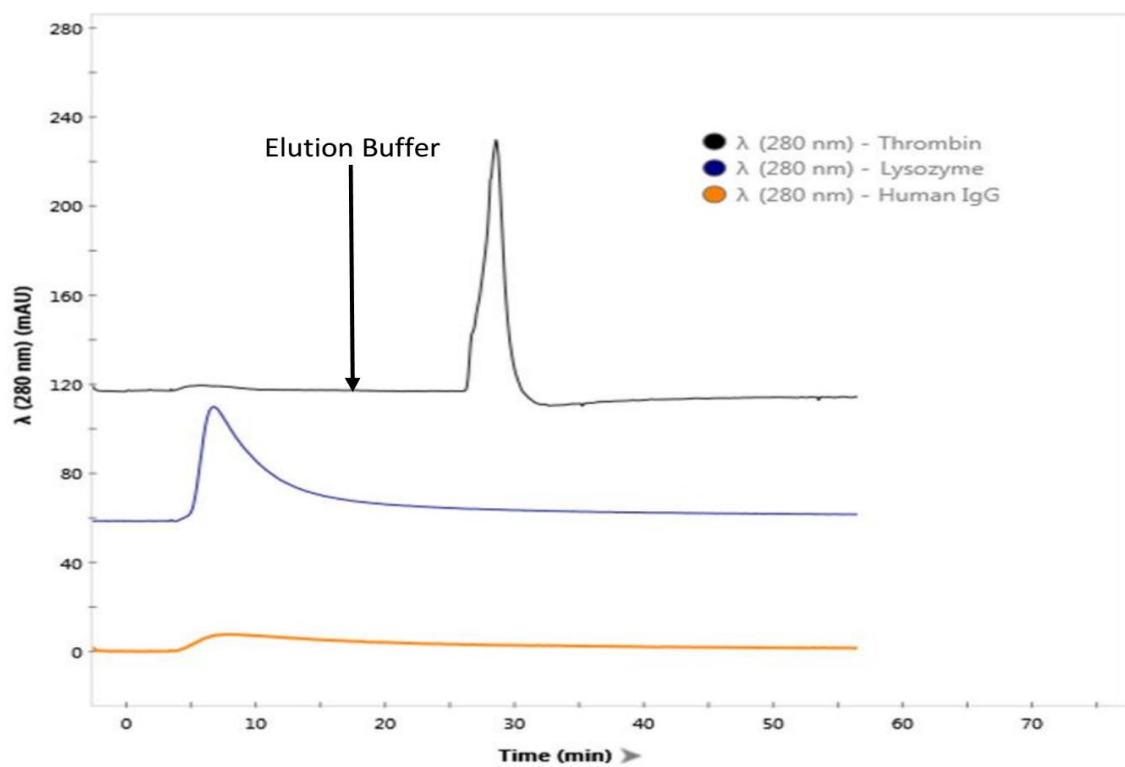
Figure 7. Target protein binding and selectivity analysis of the disk aptasensor. The aptasensor was tested with lysosyme (0.4 mg/mL), human IgG antibody (0.4 mg/mL) and

thrombin (1.0 mg/mL). The data shows effective aptasensor interaction with thrombin and minimal interaction with lysosyme (0.4 mg/mL) and human IgG antibody (0.4 mg/mL).

A mixture of lysozyme and thrombin molecules was prepared to investigate the selectivity of the aptamer-modified disk monolith towards the target thrombin molecule. Different gradient elution buffers were applied to investigate the separation efficiency of thrombin from similar non-target protein molecules. The chromatograph is shown in Figure 8. Each chromatographic analysis with different gradient elution levels resulted in the emergence of a first peak before the elution curve. This peak represents lysozyme molecules flowing through the aptamer-modified disk monolith with minimal affinity interaction. Thrombin molecules were recovered after gradient elution at 4%, 6% and 8% of the elution buffer, showing selective binding to the aptamer-modified disk monolith. The chromatograph showed three peaks under the elution curve. The first and second thrombin peaks represent thrombin molecules with different degrees of affinity interactions with the aptamer-modified disk monolith, potentially due to the unique molecular and structural characteristics of single protein molecules and their dimers formed through self-assembly mechanisms. The third peak could represent high molecular weight complexates of thrombin with low migration rate. Gradient elution at 6% elution buffer showed well resolved peaks and bandwidth for efficient separation of the non-target protein. Data from SDS-PAGE analysis further supported the peak assignments from the chromatograph. The image shows the original thrombin having a molecular weight of ~66 kDa in lanes 2 – 4, whiles lane 1 and lane 5 represented the ladder and control, respectively.
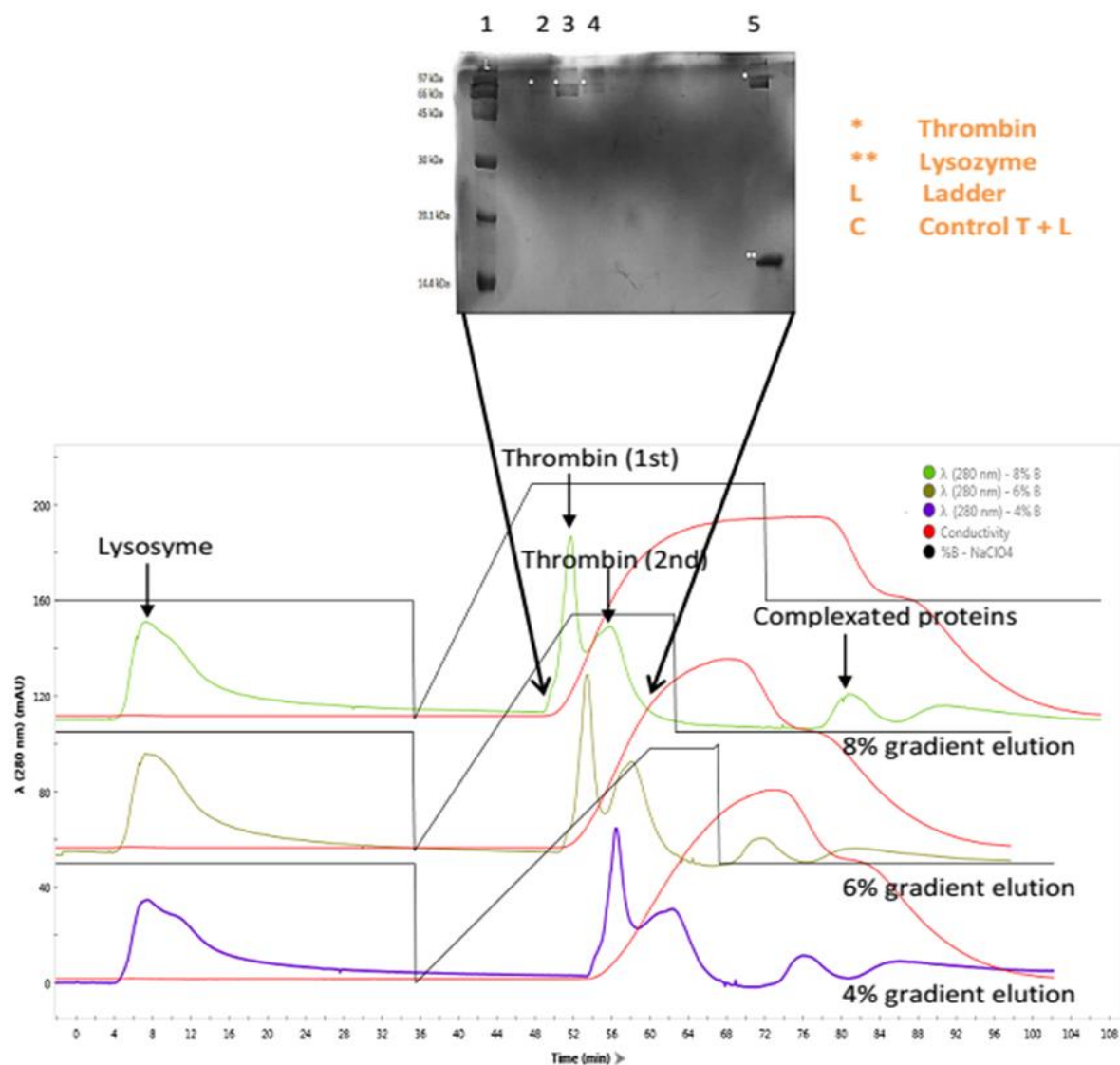
Figure 8. Thrombin separation chromatographs with varying radient elution (4%, 6%, 8% of 2 M NaClO₄). Feed sample is a protein mixture of thrombin (1.0 mg/mL) and non-target lysosyme (0.4 mg/mL). Chromatographic anlysis was performed at a flow rate of 0.3 mL/min.

4.   CONCLUSIONS

In this work, polymethacrylate disk monoliths were synthesised, characterised and functionalised with thrombin binding aptamers for selective binding and isolation of thrombin. Experimental data showed that the disk monolith possessed good permeability of $1.67 \pm 0.05 \times 10^{-14} \text{ m}^2$ (RSD =3.2%) with only a marginal drop in permeability (by 1.12 folds) after activation. An increase in the degree of aptamer immobilisation was observed with temperature increase from 4 ºC to 25 ºC. Column efficiency analysis revealed an

optimum linear velocity of 126 cm/min (≈ 0.25 mL/min) at 25±2 ºC with a theoretical plate number 128.2 and HETP of 0.022 mm. Variation in the mobile phase flow rate had minimal impact on dynamic binding capacity. However, significant differences in the dynamic binding capacity were observed with variations in thrombin concentration. The aptamer-modified disk monolith demonstrated good selectivity and isolation of thrombin and from non-target proteins in this preliminary work. Further biophysical and chromatographic evaluations are required to completely characterise the aptamer-modified monolith and transfer performance to other aptamer-target systems for high throughput biomolecular screening.

5. ACKNOWLEDGMENT

6. REFERENCES

Acquah, C., M.K. Danquah, C.K.S. Moy and C.M. Ongkudon, 2016. In-process thermochemical analysis of in situ poly(ethylene glycol methacrylate-co-glycidyl methacrylate) monolithic adsorbent synthesis. Journal of Applied Polymer Science, 133: 1-9. Available from http://dx.doi.org/10.1002/app.43507. DOI 10.1002/app.43507.

Acquah, C., M.K. Danquah, J.L.S. Yon, A. Sidhu and C.M. Ongkudon, 2015. A review on immobilised aptamers for high throughput biomolecular detection and screening. Analytica chimica acta, 888: 10-18. Available from http://www.sciencedirect.com/science/article/pii/S0003267015008016. DOI http://dx.doi.org/10.1016/j.aca.2015.05.050.

Acquah, C., C.K.S. Moy, M.K. Danquah and C.M. Ongkudon, 2016. Development and characteristics of polymer monoliths for advanced lc bioscreening applications: A review. Journal of Chromatography B, 1015–1016: 121-134. Available from http://www.sciencedirect.com/science/article/pii/S1570023216300976. DOI http://dx.doi.org/10.1016/j.jchromb.2016.02.016.

Acquah, C., E. Obeng, D. Agyei, C. Ongkudon, C. Moy and M. Danquah, 2017. Nano-doped monolithic materials for molecular separation. Separations, 4(1): 1-22. Available from http://www.mdpi.com/2297-8739/4/1/2.

Baldrich, E., A. Restrepo and C.K. O'Sullivan, 2004. Aptasensor development: Elucidation of critical parameters for optimal aptamer performance. Analytical chemistry, 76(23): 7053-7063.

Bencina, K., M. Bencina, A. Podgornik and A. Strancar, 2007. Influence of the methacrylate monolith structure on genomic DNA mechanical degradation, enzymes activity and clogging. Journal of chromatography. A, 1160(1-2): 176-

183. Available from http://www.ncbi.nlm.nih.gov/pubmed/17540390. DOI 10.1016/j.chroma.2007.05.034.

Bicho, D., C. Caramelo-Nunes, A. Sousa, F. Sousa, J. Queiroz and C. Tomaz, 2016. Purification of influenza deoxyribonucleic acid-based vaccine using agmatine monolith. Journal of Chromatography B, 1012: 153-161.

Brgles, M., T. Kurtović, L. Kovačič, I. Križaj, M. Barut, M.L. Balija, G. Allmaier, M. Marchetti-Deschmann and B. Halassy, 2014. Identification of proteins interacting with ammodytoxins in vipera ammodytes ammodytes venom by immuno-affinity chromatography. Analytical and bioanalytical chemistry, 406(1): 293-304.

Brothier, F. and V. Pichon, 2014. Miniaturized DNA aptamer-based monolithic sorbent for selective extraction of a target analyte coupled on-line to nanolc. Analytical and bioanalytical chemistry, 406(30): 7875-7886. Available from http://www.ncbi.nlm.nih.gov/pubmed/25335821. DOI 10.1007/s00216-014-8256-z.

Černigoj, U., J. Gašperšič, A. Fichtenbaum, N. Lendero Krajnc, J. Vidič, G. Mitulović and A. Štrancar, 2016. Titanium dioxide nanoparticle coating of polymethacrylate-based chromatographic monoliths for phosphopetides enrichment. Analytica chimica acta. Available from http://www.sciencedirect.com/science/article/pii/S0003267016310388. DOI http://dx.doi.org/10.1016/j.aca.2016.08.044.

Danquah, M.K. and G.M. Forde, 2007. Towards the design of a scalable and commercially viable technique for plasmid purification using a methacrylate monolithic stationary phase. Journal of Chemical Technology & Biotechnology, 82(8): 752-757. DOI 10.1002/jctb.1733.

Danquah, M.K. and G.M. Forde, 2008. Preparation of macroporous methacrylate monolithic material with convective flow properties for bioseparation: Investigating the kinetics of pore formation and hydrodynamic performance. Chemical Engineering Journal, 140(1-3): 593-599. DOI 10.1016/j.cej.2008.02.012.

Deng, N., Z. Liang, Y. Liang, Z. Sui, L. Zhang, Q. Wu, K. Yang, L. Zhang and Y. Zhang, 2012. Aptamer modified organic-inorganic hybrid silica monolithic capillary columns for highly selective recognition of thrombin. Analytical chemistry, 84(23): 10186-10190. Available from http://www.ncbi.nlm.nih.gov/pubmed/23137349. DOI 10.1021/ac302779u.

Desire, C.T., E.F. Hilder and R.D. Arrua, 2017. Monolithic high-performance liquid chromatography columns. Encyclopedia of Analytical Chemistry.

Du, K., M. Yang, Q. Zhang and S. Dan, 2015. Highly porous polymer monolith immobilized with aptamer (rna) anchored grafted tentacles and its potential for the purification of lysozyme. Industrial & Engineering Chemistry Research.

Han, B., C. Zhao, J. Yin and H. Wang, 2012. High performance aptamer affinity chromatography for single-step selective extraction and screening of basic protein lysozyme. Journal of chromatography. B, Analytical technologies in the biomedical and life sciences, 903: 112-117. Available from http://www.ncbi.nlm.nih.gov/pubmed/22841745. DOI 10.1016/j.jchromb.2012.07.003.

Isakari, Y., A. Podgornik, N. Yoshimoto and S. Yamamoto, 2016. Monolith disk chromatography separates pegylated protein positional isoforms within minutes at low pressure. Biotechnology journal, 11(1): 100-106.

Jiang, T., R. Mallik and D.S. Hage, 2005. Affinity monoliths for ultrafast immunoextraction. Analytical chemistry, 77(8): 2362-2372.

Krajacic, M., M. Ravnikar, A. Štrancar and I. Gutiérrez-Aguirre, 2017. Application of monolithic chromatographic supports in virus research. Electrophoresis.

Mihelič, I., T. Koloini, A. Podgornik and A. Štrancar, 2000. Dynamic capacity studies of cim (convective interaction media)® monolithic columns. Journal of separation science, 23(1): 39-43.

Ongkudon, C.M. and M.K. Danquah, 2010. Process optimisation for anion exchange monolithic chromatography of 4.2 kbp plasmid vaccine (pcdna3f). Journal of Chromatography B, 878(28): 2719-2725. DOI 10.1016/j.jchromb.2010.08.011.

Ongkudon, C.M., T. Kansil and C. Wong, 2014. Challenges and strategies in the preparation of large-volume polymer-based monolithic chromatography adsorbents. Journal of separation science, 37(5): 455-464.

Ongkudon, C.M., S. Pan and M.K. Danquah, 2013. An innovative monolithic column preparation for the isolation of 25 kilo base pairs DNA. Journal of chromatography. A, 1318: 156-162. Available from http://www.ncbi.nlm.nih.gov/pubmed/24209297. DOI 10.1016/j.chroma.2013.10.011.

Podgornik, A. and N.L. Krajnc, 2012. Application of monoliths for bioparticle isolation. pp: 3059-3072.

Podgornik, A., V. Smrekar, P. Krajnc and A. Strancar, 2013. Estimation of methacrylate monolith binding capacity from pressure drop data. Journal of chromatography. A, 1272: 50-55. Available from http://www.ncbi.nlm.nih.gov/pubmed/23261298. DOI 10.1016/j.chroma.2012.11.057.

Prasanna, R.R. and M.A. Vijayalakshmi, 2010. Characterization of metal chelate methacrylate monolithic disk for purification of polyclonal and monoclonal immunoglobulin g. Journal of Chromatography A, 1217(23): 3660-3667.

Roberts, M.W., C.M. Ongkudon, G.M. Forde and M.K. Danquah, 2009. Versatility of polymethacrylate monoliths for chromatographic purification of biomolecules. Journal of separation science, 32(15-16): 2485-2494. Available from http://www.ncbi.nlm.nih.gov/pubmed/19603394. DOI 10.1002/jssc.200900309.

Sharma, T.K., J.G. Bruno and A. Dhiman, 2017. Abcs of DNA aptamer and related assay development. Biotechnology advances, 35(2): 275-301. Available from http://www.sciencedirect.com/science/article/pii/S0734975017300034 [Accessed 2017/4//]. DOI https://doi.org/10.1016/j.biotechadv.2017.01.003.

Smith, B.A. and M.V. Sefton, 1988. Permeability of a heparin–polyvinyl alcohol hydrogel to thrombin and antithrombin iii. Journal of Biomedical Materials Research Part A, 22(8): 673-685.

Sousa, F., D. Prazeres and J. Queiroz, 2007. Dynamic binding capacity of plasmid DNA in histidine–agarose chromatography. Biomedical Chromatography, 21(9): 993-998.

Tan, S.Y., C. Acquah, A. Sidhu, C.M. Ongkudon, L.S. Yon and M.K. Danquah, 2016. Selex modifications and bioanalytical techniques for aptamer-target binding characterisation. Taylor & Francis: pp: 00-00.

Tan, S.Y., C. Acquah, S.Y. Tan, C.M. Ongkudon and M.K. Danquah, 2017. Characterisation of charge distribution and stability of aptamer-thrombin binding interaction. Process Biochemistry. Available from http://www.sciencedirect.com/science/article/pii/S135951131630887X. DOI https://doi.org/10.1016/j.procbio.2017.06.003.

Yamamoto, S. and A. Kita, 2005. Theoretical background of short chromatographic layers: Optimization of gradient elution in short columns. Journal of Chromatography A, 1065(1): 45-50.

Zhao, Q., X.-F. Li and X.C. Le, 2008. Aptamer-modified monolithic capillary chromatography for protein separation and detection. Analytical chemistry, 80(10): 3915-3920. DOI 10.1021/ac702567x.

Zhao, Q., X.-F. Li, Y. Shao and X.C. Le, 2008. Aptamer-based affinity chromatographic assays for thrombin. Analytical chemistry, 80(19): 7586-7593.

CHAPTER SEVEN

CONCLUSION

The main objective of this research work was to develop a robust and specific aptasensor using thrombin as the model target, thrombin binding aptamer as the ligand and disk monolith as the stationary support, providing a suitable micro-environment for affinity binding and convective transport of target molecules to occur. The main objective comprised of four specific objectives which were formulated from the underpinning research questions for this project.

The first research question sought to study the thermo-molecular relationship between in-process conditions governing the free radical polymer synthesis process and the physicochemical characteristics of the monolith as a basis of tuning the pore and surface characteristics of the monolith in Chapter Three. Results from the thermochemical parametic study of the monolith synthesis process showed that temperature in the form of *in situ* thermal build-up is the primary factor affecting the pore formation process and the surface morphology. The monolithic pore size is inversely proportional to the degree of exothermic heat released within the mould. Increasing the concentration of cross-linker monomer (EDMA) correlates with increasing polymerisation peak temperature with a reduction in polymer pore size. Similarly, an increase in the concentration of initiator (BPO) resulted in an increase in temperature build-up within the mould. In addition, different set point temperatures for polymerisation resulted in different thermal path during polymerization. Consequently, the overall internal thermal path for the reactive mixture is a function of the amount of cross-linker and initiator present as well as the set point polymerisation temperature. Kinetic modelling of polymethacrylate monolith synthesis was carried out by means of Avrami's isothermal analysis, and the results were consistent with experimental data. These findings in unravelling the first research question have been established in this research work to be useful in monitoring the thermal build-up, engineering the pore size and surface characteristics of polymethacrylate monoliths for tailored application to various targets including biomolecules, cells, proteins, ions and viruses.

The second research question for this project sought to discover the thermo-molecular relationship between in process and post-polymerisation conditions on the chemical integrity and thermal stability of polymethacrylate monoliths in Chapter Four. The thermal

stability of the polymethacrylate monolith was investigated by varying *in situ* and *ex situ* synthesis conditions. Porogen to monomer ratio and polymerisation temperature were the most influential parameters affecting the thermal stability of the monolith. The thermal stability increased with decreasing polymerisation temperature and increasing the porogen (P) to monomer (M) ratio. Increasing the total porogen (P) to monomer (M) ratio increased the thermal stability of the monolith by >62% and >50% for P40/M60-P60/M40 and P60/M40-P80/M20, respectively. Variations in the concentrations of cross-linker (EDMA) and functional monomer (GMA) were rigorously investigated. The impact on apparent activation energy was determined using Ozawa-Flynn-Wall (OFW) and Kissinger–Akahira–Sunose (KAS) isoconversional models. The relationship between apparent activation energy and the extent of conversion showed a complex multistep reaction model for polymethacrylate monoliths. Thus, the thermal stability of polymethacrylate monoliths is a function of temperature. Kinetic parameters showed that an increase in EDMA and GMA concentrations above 20% significantly enhanced the thermal stability of the monolith under elevated non-isothermal conditions. Owing to the current lack of data on the thermal stability and the synergistic relationship between in-process and *ex situ* conditions on monoliths, findings established from the second research question in this research will be critical in optimising the synthesis of polymethacrylate monoliths as robust synthetic platforms for prolonged biotechnological applications. The characteristic temperature ranges, kinetic data and activation energy correlations obtained depicts the effective temperature ranges within which polymethacrylate aptasensors can be operated without losing their molecular and structural integrity. New insights into chemical compositions which can achieve an almost homogenous morphology, tailored pore sizes, low temperature build-up and high thermal stability has been shown. The aforementioned parameters are essential in the development of a robust aptasensor with tailored pore sizes, high ligand density, and predetermined thermal stability effect.

Although aptamers have been heralded as unique ligands with superior binding characteristics over antibodies, there remain limited biophysical characterisation tools investigating their binding affinity and charge distribution under different physicochemical conditions. The effectiveness of aptamer-target interactions is affected by physicochemical conditions such as ionic strength, pH, concentration of ligand, and

temperature. The third research question comprehensively investigated the impact of aptamer hydrodynamic charge and size distribution on binding stability using zeta potential analysis via dynamic light scattering, and the development of a polymeric disk aptasensor. This was done in two sections as detailed in Chapter Five. The first section comprehensively studied how the micro-environment affected the charge distribution, hydrodynamic size and stability of aptamers and their binding complexes using zeta potential analysis via dynamic light scattering. Experimental data based on a thrombin binding aptamer (TBA) showed aptamer electronegativity at pH > 5 with improved dispersion and stability above pH 9. It was demonstrated that pH affects the binding affinity of the aptamer through protonation and deprotonation mechanisms. Thrombin-TBA complex was determined to be electronegative, and maintained electronegativity over the pH range. The presence of metal ions influenced the formation of TBA secondary structures and the resulting thrombin-TBA complexation. K^+ induced the formation of G-quadruplex in TBA under a charge distribution stability similar to thrombin-induced G-quadruplex. The presence of K^+ also reduced the electronegativity of TBA, and at low concentrations K^+ stabilizes the formation of TBA G-quadruplex structure. Thrombin-TBA complex is considered most dispersed and stable at 10 mM K^+ concentration. The presence of Mg^{2+} reduced the electronegativity of TBA significantly and favoured binding to thrombin. TBA and thrombin-TBA complex are considered stable in the presence of Mg^{2+} at concentrations > 1.5 M. TBA was found to be most stable at temperature ~20 °C with a reduction in electronegativity as temperature increased. Zeta (ζ) potential analysis via dynamic light scattering is an established useful technique in characterising interfacial distribution and electrokinetic behaviour of charged species in aqueous media. Zeta potential was therefore demonstrated to be a useful biophysical tool in the characterisation of aptamers and their targets. As such, findings established in section one of Chapter Five serve as one of the premium studies in advancing theoretical understanding of the binding behaviour of aptamers in solution in relation to surface charge distribution, hydrodynamic mobility, binding characteristics and biomolecular complex formation using dynamic light scattering prior to immobilisation.

The second section of the third research question was carried out by biophysically characterising the effect of schiff-base covalent immobilisation of aptamers on the disk

monolith and the effect of the micro-environment on the disk monolith aptasensor. The disk aptasensor was developed to have high surface area for aptamer immobilisation and convective transport features for continuous binding application. The aptamer molecules were modified with amino moiety and C-6 spacer arms to enhance the immobilisation process and reduce the occurrence of steric effect. A high ligand density of 480 pmol/uL was obtained, almost 2 fold higher than previously reported liagnd densities for polymethacrylate aptasensors. This phenomena was due to the use of microporogens in the synthesis of disk monoliths and, aldehyde cross-linkers and C-6 spacer arms during the post-polymerisation modification process. Thermal degradation analysis showed that initial polymer degradation temperature is influenced by Schiff-base activation chemistry, with an increase in endothermic heat required during the activation process. The optimum binding pH and ionic concentration under isocratic conditions was obtained at pH 8 and 5 mM Mg^{2+}, respectively, for effective bioscreening of thrombin biomolecules. The findings obtained during the biophysical characterisation of the proposed disk aptasensor demonstrated that there is formation of a covalent anchor between the aptamer-monolith system without disrupting the chemical and molecular stability of the monolith. It has also been demonstrated that polymethacrylate disk-aptasensors can be easily engineered to have high ligand density using microporogens and predetermined compositions. These findings therefore unravels the second section of the third research question in Chapter Five and contributes new knowledge to the current understanding in the development of robust aptasensors for effective bioscreening with resistivity to different micro-environmental conditions.

The fourth research question attempted to carry out extensive chromatographic studies on the proposed disk-aptasensor under different isocratic and physicochemical conditions for effective bioscreening in Chapter Six. The experimental results showed that the disk aptasensors possessed good permeability within the range $1.67 \pm 0.05 \times 10^{-14}$ m^2 (RSD =3.2%) with a marginal drop in permeability by 1.12 fold relative to the activated disk monolith. There was a significant improvement in aptamer immobilisation efficiency with temperature increase from 4 °C to 25 °C. Analysis of column efficiency revealed an optimum linear velocity of 126 cm/min ($\approx$ 0.25 mL/min) at room temperatures of 25 ± 2 °C. The theoretical number of plates for the optimum linear velocity was 128.2 with an

HETP of 0.022 mm. Binding studies demonstrated that flow rate variation had minimal impact on dynamic binding capacity of the aptasensor. However, thrombin concentration affected the dynamic binding capacity. The polymeric disk-aptasensor demonstrated good selectivity towards thrombin in a chromatographic analysis with effective gradient elution at 6% for regeneration of the aptasensor after 14 mins of applying the elution buffer. Lysosyme and IgG biomolecules which were used as non-targets were recovered at 6.73 mins and 7.86 mins, respectively, during the running of each feed. Conspicuously, findings from the chromatographic analysis in accordance with the fourth research question demonstrates the chromatographic efficiency and a satisfactory performance of the disk-aptasensor with convective flow, rapid results, biocompatibility, good permeability, high target selectivity and separation, and flow unaffected dynamic binding capacity.

In summary, all four research objectives set in Chapter One and formulated from the research questions of this dissertation have been fulfilled. The findings of this research contribute significantly in advancing current scientific knowledge and understanding in the development and characterisation of polymeric disk monolith aptasensors for bioscreening applications. It is proposed that future work considers the following aspects:

- Development of theoretical models essential in the biophysical characterisation of the morphology and binding capacity of monoliths having the same *in situ* and *ex situ conditions* during the formation of aptamer-based polymeric biosensors for affinity bioscreening. The existence of such models will be essential for the formation of standard non-destructive characterisation processes for monoliths after their synthesis for affinity applications involving immobilised aptamers.

- Investigate the thermodynamic potential and correlation between aptamers and their cognate targets via zeta potential analysis and well-established models such as Kayes, and Ottewill-Watanabe theories under different physicochemical conditions. Such further studies will contribute to the formulation of robust theoretical understandings to reinforce the use of aptamers as biosensors, drug delivery vehicles and screening of biomarkers.

- Application of rigorous biophysical and chromatographic characterisation tools to extend the applications of this research to other targets. This can be done through investigating the orientation and molecular integrity of different immobilised aptamers via atomic force microscopy, circular dichroism and further liquid chromatography. This will be essential in further understanding and formulating generic theoretical insights into their structure and binding performance. Additionally, it is recommended that chemistries that allow the tagging of target biomolecules with fluorescein isothiocyanate can be studied for an enhancement in the rapidity of results.

APPENDICES

Appendix A: Copyright and Consent Notes

Appendix A1

Consent by co-authors

Declaration for thesis section

The following co-authors attest to the candidate's contribution to a joint publication as part of his thesis. Permission by co-authors are as follows:

Name	Signature	Date
Michael K. Danquah		13/07/2017
Lau Sie Yon		13-7-17
Charles K.S. Moy		18/07/2017
Amandeep Sidhu		18-7-17
Clarence M. Ongkudon		13.7.2017
Mahmood Anwar		18-07-2017
Sze Y. Tan		17/07/2017
Sing Y. Tan		13th July, 2017
Yi Wei Chan		13/7/2017

Appendix A2

Copyright from Journal of Chromatography B

ELSEVIER LICENSE
TERMS AND CONDITIONS

Aug 16, 2017

This Agreement between Curtin University ("You") and Elsevier ("Elsevier") consists of your license details and the terms and conditions provided by Elsevier and Copyright Clearance Center.

License Number	4170820863956
License date	Aug 16, 2017
Licensed Content Publisher	Elsevier
Licensed Content Publication	Journal of Chromatography B
Licensed Content Title	Development and characteristics of polymer monoliths for advanced LC bioscreening applications: A review
Licensed Content Author	Caleb Acquah,Charles K.S. Moy,Michael K. Danquah,Clarence M. Ongkudon
Licensed Content Date	Mar 15, 2016
Licensed Content Volume	1015
Licensed Content Issue	n/a
Licensed Content Pages	14
Start Page	121
End Page	134
Type of Use	reuse in a thesis/dissertation
Intended publisher of new work	other
Portion	full article
Format	both print and electronic
Are you the author of this Elsevier article?	Yes
Will you be translating?	Yes, including English rights
Number of languages	1
Languages	English
Title of your thesis/dissertation	Development of an aptamer-based polymeric bionsensor for advanced bioscreening
Expected completion date	Aug 2017
Estimated size (number of pages)	25
Requestor Location	Curtin University Curtin University, CDT 250, 98009 Miri, Sarawak 98009 Malaysia Attn: Curtin University
Total	0.00 USD
Terms and Conditions	

INTRODUCTION

1. The publisher for this copyrighted material is Elsevier. By clicking "accept" in connection with completing this licensing transaction, you agree that the following terms and conditions

Appendix A3

Copyright from Critical Reviews in Analytical Chemistry

Appendix A4
Copyright from Analytica Chimica Acta

Appendix A5
Copyright from Journal of Applied Polymer Science

Appendix A6

Copyright from Asia-Pacific Journal of Chemical Engineering

JOHN WILEY AND SONS LICENSE
TERMS AND CONDITIONS

Aug 16, 2017

License Number	4170810380801
License date	Aug 16, 2017
Licensed Content Publisher	John Wiley and Sons
Licensed Content Publication	Asia-Pacific Journal of Chemical Engineering
Licensed Content Title	Parametric investigation of polymethacrylate monolith synthesis and stability via thermogravimetric characterisation
Licensed Content Author	Caleb Acquah,Michael K. Danquah,Charles K. S. Moy,Mahmood Anwar,Clarence M. Ongkudon
Licensed Content Date	Feb 26, 2017
Licensed Content Pages	13
Type of use	Dissertation/Thesis
Requestor type	Author of this Wiley article
Format	Print and electronic
Portion	Full article
Will you be translating?	No
Title of your thesis / dissertation	Development of an aptamer-based polymeric bionsensor for advanced bioscreening
Expected completion date	Aug 2017
Expected size (number of pages)	25
Requestor Location	Curtin University Curtin University, CDT 250, 98009 Miri, Sarawak 98009 Malaysia Attn: Curtin University
Publisher Tax ID	EU826007151
Billing Type	Invoice
Billing Address	Curtin University Curtin University, CDT 250, 98009 Miri, Malaysia 98009 Attn: Curtin University
Total	0.00 USD
Terms and Conditions	

TERMS AND CONDITIONS

Appendix A7
Copyright from Canadian Journal of Chemical Engineering

Appendix A8
Copyright from Process Biochemistry